Split-Luciferase Complementation and Molecular Dynamics Studies for the Mini-G Protein-Based Functional Characterization of GPCRs

DISSERTATION
ZUR ERLANGUNG DES DOKTORGRADES DER NATURWISSENSCHAFTEN
(DR. RER. NAT.)
AN DER FAKULTÄT FÜR CHEMIE UND PHARMAZIE
DER UNIVERSITÄT REGENSBURG

Vorgelegt von Carina Höring

aus Witten

im Jahr 2022

Diese Arbeit entstand von Juli 2017 bis Juni 2022 unter der Anleitung von PD Dr. Andrea Straßer an der Fakultät für Chemie und Pharmazie der Universität Regensburg

Promotionsgesuch eingereicht am:	28.06.2022
Vorsitzender des Prüfungsausschusses:	Prof. Dr. Sigurd Elz
Erstgutachterin:	PD Dr. Andrea Straßer
Zweitgutachter:	Prof. Dr. Pierre Koch
Drittprüfer:	Prof. Dr. Joachim Wegener

Für Christian

Everything is going to be fine in the end.

If it's not fine, it's not the end.

-Oscar Wilde-

Acknowledgments

An dieser Stelle möchte ich mich bei allen Personen bedanken, die zum Entstehen dieser Arbeit beigetragen haben und die mich über die Jahre der Promotion begleitet und unterstützt haben. Insbesondere gilt mein Dank:

Herrn Prof. Dr. Armin Buschauer für die Aufnahme in den Arbeitskreis. Leider konnte er das Entstehen dieser Arbeit nicht mehr begleiten;

Frau PD Dr. Andrea Straßer für die Betreuung, den Freiraum in der Projektgestaltung, die Durchsicht dieser Arbeit und das Erstellen des Erstgutachtens;

Herrn Prof. Dr. Günther Bernhardt für seine Betreuung zu Beginn meiner Promotion, seine Korrekturen und zahlreiche wissenschaftliche Ratschläge;

Herrn Prof. Dr. Pierre Koch für die Bereitschaft, das Zweitgutachten für diese Arbeit zu erstellen;

Herrn Prof. Dr. Joachim Wegener für den fachlichen Austausch und die Teilnahme an der Promotionsprüfung als Drittprüfer;

Herrn Prof. Dr. Sigurd Elz für die Übernahme des Vorsitzes der Promotionsprüfung;

Herrn Prof. Dr. Yinglong Miao für die Möglichkeit, einen Forschungsaufenthalt in seiner Arbeitsgruppe an der University of Kansas zu absolvieren. Ganz besonders bedanke ich mich für seine Bereitschaft, mich weiterhin zu betreuen trotz des Pandemie-bedingten verfrühten Endes des Forschungsaufenthalts, und für die damit verbundenen unzähligen Zoom-Meetings. An dieser Stelle gilt mein Dank auch Herrn Dr. Jinan Wang für die Beantwortung sämtlicher Fragen bei den GaMD Simulationen;

Herrn Prof. Dr. Heinrich Sticht für den Kurzaufenthalt in seiner Arbeitsgruppe und vor allem für die Möglichkeit die Rechensysteme und einen immensen Anteil der Speicherkapazitäten seiner Arbeitsgruppe zu nutzen. An dieser Stelle danke ich auch Herrn Dr. Anselm Horn für die technische Unterstützung auf den Rechensystemen. Ganz besonders möchte ich mich bei Herrn Dr. Christian Söldner und Herrn Marcus Conrad bedanken für ihre Geduld beim Einarbeiten in die Moleküldynamiksimulationen und fortwährende Unterstützung. Ohne euch wäre ein Teil dieser Arbeit (Kapitel 6) nicht entstanden;

Herrn PD Dr. Max Keller für die gute Zusammenarbeit und Organisation im Laboralltag und Biochemie-Praktikum. Danke auch für das Interesse an meinem Projekt und dadurch entstandene Kollaborationen zur Testung von M_2R und (fotoschaltbaren) Y_4R Liganden;

Herrn Dr. Steffen Pockes für das Interesse an meiner Arbeit, die Möglichkeit das Projekt seiner Masterandin Denise Mönnich mitzugestalten und die Unterstützung beim Verfassen meiner ersten Publikation;

Allen Co-Autoren für die angenehme und produktive Zusammenarbeit. Vor allem möchte ich Frau Ulla Seibel-Ehlert, Frau Dr. Katharina Tropmann und Frau Denise Mönnich für die Durchführung von Zellassays und Herrn Dr. Lukas Grätz, Herrn Prof. Dr. Günther Bernhardt, Herrn Dr. Christian Söldner und Herrn Marcus Conrad für die konzeptionelle Unterstützung der Projekte danken;

Frau Dr. Laura Humphrys für das Korrekturlesen, die Organisation von Lehrstuhl-Seminaren und ihren Forschergeist. Nicht zuletzt ist so ein gemeinsames Projekt und Kapitel dieser Arbeit entstanden (Kapitel 4). Thanks for teaching me how to CRISPR :-)!

Frau Maria Beer-Krön, Frau Brigitte Wenzl und Frau Susanne Bollwein für die hervorragende Unterstützung bei Experimenten und Organisation des Laboralltags und Praktikums. Besonders danke ich Frau Maria Beer-Krön für ihr sonniges Gemüt und die vielen Gespräche und aufmunternden Worte, wann immer sie nötig waren;

Herrn Peter Richthammer für seine „goldenen Hände“ und Hilfe bei technischen Problemen;

Den Pharmazie-Wahlpflichtpraktikanten und studentischen Hilfskräften Jan-Michel Oberschelp, Valerie Huber, Kathrin Hochmuth, Tim-Oliver Koch, Ahmed Omar, Julia Tettero und Sophia Mühlbauer für ihr Interesse an meinen Projekten und die experimentelle Unterstützung, die in die Kapitel 2-3 eingeflossen ist;

Der Deutschen Forschungsgemeinschaft für die finanzielle Unterstützung während meiner Promotion im Rahmen des Graduiertenkollegs GRK1910 „Medicinal Chemistry of Selective GPCR Ligands“. In diesem Zusammenhang möchte ich mich auch bei den Mitgliedern des GRK1910s bedanken für die interessanten Workshops und Retreats, sowie den lustigen Abend auf der Regensburger Dult;

Herrn Dr. Lukas Grätz, dafür dass du mich in die biochemischen/molekularbiologischen Methoden eingearbeitet hast und dabei unterstützt hast, ein eigenständiges Projekt zu entwickeln. Danke für die Kaffeepausen, und dass du immer Zeit hattest, spontane (vielleicht abwegige) Projektideen zu diskutierten. Vor allem aber Danke dafür, dass du immer an meine mich geglaubt hast;

Frau Ulla Seibel-Ehlert für die gemeinsamen Mittagspausen, die vielen Gespräche und Fachsimpelei, aber vor allem für deine Freundschaft;

Frau Denise Mönnich für die schöne Zusammenarbeit im „Dopaminiiies“-Team, deine gute Laune, dein offenes Ohr und die Milch zum Kaffee ;-)!

Frau Dr. Nicole Plank für deine Unternehmungslust, deinen Humor und deine Freundschaft. Dadurch wurde gerade die letzte Zeit zu einer der besten;

Frau Lisa Schindler für die gute Zusammenarbeit im Praktikum, deine Hilfsbereitschaft bei meinen einzigen HPLC-Läufen ;-) und vor allem für deine Empathie;

Allen aktuellen und ehemaligen Kollegen des LS Buschauer für die tolle Arbeitsatmosphäre und die lustige Zeit bei gemeinsamen Pausen, Spieleabenden, sportlichen Aktivitäten und Feierabendbieren ;-). Ohne euch wäre die Zeit nicht halb so schön gewesen;

Der „Small Gang", den besten Freundinnen, die ich mir hätte wünschen können. Danke, dass ihr immer für mich da wart, Erfolge mit mir gefeiert habt und mich bei Misserfolgen immer wieder aufgebaut habt (auch wenn ihr wahrscheinlich nur halb verstehen konntet, worum es geht);

Ganz besonders danke ich meinen Eltern Ellen und Klaus, meiner Schwester Lena, und meiner Oma Gisela, die mich auf meinem bisherigen Weg immer begleitet und unterstützt haben. Ohne euren Rückhalt wäre die Entstehung dieser Arbeit nicht möglich gewesen;

Zu guter Letzt und von Herzen möchte ich mich bei meinem Partner Christian bedanken. Danke für deine Liebe und den Rückhalt, den du mir all die Jahre gegeben hast.

Publications, Presentations and Professional Training

Peer-Reviewed Journal Articles

(Published prior to the submission of this thesis)

Gergs, U.; Büxel, M. L.; Bresinsky, M.; Kirchhefer, U.; Fehse, C.; **Höring, C.**; Hofmann, B.; Marušáková, M.; Čináková, A.; Schwarz, R.; Pockes, S.; Neumann, J., Cardiac effects of novel histamine H_2 receptor agonists. *J Pharmacol Exp Ther* **2021**, 379 (3), 223-234.

Höring, C.; Conrad, M.; Söldner, C. A.; Wang, J.; Sticht, H.; Strasser, A.; Miao, Y., Specific engineered G protein coupling to histamine receptors revealed from cellular assay experiments and accelerated molecular dynamics simulations. *Int J Mol Sci* **2021**, 22 (18).

Weinhart, C. G.; Wifling, D.; Schmidt, M. F.; Neu, E.; **Höring, C.**; Clark, T.; Gmeiner, P.; Keller, M., Dibenzodiazepinone-type muscarinic receptor antagonists conjugated to basic peptides: Impact of the linker moiety and unnatural amino acids on M_2R selectivity. *Eur J Med Chem* **2021**, 213, 113159.

Szczepańska, K.; Pockes, S.; Podlewska, S.; **Höring, C.**; Mika, K.; Latacz, G.; Bednarski, M.; Siwek, A.; Karcz, T.; Nagl, M.; Bresinsky, M.; Mönnich, D.; Seibel, U.; Kuder, K. J.; Kotańska, M.; Stark, H.; Elz, S.; Kieć-Kononowicz, K., Structural modifications in the distal, regulatory region of histamine H_3 receptor antagonists leading to the identification of a potent anti-obesity agent. *Eur J Med Chem* **2021**, 213, 113041.

Tropmann, K.; **Höring, C.**; Plank, N.; Pockes, S., Discovery of a G protein-biased radioligand for the histamine H_2 receptor with reversible binding properties. *J Med Chem* **2020**, 63 (21), 13090-13102.

Höring, C.; Seibel, U.; Tropmann, K.; Grätz, L.; Mönnich, D.; Pitzl, S.; Bernhardt, G.; Pockes, S.; Strasser, A., A dynamic, split-luciferase-based mini-G protein sensor to functionally characterize ligands at all four histamine receptor subtypes. *Int J Mol Sci* **2020**, 21 (22), 8440.

Poster Presentations

(Only contributions as presenting author are listed)

Höring, C., Seibel, U., Grätz, L., Straßer, A., Bernhardt, G. A mini-G protein recruitment assay for the human histamine H_4 receptor. *48th meeting of the European Histamine Research Society* (2019, Krakow, Poland)

Höring, C., Grätz, L., Littmann, T., Buschauer, A., Bernhardt, G., Straßer, A. Mini-G protein recruitment as an approach to the functional characterization of histamine receptor ligands. *4th German Pharm-Tox Summit* (2019, Stuttgart, Germany)

Höring, C., Grätz, L., Littmann, T., Buschauer, A., Bernhardt, G., Straßer, A. Split luciferase-based determination of mini-G protein recruitment to GPCRs demonstrated at the histamine H_1 receptor. *9th International Summer School in Medicinal Chemistry* (2018, Regensburg, Germany)

Oral Presentations

Höring, C. Specific engineered G protein coupling to histamine H_2 and H_4 receptors. *Annual retreat of the research training group 1910 "Medicinal Chemistry of Selective GPCR Ligands"* (2021, Regensburg, Germany)

Höring, C. Functional studies of the H_2R in complex with minimal G proteins. *Annual retreat of the research training group 1910 "Medicinal Chemistry of Selective GPCR Ligands"* (2020, Erlangen, Germany)

Höring, C. Mini-G protein recruitment assays - an approach for the functional characterization of GPCRs, especially of histamine receptors. *Annual retreat of the research training group 1910 "Medicinal Chemistry of Selective GPCR Ligands"* (2019, Fensterbach, Germany)

Höring, C., Seibel, U., Grätz, L., Straßer, A., Bernhardt, G. Flash presentation: A mini-G protein recruitment assay for the human histamine H_4 receptor. *48th meeting of the European Histamine Research Society* (2019, Krakow, Poland)

Professional Training

Since July 2020	Member of the research training group 1910 "Medicinal Chemistry of Selective GPCR Ligands" funded by the Deutsche Forschungsgemeinschaft *(January 2020 – July 2021: Students' Representative)*
September 2018 – June 2020	Associated member of the research training group 1910 "Medicinal Chemistry of Selective GPCR Ligands" funded by the Deutsche Forschungsgemeinschaft
March 2018	Fortbildung für Projektleiter und Beauftragte für Biologische Sicherheit (§§15 und 17 der Gentechnik-sicherheitsverordnung), Regensburg

Table of Content

1. General Introduction

1.1. G Protein-Coupled Receptor Signaling

1.1.1. G Protein-Coupled Receptors (GPCRs)

G protein-coupled receptors (GPCRs) constitute one of the largest protein superfamilies in humans.[1-3] As such, their major function is to transduce extracellular stimuli, such as by neurotransmitters and hormones or even olfactory and visual signals, into cellular responses.[4-5] Because they regulate numerous (patho)physiological processes, GPCRs play a central role in drug discovery and are targeted by approximately 30% of approved drugs.[6] More than 800 GPCRs are encoded in the human genome that are categorized into 5 main families according to their sequence similarity:[7] The rhodopsin (class A), secretin (class B), glutamate (class C), adhesion and frizzled (class F) receptor families, with the rhodopsin family representing the largest group with more than 700 members.[7] Commonly, GPCRs consist of 7 α-helical transmembrane domains (TM) separated by three extracellular and three intracellular loops, with the N-terminus located on the extracellular and the C-terminus located on the intracellular side.[8-10] Interestingly, many GPCRs tend to form dimers or even higher order oligomers in intact cells.[11-14]

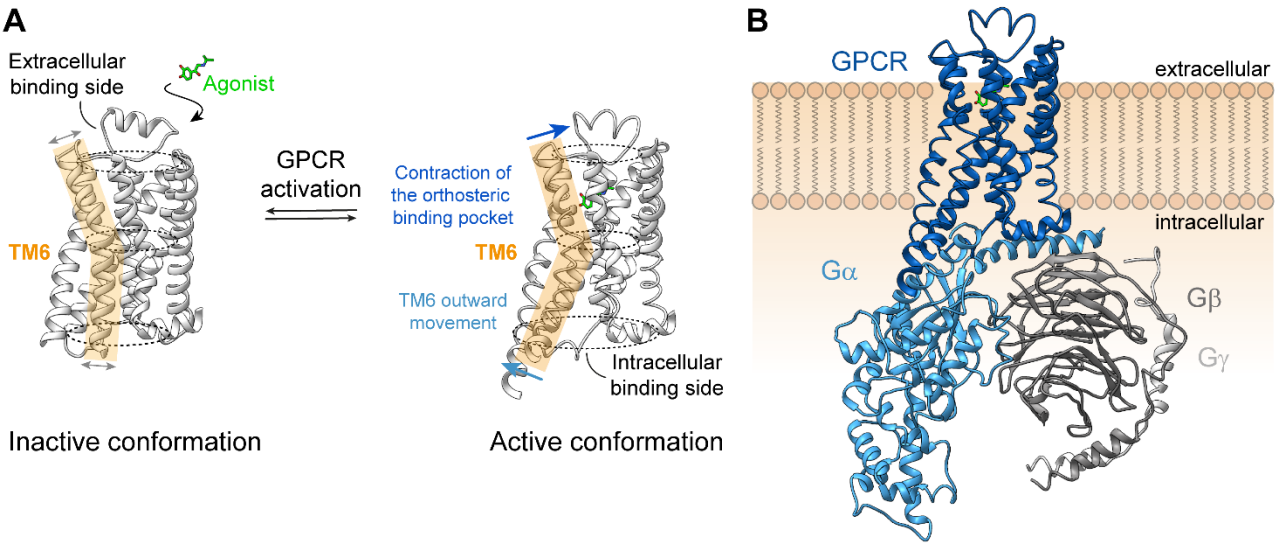

Figure 1.1. Schematic illustration of GPCR activation and intracellular coupling to a heterotrimeric G protein. A) Binding of the agonist leads to a conformational change of the GPCR, which is accompanied by contraction of the orthosteric binding pocket and outward movement of TM6. This opens an intracellular binding site for subsequent interaction with signal transducers, traditionally heterotrimeric G proteins. B) The agonist-bound active GPCR (dark blue) couples mainly to Gα (light blue) diving into the intracellular binding cavity of the receptor. Gβ (dark gray) and Gγ (light gray) support the conformation of Gα by binding to its N-terminus. Structural coordinates were taken representatively from three-dimensional structures of the inactive β_2-adrenoceptor (β_2AR) (pdb-id.: 6PS5) and the active, isoprenaline-bound β_2AR in complex with G$\alpha s\beta_1\gamma_2$ (pdb-id.: 7DHR) and processed using UCSF Chimera (version 1.16).

The activation of a GPCR upon ligand binding to the orthosteric (or allosteric) binding site leads to conformational changes, which enable the interaction with intracellular proteins and thus triggering a signal cascade. More specifically, the orthosteric binding site is a pocket within the extracellular side of the receptor, principally formed by TM3, TM5, TM6 and TM7.[15] Depending on the modality of the ligand, the orthosteric binding site undergoes distinct conformational changes after ligand binding: Starting from the ground state of the receptor, this leads to contraction for full and partial agonists (Figure 1.1A), while inverse agonists promote the opposite, an expansion.[16-17] Associated with this are global conformational changes,[15] such as the outward movement of TM6, which opens an intracellular binding site for signal transducers such as G proteins (Figure 1.1B) and β-arrestins.[18-21] Remarkably, ligand binding elicits unique receptor conformations that favor coupling to specific G proteins[22-23] or β-arrestins.[24] For example, the agonist (R,R)-fenoterol has been identified to preferentially activate Gs signaling, whereas its R,S isomer was able to stimulate both Gs and Gi proteins via the β_2AR.[25]

1.1.2. The G Protein Pathway

1.1.2.1. The Heterotrimeric G Protein Activation Cycle

In the classical view of GPCR signaling, G proteins are intermediates between the receptors expressed at the cell surface and intracellular effectors, therefore referred to as "molecular switches".[26-27] Turning on and off distinct intracellular signaling cascades in response to extracellular stimuli is principally coordinated by the activation or rather inactivation of heterotrimeric G proteins consisting of α, β and γ subunits.[28-29] More specifically, Gα comprises two conserved domains, the GTPase domain and the helical domain.[30] The β and γ subunits form a tightly associated dimer, which binds to the N-terminal region of Gα.[31-32] Of these constituents, Gα and Gγ are N-terminally attached to the cell membrane by post-translational modification, such as palmitoylation or myristoylation (Gα) and isoprenylation (Gγ).[33]

In the inactive state, G proteins exist as heterotrimers with Gα bound to GDP.[34] Activation of a G protein (Figure 1.2) involves the exchange of GDP for GTP[35-36] and the release of Gβγ in response to conformational changes at Gα.[3,37-38] Both components then are capable of activating intracellular effectors.[39-40] The intrinsic GTPase activity of Gα promotes GTP hydrolysis to GDP, thereby allowing Gβγ to return to Gα and thus the recovery of the heterotrimeric protein complex.[30,41] In the cellular context, the biochemical processes of both, G protein activation and inactivation, are tightly regulated by accessory proteins.[42] Guanine exchange factors (GEFs) encompassing activated GPCRs increase the rate of nucleotide exchange at Gα.[43] In contrast, GTPase-accelerating proteins (GAPs),[44] such as regulators of G protein signaling (RGS) proteins,[45-47] accelerate the hydrolysis of GTP, which is generally considered as the rate-limiting step

of G protein activation,[48] and guanine nucleotide dissociation inhibitors (GDIs) lock Gα in the GDP-bound state.[49-50]

1.1.2.2. G Protein-Dependent Signaling

Typically, agonist-mediated activation of GPCRs followed by G proteins elicits distinct intracellular signaling pathways, the onset of which is essentially determined by Gα. Strikingly, in contrast to the vast array of genes encoding cell surface GPCRs,[7] the human genome contains only 16 genes for Gα, 5 genes for Gβ, and 12 genes for Gγ.[51] On the basis of amino acid similarities, Gα isoforms have been clustered into four main families, Gαs, Gαi/o, Gαq/11 and Gα12/13.[52] In this thesis, Gs, Gi/o, Gq/11, or G12/13 always will refer to the heterotrimeric G protein, whereas specific G protein α subunits will be specified as Gα.

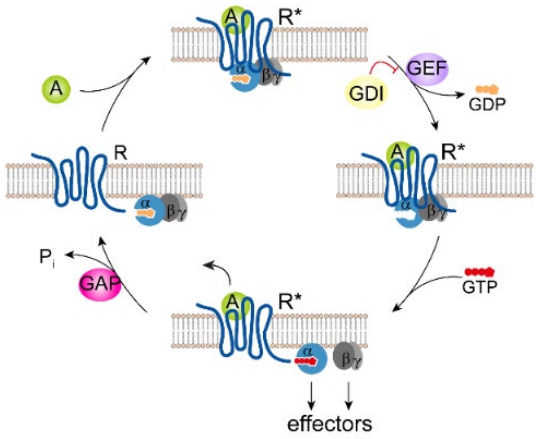

Figure 1.2. G protein activation cycle. Agonist (A)-mediated receptor activation (R*) promotes GDP exchange for GTP at Gα. The activated G protein subsequently dissociates into GTP-Gα and Gβγ, each capable of activating downstream effectors. GTP hydrolysis (GTP → GDP + P_i) restores the inactive G protein. While GTPase accelerating proteins (GAP) and GDP dissociation inhibitors (GDI) promote the inactive G protein conformation by either increasing GTP hydrolysis rate or preventing nucleotide exchange, activated receptors (R*) and other guanine nucleotide exchange factors (GEF) enhance G protein activation. Adapted from Oldham and Hamm (2008).[27]

The isoforms of two G proteins families, Gs and Gi/o, convert extracellular signals into cellular responses by interacting with membrane-bound adenylyl cyclase (AC).[53-54] However, while Gαs proteins stimulate AC, thereby catalyzing the formation of cAMP from ATP, Gαi/o proteins inhibit this reaction.[55-56] The second messenger cAMP in turn activates protein kinase A (PKA) which directly phosphorylates the cAMP-response element-binding protein (CREB) regulating gene transcription in addition to many metabolic enzymes.[57-58] Gαq/11 proteins activate phospholipase C-β (PLC-β) and thus catalyze the hydrolysis of phosphatidyl-4,5-bisphosphate (PIP_2) to inositol-1,4,5-trisphosphate (IP_3) and diacylglycerol (DAG) at the plasma membrane.[59-60] While intracellular DAG activates protein kinase C (PKC), IP_3 leads to the release of Ca^{2+} from intracellular stores.[61-63] In the Gq/11 pathway, another protein kinase, PKG, is activated by Ca^{2+}-mediated cGMP formation involving calmodulin and guanylyl cyclase.[64] In addition to the phosphorylation of proteins involved in mitogenesis, cell proliferation, and apoptosis,[65] the activation of Gq/11 ultimately regulates gene transcription.[66] The fourth G protein-dependent signaling pathway is initiated by Gα12/13 proteins that activate Rho GTPases.[67-68] These small monomeric G proteins bind to a plethora of effector proteins, the activation of which is involved in the regulation of gene transcription and cell

physiology, such as embryonal development, oncogenesis, and cancer metastasis.[69] Notably, G12/13 proteins are overexpressed in many cancers and thus may serve as prognostic factors.[70]

1.1.3. The β-Arrestin Pathway

Initially, β-arrestin function was described as "arresting" G protein-mediated signaling, which is also referred to as receptor desensitization.[71-72] G proteins and β-arrestins engage the same cytoplasmatic binding pocket and thus bind competitively to GPCRs.[18-20,73-75] Nevertheless, β-arrestin binding requires phosphorylation on serine and threonine residues at the intracellular loops and C-terminus of the GPCR,[76] which can occur by G protein-coupled receptor kinases (GRKs) upon receptor activation (homologous desensitization)[77-78] or other protein kinases, such as PKA or PKC (heterologous desensitization).[79-81] Pivotal to the desensitization mechanism is that β-arrestin binding creates a steric hindrance, which prevents further G protein activation.[82] To fully terminate GPCR signaling, β-arrestin bound receptors are removed from the cell surface mainly by clathrin-mediated endocytosis, and internalized receptors undergo a sorting process in the endosomal network, which leads to either the recycling to the plasma membrane (resensitization) or the degradation in the lysosomal pathway.[83-86]

Despite the described classical role in GPCR desensitization and internalization, β-arrestin binding induces a diverse array of cellular processes, such as mitogen-activated protein kinase (MAPK) signaling, receptor transactivation, receptor trafficking and gene transcription.[78,87-88]

1.1.4. Challenges in Drug Discovery

1.1.4.1. Crosstalk of GPCR Signaling

In drug discovery, the prospect of using selective agents to control cellular responses is clouded by the fact that GPCRs can activate multiple signaling pathways simultaneously and that crosstalk exists between these pathways.[89-90] To illustrate the magnitude of GPCR crosstalk, examples of overlap are provided in this section (Figure 1.3).

Gβγ dimers are perceived as active players in GPCR signaling[32,40] regulating K^+[91-93] and voltage-dependent Ca^{2+} ion channels,[94-95] specific isoforms of AC[96-97] or PLC,[60,98-99] and GRKs[76,100-101] independently of Gα. Thus, Gβγ of Gs and Gq/11 can cause a crosstalk from these signaling pathways by activating the opposite effector, PLC or AC, in each case.[102] Moreover, Gβγ of Gi/o is widely known to elicit Ca^{2+} release by cross-activating PLC[103-105] and Gαq/11 might also stimulate Rho GTPase activation of RhoA, a protein canonically activated in the G12/13 pathway. [68,106-107]

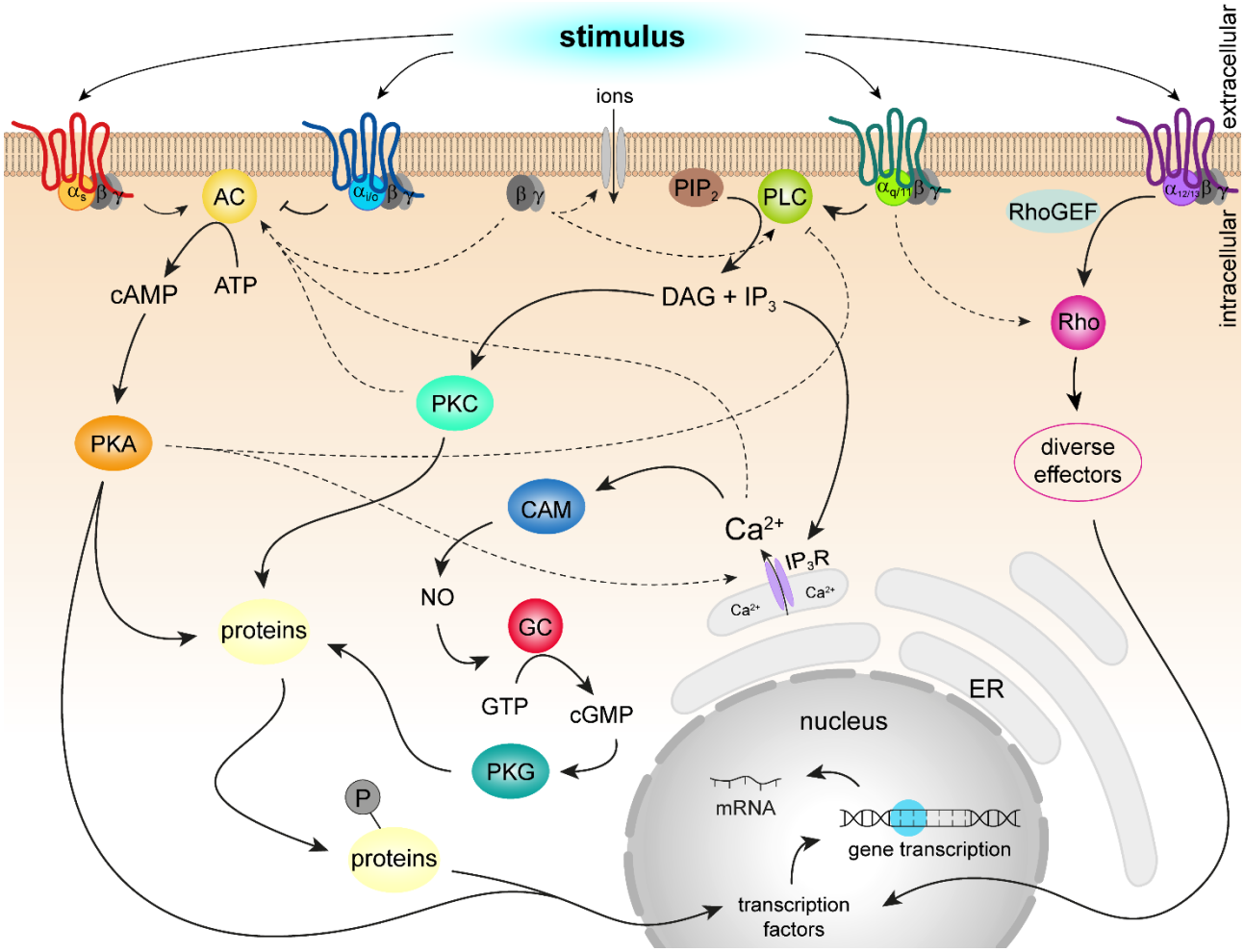

Figure 1.3. Schematic illustration of G protein-dependent GPCR signaling cascades. Canonical Gα signaling pathways of Gs- (orange), Gi/o- (blue), Gq/11- (green) and G12/13- (purple) coupled GPCRs are indicated as solid lines and involvement of signal crosstalk is indicated as dashed lines. AC, adenylyl cyclase; CAM, calcium-modulated protein; cGMP, cyclic guanine mono phosphate; DAG, diacyl glycerol; ER, endoplasmatic reticulum; GC, guanylyl cyclase; GTP, guanine triphosphate IP_3, inositol-1,4,5-trisphosphate; NO, nitric oxide; PIP_2, phosphatidylinositol-4,5-bisphosphate; PKA, protein kinase A; PKC, protein kinase C; PKG, protein kinase G; PLC, phospholipase C; Rho, Rho GTPase; RhoGEF, Rho guanine nucleotide exchange factors

In addition, pronounced crosstalk exists at the level of protein kinases. Agents that elevate cAMP might decrease intracellular DAG and IP_3 levels while increasing Ca^{2+} concentrations through PKA-mediated inhibition of PLC[108-109] or potentiation of IP_3 receptor (IP_3R) activity.[110-111] Furthermore, Gq/11-dependent PKC is able to stimulate certain isoforms of AC,[112] and Gi/o-dependent protein kinase B mediates activation of extracellular signaling kinases (ERKs),[113-114] therefore inducing a crosstalk of G protein- and β-arrestin-dependent signaling pathways.[115-116] Reciprocally, second messengers of G protein-dependent effectors, such as cAMP and DAG, can be degraded by the scaffolding effects of β-arrestin on cyclic nucleotide phosphodiesterases (PDEs) and diacylglycerol kinases (DGKs).[116]

1.1.4.2. Functional Selectivity

In contrast to the assumption that GPCRs interact only with a single intracellular binding partner, which was described by the classical ternary complex model of Black and Leff,[117-118] GPCR signaling has been shown to be multifaceted, involving various intracellular binding partners such as G proteins, β-arrestins, and GRKs.[76] In this context, the concept of functional selectivity, also referred to as "biased signaling" describes the ability of a ligand to stimulate one signaling pathway while blocking others, which the GPCR could in principle induce by stabilizing a specific receptor conformation.[24,119] Traditionally, discrimination is made for G protein- and β-arrestin-mediated signaling pathways.[24,120] However, there is increasing evidence that ligands can also modulate binding to different G protein families or rather Gα isoforms.[121-123]

Encouraged by the hope that therapeutic efficacy is related to individual signaling pathways, the development of functionally selective agents has become the focus of many drug discovery programs,[124-126] in addition to the design of highly affine ligands.[127] For example, since μ-opioid receptor (MOR)-mediated analgesia has been suggested to result from Gi/o signaling but the on-target side effect of respiratory depression might be related to β-arrestin signaling, several studies have aimed at the development of Gi/o-biased MOR agonists.[128] By solely activating the beneficial signaling pathway, researchers hope to minimize undesirable side effects.[129-130] At the developmental stage, the choice of assay systems is therefore critical. Particularly for the determination of (weak) partial agonism, proximal assays at the G protein or β-arrestin level seem desirable because these are less subject to receptor reserve or signaling crosstalk regulated by other cellular processes than distal events determined in traditional functional assays monitoring second messenger (cAMP, Ca^{2+}) generation or gene transcription.[131-132]

1.2. A Historical Perspective of G protein Level Assays

1.2.1. Guanine Nucleotide Exchange at Gα

In the 1970s, cooperativity between AC activity and guanine nucleotides was observed in preparations from rat liver and turkey erythrocytes.[133-134] Shortly thereafter, the proposed "guanine nucleotide-binding regulatory component" was found to activate AC only in presence of a "hormone", suggesting that the guanine binding site was not at AC.[135] The subsequent purification of Gs and Gi proteins has enabled first functional studies of G proteins using radiolabeled guanine nucleotides,[136-138] and agonists were shown not only to increase G protein activation but also to accelerate GTP hydrolysis.[139-141] More specifically, G protein activation was determined by the use of nonhydrolyzable [^{35}S]GTPγS, which promotes the accumulation of [^{35}S]GTPγS-bound Gα, whereas the rate of GTP hydrolysis has been assessed by quantifying [^{32}P]P_i cleaved from [γ-^{32}P]GTP.[142-143] Originally, [^{35}S]GTPγS binding and steady-state GTPase assays were performed on reconstituted receptors and G proteins or on native tissue preparations.[144] Later, using membrane or homogenate preparations of recombinant cells, these assays have been implemented in drug discovery for functional characterization of putative ligands.[143,145-147] Because of the irreversible activation of Gα in [^{35}S]GTPγS binding assays, the signal strength tends to be greater than in steady-state GTPase assays monitoring the GTP conversion rate[148], and has therefore been used more commonly. A particular advantage of [^{35}S]GTPγS binding assays is that they allow direct measurement of G protein activation.

1.2.2. Proximity-Based Assays at the G Protein Level

Activation of a heterotrimeric G protein typically results in spatial changes that is largely due to dissociation of Gβγ. For this reason, the examination of G protein activation using techniques developed for the detection of protein - protein interactions (PPI) has become an attractive alternative.[149] These methods are basically reliant on genetically encoded bioluminescent and fluorescent proteins, and can be used in living cells, thus enabling real-time measurements.[150-152]

1.2.2.1. Determination of Protein – Protein Interactions

1.2.2.1.1. Bioluminescent and Fluorescent Proteins Enabling Resonance Energy Transfer

In nature, a variety of living organisms, including species of insects, marine organisms, bacteria, and fungi, have been found to produce bioluminescence for attracting mates, luring prey, or repelling predators.[153-155] In spite of major structural differences in the luciferase-luciferin systems, the biochemical reaction follows a similar mechanism: An enzyme, called luciferase, catalyzes the oxidative decarboxylation of a substrate (luciferin) accompanied by the formation of a high-energy intermediate state whose relaxation to the ground state releases light (Figure 1.4).[156-157]

In GPCR research, mainly two types of luciferase-luciferin systems have been utilized. The D-luciferin-dependent luciferases from insects, such as Firefly luciferase (FLuc, 61 kDa) from firefly *Photinus pyralis,*[158] require ATP and Mg^{2+} for oxidation of the luciferin.[156] The emission wavelength of FLuc is usually sensitive to changes in pH and metal cations, although it is generally yellow - green (λ_{max}: ~560 nm).[159-162] However, the emission wavelength released by luciferases from other luminescent insects might vary, sometimes even within a single species,[163] as with the different luciferases isolated from the Caribbean click beetle *Pyrophorus plagiophthalamus*, which emit light ranging from green (λ_{max}: ~545 nm) to orange (λ_{max}: ~590 nm).[164] In contrast, coelenterazine-dependent luciferases isolated from marine organisms, such as Renilla luciferase (RLuc, 36 kDa) derived from sea pansy *Renilla reniformis,*[165] all release blue light (λ_{max}: ~460-480 nm) without the need for additional ATP or Mg^{2+}.[157,166]

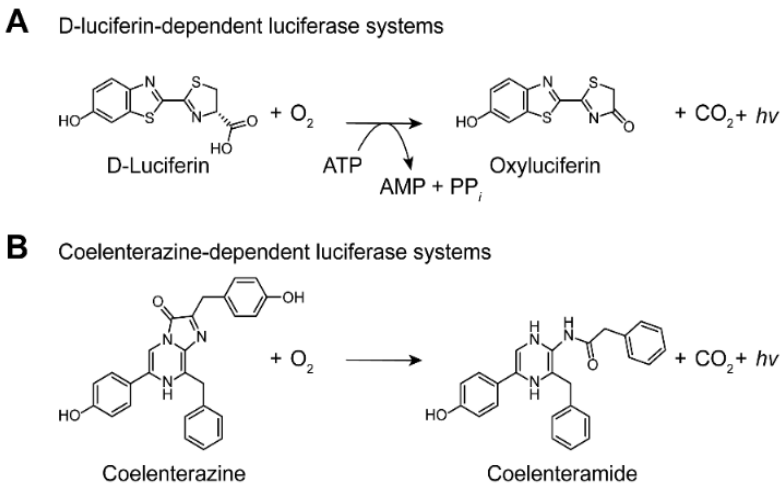

Figure 1.4. Luciferase reactions of luciferases commonly used in GPCR research. Both luciferase types require oxygen to catalyze the oxidative decarboxylation of their substrates A) D-luciferin and B) coelenterazine resulting in the release of light (*hv*). In contrast to coelenterarzine converting luciferases, the oxidation of D-luciferin requires ATP.

However, the emission of green light has also observed in marine organisms, such as in the jellyfish *Aquorea victoria*, which is due to a phenomenon termed bioluminescence resonance energy transfer (BRET).[167] This phenomenon is based on the same principles as Förster resonance energy transfer (FRET), which was originally described by Theodor Förster and is a physical process in which a fluorescent (or bioluminescent) donor transfers energy to a fluorescent acceptor.[168] RET efficiency depends on the donor's emission spectrum overlapping with the acceptor's excitation spectrum, the donor and acceptor being less than 100 Å apart, and their dipole moments having the correct relative orientation (e.g., the highest RET is observed with parallel dipole orientation).[169] In jellyfish *A. victoria*, BRET occurs between the bioluminescent photoprotein aequorin, which contains an oxygen-activated coelenterazine, and the green fluorescent protein (GFP)[170] shifting the emission wavelength of coelenterazine to green light (λ_{max}: ~510 nm).[166-167]

In drug discovery, BRET- and FRET-based assays have been successfully used to study ligand binding to GPCRs, associated conformational changes of the receptor itself, interaction with signal transducers, and subsequent formation of second messengers. Overall, these assays have benefited from the development of brighter luciferases with improved stability (e.g., ELuc[171]) and

smaller size (e.g., NanoLuc[172]), as well as monomeric GFP color variants with faster maturation in cells (e.g., YFP[173] and mVenus[174-175]). While FRET-based assays have higher temporal resolution due to the overall high light intensities, BRET-based assays offer a higher signal-to-noise ratio because no external light needs to be introduced into the system, resulting in higher assay sensitivity. In particular, the higher light intensity compared to D-luciferin-converting luciferases has made coelenterazine-dependent luciferases powerful analytical tools for BRET-based detection of PPI (Figure 1.5).[152,167]

1.2.2.1.2. Split-Luciferase Complementation

Typically, RET requires the addition of two bulky labels in the ~30-60 kDa range to the proteins of interest, which may present a steric hindrance to PPI.[176] Therefore, the concept of protein complementation assay (PCA) has become an attractive alternative for designing functional assays in drug discovery (Figure 1.5).[177] The principle of this technique is based on the dissection of a reporter protein that restores catalytic function unless these fragments are separated.[178-179] Principally, PCAs have been designed on the basis of fluorescent and bioluminescent proteins. Nevertheless, split-proteins derived from GFP[180] and its color variants[181] suffer from irreversible complementation and long maturation time for folding and reconstitution of the fluorophore,[182-183] making them poorly suited for the elucidation of rapid or transient processes. Although the initial approach for generating a split-luciferase involved an intein-assisted and thus irreversible reaction,[184] the split-luciferases used today are fully reversible.[185] Furthermore, compared to split-FPs, reconstituted luciferases provide a higher degree to assay sensitivity due to the combination of rapid maturation and independence from external light excitation.[177,185]

Split-luciferase complementation (SLC) was first applied to FLuc by dissection into two distinct domains of different size,[184] which surround the active site as identified from its three-dimensional structure.[186-187] Initially, this resulted in a substantial loss of intensity,[184] but the incremental truncation of the N- and C-terminal domains resulting in an overlap of 18 amino acids significantly improved the intensity of split-FLuc, most likely due to better reconstitution of the active site.[188] While the generation of split-luciferases derived from D-luciferin-dependent luciferases has provided multicolor systems, such as split-ELuc (λ_{max}: ~540 nm),[171,189] or split-CBR (λ_{max}: ~610 nm),[190] generation of split-luciferases from coelenterazine-dependent systems, such as split-RLuc,[191] has resulted in particularly bright and small reporters.[177,185]

One of the most recently developed luciferases in molecular biology, is NanoLuc,[172] which has been developed from the native heterotetrameric *Oplophorus* luciferase (OLuc) of the deep-sea shrimp *Oplophorus gracilirostris*.[192] Its dissection gave rise to split-NanoLuc that has become a powerful tool for the detection of PPI (Figure 1.5B),[193] particularly due to its small size of 19 kDa and more than 150-fold higher brightness compared to FLuc or RLuc.[177] Of note, different C-terminal fragments consisting of only 11 amino acids are available with either low (K_d = 190 µM), moderate (K_d = 0.9 µM) or high (K_d = 0.7 nM) affinity for the 159 amino acid sized N-terminal fragment.[193]

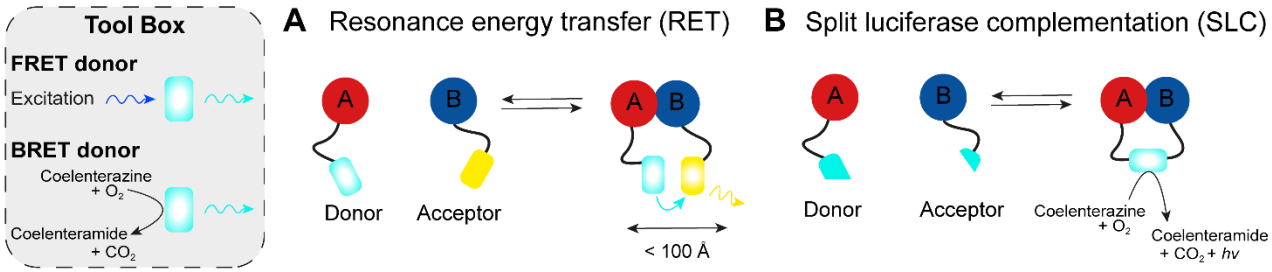

Figure 1.5. Schematic principle of methods for detection of protein – protein interactions commonly used in GPCR research. A) Resonance energy transfer (RET) is facilitated by overlapping emission and excitation spectra of a fluorescent or bioluminescent donor (FRET or BRET donor, bright blue) and a fluorescent acceptor (yellow). When the proteins of interest (protein A and protein B) allow a distance <100 Å between RET labels during the interaction, the donor can excite the acceptor. B) Instead, split-luciferase fragments can be attached to the proteins of interest to detect split-luciferase complementation (SLC). After protein - protein interaction, the luciferase reconstitutes a functional enzyme that releases bioluminescence.

1.2.2.2. Classical Interactions within G protein Activation Cycle

1.2.2.2.1. Determination of G protein Activation

At the turn of the millennium, a milestone in the field of optical sensor development has been achieved by Janetopoulos et al., who were the first to measure changes in FRET in response to G protein activation in *Dictyostelium*.[194] Since then, the principle of the sensor, which is the attachment of RET labels to Gα and Gβγ subunits and thus monitoring the dissociation of Gβγ upon G protein activation, has been applied to nearly all G protein isoforms expressed in humans (Figure 1.6A).[195] For maintaining functional interaction with Gα, possible labeling sites at the βγ dimer comprise the N-termini of either Gβ or Gγ as well as, interestingly, the C-terminus Gγ.[196-198] Nevertheless, attaching a label to Gγ would disturb effector coupling.[196] Labeling of Gα has been more difficult because modification of the N-terminus would remove Gα from the plasma membrane,[33] whereas labeling of the C-terminus, which constitutes the main contact surface of Gα to GPCRs, would prevent binding to the receptor.[176] Therefore, suitable labeling positions had to be identified for each α subunit that are typically within the loop regions of the α-helical domain.[194-196,199-200]

At the same time, GPCR activation sensors have been developed by attaching RET labels to the C-terminus and the intracellular ends of TM6, thereby monitoring agonist-induced outward movement of TM6.[201-202] Compared with these GPCR activation sensors, G protein activation occurs approximately 10 times slower than GPCR activation and has been observed in the range of 500 ms.[176] In addition, the use of fluorescently labeled G protein subunits has provided important insight to the spatiotemporal dynamics of G protein localization at the plasma membrane and has visualized G protein trafficking to intracellular compartments,[199,203] which e.g., is enabled by de-palmitoylation upon activation.[204-205] Consistent with the classical opinion that a single receptor can activate multiple G proteins (receptor reserve[206]), sensor activation mediated by a partial agonist has been significantly greater at the G protein level than at the receptor level.[207] An important consideration when using G protein activation sensors is that an unbalanced expression of G protein components can lead to decreased sensitivity of the assay, as the underlying reaction is highly dependent on stoichiometry.[208] In practical applications, this means that all G protein components, regardless of labeling sites, need to be co-transfected, preferably encoded as unimolecular sensor on a single plasmid.[209-211]

1.2.2.2.2. Determination of GPCR – G Protein Interaction

An alternative to measuring G protein activation is the direct assessment of specific GPCR – G protein interaction by placing one RET label at the C-terminus of the receptor and the other at the G protein (Gα or Gγ) (Figure 1.6B).[212-214] Interestingly, FRET sensors have shown that this interaction occurs within the same timeframe as GPCR activation (~50 ms) suggesting that GPCR activation and G protein engagement precede G protein activation.[213] Compared with RET based techniques, split-luciferase complementation (SLC) has been far less popular for detecting GPCR - G protein interactions,[215] largely because split-luciferases engineered from naturally occurring luciferases, such as FLuc or *Gaussia* luciferase (GLuc) from copepod *Gaussia princeps*[216], provide some affinity and were not very bright.[217-218] More recently, the introduction of brighter split-NanoLuc with low affinity fragments has changed the situation.[219] As with RET-based sensors, labels were conjugated to the receptor C-terminus and Gα , the insertion sites of which had to be selected individually for each isoform.[215,220]

Similar concepts have been used to study the interaction of GPCRs with other signal transducers, such as β-arrestins or GRKs, in response to agonists.[221-225] Since more than 800 GPCRs elicit specific cellular responses by interacting with only few signal transducers, structural biologists are particularly interested in determining which receptor conformations are decisive for obtaining specific coupling patterns.[17,226-227] The question of whether these receptor conformations can be stabilized by specific ligands or even modulated by biased ligands represents a smooth transition to drug discovery.[120,228]

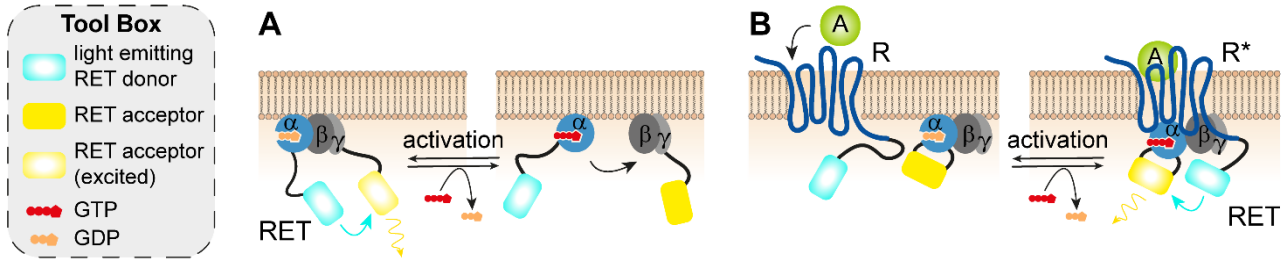

Figure 1.6. Resonance energy transfer (RET)-based G protein biosensors. A) Heterotrimeric G protein activation leads to the dissociation of Gβγ and thus a decrease in RET between donor (light blue) and acceptor (yellow) attached to Gα and Gβγ. B) Specific GPCR – G protein interaction upon agonist (A)-mediated receptor activation (R*) is revealed by RET between the donor attached to the receptor C-terminus and acceptor fused to Gα. Adapted from Galés et al. (2006).[197]

1.2.2.3. Novel Assay Platforms at the G protein Level

1.2.2.3.1. Approaches to Reduce Labels at the Heterotrimeric G protein

A concern with classical RET-based G protein activation sensors is the use of relatively large donor and acceptor proteins (~30-60 kDa), as these could interfere with native PPI due to steric hindrance.[176] Therefore, researchers have sought ways to reduce bulky labels on native G protein components.[229] Initial approaches included RET sensors that detect G protein activation indirectly through the release of the Gβγ dimer. For this purpose, RET labels were attached to Gβγ and masGRK3ct constructed from the Gβγ-binding C-terminal peptide of GRK3 and the plasma membrane marker CAAX (Figure 1.7A).[208,230-231] Noteworthily, in addition to the plasma membrane marker CAAX, several compartment specific markers have become available including endosome marker FYVE, endoplasmatic reticulum marker PTP1B, mitochondrial marker Bcl-xL and Golgi marker giantin that particularly serve for studying GPCR trafficking.[222,232-233]

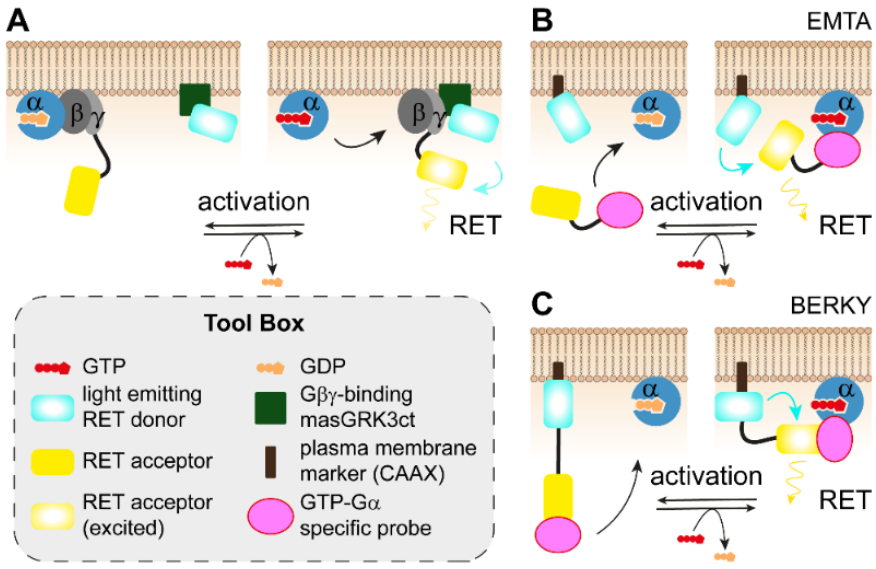

Figure 1.7. Schematic illustration of novel biosensors at the G protein level. A) RET labels attached to Gβγ and engineered Gβγ-binding, membrane associated C-terminal peptide of GRK3 (masGRK3ct) allow for indirect quantification of G protein activation. B) Effector membrane translocalization assays (EMTA) and C) unimolecular BRET sensor with flexible ER/K-linker and YFP (BERKY) allow for detecting nucleotide exchange on Gα upon G protein activation using RET labels fused to GTP-Gα specific effectors and a plasma membrane marker (CAAX). Adapted from Avet et al. (2020)[234] and Maziarz et al. (2020).[235]

To overcome the limitation that RET-based G protein activation sensors typically detect conformational changes at the heterotrimeric G protein upon activation, rather than measuring the exchange of GDP for GTP, researchers lately have focused on the use of effectors that specifically recognize GTP-bound Gα. Instead of labeling heterotrimeric G protein constituents, Wright et al. and Avet et al. have provided effector membrane translocalization assays (EMTA) that determine G protein activation by BRET between RLucII conjugated G protein-specific effectors (e.g. Rap1 GTPase-activating protein 1 for Gi/o and p63 Rho guanine nucleotide exchange factor for Gq/11) and rGFP attached to the plasma membrane (rGFP-CAAX) (Figure 1.7B).[233-234] Based on the same concept, Maziarz et al. have developed a unimolecular BRET sensor with flexible ER/K-linker and YFP (BERKY).[235] This sensor molecule consists of a BRET donor bound to the plasma membrane and separated from the BRET acceptor by a flexible ER/K linker. The effectors specifically recognizing GTP-bound Gα have been fused to the N-terminus of this sensor, which can bend toward the membrane upon activation of the G protein, thus enabling BRET (Figure 1.7C).[235]

1.2.2.3.2. GPCR Conformation-Specific Probes

Overall, agonist-mediated activation of a GPCR is the key process for triggering a G protein-dependent signaling cascade. Based on X-ray or cryo-EM structures, the understanding of the underlying molecular mechanism is emerging,[15] particularly with respect to the conformational differences induced by ligands that either fully or partially activate signaling pathways — sometimes even in a functionally selective manner.[236-237] The development of GPCR conformation-specific probes has significantly contributed to the resolution of active GPCR structures by rigidizing the otherwise highly flexible receptor complexes.[73,238-249]

Nanobodies (Nb), which represent the antigen-binding domain of heavy-chain only camelid antibodies, have been developed for stabilizing different GPCR conformations, such as the active (Nb80[250-251]) and inactive (Nb60[252-253]) β_2-adrenoceptor (β_2AR) states.[238,254] In a more natural approach, mini-G proteins were designed based on the GTPase domain of Gαs.[255-256] Specifically, several genetic modifications, including removal of the helical domain, truncation of the N-terminus, thus removing the Gβγ binding site and ability to bind to the plasma membrane, as well as the introduction of additional point mutations to increase in-vitro stability, gave birth to the first mini-G protein, mGs.[255] Analogously, the strategy could be applied to Gα12 yielding mG12 but was not suitable for proteins of the Gi/o and Gq/11 families.[257] Instead, chimeric G proteins[258-259] were generated by replacing the α5 helix of mGs with that of $G\alpha i_1$ and Gαq resulting in mGsi and mGsq.[257] A scheme of nanobody and mini-G protein binding to GPCRs is given in Figure 1.8.

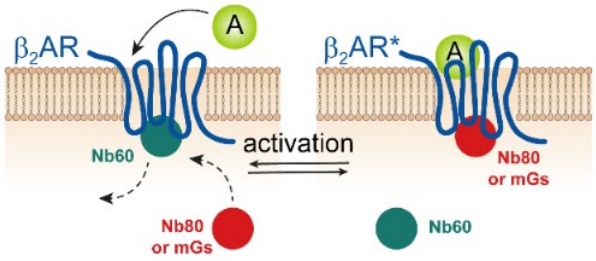

Figure 1.8. Schematic principle of nanobody and mini-G protein binding to the β_2-adrenoceptor (β_2AR). The inactive β_2AR state is stabilized by Nb60, whereas activation of the receptor (β_2AR*) by an agonist (A) allows for binding to either Nb80 or mGs. Adapted from Jullié et al. (2022).[256]

When conjugated to labels for RET or SLC, both nanobodies and mini-G proteins can be expressed as biosensors in living cells to monitor ligand-mediated conformational changes of GPCRs in real-time.[232,260-263] However, in terms of developing a universally applicable sensor suite for GPCRs, the use of mini-G proteins seems more favorable for the following reasons: On one hand, the nanobody manufacturing process typically involves time-consuming and costly steps, including immunization of camelids, such as llamas, the isolation from blood, creation of cDNA libraries, and subsequent screening for positive clones.[254] Therefore, nanobodies are available only for a limited number of GPCRs,[151] including β_2-adrenoceptor,[250-251,264] muscarininc M_2 receptor,[265] opioid receptors (μ-OR, κ-OR and δ-OR),[266-268] the viral chemokine receptor US28,[269] and angiotensin AT_1 receptor.[270] On the other hand, despite data still being sparse, there is strong evidence that some nanobodies might recognize GPCR conformations that are divergent from those relevant for G protein binding, not least by three-dimensional structures of κ-OR or μ-OR in complex with Nb39 or heterotrimeric Gi.[266,268,271] Expressed as biosensors in living cells, Nb39 and Nb33 recognized different opioid receptor conformations than mGsi, potentially in a GRK2-dependent manner in the case of Nb33.[272-273]

By contrast, mini-G proteins acquire GPCR coupling specificity due to the α5 helix and therefore shall recognize GPCR conformations relevant to G protein binding.[232,257] Since mini-G proteins are expected to be universally applicable to GPCRs, they represent valuable tools for the functional characterization in drug discovery.[274]

1.3. Objective and Aim of the Thesis

In GPCR research, there is great interest in developing high-affinity and selective ligands as pharmacological tools and ultimately as drugs.[5-6,275] In addition, the idea that biased agonists could improve drug therapy by "not activating" unfavorable signaling pathways to reduce associated adverse effects has led to new paradigms in drug discovery.[119,126,276] Traditionally, biased ligands have been evaluated based on their ability to discriminate for G protein or β-arrestin signaling pathways.[119,277] However, there is growing research interest in how conformational changes in GPCRs enable signaling bias with respect to G protein families or rather Gα isoforms.[17,121-123,226] At the developmental stage, there is thus a reasonable need for appropriate cellular assays that allow accurate determination of ligand potency and efficacy and bias analysis. Since intracellular signaling is subject to signal amplification and even crosstalk of different signaling pathways, proximal assays seem to be particularly well suited for functional characterization of ligands, especially with respect to ligand modality including complete, partial, and inverse agonism or antagonism.[132,142]

Previously, the [^{35}S]GTPγS binding assay was commonly used at the institute for the functional characterization of prospective ligands. Despite its usefulness for quantifying the exchange of GDP for GTP during the G protein activation process and even GPCR – G protein stoichiometry, the assay has some general drawbacks, including safety precautions and increasing costs for waste disposal. In addition, the limited number of suppliers causes high acquisition costs for radiolabeled GTP analogs. Therefore, it was even more serious that we were repeatedly confronted with insufficient quality of the purchased [^{35}S]GTPγS batches containing less than 21% of the intact molecule (Figure 1.9).

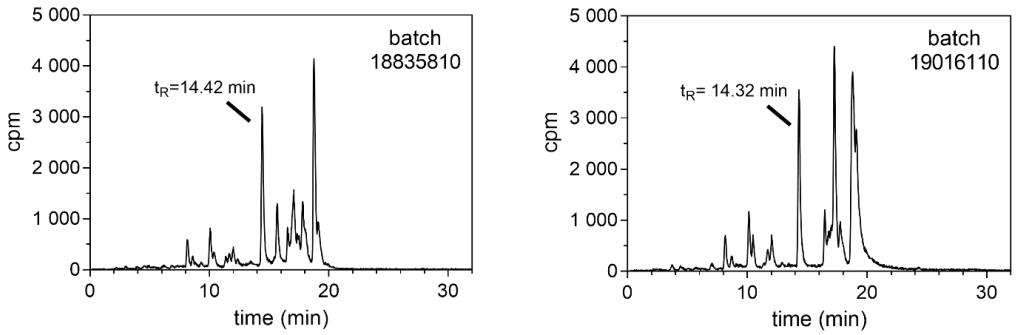

Figure 1.9. Radiochromatograms of [^{35}S]GTPγS batches 18835810 (S22) and 19016110 (S23). Peaks at t_R= 14.42 min or rather t_R= 14.32 min in the radio-chromatograms were identified as intact [^{35}S]GTPγS by spiking with "cold" GTPγS (UV 260 nm, not shown). [^{35}S]GTPγS peaks represent only 20.89% or rather 14.6% of the total area. HPLC system used: Waters pump 510, Waters Pump Control Modul; Waters UV-Detector 486; Radiometric Flow-1 beta Series A-500 detector; column: Phenomenex Luna C18 (150 x 4.6 mm, 3 µm); mobile phase: A: acetonitrile, B: 20 mM NH_4OAc/10 mM tetrapentylammoniumbromide, pH = 5; gradient: 0 min: A/B 20:80, 15 min: A/B 60:40, 25 min: A/B 95:5, 30 min: A/B 95:5, 32 min: A/B 20:80; flow: 0.8 mL/min (HPLC), 4 mL/min (liquid scintillator (Rotiscint eco plus, Carl Roth)); injection volume: 100 µL.

Therefore, the aim of this thesis was the development and characterization of a modern G protein-dependent assay platform with proximal assay readout applicable to the GPCRs of interest at the institute. This new assay platform should overcome some general limitations of the [^{35}S]GTPγS binding assay. Due to low membrane permeability of nucleotides, the assay performance was greatly limited to membrane or homogenate preparations instead of using intact cells,[142-143] resulting in the destruction of the native cellular environment and thus accessory proteins, such as GAPs accelerating GTP hydrolysis,[44] as well as other strictly necessary components, such as GDP and sodium and magnesium ions.[278] In practical terms, a mostly elaborate optimization of cellular system (e.g., using fusion proteins[279-280] and assay buffer components[281-282]) is mandatory to obtain optimal assay signals. In addition, the filtration step to separate [^{35}S]GTPγS bound to Gα from unbound prevented assay homogeneity and thus the possibility of real-time measurements.[143] Although the use of microspheres for scintillation proximity assays (SPAs)[283-284] or fluorescently labeled (N-methyl-3'O-anthanilate (MANT)[285], BODIPY[286], europium chelates[284,287]) GTP analogs would enable such real time character, these alternatives seemed unfavorable due to costs, the (sometimes) ineffective G protein activation and poor assay signals.[143,288]

In 2017, miniaturized G-proteins (mini-G-proteins) have been reported.[257] Although originally designed for crystallization purposes by stabilizing active GPCR conformations,[255] mini-G proteins can also be used to monitor agonist-mediated GPCR activation in living cells when fused with corresponding genetically encoded luminescent and fluorescent proteins.[232] Compared with the commonly used BRET-based G protein activation sensors, the mini-G proteins in combination with SLC seemed to be particularly advantageous for weakly expressed and constitutively active GPCRs, such as H_4R. The cytosolic nature of the mini-G proteins (instead of membrane-bound G proteins in proximity to the receptor) combined with the low catalytic activity of the split-luciferase fragments, unless complemented, significantly reduces assay background signals, resulting in generally higher signal amplitudes.

Methodologically, the present work involves the fusion of split-luciferase fragments derived from the particularly small and bright luciferase NanoLuc® (19 kDa; λ_{max}: ~ 460 nm) to various GPCRs of interest at the institute and the mini-G proteins mGs, mGsi, and mGsq, their stable or transient expression in HEK293T cells, and the application of computational Gaussian accelerated molecular dynamics (GaMD) simulations. Overall, the focus has been on assay quality (Z' factor, signal-to-background), the pharmacological characterization of standard ligands, and the exploration of GPCR coupling profiles. In addition, the usefulness of mini-G protein recruitment to endogenously expressed receptors was assessed for mGs and $\beta_{1,2}$AR after CRISPR/Cas9-mediated genome editing.

1.4. References

1. Venter, J. C., Adams, M. D., Myers, E. W., Li, P. W., Mural, R. J., Sutton, G. G., Smith, H. O., Yandell, M., Evans, C. A., Holt, R. A., et al., The sequence of the human genome. *Science* **2001,** *291* (5507), 1304-1351, doi: 10.1126/science.1058040.
2. Lander, E. S., Linton, L. M., Birren, B., Nusbaum, C., Zody, M. C., Baldwin, J., Devon, K., Dewar, K., Doyle, M., FitzHugh, W., et al., Initial sequencing and analysis of the human genome. *Nature* **2001,** *409* (6822), 860-921, doi: 10.1038/35057062.
3. Goricanec, D., Stehle, R., Egloff, P., Grigoriu, S., Pluckthun, A., Wagner, G. & Hagn, F., Conformational dynamics of a G-protein α subunit is tightly regulated by nucleotide binding. *Proc Natl Acad Sci U S A* **2016,** *113* (26), E3629-3638, doi: 10.1073/pnas.1604125113.
4. Katritch, V., Cherezov, V. & Stevens, R. C., Structure-function of the G protein-coupled receptor superfamily. *Annu Rev Pharmacol Toxicol* **2013,** *53*, 531-556, doi: 10.1146/annurev-pharmtox-032112-135923.
5. Wacker, D., Stevens, R. C. & Roth, B. L., How ligands illuminate GPCR molecular pharmacology. *Cell* **2017,** *170* (3), 414-427, doi: 10.1016/j.cell.2017.07.009.
6. Hauser, A. S., Attwood, M. M., Rask-Andersen, M., Schioth, H. B. & Gloriam, D. E., Trends in GPCR drug discovery: New agents, targets and indications. *Nat Rev Drug Discov* **2017,** *16* (12), 829-842, doi: 10.1038/nrd.2017.178.
7. Fredriksson, R., Lagerström, M. C., Lundin, L. G. & Schiöth, H. B., The G-protein-coupled receptors in the human genome form five main families. Phylogenetic analysis, paralogon groups, and fingerprints. *Mol Pharmacol* **2003,** *63* (6), 1256-1272, doi: 10.1124/mol.63.6.1256.
8. Venkatakrishnan, A. J., Deupi, X., Lebon, G., Tate, C. G., Schertler, G. F. & Babu, M. M., Molecular signatures of G-protein-coupled receptors. *Nature* **2013,** *494* (7436), 185-194, doi: 10.1038/nature11896.
9. Katritch, V., Cherezov, V. & Stevens, R. C., Diversity and modularity of G protein-coupled receptor structures. *Trends Pharmacol Sci* **2012,** *33* (1), 17-27, doi: 10.1016/j.tips.2011.09.003.
10. Rosenbaum, D. M., Rasmussen, S. G. & Kobilka, B. K., The structure and function of G-protein-coupled receptors. *Nature* **2009,** *459* (7245), 356-363, doi: 10.1038/nature08144.
11. Hébert, T. E. & Bouvier, M., Structural and functional aspects of G protein-coupled receptor oligomerization. *Biochemistry and cell biology = Biochimie et biologie cellulaire* **1998,** *76* (1), 1-11, doi: 10.1139/bcb-76-1-1.
12. Overton, M. C. & Blumer, K. J., G-protein-coupled receptors function as oligomers in vivo. *Current biology : CB* **2000,** *10* (6), 341-344, doi: 10.1016/s0960-9822(00)00386-9.
13. Milligan, G., Ramsay, D., Pascal, G. & Carrillo, J. J., GPCR dimerisation. *Life sciences* **2003,** *74* (2-3), 181-188, doi: 10.1016/j.lfs.2003.09.005.
14. Lohse, M. J., Dimerization in GPCR mobility and signaling. *Current opinion in pharmacology* **2010,** *10* (1), 53-58, doi: 10.1016/j.coph.2009.10.007.
15. Weis, W. I. & Kobilka, B. K., The molecular basis of G protein-coupled receptor activation. *Annu Rev Biochem* **2018,** *87*, 897-919, doi: 10.1146/annurev-biochem-060614-033910.
16. Deluigi, M., Klipp, A., Klenk, C., Merklinger, L., Eberle, S. A., Morstein, L., Heine, P., Mittl, P. R. E., Ernst, P., Kamenecka, T. M., et al., Complexes of the neurotensin receptor 1 with small-molecule ligands reveal structural determinants of full, partial, and inverse agonism. *Sci Adv* **2021,** *7* (5), eabe5504, doi: doi:10.1126/sciadv.abe5504.

17. Fleetwood, O., Carlsson, J. & Delemotte, L., Identification of ligand-specific G protein-coupled receptor states and prediction of downstream efficacy via data-driven modeling. *Elife* **2021,** *10*, doi: 10.7554/eLife.60715.

18. Rasmussen, S. G., DeVree, B. T., Zou, Y., Kruse, A. C., Chung, K. Y., Kobilka, T. S., Thian, F. S., Chae, P. S., Pardon, E., Calinski, D., et al., Crystal structure of the β2 adrenergic receptor–Gs protein complex. *Nature* **2011,** *477* (7366), 549-555, doi: 10.1038/nature10361.

19. Kang, Y., Zhou, X. E., Gao, X., He, Y., Liu, W., Ishchenko, A., Barty, A., White, T. A., Yefanov, O., Han, G. W., et al., Crystal structure of rhodopsin bound to arrestin by femtosecond X-ray laser. *Nature* **2015,** *523* (7562), 561-567, doi: 10.1038/nature14656.

20. Szczepek, M., Beyrière, F., Hofmann, K. P., Elgeti, M., Kazmin, R., Rose, A., Bartl, F. J., von Stetten, D., Heck, M., Sommer, M. E., et al., Crystal structure of a common GPCR-binding interface for G protein and arrestin. *Nat Commun* **2014,** *5*, 4801, doi: 10.1038/ncomms5801.

21. Janz, J. M. & Farrens, D. L., Rhodopsin activation exposes a key hydrophobic binding site for the transducin α-subunit C terminus. *J Biol Chem* **2004,** *279* (28), 29767-29773, doi: 10.1074/jbc.M402567200.

22. Kenakin, T., Ligand-selective receptor conformations revisited: The promise and the problem. *Trends Pharmacol Sci* **2003,** *24* (7), 346-354, doi: 10.1016/s0165-6147(03)00167-6.

23. Perez, D. M. & Karnik, S. S., Multiple signaling states of G-protein-coupled receptors. *Pharmacol Rev* **2005,** *57* (2), 147-161, doi: 10.1124/pr.57.2.2.

24. Violin, J. D. & Lefkowitz, R. J., β-arrestin-biased ligands at seven-transmembrane receptors. *Trends Pharmacol Sci* **2007,** *28* (8), 416-422, doi: 10.1016/j.tips.2007.06.006.

25. Woo, A. Y., Wang, T. B., Zeng, X., Zhu, W., Abernethy, D. R., Wainer, I. W. & Xiao, R. P., Stereochemistry of an agonist determines coupling preference of β2-adrenoceptor to different G proteins in cardiomyocytes. *Mol Pharmacol* **2009,** *75* (1), 158-165, doi: 10.1124/mol.108.051078.

26. Gilman, A. G., G proteins: transducers of receptor-generated signals. *Annu Rev Biochem* **1987,** *56*, 615-649, doi: 10.1146/annurev.bi.56.070187.003151.

27. Oldham, W. M. & Hamm, H. E., Heterotrimeric G protein activation by G-protein-coupled receptors. *Nat Rev Mol Cell Biol* **2008,** *9* (1), 60-71, doi: 10.1038/nrm2299.

28. Milligan, G. & Kostenis, E., Heterotrimeric G-proteins: A short history. *Br J Pharmacol* **2006,** *147 Suppl 1*, S46-55, doi: 10.1038/sj.bjp.0706405.

29. Syrovatkina, V., Alegre, K. O., Dey, R. & Huang, X. Y., Regulation, signaling, and physiological functions of G proteins. *J Mol Biol* **2016,** *428* (19), 3850-3868, doi: 10.1016/j.jmb.2016.08.002.

30. Cabrera-Vera, T. M., Vanhauwe, J., Thomas, T. O., Medkova, M., Preininger, A., Mazzoni, M. R. & Hamm, H. E., Insights into G protein structure, function, and regulation. *Endocr Rev* **2003,** *24* (6), 765-781, doi: 10.1210/er.2000-0026.

31. Sondek, J., Bohm, A., Lambright, D. G., Hamm, H. E. & Sigler, P. B., Crystal structure of a G-protein $\beta\ \gamma$ dimer at 2.1A resolution. *Nature* **1996,** *379* (6563), 369-374, doi: 10.1038/379369a0.

32. Clapham, D. E. & Neer, E. J., G protein $\beta\ \gamma$ subunits. *Annu Rev Pharmacol Toxicol* **1997,** *37*, 167-203, doi: 10.1146/annurev.pharmtox.37.1.167.

33. Vögler, O., Barcelo, J. M., Ribas, C. & Escriba, P. V., Membrane interactions of G proteins and other related proteins. *Biochim Biophys Acta* **2008,** *1778* (7-8), 1640-1652, doi: 10.1016/j.bbamem.2008.03.008.

34. Ferguson, K. M., Higashijima, T., Smigel, M. D. & Gilman, A. G., The influence of bound GDP on the kinetics of guanine nucleotide binding to G proteins. *J Biol Chem* **1986,** *261* (16), 7393-7399, doi: 10.1016/S0021-9258(17)38404-1.

35. Gilman, A. G., G proteins and dual control of adenylate cyclase. *Cell* **1984,** *36* (3), 577-579, doi: 10.1016/0092-8674(84)90336-2.

36. Bourne, H. R., Sanders, D. A. & McCormick, F., The GTPase superfamily: conserved structure and molecular mechanism. *Nature* **1991,** *349* (6305), 117-127, doi: 10.1038/349117a0.

37. Medkova, M., Preininger, A. M., Yu, N. J., Hubbell, W. L. & Hamm, H. E., Conformational changes in the amino-terminal helix of the G protein αi1 following dissociation from G$\beta\gamma$ subunit and activation. *Biochemistry* **2002,** *41* (31), 9962-9972, doi: 10.1021/bi0255726.

38. Martemyanov, K. A., Mechanisms of G$\beta\gamma$ release upon GPCR activation. *Trends Biochem Sci* **2021,** *46* (9), 703-704, doi: 10.1016/j.tibs.2021.05.002.

39. Wettschureck, N. & Offermanns, S., Mammalian G proteins and their cell type specific functions. *Physiol Rev* **2005,** *85* (4), 1159-1204, doi: 10.1152/physrev.00003.2005.

40. Khan, S. M., Sleno, R., Gora, S., Zylbergold, P., Laverdure, J. P., Labbe, J. C., Miller, G. J. & Hebert, T. E., The expanding roles of G$\beta\gamma$ subunits in G protein-coupled receptor signaling and drug action. *Pharmacol Rev* **2013,** *65* (2), 545-577, doi: 10.1124/pr.111.005603.

41. Spiegel, A. M., Signal transduction by guanine nucleotide binding proteins. *Mol Cell Endocrinol* **1987,** *49* (1), 1-16, doi: 10.1016/0303-7207(87)90058-x.

42. Siderovski, D. P. & Willard, F. S., The GAPs, GEFs, and GDIs of heterotrimeric G-protein alpha subunits. *Int J Biol Sci* **2005,** *1* (2), 51-66, doi: 10.7150/ijbs.1.51.

43. Ross, E. M., G Protein-coupled receptors: Multi-turnover GDP/GTP exchange catalysis on heterotrimeric G proteins. *Cell Logist* **2014,** *4*, e29391-e29391, doi: 10.4161/cl.29391.

44. Ross, E. M. & Wilkie, T. M., GTPase-activating proteins for heterotrimeric G proteins: regulators of G protein signaling (RGS) and RGS-like proteins. *Annu Rev Biochem* **2000,** *69*, 795-827, doi: 10.1146/annurev.biochem.69.1.795.

45. Berman, D. M., Wilkie, T. M. & Gilman, A. G., GAIP and RGS4 are GTPase-activating proteins for the Gi subfamily of G protein α subunits. *Cell* **1996,** *86* (3), 445-452, doi: 10.1016/s0092-8674(00)80117-8.

46. Watson, N., Linder, M. E., Druey, K. M., Kehrl, J. H. & Blumer, K. J., RGS family members: GTPase-activating proteins for heterotrimeric G-protein α-subunits. *Nature* **1996,** *383* (6596), 172-175, doi: 10.1038/383172a0.

47. Hepler, J. R., Berman, D. M., Gilman, A. G. & Kozasa, T., RGS4 and GAIP are GTPase-activating proteins for Gq α and block activation of phospholipase C β by γ-thio-GTP-Gq α. *Proc Natl Acad Sci U S A* **1997,** *94* (2), 428-432, doi: 10.1073/pnas.94.2.428.

48. Ross, E. M., Coordinating speed and amplitude in G-protein signaling. *Current biology : CB* **2008,** *18* (17), R777-R783, doi: 10.1016/j.cub.2008.07.035.

49. Sato, M., Blumer, J. B., Simon, V. & Lanier, S. M., Accessory proteins for G proteins: Partners in signaling. *Annu Rev Pharmacol Toxicol* **2006,** *46*, 151-187, doi: 10.1146/annurev.pharmtox.46.120604.141115.

50. Willard, F. S., Kimple, R. J. & Siderovski, D. P., Return of the GDI: the GoLoco motif in cell division. *Annu Rev Biochem* **2004,** *73*, 925-951, doi: 10.1146/annurev.biochem.73.011303.073756.

51. Downes, G. B. & Gautam, N., The G protein subunit gene families. *Genomics* **1999,** *62* (3), 544-552, doi: 10.1006/geno.1999.5992.

52. Simon, M. I., Strathmann, M. P. & Gautam, N., Diversity of G proteins in signal transduction. *Science* **1991,** *252* (5007), 802-808, doi: 10.1126/science.1902986.

53. Simonds, W. F., G protein regulation of adenylate cyclase. *Trends Pharmacol Sci* **1999,** *20* (2), 66-73, doi: 10.1016/s0165-6147(99)01307-3.

54. Sadana, R. & Dessauer, C. W., Physiological roles for G protein-regulated adenylyl cyclase isoforms: Insights from knockout and overexpression studies. *Neuro-Signals* **2009,** *17* (1), 5-22, doi: 10.1159/000166277.

55. Hepler, J. R. & Gilman, A. G., G proteins. *Trends Biochem Sci* **1992,** *17* (10), 383-387, doi: 10.1016/0968-0004(92)90005-t.

56. Sunahara, R. K. & Insel, P. A., The molecular pharmacology of G protein signaling then and now: A tribute to Alfred G. Gilman. *Mol Pharmacol* **2016,** *89* (5), 585-592, doi: 10.1124/mol.116.104216.

57. Sutherland, E. W., On the biological role of cyclic AMP. *JAMA* **1970,** *214* (7), 1281-1288.

58. Sassone-Corsi, P., The cyclic AMP pathway. *Cold Spring Harb Perspect Biol* **2012,** *4* (12), a011148, doi: 10.1101/cshperspect.a011148.

59. Lee, C. H., Park, D., Wu, D., Rhee, S. G. & Simon, M. I., Members of the Gq α subunit gene family activate phospholipase C β isozymes. *J Biol Chem* **1992,** *267* (23), 16044-16047.

60. Park, D., Jhon, D. Y., Lee, C. W., Lee, K. H. & Rhee, S. G., Activation of phospholipase C isozymes by G protein β γ subunits. *J Biol Chem* **1993,** *268* (7), 4573-4576.

61. Berridge, M. J., Inositol trisphosphate and diacylglycerol: Two interacting second messengers. *Annu Rev Biochem* **1987,** *56*, 159-193, doi: 10.1146/annurev.bi.56.070187.001111.

62. Kadamur, G. & Ross, E. M., Mammalian phospholipase C. *Annual review of physiology* **2013,** *75*, 127-154, doi: 10.1146/annurev-physiol-030212-183750.

63. Black, A. & Black, J., Protein kinase C signaling and cell cycle regulation. *Front Immunol* **2013,** *3*, doi: 10.3389/fimmu.2012.00423.

64. Francis, S. H., Busch, J. L., Corbin, J. D. & Sibley, D., cGMP-dependent protein kinases and cGMP phosphodiesterases in nitric oxide and cGMP action. *Pharmacol Rev* **2010,** *62* (3), 525-563, doi: 10.1124/pr.110.002907.

65. Yang, C. & Kazanietz, M. G., Divergence and complexities in DAG signaling: Looking beyond PKC. *Trends Pharmacol Sci* **2003,** *24* (11), 602-608, doi: 10.1016/j.tips.2003.09.003.

66. Boss, V., Talpade, D. J. & Murphy, T. J., Induction of NFAT-mediated transcription by Gq-coupled receptors in lymphoid and non-lymphoid cells. *J Biol Chem* **1996,** *271* (18), 10429-10432, doi: 10.1074/jbc.271.18.10429.

67. Bishop, A. L. & Hall, A., Rho GTPases and their effector proteins. *Biochem J* **2000,** *348 Pt 2* (Pt 2), 241-255.

68. Riobo, N. A. & Manning, D. R., Receptors coupled to heterotrimeric G proteins of the G12 family. *Trends Pharmacol Sci* **2005,** *26* (3), 146-154, doi: 10.1016/j.tips.2005.01.007.

69. Kozasa, T., Hajicek, N., Chow, C. R. & Suzuki, N., Signalling mechanisms of RhoGTPase regulation by the heterotrimeric G proteins G12 and G13. *J Biochem* **2011,** *150* (4), 357-369, doi: 10.1093/jb/mvr105.

70. Yang, Y. M., Kuen, D. S., Chung, Y., Kurose, H. & Kim, S. G., G α 12/13 signaling in metabolic diseases. *Exp Mol Med* **2020,** *52* (6), 896-910, doi: 10.1038/s12276-020-0454-5.

71. Kühn, H., Hall, S. W. & Wilden, U., Light-induced binding of 48-kDa protein to photoreceptor membranes is highly enhanced by phosphorylation of rhodopsin. *FEBS Lett* **1984,** *176* (2), 473-478, doi: 10.1016/0014-5793(84)81221-1.

72. Lohse, M. J., Benovic, J. L., Codina, J., Caron, M. G. & Lefkowitz, R. J., β-Arrestin: A protein that regulates β-adrenergic receptor function. *Science* **1990,** *248* (4962), 1547-1550, doi: 10.1126/science.2163110.

73. Carpenter, B., Nehmé, R., Warne, T., Leslie, A. G. & Tate, C. G., Structure of the adenosine A2A receptor bound to an engineered G protein. *Nature* **2016,** *536* (7614), 104-107, doi: 10.1038/nature18966.

74. Zhou, X. E., He, Y., de Waal, P. W., Gao, X., Kang, Y., Van Eps, N., Yin, Y., Pal, K., Goswami, D., White, T. A., et al., Identification of phosphorylation codes for arrestin recruitment by G protein-coupled receptors. *Cell* **2017,** *170* (3), 457-469.e413, doi: 10.1016/j.cell.2017.07.002.

75. Kumari, P., Srivastava, A., Banerjee, R., Ghosh, E., Gupta, P., Ranjan, R., Chen, X., Gupta, B., Gupta, C., Jaiman, D., et al., Functional competence of a partially engaged GPCR-β-arrestin complex. *Nat Commun* **2016,** *7*, 13416, doi: 10.1038/ncomms13416.

76. Gurevich, V. V. & Gurevich, E. V., GPCR signaling regulation: The role of GRKs and arrestins. *Front Pharmacol* **2019,** *10*, 125, doi: 10.3389/fphar.2019.00125.

77. Benovic, J. L., Kühn, H., Weyand, I., Codina, J., Caron, M. G. & Lefkowitz, R. J., Functional desensitization of the isolated β-adrenergic receptor by the β-adrenergic receptor kinase: Potential role of an analog of the retinal protein arrestin (48-kDa protein). *Proc Natl Acad Sci U S A* **1987,** *84* (24), 8879-8882, doi: 10.1073/pnas.84.24.8879.

78. Sun, N. & Kim, K. M., Mechanistic diversity involved in the desensitization of G protein-coupled receptors. *Archives of pharmacal research* **2021,** *44* (4), 342-353, doi: 10.1007/s12272-021-01320-y.

79. Cho, E. Y., Cho, D. I., Park, J. H., Kurose, H., Caron, M. G. & Kim, K. M., Roles of protein kinase C and actin-binding protein 280 in the regulation of intracellular trafficking of dopamine D3 receptor. *Mol Endocrinol* **2007,** *21* (9), 2242-2254, doi: 10.1210/me.2007-0202.

80. Benovic, J. L., Pike, L. J., Cerione, R. A., Staniszewski, C., Yoshimasa, T., Codina, J., Caron, M. G. & Lefkowitz, R. J., Phosphorylation of the mammalian β-adrenergic receptor by cyclic AMP-dependent protein kinase. Regulation of the rate of receptor phosphorylation and dephosphorylation by agonist occupancy and effects on coupling of the receptor to the stimulatory guanine nucleotide regulatory protein. *J Biol Chem* **1985,** *260* (11), 7094-7101.

81. Kelly, E., Bailey, C. P. & Henderson, G., Agonist-selective mechanisms of GPCR desensitization. *Br J Pharmacol* **2008,** *153* (S1), S379-S388, doi: 10.1038/sj.bjp.0707604.

82. Gurevich, V. V. & Gurevich, E. V., The molecular acrobatics of arrestin activation. *Trends Pharmacol Sci* **2004,** *25* (2), 105-111, doi: 10.1016/j.tips.2003.12.008.

83. Pavlos, N. J. & Friedman, P. A., GPCR signaling and trafficking: The long and short of iz. *Trends in endocrinology and metabolism: TEM* **2017,** *28* (3), 213-226, doi: 10.1016/j.tem.2016.10.007.

84. January, B., Seibold, A., Whaley, B., Hipkin, R. W., Lin, D., Schonbrunn, A., Barber, R. & Clark, R. B., β2-adrenergic receptor desensitization, internalization, and phosphorylation in response to full and partial agonists. *J Biol Chem* **1997,** *272* (38), 23871-23879, doi: 10.1074/jbc.272.38.23871.

85. Pearse, B. M., Clathrin: A unique protein associated with intracellular transfer of membrane by coated vesicles. *Proc Natl Acad Sci U S A* **1976,** *73* (4), 1255-1259, doi: 10.1073/pnas.73.4.1255.

86. Traub, L. M., Tickets to ride: Selecting cargo for clathrin-regulated internalization. *Nat Rev Mol Cell Biol* **2009,** *10* (9), 583-596, doi: 10.1038/nrm2751.

87. Kang, D. S., Tian, X. & Benovic, J. L., Role of β-arrestins and arrestin domain-containing proteins in G protein-coupled receptor trafficking. *Current opinion in cell biology* **2014,** *27*, 63-71, doi: 10.1016/j.ceb.2013.11.005.

88. DeWire, S. M., Ahn, S., Lefkowitz, R. J. & Shenoy, S. K., β-arrestins and cell signaling. *Annual review of physiology* **2007,** *69*, 483-510, doi: 10.1146/annurev.physiol.69.022405.154749.

89. Hur, E.-M. & Kim, K.-T., G protein-coupled receptor signalling and cross-talk: Achieving rapidity and specificity. *Cell Signal* **2002,** *14* (5), 397-405, doi: 10.1016/S0898-6568(01)00258-3.

90. Werry, T. D., Wilkinson, G. F. & Willars, G. B., Mechanisms of cross-talk between G-protein-coupled receptors resulting in enhanced release of intracellular Ca2+. *Biochem J* **2003,** *374* (Pt 2), 281-296, doi: 10.1042/BJ20030312.

91. Logothetis, D. E., Kurachi, Y., Galper, J., Neer, E. J. & Clapham, D. E., The $\beta\gamma$ subunits of GTP-binding proteins activate the muscarinic K+ channel in heart. *Nature* **1987,** *325* (6102), 321-326, doi: 10.1038/325321a0.

92. Lüscher, C., Jan, L. Y., Stoffel, M., Malenka, R. C. & Nicoll, R. A., G protein-coupled inwardly rectifying K+ channels (GIRKs) mediate postsynaptic but not presynaptic transmitter actions in hippocampal neurons. *Neuron* **1997,** *19* (3), 687-695, doi: 10.1016/S0896-6273(00)80381-5.

93. Quallo, T., Alkhatib, O., Gentry, C., Andersson, D. A. & Bevan, S., G protein $\beta\gamma$ subunits inhibit TRPM3 ion channels in sensory neurons. *eLife* **2017,** *6*, e26138, doi: 10.7554/eLife.26138.

94. Currie, K. P., G protein modulation of CaV2 voltage-gated calcium channels. *Channels (Austin)* **2010,** *4* (6), 497-509, doi: 10.4161/chan.4.6.12871.

95. Zamponi, G. W. & Currie, K. P., Regulation of Ca(V)2 calcium channels by G protein coupled receptors. *Biochim Biophys Acta* **2013,** *1828* (7), 1629-1643, doi: 10.1016/j.bbamem.2012.10.004.

96. Sunahara, R. K., Dessauer, C. W. & Gilman, A. G., Complexity and diversity of mammalian adenylyl cyclases. *Annu Rev Pharmacol Toxicol* **1996,** *36*, 461-480, doi: 10.1146/annurev.pa.36.040196.002333.

97. Steiner, D., Saya, D., Schallmach, E., Simonds, W. F. & Vogel, Z., Adenylyl cyclase type-VIII activity is regulated by G$\beta\gamma$ subunits. *Cell Signal* **2006,** *18* (1), 62-68, doi: 10.1016/j.cellsig.2005.03.014.

98. Smrcka, A. V. & Sternweis, P. C., Regulation of purified subtypes of phosphatidylinositol-specific phospholipase C β by G protein α and $\beta\gamma$ subunits. *J Biol Chem* **1993,** *268* (13), 9667-9674, doi: 10.1016/S0021-9258(18)98401-2.

99. Fisher, I., Jenkins, M., Tall, G., Burke, J. E. & Smrcka, A. V., Activation of phospholipase C β by G$\beta\gamma$ and Gαq involves C-terminal rearrangement to release auto-inhibition. *bioRxiv* **2019**, 810994, doi: 10.1101/810994.

100. Daaka, Y., Pitcher, J. A., Richardson, M., Stoffel, R. H., Robishaw, J. D. & Lefkowitz, R. J., Receptor and G $\beta\gamma$ isoform-specific interactions with G protein-coupled receptor kinases. *Proc Natl Acad Sci U S A* **1997,** *94* (6), 2180-2185, doi: 10.1073/pnas.94.6.2180.

101. Kozasa, T., The structure of GRK2-G$\beta\gamma$ complex: Intimate association of G-protein signaling modules. *Trends Pharmacol Sci* **2004,** *25* (2), 61-63, doi: 10.1016/j.tips.2003.12.006.

102. Cordeaux, Y. & Hill, S. J., Mechanisms of cross-talk between G-protein-coupled receptors. *Neuro-Signals* **2002,** *11* (1), 45-57, doi: 10.1159/000057321.

103. Tsu, R. & Wong, Y., Gi-mediated stimulation of type II adenylyl cyclase is augmented by Gq-coupled receptor activation and phorbol ester treatment. *J Neurosci* **1996,** *16* (4), 1317-1323, doi: 10.1523/jneurosci.16-04-01317.1996.

104. Selbie, L. A. & Hill, S. J., G protein-coupled-receptor cross-talk: The fine-tuning of multiple receptor-signalling pathways. *Trends Pharmacol Sci* **1998,** *19* (3), 87-93, doi: 10.1016/s0165-6147(97)01166-8.

105. Carroll, R. C., Morielli, A. D. & Peralta, E. G., Coincidence detection at the level of phospholipase C activation mediated by the M4 muscarinic acetylcholine receptor. *Current biology : CB* **1995,** *5* (5), 536-544, doi: 10.1016/s0960-9822(95)00106-0.

106. Booden, M. A., Siderovski, D. P. & Der, C. J., Leukemia-associated Rho guanine nucleotide exchange factor promotes Gαq-coupled activation of RhoA. *Mol Cell Biol* **2002,** *22* (12), 4053-4061, doi: 10.1128/MCB.22.12.4053-4061.2002.

107. Chikumi, H., Vázquez-Prado, J., Servitja, J. M., Miyazaki, H. & Gutkind, J. S., Potent activation of RhoA by Gαq and Gq-coupled receptors. *J Biol Chem* **2002,** *277* (30), 27130-27134, doi: 10.1074/jbc.M204715200.

108. Liu, M. & Simon, M. I., Regulation by cAMP-dependent protein kinase of a G-protein-mediated phospholipase C. *Nature* **1996,** *382* (6586), 83-87, doi: 10.1038/382083a0.

109. Ding, K. H., Husain, S., Akhtar, R. A., Isales, C. M. & Abdel-Latif, A. A., Inhibition of muscarinic-stimulated polyphosphoinositide hydrolysis and Ca2+ mobilization in cat iris sphincter smooth muscle cells by cAMP-elevating agents. *Cell Signal* **1997,** *9* (6), 411-421, doi: 10.1016/s0898-6568(97)00018-1.

110. Bugrim, A. E., Regulation of Ca2+ release by cAMP-dependent protein kinase. A mechanism for agonist-specific calcium signaling? *Cell calcium* **1999,** *25* (3), 219-226, doi: 10.1054/ceca.1999.0027.

111. Taylor, C. W., Regulation of IP3 receptors by cyclic AMP. *Cell calcium* **2017,** *63*, 48-52, doi: 10.1016/j.ceca.2016.10.005.

112. Halls, M. L. & Cooper, D. M., Regulation by Ca2+-signaling pathways of adenylyl cyclases. *Cold Spring Harb Perspect Biol* **2011,** *3* (1), a004143, doi: 10.1101/cshperspect.a004143.

113. Luttrell, L. M., Roudabush, F. L., Choy, E. W., Miller, W. E., Field, M. E., Pierce, K. L. & Lefkowitz, R. J., Activation and targeting of extracellular signal-regulated kinases by β-arrestin scaffolds. *Proc Natl Acad Sci U S A* **2001,** *98* (5), 2449-2454, doi: 10.1073/pnas.041604898.

114. Eishingdrelo, H., Sun, W., Li, H., Wang, L., Eishingdrelo, A., Dai, S., McKew, J. C. & Zheng, W., ERK and β-arrestin interaction: A converging point of signaling pathways for multiple types of cell surface receptors. *J Biomol Screen* **2015,** *20* (3), 341-349, doi: 10.1177/1087057114557233.

115. Rai, S. N., Dilnashin, H., Birla, H., Singh, S. S., Zahra, W., Rathore, A. S., Singh, B. K. & Singh, S. P., The role of PI3K/Akt and ERK in neurodegenerative disorders. *Neurotox Res* **2019,** *35* (3), 775-795, doi: 10.1007/s12640-019-0003-y.

116. Randakova, A. & Jakubik, J., Functionally selective and biased agonists of muscarinic receptors. *Pharmacol Res* **2021,** *169*, 105641, doi: 10.1016/j.phrs.2021.105641.

117. Black, J. W. & Leff, P., Operational models of pharmacological agonism. *Proceedings of the Royal Society of London. Series B, Biological sciences* **1983,** *220* (1219), 141-162, doi: 10.1098/rspb.1983.0093.

118. Black, J. W., Leff, P., Shankley, N. P. & Wood, J., An operational model of pharmacological agonism: the effect of E/[A] curve shape on agonist dissociation constant estimation. *Br J Pharmacol* **1985,** *84* (2), 561-571, doi: 10.1111/j.1476-5381.1985.tb12941.x.

119. Kenakin, T. & Christopoulos, A., Signalling bias in new drug discovery: Detection, quantification and therapeutic impact. *Nat Rev Drug Discov* **2013,** *12* (3), 205-216, doi: 10.1038/nrd3954.

120. Kenakin, T., Signaling bias in drug discovery. *Expert Opin Drug Discov* **2017,** *12* (4), 321-333, doi: 10.1080/17460441.2017.1297417.

121. Sauliere, A., Bellot, M., Paris, H., Denis, C., Finana, F., Hansen, J. T., Altie, M. F., Seguelas, M. H., Pathak, A., Hansen, J. L., et al., Deciphering biased-agonism complexity reveals a new active AT1 receptor entity. *Nat Chem Biol* **2012,** *8* (7), 622-630, doi: 10.1038/nchembio.961.

122. Griffin, M. T., Figueroa, K. W., Liller, S. & Ehlert, F. J., Estimation of agonist activity at G protein-coupled receptors: Analysis of M2 muscarinic receptor signaling through Gi/o, Gs, and G15. *J Pharmacol Exp Ther* **2007,** *321* (3), 1193-1207, doi: 10.1124/jpet.107.120857.

123. Holze, J., Bermudez, M., Pfeil, E. M., Kauk, M., Bodefeld, T., Irmen, M., Matera, C., Dallanoce, C., De Amici, M., Holzgrabe, U., et al., Ligand-specific allosteric coupling controls G-protein-coupled receptor signaling. *ACS Pharmacol Transl Sci* **2020,** *3* (5), 859-867, doi: 10.1021/acsptsci.0c00069.

124. Mailman, R. B., GPCR functional selectivity has therapeutic impact. *Trends Pharmacol Sci* **2007,** *28* (8), 390-396, doi: 10.1016/j.tips.2007.06.002.

125. Bock, A., Kostenis, E., Trankle, C., Lohse, M. J. & Mohr, K., Pilot the pulse: Controlling the multiplicity of receptor dynamics. *Trends Pharmacol Sci* **2014,** *35* (12), 630-638, doi: 10.1016/j.tips.2014.10.002.

126. Violin, J. D., Crombie, A. L., Soergel, D. G. & Lark, M. W., Biased ligands at G-protein-coupled receptors: promise and progress. *Trends Pharmacol Sci* **2014,** *35* (7), 308-316, doi: 10.1016/j.tips.2014.04.007.

127. Jacobson, K. A., New paradigms in GPCR drug discovery. *Biochem Pharmacol* **2015,** *98* (4), 541-555, doi: 10.1016/j.bcp.2015.08.085.

128. Tan, L., Yan, W., McCorvy, J. D. & Cheng, J., Biased ligands of G protein-coupled receptors (GPCRs): Structure–functional selectivity relationships (SFSRs) and therapeutic potential. *J Med Chem* **2018,** *61* (22), 9841-9878, doi: 10.1021/acs.jmedchem.8b00435.

129. Thompson, G. L., Kelly, E., Christopoulos, A. & Canals, M., Novel GPCR paradigms at the μ-opioid receptor. *Br J Pharmacol* **2015,** *172* (2), 287-296, doi: 10.1111/bph.12600.

130. Michel, M. C. & Charlton, S. J., Biased agonism in drug discovery-Is it too soon to choose a path? *Mol Pharmacol* **2018,** *93* (4), 259-265, doi: 10.1124/mol.117.110890.

131. Hill, S. J., Baker, J. G. & Rees, S., Reporter-gene systems for the study of G-protein-coupled receptors. *Current opinion in pharmacology* **2001,** *1* (5), 526-532, doi: 10.1016/s1471-4892(01)00091-1.

132. Zhang, R. & Xie, X., Tools for GPCR drug discovery. *Acta Pharmacol Sin* **2012,** *33* (3), 372-384, doi: 10.1038/aps.2011.173.

133. Rodbell, M., Birnbaumer, L., Pohl, S. L. & Krans, H. M., The glucagon-sensitive adenyl cyclase system in plasma membranes of rat liver. V. An obligatory role of guanylnucleotides in glucagon action. *J Biol Chem* **1971,** *246* (6), 1877-1882.

134. Cassel, D. & Selinger, Z., Catecholamine-stimulated GTPase activity in turkey erythrocyte membranes. *Biochim Biophys Acta* **1976,** *452* (2), 538-551, doi: 10.1016/0005-2744(76)90206-0.

135. Cassel, D. & Selinger, Z., Mechanism of adenylate cyclase activation through the β-adrenergic receptor: Catecholamine-induced displacement of bound GDP by GTP. *Proc Natl Acad Sci U S A* **1978,** *75* (9), 4155-4159, doi: 10.1073/pnas.75.9.4155.

136. Sternweis, P. C., Northup, J. K., Smigel, M. D. & Gilman, A. G., The regulatory component of adenylate cyclase. Purification and properties. *J Biol Chem* **1981,** *256* (22), 11517-11526.

137. Northup, J. K., Sternweis, P. C., Smigel, M. D., Schleifer, L. S., Ross, E. M. & Gilman, A. G., Purification of the regulatory component of adenylate cyclase. *Proc Natl Acad Sci U S A* **1980,** *77* (11), 6516-6520, doi: 10.1073/pnas.77.11.6516.

138. Bokoch, G. M., Katada, T., Northup, J. K., Ui, M. & Gilman, A. G., Purification and properties of the inhibitory guanine nucleotide-binding regulatory component of adenylate cyclase. *J Biol Chem* **1984,** *259* (6), 3560-3567.

139. Asano, T., Pedersen, S. E., Scott, C. W. & Ross, E. M., Reconstitution of catecholamine-stimulated binding of guanosine 5'-O-(3-thiotriphosphate) to the stimulatory GTP-binding protein of adenylate cyclase. *Biochemistry* **1984,** *23* (23), 5460-5467, doi: 10.1021/bi00318a013.

140. Kurose, H., Katada, T., Haga, T., Haga, K., Ichiyama, A. & Ui, M., Functional interaction of purified muscarinic receptors with purified inhibitory guanine nucleotide regulatory proteins reconstituted in phospholipid vesicles. *J Biol Chem* **1986,** *261* (14), 6423-6428.

141. Higashijima, T., Ferguson, K. M., Smigel, M. D. & Gilman, A. G., The effect of GTP and Mg2+ on the GTPase activity and the fluorescent properties of Go. *J Biol Chem* **1987,** *262* (2), 757-761.

142. Milligan, G., Principles: Extending the utility of [35S]GTP γ S binding assays. *Trends Pharmacol Sci* **2003,** *24* (2), 87-90, doi: 10.1016/s0165-6147(02)00027-5.

143. Strange, P. G., Use of the GTP γ S ([35S]GTP γ S and Eu-GTP γ S) binding assay for analysis of ligand potency and efficacy at G protein-coupled receptors. *Br J Pharmacol* **2010,** *161* (6), 1238-1249, doi: 10.1111/j.1476-5381.2010.00963.x.

144. Harrison, C. & Traynor, J. R., The [35S]GTP γ S binding assay: Approaches and applications in pharmacology. *Life sciences* **2003,** *74* (4), 489-508, doi: 10.1016/j.lfs.2003.07.005.

145. Lazareno, S. & Birdsall, N. J., Pharmacological characterization of acetylcholine-stimulated [35S]-GTP γ S binding mediated by human muscarinic M1-M4 receptors: Antagonist studies. *Br J Pharmacol* **1993,** *109* (4), 1120-1127, doi: 10.1111/j.1476-5381.1993.tb13738.x.

146. Houston, C., Wenzel-Seifert, K., Burckstummer, T. & Seifert, R., The human histamine H2-receptor couples more efficiently to Sf9 insect cell Gs-proteins than to insect cell Gq-proteins: Limitations of Sf9 cells for the analysis of receptor/Gq-protein coupling. *J Neurochem* **2002,** *80* (4), 678-696, doi: 10.1046/j.0022-3042.2001.00746.x.

147. Strasser, A., Striegl, B., Wittmann, H. J. & Seifert, R., Pharmacological profile of histaprodifens at four recombinant histamine H1 receptor species isoforms. *J Pharmacol Exp Ther* **2008,** *324* (1), 60-71, doi: 10.1124/jpet.107.129601.

148. Windh, R. T. & Manning, D. R., Analysis of G protein activation in Sf9 and mammalian cells by agonist-promoted [35S]GTP γ S binding. *Methods Enzymol* **2002,** *344*, 3-14, doi: 10.1016/s0076-6879(02)44702-7.

149. Bondar, A. & Lazar, J., Optical sensors of heterotrimeric G protein signaling. *The FEBS journal* **2021,** *288* (8), 2570-2584, doi: 10.1111/febs.15655.

150. Ayoub, M. A., Resonance energy transfer-based approaches to study GPCRs. *Methods Cell Biol* **2016,** *132*, 255-292, doi: 10.1016/bs.mcb.2015.10.008.

151. Zhou, Y., Meng, J., Xu, C. & Liu, J., Multiple GPCR functional assays based on resonance energy transfer sensors. *Frontiers in cell and developmental biology* **2021,** *9*, 611443, doi: 10.3389/fcell.2021.611443.

152. El Khamlichi, C., Reverchon-Assadi, F., Hervouet-Coste, N., Blot, L., Reiter, E. & Morisset-Lopez, S., Bioluminescence resonance energy transfer as a method to study protein-protein interactions: Application to G protein coupled receptor biology. *Molecules* **2019,** *24* (3), doi: 10.3390/molecules24030537.

153. Kahlke, T. & Umbers, K. D., Bioluminescence. *Current biology : CB* **2016,** *26* (8), R313-314, doi: 10.1016/j.cub.2016.01.007.

154. Haddock, S. H., Moline, M. A. & Case, J. F., Bioluminescence in the sea. *Annual review of marine science* **2010,** *2*, 443-493, doi: 10.1146/annurev-marine-120308-081028.

155. Widder, E. A., Bioluminescence in the ocean: Origins of biological, chemical, and ecological diversity. *Science* **2010,** *328* (5979), 704-708, doi: doi:10.1126/science.1174269.

156. Marques, S. M. & Esteves da Silva, J. C. G., Firefly bioluminescence: A mechanistic approach of luciferase catalyzed reactions. *IUBMB Life* **2009,** *61* (1), 6-17, doi: 10.1002/iub.134.

157. Jiang, T., Du, L. & Li, M., Lighting up bioluminescence with coelenterazine: Strategies and applications. *Photochem Photobiol Sci* **2016,** *15* (4), 466-480, doi: 10.1039/c5pp00456j.

158. de Wet, J. R., Wood, K. V., Helinski, D. R. & DeLuca, M., Cloning of firefly luciferase cDNA and the expression of active luciferase in Escherichia coli. *Proc Natl Acad Sci U S A* **1985,** *82* (23), 7870-7873, doi: 10.1073/pnas.82.23.7870.

159. Seliger, H. H. & McElroy, W. D., The colors of firefly bioluminescence: Enzyme configuration and species specificity. *Proc Natl Acad Sci U S A* **1964,** *52* (1), 75-81, doi: 10.1073/pnas.52.1.75.

160. Ando, Y., Niwa, K., Yamada, N., Enomoto, T., Irie, T., Kubota, H., Ohmiya, Y. & Akiyama, H., Firefly bioluminescence quantum yield and colour change by pH-sensitive green emission. *Nat Photonics* **2008,** *2* (1), 44-47, doi: 10.1038/nphoton.2007.251.

161. Hosseinkhani, S., Molecular enigma of multicolor bioluminescence of firefly luciferase. *Cell Mol Life Sci* **2011,** *68* (7), 1167-1182, doi: 10.1007/s00018-010-0607-0.

162. Viviani, V. R., Gabriel, G. V. M., Bevilaqua, V. R., Simoes, A. F., Hirano, T. & Lopes-de-Oliveira, P. S., The proton and metal binding sites responsible for the pH-dependent green-red bioluminescence color tuning in firefly luciferases. *Sci Rep* **2018,** *8* (1), 17594, doi: 10.1038/s41598-018-33252-x.

163. Thorne, N., Inglese, J. & Auld, D. S., Illuminating insights into firefly luciferase and other bioluminescent reporters used in chemical biology. *Chem Biol* **2010,** *17* (6), 646-657, doi: 10.1016/j.chembiol.2010.05.012.

164. Wood, K. V., Lam, Y. A., Seliger, H. H. & McElroy, W. D., Complementary DNA coding click beetle luciferases can elicit bioluminescence of different colors. *Science* **1989,** *244* (4905), 700-702, doi: 10.1126/science.2655091.

165. Lorenz, W. W., McCann, R. O., Longiaru, M. & Cormier, M. J., Isolation and expression of a cDNA encoding Renilla reniformis luciferase. *Proc Natl Acad Sci U S A* **1991,** *88* (10), 4438-4442, doi: 10.1073/pnas.88.10.4438.

166. Markova, S. V. & Vysotski, E. S., Coelenterazine-dependent luciferases. *Biochemistry. Biokhimiia* **2015,** *80* (6), 714-732, doi: 10.1134/s0006297915060073.

167. Krasitskaya, V. V., Bashmakova, E. E. & Frank, L. A., Coelenterazine-dependent luciferases as a powerful analytical tool for research and biomedical applications. *Int J Mol Sci* **2020,** *21* (20), doi: 10.3390/ijms21207465.

168. Förster, T., Zwischenmolekulare Energiewanderung und Fluoreszenz. *Annalen der Physik* **1948,** *437* (1-2), 55-75, doi: 10.1002/andp.19484370105.

169. Stryer, L., Fluorescence energy transfer as a spectroscopic ruler. *Annu Rev Biochem* **1978,** *47*, 819-846, doi: 10.1146/annurev.bi.47.070178.004131.

170. Tsien, R. Y., The green fluorescent protein. *Annu Rev Biochem* **1998,** *67*, 509-544, doi: 10.1146/annurev.biochem.67.1.509.

171. Nakajima, Y., Yamazaki, T., Nishii, S., Noguchi, T., Hoshino, H., Niwa, K., Viviani, V. R. & Ohmiya, Y., Enhanced beetle luciferase for high-resolution bioluminescence imaging. *PLoS One* **2010,** *5* (4), e10011, doi: 10.1371/journal.pone.0010011.

172. Hall, M. P., Unch, J., Binkowski, B. F., Valley, M. P., Butler, B. L., Wood, M. G., Otto, P., Zimmerman, K., Vidugiris, G., Machleidt, T., et al., Engineered luciferase reporter from a deep sea shrimp utilizing a novel imidazopyrazinone substrate. *ACS Chem Biol* **2012,** *7* (11), 1848-1857, doi: 10.1021/cb3002478.

173. Heim, R. & Tsien, R. Y., Engineering green fluorescent protein for improved brightness, longer wavelengths and fluorescence resonance energy transfer. *Current biology : CB* **1996,** *6* (2), 178-182, doi: 10.1016/s0960-9822(02)00450-5.

174. Shaner, N. C., Campbell, R. E., Steinbach, P. A., Giepmans, B. N., Palmer, A. E. & Tsien, R. Y., Improved monomeric red, orange and yellow fluorescent proteins derived from Discosoma sp. red fluorescent protein. *Nat Biotechnol* **2004,** *22* (12), 1567-1572, doi: 10.1038/nbt1037.

175. Shaner, N. C., Patterson, G. H. & Davidson, M. W., Advances in fluorescent protein technology. *J Cell Sci* **2007,** *120* (Pt 24), 4247-4260, doi: 10.1242/jcs.005801.

176. Lohse, M. J., Nuber, S. & Hoffmann, C., Fluorescence/bioluminescence resonance energy transfer techniques to study G-protein-coupled receptor activation and signaling. *Pharmacol Rev* **2012,** *64* (2), 299-336, doi: 10.1124/pr.110.004309.

177. Wouters, E., Vasudevan, L., Crans, R. A. J., Saini, D. K. & Stove, C. P., Luminescence- and fluorescence-based complementation assays to screen for GPCR oligomerization: Current state of the art. *Int J Mol Sci* **2019,** *20* (12), doi: 10.3390/ijms20122958.

178. Richards, F. M., On the enzymatic activity of subtilisin-modified ribonuclease. *Proc Natl Acad Sci U S A* **1958,** *44* (2), 162-166, doi: 10.1073/pnas.44.2.162.

179. Michnick, S. W., Remy, I., Campbell-Valois, F. X., Vallée-Bélisle, A. & Pelletier, J. N., Detection of protein-protein interactions by protein fragment complementation strategies. *Methods Enzymol* **2000,** *328*, 208-230, doi: 10.1016/s0076-6879(00)28399-7.

180. Ozawa, T., Takeuchi, T. M., Kaihara, A., Sato, M. & Umezawa, Y., Protein splicing-based reconstitution of split green fluorescent protein for monitoring protein-protein interactions in bacteria: improved sensitivity and reduced screening time. *Anal Chem* **2001,** *73* (24), 5866-5874, doi: 10.1021/ac010717k.

181. Kodama, Y. & Hu, C.-D., Bimolecular fluorescence complementation (BiFC): A 5-year update and future perspectives. *BioTechniques* **2012,** *53* (5), 285-298, doi: 10.2144/000113943.

182. Magliery, T. J., Wilson, C. G., Pan, W., Mishler, D., Ghosh, I., Hamilton, A. D. & Regan, L., Detecting protein-protein interactions with a green fluorescent protein fragment reassembly trap: Scope and mechanism. *J Am Chem Soc* **2005,** *127* (1), 146-157, doi: 10.1021/ja046699g.

183. Hu, C.-D., Chinenov, Y. & Kerppola, T. K., Visualization of interactions among bZIP and Rel family proteins in living cells using bimolecular fluorescence complementation. *Molecular Cell* **2002,** *9* (4), 789-798, doi: 10.1016/S1097-2765(02)00496-3.

184. Ozawa, T., Kaihara, A., Sato, M., Tachihara, K. & Umezawa, Y., Split luciferase as an optical probe for detecting protein-protein interactions in mammalian cells based on protein splicing. *Anal Chem* **2001,** *73* (11), 2516-2521, doi: 10.1021/ac0013296.

185. Hattori, M. & Ozawa, T., Split luciferase complementation for analysis of intracellular signaling. *Anal Sci* **2014,** *30* (5), 539-544, doi: 10.2116/analsci.30.539.

186. Conti, E., Franks, N. P. & Brick, P., Crystal structure of firefly luciferase throws light on a superfamily of adenylate-forming enzymes. *Structure* **1996,** *4* (3), 287-298, doi: 10.1016/S0969-2126(96)00033-0.

187. Franks, N. P., Jenkins, A., Conti, E., Lieb, W. R. & Brick, P., Structural basis for the inhibition of firefly luciferase by a general anesthetic. *Biophys J* **1998,** *75* (5), 2205-2211, doi: 10.1016/S0006-3495(98)77664-7.

188. Luker, K. E., Smith, M. C., Luker, G. D., Gammon, S. T., Piwnica-Worms, H. & Piwnica-Worms, D., Kinetics of regulated protein-protein interactions revealed with firefly luciferase complementation imaging in cells and living animals. *Proc Natl Acad Sci U S A* **2004,** *101* (33), 12288-12293, doi: 10.1073/pnas.0404041101.

189. Misawa, N., Kafi, A. K., Hattori, M., Miura, K., Masuda, K. & Ozawa, T., Rapid and high-sensitivity cell-based assays of protein-protein interactions using split click beetle luciferase complementation: An approach to the study of G-protein-coupled receptors. *Anal Chem* **2010,** *82* (6), 2552-2560, doi: 10.1021/ac100104q.

190. Hida, N., Awais, M., Takeuchi, M., Ueno, N., Tashiro, M., Takagi, C., Singh, T., Hayashi, M., Ohmiya, Y. & Ozawa, T., High-sensitivity real-time imaging of dual protein-protein interactions in living subjects using multicolor luciferases. *PLoS One* **2009,** *4* (6), e5868, doi: 10.1371/journal.pone.0005868.

191. Paulmurugan, R. & Gambhir, S. S., Monitoring protein−protein interactions using split synthetic Renilla luciferase protein-fragment-assisted complementation. *Anal Chem* **2003,** *75* (7), 1584-1589, doi: 10.1021/ac020731c.

192. Inouye, S., Watanabe, K., Nakamura, H. & Shimomura, O., Secretional luciferase of the luminous shrimp Oplophorus gracilirostris: cDNA cloning of a novel imidazopyrazinone luciferase(1). *FEBS Lett* **2000,** *481* (1), 19-25, doi: 10.1016/s0014-5793(00)01963-3.

193. Dixon, A. S., Schwinn, M. K., Hall, M. P., Zimmerman, K., Otto, P., Lubben, T. H., Butler, B. L., Binkowski, B. F., Machleidt, T., Kirkland, T. A., et al., NanoLuc complementation reporter optimized for accurate measurement of protein interactions in cells. *ACS Chem Biol* **2016,** *11* (2), 400-408, doi: 10.1021/acschembio.5b00753.

194. Janetopoulos, C., Jin, T. & Devreotes, P., Receptor-mediated activation of heterotrimeric G-proteins in living cells. *Science* **2001,** *291* (5512), 2408-2411, doi: 10.1126/science.1055835.

195. Olsen, R. H. J., DiBerto, J. F., English, J. G., Glaudin, A. M., Krumm, B. E., Slocum, S. T., Che, T., Gavin, A. C., McCorvy, J. D., Roth, B. L., et al., TRUPATH, an open-source biosensor platform for interrogating the GPCR transducerome. *Nat Chem Biol* **2020,** *16* (8), 841-849, doi: 10.1038/s41589-020-0535-8.

196. Bünemann, M., Frank, M. & Lohse, M. J., Gi protein activation in intact cells involves subunit rearrangement rather than dissociation. *Proc Natl Acad Sci U S A* **2003,** *100* (26), 16077-16082, doi: 10.1073/pnas.2536719100.

197. Gales, C., Van Durm, J. J., Schaak, S., Pontier, S., Percherancier, Y., Audet, M., Paris, H. & Bouvier, M., Probing the activation-promoted structural rearrangements in preassembled receptor-G protein complexes. *Nat Struct Mol Biol* **2006,** *13* (9), 778-786, doi: 10.1038/nsmb1134.

198. Hein, P., Rochais, F., Hoffmann, C., Dorsch, S., Nikolaev, V. O., Engelhardt, S., Berlot, C. H., Lohse, M. J. & Bünemann, M., Gs activation is time-limiting in initiating receptor-mediated signaling. *J Biol Chem* **2006,** *281* (44), 33345-33351, doi: 10.1074/jbc.M606713200.

199. Hynes, T. R., Mervine, S. M., Yost, E. A., Sabo, J. L. & Berlot, C. H., Live cell imaging of Gs and the β 2-adrenergic receptor demonstrates that both αs and $\beta 1 \gamma 7$ internalize upon stimulation and exhibit similar trafficking patterns that differ from that of the β 2-adrenergic receptor. *J Biol Chem* **2004,** *279* (42), 44101-44112, doi: 10.1074/jbc.M405151200.

200. Adjobo-Hermans, M. J., Goedhart, J., van Weeren, L., Nijmeijer, S., Manders, E. M., Offermanns, S. & Gadella, T. W., Jr., Real-time visualization of heterotrimeric G protein Gq activation in living cells. *BMC Biol* **2011,** *9*, 32, doi: 10.1186/1741-7007-9-32.

201. Vilardaga, J.-P., Bünemann, M., Krasel, C., Castro, M. & Lohse, M. J., Measurement of the millisecond activation switch of G protein–coupled receptors in living cells. *Nat Biotechnol* **2003,** *21* (7), 807-812, doi: 10.1038/nbt838.

202. Schihada, H., Vandenabeele, S., Zabel, U., Frank, M., Lohse, M. J. & Maiellaro, I., A universal bioluminescence resonance energy transfer sensor design enables high-sensitivity screening of GPCR activation dynamics. *Commun Biol* **2018,** *1*, 105, doi: 10.1038/s42003-018-0072-0.

203. Chisari, M., Saini, D. K., Kalyanaraman, V. & Gautam, N., Shuttling of G protein subunits between the plasma membrane and intracellular membranes. *J Biol Chem* **2007,** *282* (33), 24092-24098, doi: 10.1074/jbc.M704246200.

204. Wedegaertner, P. B. & Bourne, H. R., Activation and depalmitoylation of Gs α. *Cell* **1994,** *77* (7), 1063-1070, doi: 10.1016/0092-8674(94)90445-6.

205. Polit, A., Mystek, P. & Blasiak, E., Every detail matters. That is, how the interaction between Gα proteins and membrane affects their function. *Membranes (Basel)* **2021,** *11* (3), doi: 10.3390/membranes11030222.

206. Kenakin, T. P., Receptor reserve as a tissue misnomer. *Trends Pharmacol Sci* **1986,** *7*, 93-95, doi: 10.1016/0165-6147(86)90271-3.

207. Nikolaev, V. O., Hoffmann, C., Bünemann, M., Lohse, M. J. & Vilardaga, J. P., Molecular basis of partial agonism at the neurotransmitter α2A-adrenergic receptor and Gi-protein heterotrimer. *J Biol Chem* **2006,** *281* (34), 24506-24511, doi: 10.1074/jbc.M603266200.

208. Hollins, B., Kuravi, S., Digby, G. J. & Lambert, N. A., The C-terminus of GRK3 indicates rapid dissociation of G protein heterotrimers. *Cell Signal* **2009,** *21* (6), 1015-1021, doi: 10.1016/j.cellsig.2009.02.017.

209. van Unen, J., Stumpf, A. D., Schmid, B., Reinhard, N. R., Hordijk, P. L., Hoffmann, C., Gadella, T. W., Jr. & Goedhart, J., A new generation of FRET sensors for robust measurement of Gαi1, Gαi2 and Gαi3 activation kinetics in single cells. *PLoS One* **2016,** *11* (1), e0146789, doi: 10.1371/journal.pone.0146789.

210. Mastop, M., Reinhard, N. R., Zuconelli, C. R., Terwey, F., Gadella, T. W. J., Jr., van Unen, J., Adjobo-Hermans, M. J. W. & Goedhart, J., A FRET-based biosensor for measuring Gα13 activation in single cells. *PLoS One* **2018,** *13* (3), e0193705, doi: 10.1371/journal.pone.0193705.

211. Schihada, H., Shekhani, R. & Schulte, G., Quantitative assessment of constitutive G protein-coupled receptor activity with BRET-based G protein biosensors. *Science signaling* **2021,** *14* (699), eabf1653, doi: doi:10.1126/scisignal.abf1653.

212. Galés, C., Rebois, R. V., Hogue, M., Trieu, P., Breit, A., Hébert, T. E. & Bouvier, M., Real-time monitoring of receptor and G-protein interactions in living cells. *Nat Methods* **2005,** *2* (3), 177-184, doi: 10.1038/nmeth743.

213. Hein, P., Frank, M., Hoffmann, C., Lohse, M. J. & Bunemann, M., Dynamics of receptor/G protein coupling in living cells. *EMBO J* **2005,** *24* (23), 4106-4114, doi: 10.1038/sj.emboj.7600870.

214. Okashah, N., Wan, Q., Ghosh, S., Sandhu, M., Inoue, A., Vaidehi, N. & Lambert, N. A., Variable G protein determinants of GPCR coupling selectivity. *Proc Natl Acad Sci U S A* **2019,** *116* (24), 12054-12059, doi: 10.1073/pnas.1905993116.

215. Laschet, C., Dupuis, N. & Hanson, J., A dynamic and screening-compatible nanoluciferase-based complementation assay enables profiling of individual GPCR-G protein interactions. *J Biol Chem* **2019,** *294* (11), 4079-4090, doi: 10.1074/jbc.RA118.006231.

216. Inouye, S. & Sahara, Y., Identification of two catalytic domains in a luciferase secreted by the copepod Gaussia princeps. *Biochem Biophys Res Commun* **2008,** *365* (1), 96-101, doi: 10.1016/j.bbrc.2007.10.152.

217. Dupuis, N., Laschet, C., Franssen, D., Szpakowska, M., Gilissen, J., Geubelle, P., Soni, A., Parent, A. S., Pirotte, B., Chevigné, A., et al., Activation of the orphan G protein-coupled receptor GPR27 by surrogate ligands promotes β-arrestin 2 recruitment. *Mol Pharmacol* **2017,** *91* (6), 595-608, doi: 10.1124/mol.116.107714.

218. Hattori, M., Tanaka, M., Takakura, H., Aoki, K., Miura, K., Anzai, T. & Ozawa, T., Analysis of temporal patterns of GPCR-β-arrestin interactions using split luciferase-fragment complementation. *Molecular bioSystems* **2013,** *9* (5), 957-964, doi: 10.1039/c2mb25443c.

219. England, C. G., Ehlerding, E. B. & Cai, W., NanoLuc: A small luciferase is brightening up the field of bioluminescence. *Bioconjug Chem* **2016,** *27* (5), 1175-1187, doi: 10.1021/acs.bioconjchem.6b00112.

220. Yano, H., Cai, N. S., Javitch, J. A. & Ferré, S., Luciferase complementation based-detection of G-protein-coupled receptor activity. *BioTechniques* **2018,** *65* (1), 9-14, doi: 10.2144/btn-2018-0039.

221. Jorgensen, R., Kubale, V., Vrecl, M., Schwartz, T. W. & Elling, C. E., Oxyntomodulin differentially affects glucagon-like peptide-1 receptor β-arrestin recruitment and signaling through Gαs. *J Pharmacol Exp Ther* **2007,** *322* (1), 148-154, doi: 10.1124/jpet.107.120006.

222. Namkung, Y., Le Gouill, C., Lukashova, V., Kobayashi, H., Hogue, M., Khoury, E., Song, M., Bouvier, M. & Laporte, S. A., Monitoring G protein-coupled receptor and β-arrestin trafficking in live cells using enhanced bystander BRET. *Nat Commun* **2016,** *7* (1), 12178, doi: 10.1038/ncomms12178.

223. Littmann, T., Buschauer, A. & Bernhardt, G., Split luciferase-based assay for simultaneous analyses of the ligand concentration- and time-dependent recruitment of β-arrestin2. *Anal Biochem* **2019,** *573*, 8-16, doi: 10.1016/j.ab.2019.02.023.

224. Forster, L., Grätz, L., Mönnich, D., Bernhardt, G. & Pockes, S., A split luciferase complementation assay for the quantification of β-arrestin2 recruitment to dopamine D2-like receptors. *Int J Mol Sci* **2020,** *21* (17), 6103.

225. Flöser, A., Becker, K., Kostenis, E., Konig, G., Krasel, C., Kolb, P. & Bünemann, M., Disentangling bias between Gq, GRK2, and arrestin3 recruitment to the M3 muscarinic acetylcholine receptor. *Elife* **2021,** *10*, doi: 10.7554/eLife.58442.

226. Flock, T., Hauser, A. S., Lund, N., Gloriam, D. E., Balaji, S. & Babu, M. M., Selectivity determinants of GPCR-G-protein binding. *Nature* **2017,** *545* (7654), 317-322, doi: 10.1038/nature22070.

227. Lim, S. M., Decoding principles of selective GPCR-Gα coupling. *Biochemistry* **2020,** *59* (2), 130-131, doi: 10.1021/acs.biochem.9b00828.

228. Gurevich, V. V. & Gurevich, E. V., Biased GPCR signaling: Possible mechanisms and inherent limitations. *Pharmacol Ther* **2020,** *211*, 107540, doi: 10.1016/j.pharmthera.2020.107540.

229. Wright, S. C. & Bouvier, M., Illuminating the complexity of GPCR pathway selectivity – advances in biosensor development. *Curr Opin Struct Biol* **2021,** *69*, 142-149, doi: 10.1016/j.sbi.2021.04.006.

230. Kumar, K. R., Lohmann, K., Masuho, I., Miyamoto, R., Ferbert, A., Lohnau, T., Kasten, M., Hagenah, J., Brüggemann, N., Graf, J., et al., Mutations in GNAL: A novel cause of craniocervical dystonia. *JAMA neurology* **2014,** *71* (4), 490-494, doi: 10.1001/jamaneurol.2013.4677.

231. Masuho, I., Martemyanov, K. A. & Lambert, N. A., Monitoring G protein activation in cells with BRET. *Methods Mol Biol* **2015,** *1335*, 107-113, doi: 10.1007/978-1-4939-2914-6_8.

232. Wan, Q., Okashah, N., Inoue, A., Nehmé, R., Carpenter, B., Tate, C. G. & Lambert, N. A., Mini G protein probes for active G protein-coupled receptors (GPCRs) in live cells. *J Biol Chem* **2018,** *293* (19), 7466-7473, doi: 10.1074/jbc.RA118.001975.

233. Wright, S. C., Lukasheva, V., Le Gouill, C., Kobayashi, H., Breton, B., Mailhot-Larouche, S., Blondel-Tepaz, É., Antunes Vieira, N., Costa-Neto, C., Héroux, M., et al., BRET-based effector membrane translocation assay monitors GPCR-promoted and endocytosis-mediated Gq activation at early endosomes. *Proc Natl Acad Sci U S A* **2021,** *118* (20), doi: 10.1073/pnas.2025846118.

234. Avet, C., Mancini, A., Breton, B., Le Gouill, C., Hauser, A. S., Normand, C., Kobayashi, H., Gross, F., Hogue, M., Lukasheva, V., et al., Selectivity landscape of 100 therapeutically relevant GPCR profiled by an effector translocation-based BRET platform. *bioRxiv* **2020**, 2020.2004.2020.052027, doi: 10.1101/2020.04.20.052027.

235. Maziarz, M., Park, J. C., Leyme, A., Marivin, A., Garcia-Lopez, A., Patel, P. P. & Garcia-Marcos, M., Revealing the activity of trimeric G-proteins in live cells with a versatile biosensor design. *Cell* **2020,** *182* (3), 770-785.e716, doi: 10.1016/j.cell.2020.06.020.

236. Manglik, A. & Kobilka, B., The role of protein dynamics in GPCR function: Insights from the β2AR and rhodopsin. *Current opinion in cell biology* **2014,** *27*, 136-143, doi: 10.1016/j.ceb.2014.01.008.

237. Rankovic, Z., Brust, T. F. & Bohn, L. M., Biased agonism: An emerging paradigm in GPCR drug discovery. *Bioorg Med Chem Lett* **2016,** *26* (2), 241-250, doi: 10.1016/j.bmcl.2015.12.024.

238. Manglik, A., Kobilka, B. K. & Steyaert, J., Nanobodies to study G protein-coupled receptor structure and function. *Annu Rev Pharmacol Toxicol* **2017,** *57*, 19-37, doi: 10.1146/annurev-pharmtox-010716-104710.

239. Tsai, C. J., Pamula, F., Nehmé, R., Muhle, J., Weinert, T., Flock, T., Nogly, P., Edwards, P. C., Carpenter, B., Gruhl, T., et al., Crystal structure of rhodopsin in complex with a mini-Go sheds light on the principles of G protein selectivity. *Sci Adv* **2018,** *4* (9), eaat7052, doi: 10.1126/sciadv.aat7052.

240. Kim, K., Che, T., Panova, O., DiBerto, J. F., Lyu, J., Krumm, B. E., Wacker, D., Robertson, M. J., Seven, A. B., Nichols, D. E., et al., Structure of a hallucinogen-activated Gq-coupled 5-HT2A serotonin receptor. *Cell* **2020,** *182* (6), 1574-1588 e1519, doi: 10.1016/j.cell.2020.08.024.

241. Liu, Q., Yang, D., Zhuang, Y., Croll, T. I., Cai, X., Dai, A., He, X., Duan, J., Yin, W., Ye, C., et al., Ligand recognition and G-protein coupling selectivity of cholecystokinin A receptor. *Nat Chem Biol* **2021,** *17* (12), 1238-1244, doi: 10.1038/s41589-021-00841-3.

242. Lin, X., Li, M., Wang, N., Wu, Y., Luo, Z., Guo, S., Han, G. W., Li, S., Yue, Y., Wei, X., et al., Structural basis of ligand recognition and self-activation of orphan GPR52. *Nature* **2020,** *579* (7797), 152-157, doi: 10.1038/s41586-020-2019-0.

243. Hong, C., Byrne, N. J., Zamlynny, B., Tummala, S., Xiao, L., Shipman, J. M., Partridge, A. T., Minnick, C., Breslin, M. J., Rudd, M. T., et al., Structures of active-state orexin receptor 2 rationalize peptide and small-molecule agonist recognition and receptor activation. *Nat Commun* **2021,** *12* (1), 815, doi: 10.1038/s41467-021-21087-6.

244. Zhuang, Y., Xu, P., Mao, C., Wang, L., Krumm, B., Zhou, X. E., Huang, S., Liu, H., Cheng, X., Huang, X. P., et al., Structural insights into the human D1 and D2 dopamine receptor signaling complexes. *Cell* **2021,** *184* (4), 931-942.e918, doi: 10.1016/j.cell.2021.01.027.

245. Wang, Y., Guo, S., Zhuang, Y., Yun, Y., Xu, P., He, X., Guo, J., Yin, W., Xu, H. E., Xie, X., et al., Molecular recognition of an acyl-peptide hormone and activation of ghrelin receptor. *Nat Commun* **2021,** *12* (1), 5064, doi: 10.1038/s41467-021-25364-2.

246. Thom, C., Ehrenmann, J., Vacca, S., Waltenspuhl, Y., Schoppe, J., Medalia, O. & Pluckthun, A., Structures of neurokinin 1 receptor in complex with Gq and Gs proteins reveal substance P binding mode and unique activation features. *Sci Adv* **2021,** *7* (50), eabk2872, doi: 10.1126/sciadv.abk2872.

247. Cao, C., Kang, H. J., Singh, I., Chen, H., Zhang, C., Ye, W., Hayes, B. W., Liu, J., Gumpper, R. H., Bender, B. J., et al., Structure, function and pharmacology of human itch GPCRs. *Nature* **2021,** *600* (7887), 170-175, doi: 10.1038/s41586-021-04126-6.

248. Garcia-Nafria, J., Lee, Y., Bai, X., Carpenter, B. & Tate, C. G., Cryo-EM structure of the adenosine A2A receptor coupled to an engineered heterotrimeric G protein. *Elife* **2018,** *7*, doi: 10.7554/eLife.35946.

249. Garcia-Nafria, J., Nehmé, R., Edwards, P. C. & Tate, C. G., Cryo-EM structure of the serotonin 5-HT1B receptor coupled to heterotrimeric Go. *Nature* **2018,** *558* (7711), 620-623, doi: 10.1038/s41586-018-0241-9.

250. Rasmussen, S. G., Choi, H. J., Fung, J. J., Pardon, E., Casarosa, P., Chae, P. S., Devree, B. T., Rosenbaum, D. M., Thian, F. S., Kobilka, T. S., et al., Structure of a nanobody-stabilized active state of the β2 adrenoceptor. *Nature* **2011,** *469* (7329), 175-180, doi: 10.1038/nature09648.

251. Rosenbaum, D. M., Zhang, C., Lyons, J. A., Holl, R., Aragao, D., Arlow, D. H., Rasmussen, S. G., Choi, H. J., Devree, B. T., Sunahara, R. K., et al., Structure and function of an irreversible agonist-β2 adrenoceptor complex. *Nature* **2011,** *469* (7329), 236-240, doi: 10.1038/nature09665.

252. Staus, D. P., Wingler, L. M., Strachan, R. T., Rasmussen, S. G., Pardon, E., Ahn, S., Steyaert, J., Kobilka, B. K. & Lefkowitz, R. J., Regulation of β2-adrenergic receptor function by conformationally selective single-domain intrabodies. *Mol Pharmacol* **2014,** *85* (3), 472-481, doi: 10.1124/mol.113.089516.

253. Staus, D. P., Strachan, R. T., Manglik, A., Pani, B., Kahsai, A. W., Kim, T. H., Wingler, L. M., Ahn, S., Chatterjee, A., Masoudi, A., et al., Allosteric nanobodies reveal the dynamic range and diverse mechanisms of G-protein-coupled receptor activation. *Nature* **2016,** *535* (7612), 448-452, doi: 10.1038/nature18636.

254. De Groof, T. W. M., Bobkov, V., Heukers, R. & Smit, M. J., Nanobodies: New avenues for imaging, stabilizing and modulating GPCRs. *Mol Cell Endocrinol* **2019,** *484*, 15-24, doi: 10.1016/j.mce.2019.01.021.

255. Carpenter, B. & Tate, C. G., Engineering a minimal G protein to facilitate crystallisation of G protein-coupled receptors in their active conformation. *Protein Eng Des Sel* **2016,** *29* (12), 583-594, doi: 10.1093/protein/gzw049.

256. Jullié, D., Valbret, Z. & Stoeber, M., Optical tools to study the subcellular organization of GPCR neuromodulation. *J Neurosci Methods* **2022,** *366*, 109408, doi: 10.1016/j.jneumeth.2021.109408.

257. Nehmé, R., Carpenter, B., Singhal, A., Strege, A., Edwards, P. C., White, C. F., Du, H., Grisshammer, R. & Tate, C. G., Mini-G proteins: Novel tools for studying GPCRs in their active conformation. *PLoS One* **2017,** *12* (4), e0175642, doi: 10.1371/journal.pone.0175642.

258. Conklin, B. R., Farfel, Z., Lustig, K. D., Julius, D. & Bourne, H. R., Substitution of three amino acids switches receptor specificity of Gqα to that of Giα. *Nature* **1993,** *363* (6426), 274-276, doi: 10.1038/363274a0.

259. Milligan, G. & Rees, S., Chimaeric G α proteins: Their potential use in drug discovery. *Trends Pharmacol Sci* **1999,** *20* (3), 118-124, doi: 10.1016/s0165-6147(99)01320-6.

260. Irannejad, R., Tomshine, J. C., Tomshine, J. R., Chevalier, M., Mahoney, J. P., Steyaert, J., Rasmussen, S. G., Sunahara, R. K., El-Samad, H., Huang, B., et al., Conformational biosensors reveal GPCR signalling from endosomes. *Nature* **2013,** *495* (7442), 534-538, doi: 10.1038/nature12000.

261. Lan, T.-H., Liu, Q., Li, C., Wu, G., Steyaert, J. & Lambert, N. A., BRET evidence that β2 adrenergic receptors do not oligomerize in cells. *Sci Rep* **2015,** *5* (1), 10166, doi: 10.1038/srep10166.

262. Che, T., English, J., Krumm, B. E., Kim, K., Pardon, E., Olsen, R. H. J., Wang, S., Zhang, S., Diberto, J. F., Sciaky, N., et al., Nanobody-enabled monitoring of κ opioid receptor states. *Nat Commun* **2020,** *11* (1), 1145, doi: 10.1038/s41467-020-14889-7.

263. Vasudevan, L. & Stove, C. P., A novel nanobody-based bio-assay using functional complementation of a split nanoluciferase to monitor μ-opioid receptor activation. *Anal Bioanal Chem* **2020,** *412* (29), 8015-8022, doi: 10.1007/s00216-020-02945-6.

264. Ring, A. M., Manglik, A., Kruse, A. C., Enos, M. D., Weis, W. I., Garcia, K. C. & Kobilka, B. K., Adrenaline-activated structure of β2-adrenoceptor stabilized by an engineered nanobody. *Nature* **2013,** *502* (7472), 575-579, doi: 10.1038/nature12572.

265. Kruse, A. C., Ring, A. M., Manglik, A., Hu, J., Hu, K., Eitel, K., Hübner, H., Pardon, E., Valant, C., Sexton, P. M., et al., Activation and allosteric modulation of a muscarinic acetylcholine receptor. *Nature* **2013,** *504* (7478), 101-106, doi: 10.1038/nature12735.

266. Huang, W., Manglik, A., Venkatakrishnan, A. J., Laeremans, T., Feinberg, E. N., Sanborn, A. L., Kato, H. E., Livingston, K. E., Thorsen, T. S., Kling, R. C., et al., Structural insights into μ-opioid receptor activation. *Nature* **2015,** *524* (7565), 315-321, doi: 10.1038/nature14886.

267. Sounier, R., Mas, C., Steyaert, J., Laeremans, T., Manglik, A., Huang, W., Kobilka, B. K., Déméné, H. & Granier, S., Propagation of conformational changes during μ-opioid receptor activation. *Nature* **2015,** *524* (7565), 375-378, doi: 10.1038/nature14680.

268. Che, T., Majumdar, S., Zaidi, S. A., Ondachi, P., McCorvy, J. D., Wang, S., Mosier, P. D., Uprety, R., Vardy, E., Krumm, B. E., et al., Structure of the nanobody-stabilized active state of the κ opioid receptor. *Cell* **2018,** *172* (1), 55-67.e15, doi: 10.1016/j.cell.2017.12.011.

269. Burg, J. S., Ingram, J. R., Venkatakrishnan, A. J., Jude, K. M., Dukkipati, A., Feinberg, E. N., Angelini, A., Waghray, D., Dror, R. O., Ploegh, H. L., et al., Structural biology. Structural basis for chemokine recognition and activation of a viral G protein-coupled receptor. *Science* **2015,** *347* (6226), 1113-1117, doi: 10.1126/science.aaa5026.

270. Wingler, L. M., McMahon, C., Staus, D. P., Lefkowitz, R. J. & Kruse, A. C., Distinctive activation mechanism for angiotensin receptor revealed by a synthetic nanobody. *Cell* **2019,** *176* (3), 479-490.e412, doi: 10.1016/j.cell.2018.12.006.

271. Koehl, A., Hu, H., Maeda, S., Zhang, Y., Qu, Q., Paggi, J. M., Latorraca, N. R., Hilger, D., Dawson, R., Matile, H., et al., Structure of the μ-opioid receptor-Gi protein complex. *Nature* **2018,** *558* (7711), 547-552, doi: 10.1038/s41586-018-0219-7.

272. Stoeber, M., Jullie, D., Li, J., Chakraborty, S., Majumdar, S., Lambert, N. A., Manglik, A. & von Zastrow, M., Agonist-selective recruitment of engineered protein probes and of GRK2 by opioid receptors in living cells. *Elife* **2020,** *9*, doi: 10.7554/eLife.54208.

273. Crilly, S. E., Ko, W., Weinberg, Z. Y. & Puthenveedu, M. A., Conformational specificity of opioid receptors is determined by subcellular location irrespective of agonist. *Elife* **2021,** *10*, doi: 10.7554/eLife.67478.

274. Martemyanov, K. A. & Garcia-Marcos, M., Making useful gadgets with miniaturized G proteins. *J Biol Chem* **2018,** *293* (19), 7474-7475, doi: 10.1074/jbc.H118.002879.

275. Conner, J. W., Poole, D. P., Jorg, M. & Veldhuis, N. A., New small molecule fluorescent probes for G protein-coupled receptors: Valuable tools for drug discovery. *Future Med Chem* **2021,** *13* (1), 63-90, doi: 10.4155/fmc-2019-0327.

276. Rajagopal, S., Rajagopal, K. & Lefkowitz, R. J., Teaching old receptors new tricks: Biasing seven-transmembrane receptors. *Nat Rev Drug Discov* **2010,** 9 (5), 373-386, doi: 10.1038/nrd3024.

277. Gundry, J., Glenn, R., Alagesan, P. & Rajagopal, S., A practical guide to approaching biased agonism at G protein coupled receptors. *Front Neurosci* **2017,** *11* (17), doi: 10.3389/fnins.2017.00017.

278. Hilf, G., Gierschik, P. & Jakobs, K. H., Muscarinic acetylcholine receptor-stimulated binding of guanosine 5'-O-(3-thiotriphosphate) to guanine-nucleotide-binding proteins in cardiac membranes. *Eur J Biochem* **1989,** *186* (3), 725-731, doi: 10.1111/j.1432-1033.1989.tb15266.x.

279. Wenzel-Seifert, K., Lee, T. W., Seifert, R. & Kobilka, B. K., Restricting mobility of Gsα relative to the β 2-adrenoceptor enhances adenylate cyclase activity by reducing Gsα GTPase activity. *Biochem J* **1998,** *334 (Pt 3)*, 519-524, doi: 10.1042/bj3340519.

280. Schneider, E. H. & Seifert, R., Histamine H4 receptor-RGS fusion proteins expressed in Sf9 insect cells: A sensitive and reliable approach for the functional characterization of histamine H4 receptor ligands. *Biochem Pharmacol* **2009,** *78* (6), 607-616, doi: 10.1016/j.bcp.2009.05.015.

281. Singh, J. K., Maniyar, R. C. & Shirsath, V. S., Development of time-resolved fluorescent based [EU]-GTP binding assay for selection of human histamine 3 receptor antagonists/inverse agonist: a potential target for Alzheimer's treatment. *Annals of neurosciences* **2012,** *19* (2), 71-75, doi: 10.5214/ans.0972.7531.12190205.

282. Panchalingam, S. & Undie, A. S., Optimized binding of [35S]GTPγS to Gq-like proteins stimulated with dopamine D1-like receptor agonists. *Neurochem Res* **2000,** *25* (6), 759-767, doi: 10.1023/a:1007553004615.

283. DeLapp, N. W., The antibody-capture [(35)S]GTPγS scintillation proximity assay: A powerful emerging technique for analysis of GPCR pharmacology. *Trends Pharmacol Sci* **2004,** *25* (8), 400-401, doi: 10.1016/j.tips.2004.06.003.

284. Koval, A., Kopein, D., Purvanov, V. & Katanaev, V. L., Europium-labeled GTP as a general nonradioactive substitute for [35S]GTP γ S in high-throughput G protein studies. *Anal Biochem* **2010,** *397* (2), 202-207, doi: 10.1016/j.ab.2009.10.028.

285. Remmers, A. E., Posner, R. & Neubig, R. R., Fluorescent guanine nucleotide analogs and G protein activation. *J Biol Chem* **1994,** *269* (19), 13771-13778.

286. Jameson, E. E., Roof, R. A., Whorton, M. R., Mosberg, H. I., Sunahara, R. K., Neubig, R. R. & Kennedy, R. T., Real-time detection of basal and stimulated G protein GTPase activity using fluorescent GTP analogues. *J Biol Chem* **2005,** *280* (9), 7712-7719, doi: 10.1074/jbc.M413810200.

287. Frang, H., Mukkala, V. M., Syystö, R., Ollikka, P., Hurskainen, P., Scheinin, M. & Hemmilä, I., Nonradioactive GTP binding assay to monitor activation of G protein-coupled receptors. *Assay Drug Dev Technol* **2003,** *1* (2), 275-280, doi: 10.1089/15406580360545080.

288. Rozwandowicz-Jansen, A., Laurila, J., Martikkala, E., Frang, H., Hemmilä, I., Scheinin, M., Hänninen, P. & Härmä, H., Homogeneous GTP binding assay employing QRET technology. *J Biomol Screen* **2010,** *15* (3), 261-267, doi: 10.1177/1087057109358921.

2. A Dynamic, Split-Luciferase-Based Mini-G Protein Sensor to Functionally Characterize Ligands at All Four Histamine Receptor Subtypes

Note: Prior to the submission of this thesis, the content of this chapter, except for minor changes, was published in collaboration with partners:

Höring, C.; Seibel, U.; Tropmann, K.; Grätz, L.; Mönnich, D.; Pitzl, S.; Bernhardt, G.; Pockes, S.; Strasser, A., A dynamic, split-luciferase-based mini-G protein sensor to functionally characterize ligands at all four histamine receptor subtypes. *Int J Mol Sci* **2020,** 21 (22), 8440, doi: 10.3390/ijms21228440.

The following experimental work was performed by co-workers:

Ulla Seibel-Ehlert:	Radioligand saturation binding experiments and [^{35}S]GTPγS binding assays at the H_1R
Dr. Katharina Tropmann:	Radioligand competition binding experiments

2.1. Introduction

G protein-coupled receptors (GPCRs) transduce external stimuli to intracellular events by the activation of heterotrimeric G proteins. Upon receptor activation, the heterotrimeric G protein binds to the receptor, which is followed by a GDP-GTP nucleotide exchange at the Gα subunit. The resulting conformational change of Gα promotes the uncoupling of the G protein from the receptor and the dissociation of the heterotrimer into a Gα monomer and a Gβγ dimer.[1-2] Both are then capable to modulate effector proteins inside the cell. Canonical GPCR-mediated signaling is determined by Gα, the subtypes of which target different membrane-bound effectors, such as phospholipase C (PLC),[3-4] and adenylyl cyclase (AC).[5-6] In drug discovery, GPCRs are the most studied drug targets and are addressed by more than 30% of approved drugs.[7] Fundamental criteria for successful drugs are a high binding affinity and potency at the target receptor, as well as a distinct pharmacological action ((full, partial, inverse) agonism, antagonism). The further downstream in the signaling cascade, the more pronounced the signal, irrespective of the ultimate cellular response. Thus, the characterization of the proximal functional response as a target-specific effect is desirable, particularly for lead-structure identification and bias analysis of compounds.

Classical methods have successfully focused on the key events of receptor-G protein interaction and G protein activation using radiolabeled GTP analogs ([^{35}S]GTPγS,[8-10] [γ-^{32}P]GTP[11-13]). Unfortunately, we have repeatedly experienced insufficient quality with batches of commercially available radiolabeled GTP analogs. For this reason, compounded by economic considerations, such as the increased cost of radioactive waste disposal, it may be preferable to implement a different proximal functional assay, both for routine testing and detailed pharmacological studies of ligand-GPCR interaction. Non-radioactive labels of GTP analogs, such as europium,[14] TAMRA, Cy3, and Cy5,[15] as well as the utilization of the commercial GTPase-Glo™ technique,[16] in which native GTP is converted to ATP, which is then involved in an enzyme reaction, allow for a fluorescent or bioluminescent readout. However, these methods are restricted to membrane preparations, cell homogenates or fixed cells.[16-17] Moreover, nucleotide exchange and GTP hydrolysis represent limiting steps according to the respective Gα subtype.[18] Modern FRET-/BRET-based G protein activation sensors monitoring the interaction of appropriate donor-acceptor pairs (GPCR and Gα/Gβγ[19], Gα and Gβγ[20] or Gβγ and a membrane anchor[21]) provide valuable insight into signaling kinetics and can visualize signal compartmentalization. However, for routine characterization of potential ligands, the application of these sensors is unfavorable due to the requirement for specialized equipment (e.g., multiple wavelength monitoring) and comprehensive expertise in performing the time-sensitive technique (millisecond timescale).

Additionally, the spectral properties of the donor/acceptor pairs (intensity and spectral overlap of the excitation and emission wavelengths) can affect the signal amplitude.[18] This is an issue in case of weakly expressed GPCRs.

In 2017, a new class of minimal G protein chimeras (mini-G) was developed.[22] All mini-G constructs are surrogates of the Gαs subunit and comprise the following key features: Minimization to the GTPase domain, a mutation that uncouples the binding to active state GPCRs from nucleotide exchange, and the deletion of the N-terminal membrane anchor as well as the Gβγ binding site. By replacing the α5 helix of the minimal Gαs protein (mGs) with the respective sequence of other Gα subunits, mini-G proteins covering all major Gα families were derived and appropriate coupling specificities were demonstrated.[22-23] The application of BRET and split-luciferase complementation (SLC) techniques to GPCRs and mini-G proteins has created new G protein sensors that monitor functional responses in real-time.[23-31] Of particular note, the dynamic assay ranges benefited from the cytosolic nature of the mini-G proteins, as native, membrane-anchored G proteins produce high baseline values due to their closer proximity to membrane-bound GPCRs.[23-25]

The aim of this study was to implement a modern, live cell-based assay to study the molecular signaling mechanisms of putative histamine receptor agonists and antagonists. Moreover, the method needed to provide a proximal readout with improved signal amplitudes, which was essential for the weakly expressed H_4R.[32] For these purposes, the mini-G protein concept was considered suitable. We applied the split-NanoLuc technology[33] to all four histamine receptor subtypes (H_1R, H_2R, H_3R and H_4R) and the respective (chimeric) mini-G proteins mGsq, mGs and mGsi, where mGsq and mGsi represent chimeras of mGs with respective α5 helices of $G\alpha i_1$ and Gαq.[22] The present study reports on the evaluation of mini-G protein sensors for the entire histamine receptor family, including functional characterization of standard histamine receptor ligands.

2.2. Materials and Methods

2.2.1. Materials

Dulbecco's modified Eagle's medium (DMEM) was purchased from Sigma-Aldrich (Taufkirchen, Germany) and Leibovitz' L-15 medium (L-15) from Fisher Scientific (Nidderau, Germany). FCS, trypsin/EDTA and geneticin (G418) were from Merck Biochrom (Darmstadt, Germany), whereas puromycin was from InvivoGen (Toulouse, France) and furimazine from Promega (Mannheim, Germany). The pcDNA3.1 vector was from Thermo Scientific (Nidderau, Germany) and the pIRESpuro3 vector was a kind gift from Prof. Dr. Gunter Meister (University of Regensburg). Histamine dihydrochloride (his) was purchased from Tokyo Chemical Industry (Eschborn, Germany), whereas 4-methylhistamine dihydrochloride (4mhis), mepyramine maleate (mep), imetit dihydrobromide (imet), immepip dihydrobromide (immep), thioperamide maleate (thio), clobenpropit dihydrobromide (clob) and A943931 dihydrochloride (A943931) were from Tocris Bioscience (Bristol, United Kingdom). N^{α}-methylhistamine dihydrochloride (Namh), betahistine dihydrochloride (betahis), diphenhydramine hydrochloride (dph), maprotiline hydrochloride (map), cyproheptadine hydrochloride sesquihydrate (cyp), amthamine dihydrobromide (amt), dimaprit dihydrochloride (dim), cimetidine (cim), famotidine (fam) and ranitidine hydrochloride (ran) were purchased from Sigma. Histaprodifen (histapro),[34] suprahistaprodifen (suprahis),[34] UR-KUM530 (KUM530),[12] impromidine (impro),[35] UR-PI294 (PI294),[36] VUF8430 (VUF8430),[37] and JNJ7777120 (JNJ)[38] were synthesized in-house according to published procedures. Pitolisant hydrochloride (pito) was kindly provided by Prof. Dr. Katarzyna Kiec-Kononowicz (Jagiellonian University, Krakow). All ligands were dissolved, according to their physicochemical properties. Preferably, stock solutions of the ligands were prepared in Millipore water, except for histaprodifen (histapro), suprahistaprodifen (suprahis), maprotiline (map), cimetidine (cim) and famotidine (fam). In these cases, DMSO (Merck) was (proportionally) used as solvent (DMSO/H_2O: histapro, suprahis: 50/50; map: 30/70; cim, fam: 100% DMSO).

2.2.2. Molecular Cloning

The human codon-optimized cDNA fragments encoding the mini-G proteins mGs, mGsi and mGsq (corresponding to mini-Gs393, mini-Gs/i43 and mini-Gs/q71 published by Nehmé et al.,[22] cf. Appendix Figure A1), were synthesized by Eurofins Genomics (Eurofins Genomics LLC, Ebersberg, Germany). Plasmids containing the split-NanoLuc fragments (NlucN: 159 N-terminal NanoLuc amino acids; NlucC: 11 C-terminal NanoLuc amino acids) were from Promega and cDNAs encoding the histamine receptors were purchased from the Missouri cDNA research center (Rolla, MO, USA). All cDNAs were amplified by PCR and subcloned into vector backbones by standard molecular cloning techniques. For this purpose, a set of pIRESpuro3 vectors was generated

encoding the respective mini-G protein, which was N-terminally fused to the large split-luciferase fragment (NlucN) separated by a flexible glycine-serine-linker (encoding -GSSGGGGSGGGGSS-).[39-40] The sequence encoding the H_1R-NlucC described by Littmann et al. (2019) was subcloned into pcDNA3.1 using the restriction enzymes *Hin*dIII and *Sac*II, and the receptor sequence was then replaced by either the H_2R, H_3R or H_4R gene using *Hin*dIII and *Xba*I.[39] The optimal arrangement of a split-luciferase system to study the interaction of GPCRs and intracellular proteins of interest (GPCR-NlucC and NlucN-protein) was reported previously.[23,39] Plasmid DNA was quantified by UV-Vis absorbance using a NanoDrop spectrophotometer (ThermoFisher, Braunschweig, Germany). All sequences were verified by sequencing performed by Eurofins Genomics.

2.2.3. Cell Culture

HEK293T cells were a kind gift from Prof. Dr. Wulf Schneider (Institute for Medical Microbiology and Hygiene, Regensburg, Germany) and cultured in DMEM supplemented with 10% FCS at 37 °C in a water-saturated atmosphere containing 5% CO_2. Cells were periodically inspected for mycoplasma contamination by means of the Venor GeM Mycoplasma Detection Kit (Minerva Biolabs, Berlin, Germany) and proven negative.

2.2.4. Generation of Stable Transfectants

To generate stable cell lines, wildtype HEK293T cells were stepwise transfected with a pIRESpuro3 vector encoding either the NlucN-mGs, NlucN-mGsi or NlucN-mGsq fusion protein, and with the respective pcDNA3.1 plasmid encoding the histamine $H_{1,2,3,4}$R-NlucC fusion protein according to the XtremeGene HP transfection protocol (Merck). The cells were then cultured in DMEM supplemented with 10% FCS, 1 µg/mL puromycin and 600 µg/mL G418 for sustained selection pressure.

2.2.5. Generation of Transient Transfectants

Adjusted to a cell density of 0.3 x 10^6 cells/mL, HEK293T cells were seeded into a 6-well cell culture plate (Sarstedt, Nümbrecht, Germany) and allowed to attach overnight. The next day, the cells were transfected using linear polyethyleneimine (PEI, 1 mg/mL in PBS; 1:5 ratio (2 µg DNA: 10 µL PEI)) and incubated for another 48 h to allow for adequate protein expression. For mini-G protein recruitment assays and radioligand competition binding experiments, we applied a constant amount of 2 µg of total DNA per 6-well (total volume of 2 mL) comprising 1 µg of pcDNA3.1 $H_{1/2/3}$R-NlucC and increasing amounts of the pIRESpuro3 NlucN-mGsq/-mGs/-mGsi DNA (0.125, 0.25, 0.5, or 1.0 µg). To ensure a uniform transfection efficiency, the empty pIRESpuro3 vector was co-transfected as mock DNA (0.875, 0.75, 0.5 µg or none). For Western blot analysis of the mini-G protein expression, the cells were transfected with a total amount of 2 µg DNA comprising 0.125,

0.25, 0.5 or 1.0 µg of the pIRESpuro3 NlucN-mGsq/-mGs/-mGsi and 1.875, 1.750, 1.5 and 1.0 µg, respectively, of the empty pIRESpuro3 vector as mock DNA.

2.2.6. Western Blot Analysis

Cells were lysed using a RIPA lysis buffer (50 mM Tris, 0.1% sodium dodecyl sulfate, 0.5% sodium deoxycholate, 1% Triton X-100, 150 mM NaCl) supplemented with SIGMAFAST protease inhibitor cocktail tablets according to the manufacturer's protocol (Sigma-Aldrich). Lysates (15 µg protein) and 10 µL of the Precision Plus ProteinTM Dual Color Standard (Bio-Rad, Feldkirchen, Germany) were loaded to an 8–16% Novex Tris-glycine polyacrylamide gel (Thermo Scientific) and SDS-page was performed at 225 V for 1 h. Thereafter, the proteins were blotted on a nitrocellulose membrane (0.2 A, 1 h). By incubation with 5% skim milk powder in phosphate-buffered saline supplemented with 0.05% Tween 20 (PBS-T) for 1 h at RT, nonspecific binding sites of the membrane were blocked. After three washing steps with PBS-T, blots were incubated overnight at 4 °C with the primary antibodies α-Nluc (1:5000; in PBS-T; polyclonal, produced in rabbit, kindly provided by Promega) and α-vinculin (1:500; in PBS-T; monoclonal; MAB6896, produced in mouse, R&D Systems Inc., MN, USA). After additional three washing steps on the next day, the membranes were incubated with the HRP-conjugated secondary antibodies (raised against IgG, respectively) α-rabbit (1:10,000 in PBS-T; sc-2313, produced in donkey, Santa Cruz, TX, USA) and α-mouse (1:100,000 in PBS-T; A0168, produced in goat; Sigma-Aldrich) for 3 h at RT. The blots were washed three times with PBS-T and developed using the Clarity Western ECL substrate (Bio-Rad, Feldkirchen, Germany). Subsequently, the colorimetric and luminescent images of the stained blots were captured using a ChemiDoc MP imager (Bio-Rad).

2.2.7. Mini-G Protein Recruitment Assays

The day before the experiment, cells were detached by trypsinization (0.05% trypsin, 0.02% EDTA in PBS) and centrifuged (700 g, 5 min). Subsequently, the cells were resuspended in L-15 supplemented with 10 mM HEPES (Serva, Heidelberg, Germany) and 5% FCS. Thereafter, 100.000 cells per well were seeded onto a white flat-bottom 96-well microtiter plate (Brand GmbH + CoKG, Wertheim, Germany) and incubated at 37 °C in a water-saturated atmosphere without additional CO_2 overnight. The substrate furimazine and all ligands were diluted in L-15, and shortly before the experiment, 10 µL of the substrate were added to the cells (final dilution 1:1000). Then, the plate was transferred to a pre-heated (37 °C) EnSpire plate reader (Perkin Elmer Inc., Rodgau, Germany). After recording the basal luminescence for 15 min, 10 µL of the agonist serial dilutions were added to the cells (final volume: 100 µL) and luminescence traces were recorded for 45 min (agonist mode). For antagonist assays, after basal luminescence was measured, cells were incubated with antagonists at different concentrations for 15 min. To elicit split-NanoLuc

complementation by mini-G protein recruitment, the reference agonist histamine was added to the cells at a concentration of approximately EC_{80} (H_1R: 10 µM, $H_{2\text{-}4}R$: 1 µM), previously determined in the agonist mode for each system. Overall, luminescence was captured with an integration time of 0.1 s per well. Data were analyzed using GraphPad Prism8 software (San Diego, CA, USA). The relative luminescence units (RLU) were corrected for slight inter-well variation caused by differences in cell density and substrate concentration, as well as for baseline drift, by dividing all data by the mean luminescence intensity of the respective L-15 control. AUCs of the luminescence traces within45 min ($AUC_{45\ min}$) were calculated for each concentration and normalized to the maximum response of 100 µM histamine (100% control) and L-15 (0% control). The logarithmic ligand concentrations were fitted against the normalized intensities with variable slope (log(c) vs. response – variable slope (four parameters)). The fit yielded pEC_{50} and E_{max} values in the case of agonists, and pIC_{50} values in the case of antagonists, which were used to calculate pK_b values according to the Cheng-Prusoff-equation.[41] In order to assess Z' factors, the baseline-corrected relative luminescence units (RLU) of 100 µM histamine and L-15 were inter-well corrected and AUCs were used for the calculation of means and standard deviations.[42]

Specifically, Z' factors were calculated according to the following equation:

$$Z' = 1 - \frac{3(\sigma_{his} + \sigma_{L-15})}{|\mu_{his} - \mu_{L-15}|}$$

where, σ_{his} and σ_{L-15} represent the standard deviation and μ_{his} and μ_{L-15} the means of $AUC_{45\ min}$ obtained for wells containing 100 µM histamine or L-15 buffer.

Significant differences in the efficacies obtained in the mini-G protein recruitment assay were assessed using a one-sample t-test (N = 5, α = 0.05). When investigating the influence of the mini-G protein expression level, significant differences between AUCs and pEC_{50} values were calculated using one-way ANOVA followed by Tukey's multiple comparison test (N = 5, α = 0.05).

2.2.8. Radioligand Binding Experiments

Radioligand saturation binding experiments were performed using intact HEK293T cells co-expressing either NlucN-mGsq/H_1R-NlucC, NlucN-mGs/H_2R-NlucC, NlucN-mGsi/H_3R-NlucC or NlucN-mGsi/H_4R-NlucC. The following radioligands were used to verify the receptor expressions: [^{3}H]mepyramine (α_s = 20 Ci/mmol, Hartmann Analytics GmbH, Braunschweig, Germany) for the H_1R, [^{3}H]UR-DE257[43] (α_s = 32.9 Ci/mmol) for the H_2R and [^{3}H]UR-PI294[44] (α_s = 93.3 Ci/mmol) for the H_3R and H_4R. The specific binding of each radioligand was determined by subtracting the non-specific binding from the corresponding total binding. The cells were incubated with various concentrations of the radioligands in the absence (L-15) (total binding) or presence of a competitor at a final concentration of 10 µM (nonspecific binding). As competitors,

diphenhydramine for the H_1R, famotidine for the H_2R, thioperamide for the H_3R and histamine for the H_4R were applied. Radioligand competition binding experiments were performed using intact HEK293T cells expressing NlucN-mGs and H_2R-NlucC fusion proteins. The cells were incubated with 50 nM [^{3}H]UR-DE257 and with the ligands in serial dilution and with L-15 (negative control). The non-specific binding of the radioligand was determined in the presence of famotidine at a final concentration of 10 µM and subtracted from all values.

For both, radioligand saturation and competition binding experiments, all (radio)ligand dilutions were prepared 10-fold concentrated in L-15 and 10 µL/well were transferred to a round bottom polypropylene 96-well microtiter plate (Greiner Bio-One, Frickenhausen, Germany). The cells were detached by trypsinization (0.05% trypsin + 0.02% EDTA), harvested by centrifugation (700 g, 5 min) and resuspended in L-15. The cells were adjusted to a density of 1.0 x 10^6 cells/mL and 80 µL of the cell suspension were added to each well (final assay volume: 100 µL). Then, the cells were incubated at room temperature under shaking ($H_{1,3,4}R$: 120 min, H_2R: 60 min) and then collected by filtration and washed with ice-cold PBS using a 96-well harvester (Brandel Inc., Unterföhring, Germany). The cell-associated radioactivity was measured by liquid scintillation counting, as previously described.[45]

All data were analyzed using GraphPad Prism8 software. In the case of saturation binding experiments, all data were best fitted to a one-site saturation binding model (one site – total and nonspecific binding; one site – specific binding) yielding K_d values. For competition binding experiments, data of the agonist histamine were best fitted to a two-sites competition binding model (two sites – fit logIC$_{50}$) yielding pIC$_{50,high}$ and pIC$_{50,low}$. Except, competition binding data of histamine using cells transiently transfected with the H_2R alone and data of the antagonist famotidine obtained at cells stably co-expressing the H_2R and mGs were fitted to the one-site three parameter logistic fit (one-site – fit logIC$_{50}$) to determine pIC$_{50}$ values. Obtained pIC$_{50}$ values (pIC$_{50}$, pIC$_{50,high}$, pIC$_{50,low}$) were then used to calculate pK_b values according to the Cheng-Prusoff-equation.[41]

2.3. Results

2.3.1. Principle and Characteristics of the Mini-G Protein Recruitment Assay

To study G protein signaling in response to histamine receptor ligands, the split-NanoLuc technology[33] was applied to the human histamine H_1, H_2, H_3 and H_4 receptor subtypes ($H_{1,2,3,4}$R-NlucC) and the corresponding mini-G proteins mGsq, mGs and mGsi (NlucN-mini-G). Respective mini-G protein sequences are given in the Appendix (Figure A1). Upon receptor activation, the mini-G protein was recruited by the receptor leading to the formation of a functional NanoLuc (Figure 2.1A). Thus, agonist concentration-dependent luminescence signals were obtained in the presence of the substrate furimazine (Figure 2.1B). To investigate antagonists, the response of the reference agonist histamine at EC_{80} concentration (H_1R: 10 µM, $H_{2\text{-}4}$R: 1 µM) was measured after a pre-incubation period of the respective antagonists. To verify the histamine receptor expression, radioligand saturation binding experiments were performed, and adequate binding of [^{3}H]mepyramine to the H_1R co-expressed with mGsq, [^{3}H]UR-DE257 to the H_2R co-expressed with mGs and [^{3}H]UR-PI294 to the H_3R and H_4R each co-expressed with mGsi were observed (cf. Appendix, Figure A2 and Table A1).

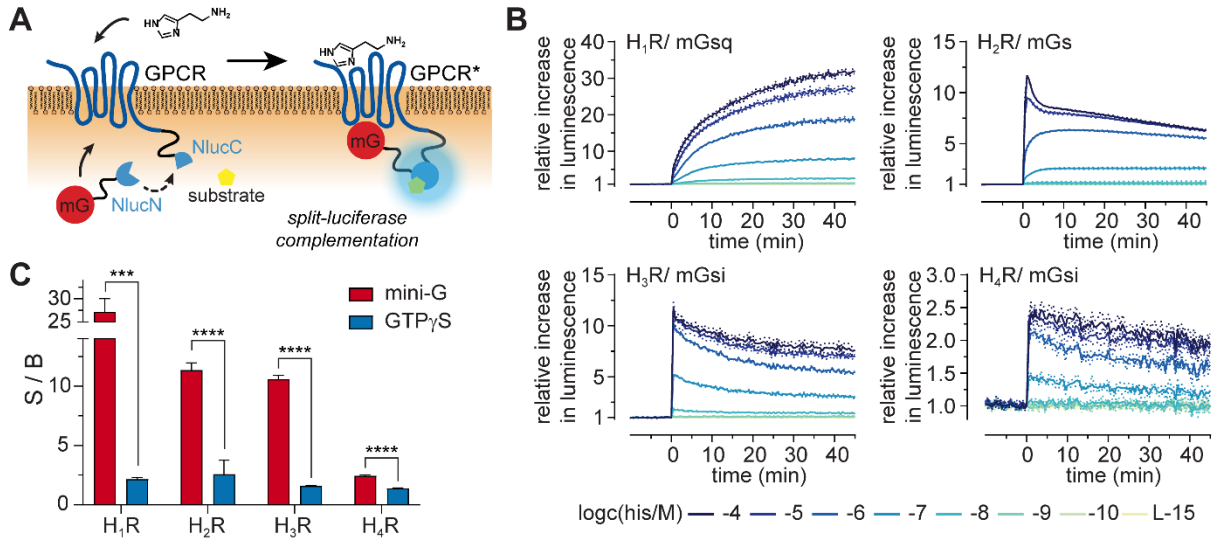

Figure 2.1. Principle of the mini-G protein recruitment assay and signals obtained at the $H_{1\text{-}4}$R. A) Scheme of the mini-G protein recruitment assay. Split-NanoLuc fragments NlucC and NlucN were applied to $H_{1\text{-}4}$R (C-terminus) and mini-G proteins (mini-G; N-terminus), respectively. Upon receptor activation, the mini-G protein is recruited to the GPCR facilitating split-luciferase complementation. The functional enzyme formed subsequently catalyzes the oxidation of the substrate resulting in luminescent signals in an agonist concentration-dependent manner. B) Representative luminescence traces of the mini-G protein recruitment of mGsq to H_1R, mGs to H_2R and mGsi to H_3R and H_4R. Baseline and inter-well corrected luminescence traces of histamine at various concentrations and the assay medium Leibovitz's L-15 (L-15) as negative control are plotted. C) Plotted signal-to-background ratios (S/Bs) were calculated from 100% and 0% values of the respective assays, representing top and bottom values of the concentration response curves. For the mini-G protein recruitment assay (mini-G), peak or plateau values of the response to 100 µM histamine (100%) and L-15 (0%) are displayed, whereas for the [^{35}S]GTPγS binding assay (GTPγS) responses to 1 mM histamine for $H_{1,2}$R or to 10 µM histamine for $H_{3,4}$R (100%) and H_2O (0%) were taken. Presented data are the means ± SEM of at least five independent experiments ($N \geq 5$), each performed in triplicate. Statistical significance of S/B values (****: $p < 0.0001$) was assessed using a Welch's two-sample t-test for unpaired samples.

2.3.2. Kinetics and Dynamic Ranges of Mini-G Protein Recruitment

The dynamic split-NanoLuc approach allowed for monitoring the G protein response to a ligand in real-time, demonstrating differences in kinetics for each receptor and mini-G protein combination upon histamine stimulation (Figure 2.1B). The mGsq recruitment to the H_1R is comparatively slow, leading to a plateau, whereas the luminescence signals of the mGs and mGsi recruitment to the H_2R, H_3R and H_4R reach very sharp maxima and then flatten gradually. However, since deletions of the membrane anchor and the Gβγ binding site were among the key modifications in the development of the utilized mini-G proteins, one can speculate that kinetics observed might differ to the behavior of endogenous heterotrimeric G proteins. More specifically, mini-G protein recruitment signaling is composed of a series of molecular processes that include ligand binding, receptor activation, split-luciferase complementation, and substrate oxidation, all of which can affect the kinetics of signal output. Nevertheless, tracing given luminescent traces in real-time upon receptor activation could help to unveil differences in receptor regulation (e.g., receptor desensitization and internalization) when exposed to different ligands.[46-47] Moreover, as GPCR conformation specific probes mini-G protein sensors may also serve as useful tools to supplement studies of ligand binding kinetics, such as the determination of association and dissociation rate constants ($k_{on/off}$) and residence time always with respect to a reference ligand.[48-49]

At this point it should be mentioned that, in order to uniformly compare signal-to-background (S/B) ratios, the [^{35}S]GTPγS binding assay had to be implemented for the H_1R, the method of which is described in the Appendix (Method A1). Thus, it could be demonstrated that mini-G protein recruitment assay signal amplitudes were significantly increased at all four receptor subtypes compared to [^{35}S]GTPγS binding assays (Figure 2.1C). Remarkably, in the case of the H_1R, the S/B ratio was up to 12-fold higher in the mini-G protein recruitment assay than in the [^{35}S]GTPγS binding assay (27.16 ± 2.89 (mini-G) vs. 2.16 ± 0.16 (GTPγS); Figure 2.1C). Such favorable S/B ratios should be beneficial in determining agonist efficacy and allow for a reduction in agonist concentration when exploring antagonists.

To evaluate the overall assay quality, Z' factors were calculated as a dimensionless figure of statistical effect size. Classically, the Z' factor has been used in the validation process of HTS methods, as it numerically evaluates the dynamic range of an assay and its ability to identify biologically active molecules.[42] For all four receptor subtypes, Z' factors that were between 0.5 and 1.0 were obtained (H_1R: 0.78 ± 0.07, H_2R: 0.85 ± 0.02, H_3R: 0.79 ± 0.04, H_4R: 0.68 ± 0.05; cf. Appendix Figure A3) indicating a sufficient separation of maximal effect and baseline values. Consequently, the presented mini-G protein recruitment assays can be classified as excellent screening methods.[42]

2.3.3. Mini-G Protein Recruitment-Based Investigation of Histamine Receptor Ligands

To demonstrate the applicability of these novel assays for future drug research, a set of standard ligands was tested (cf. Appendix, Figure A4) that are described as (inverse) agonists or antagonists. First, the mini-G protein recruitment approach was validated for the investigation of agonists and at all four receptor subtypes a multifaceted spectrum of pharmacological actions was obtained (Figure 2.2, Tables 2.1-2.4). Efficacies ranged from weak partial agonism, discovered for histaprodifen at the H_1R (E_{max} = 33 ± 2.0%) and PI294 at the H_1R and H_3R (E_{max} = 27 ± 0.5% and 11 ± 1.1%, respectively), to full agonism, demonstrated by e.g., N^{α}-methylhistamine at the H_1R (E_{max} = 93 ± 5.3%), dimaprit at the H_2R (E_{max} = 97 ± 1.1%) and histamine (by definition: 100%) at all four receptor subtypes (Tables 2.1–2.4). Strikingly, the efficacies of KUM530 at the H_1R (E_{max} = 112 ± 1.0%) and N^{α}-methylhistamine at the H_3R (E_{max} = 111 ± 1.6%) were significantly higher ($\alpha < 0.05$) as those of the endogenous ligand histamine (Tables 2.1, 2.3), which is hypothesized as 'superagonism'.[53] Similar results were previously observed for KUM530 and were suggested to originate from a differing orientation in the binding pocket of the H_1R compared to histamine.[54-55] In contrast, N^{α}-methylhistamine has always been reported as a full agonist at the H_3R.[10] It is worth mentioning that, although all orders of potency of the studied agonists were in good agreement with literature data (Figure 2.2A, Tables 2.1–2.4), agonists probed at the H_3R and the H_4R generally displayed lower potencies (up to one magnitude) than in published [^{35}S]GTPγS binding and steady-state GTPase activity assays (Tables 2.3, 2.4). Earlier, a similar phenomenon has been observed with agonists studied in NanoBRET binding assays using intact cells expressing either the H_3R or the H_4R, as well as with agonists investigated with an H_3R conformational sensor.[50-52] It is likely that such differences rise from an altered GPCR - G protein-guanine nucleotide composition in intact cells resulting in a more transient formation of the ternary complex compared to cell membrane preparations or cell homogenates thus reducing the occurrence of high-affinity binding sites.[17]

In addition, the application of mini-G protein sensors was extended for the characterization of antagonists. Therefore, after pre-incubation with the antagonists the reference agonist histamine was added to the cells at a concentration of approximately EC_{80} (H_1R: 10 µM, $H_{2\text{-}4}R$: 1 µM) to elicit split-NanoLuc complementation after mini-G protein recruitment. In this setting, standard antagonists displayed expected pK_b values at all receptor subtypes (Figure 2.2B, Tables 2.1–2.4). Only in the cases of the tricyclic H_1R antagonists maprotiline (pK_b = 10.33 ± 0.08) and cyproheptadine (pK_b = 10.04 ± 0.11), we determined up to two magnitudes higher pK_b values than reported (Table 2.1).

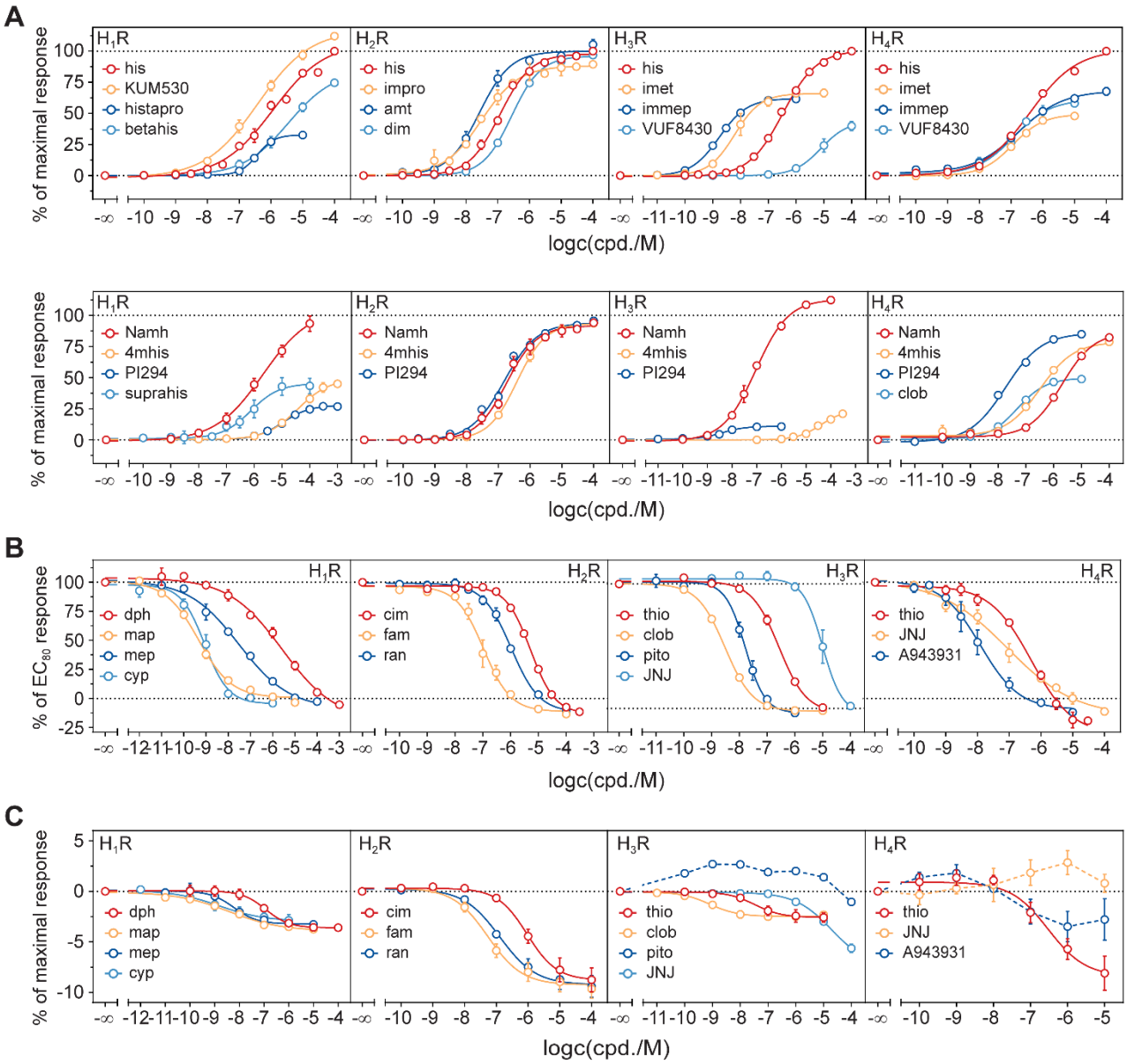

Figure 2.2. Concentration response curves of histamine receptor ligands obtained in the mini-G protein recruitment assay. Agonists were tested in the assay agonist mode (A) and antagonists or rather inverse agonists were tested in the assay antagonist (B) and agonist (C) modes, respectively. HEK293T cells stably co-expressing a combination of either the H_1R-NlucC/NlucN-mGsq, H_2R-NlucC/NlucN-mGs, H_3R-NlucC/NlucN-mGsi or H_4R-NlucC/NlucN-mGsi were used. In the agonist mode, ligands were added to the cells and split-luciferase complementation (SLC) enabled by mini-G protein recruitment to the activated receptor was assessed. In the antagonist mode, cells were pre-incubated with the ligand and SLC was assessed after the addition of histamine (H_1R: 10 µM, $H_{2\text{-}4}$R: 1 µM). Data were normalized to L-15 as solvent control (0%) and to maximal responses elicited by 100 µM histamine for experiments conducted in the agonist mode and 10 µM (H_1R) or 1 µM histamine ($H_{2\text{-}4}$R) for assays conducted in the antagonist mode (100%). Data represent means ± SEM from at least three independent experiments ($N \geq 3$), each performed in triplicate.

Table 2.1. Potencies (pEC_{50}/pK_b) and efficacies (E_{max}) of ligands at the H_1R explored in the mini-G protein recruitment assay. Data represent means ± SEM of at least three independent experiments ($N \geq 3$), each performed in triplicate. Statistical differences (*) of $E_{max} > 100\%$ or rather $E_{max} < 0\%$ were tested using a one-sample t-test ($\alpha = 0.05$). Functional data obtained from [^{35}S]GTPγS and steady-state GTPase assays and ligand binding affinities (pK_i) determined in radioligand competition binding assays are included for comparison.

	Mini-G Protein Recruitment		GTPγS[a]/GTPase[b]		Competition Binding[c]
Cpd.	pEC_{50}/(pK_b) ± SEM	E_{max} ± SEM [%]	pEC_{50}/(pK_b)	E_{max} [%]	pK_i
his	5.94 ± 0.12	100	5.21 ± 0.06[a] 6.92[b,12]	100[a] 100[b,12]	5.62[12]
KUM530	6.41 ± 0.12	112 ± 1.0*	6.22 ± 0.10[a] 7.75[c,55]	95 ± 5.7[a] 94[c,55]	6.43[55]
betahis	5.49 ± 0.13	75 ± 2.0	5.84[d,56]	86[d,56]	
histapro	6.42 ± 0.02	33 ± 2.0	5.86 ± 0.07[a] 6.95[b,12]	31 ± 2.8[a] 62[b,12]	6.47[12]
Namh	5.53 ± 0.10	93 ± 5.3			
4mhis	4.41 ± 0.12	45 ± 1.6	4.80[e,57]	90[e,57]	
PI294	4.88 ± 0.09	27 ± 0.5	5.46[f,36]	30[f,36]	
suprahis	6.14 ± 0.14	43 ± 5.1	6.83[b,12]	64[b,12]	6.58[12]
dph	6.95 ± 0.04 (6.53) ± 0.17	-4 ± 0.04*	(6.98) ± 0.07[a] (7.81)[d,56]		7.40[54]
map	8.36 ± 0.11 (10.33) ± 0.08	-4 ± 0.2*	(8.54)[g,58]		8.50[54]
mep	8.3 ± 0.13 (8.63) ± 0.08	-3 ± 0.2*	(8.00) ± 0.17[a], (8.25)[d,56]		8.39[54] 8.7[59]
cyp	8.85 ± 0.28 (10.04) ± 0.11	-3 ± 0.5*	(8.72)[d,56]		8.63[54]

Reference data are taken from (unless otherwise stated, E_{max} values refer to histamine = 100%): [a]functional [^{35}S]GTPγS binding assays using *Sf*9 cells co-expressing either hH_1R, Gαq, Gβ$_1$ and Gγ$_2$ (cf. Appendix, Method A1). [b]functional [^{32}P]GTPase activity assays using membrane preparations of *Sf*9 cells co-expressing hH_1R and RGS4.[12,36,55-58] [c][^{3}H]mepyramine displacement assays using *Sf*9 cells co-expressing hH_1R and RGS4,[12,55] HEK293T hH_1R CRE-Luc cells,[54] or whole cell homogenates of COS-7 cells expressing hH_1R.[59]

In the past, histamine receptors were frequently reported to be constitutively active in recombinant systems.[60-63] Thus, the inverse agonistic potential of antagonists was assessed in the mini-G protein recruitment assay revealing that nearly all investigated antagonists significantly reduced the basal activity of the receptors, except for H_4R, in a concentration-dependent manner (Figure 2.2C, Tables 2.1–2.4). However, in the studied systems, the maximal inverse efficacies were relatively small when normalized to 100 µM histamine (H_1R: -4%, H_2R: -10%, H_3R: −6%, H_4R: −8%). Notably, the constitutive activity of Gi-coupled H_3R and H_4R was less pronounced in mini-G protein recruitment assays than in [^{35}S]GTPγS binding or GTPase activity assays,[9-10,64-65] consistent with the earlier hypothesis that fewer high-affinity states of these receptors are formed in intact cells than in membrane preparations because of an altered nucleotide composition.[17]

Table 2.2. Potencies (pEC_{50}/pK_b) and efficacies (E_{max}) of ligands at the H_2R explored in the mini-G protein recruitment assay. Data represent means ± SEM of at least three independent experiments ($N \geq 3$), each performed in triplicate. Statistical differences (*) of $E_{max} < 0\%$ were tested using a one-sample t-test ($\alpha = 0.05$). Functional data obtained in steady-state GTPase assays and ligand binding affinities (pK_i) determined in radioligand competition binding assays are included for comparison.

	Mini-G Protein Recruitment		GTPase[a]		Competition Binding[b]
Cpd.	pEC_{50}/(pK_b) ± SEM	E_{max} ± SEM [%]	pEC_{50}/(pK_b)	E_{max} [%]	pK_i
his	6.93 ± 0.05	100	6.00[11]	100[11]	6.27[43]
impro	7.51 ± 0.02	90 ± 1.4	6.80[11]	82[11]	6.3[66]
amt	7.57 ± 0.10	105 ± 3.5	6.72[11]	85[11]	6.61[43]
dim	6.56 ± 0.02	97 ± 1.1	6.04[11]	91[11]	4.6[66]
Namh	6.74 ± 0.08	94 ± 1.4			
4mhis	6.41 ± 0.05	94 ± 2.5	5.54[57]	101[57]	5.1[67]
PI294	6.83 ± 0.07	96 ± 0.7	6.43[36]	83[36]	
cim	6.02 ± 0.03 (6.26) ± 0.02	-9 ± 1.1*	(5.77)[11]	−8[11]	6.2[66]
fam	7.27 ± 0.07 (7.99) ± 0.12	-10 ± 0.9*	(7.32)[11]	−1[11]	7.8[66] 6.87[43]
ran	6.95 ± 0.11 (6.97) ± 0.01	-9 ± 1*	(6.08)[11]	−9[11]	7.1[66] 5.76[43]

Reference data are taken from (unless otherwise stated, E_{max} values refer to histamine = 100%): [a]functional [^{32}P]GTPase activity assays using membrane preparations of *Sf*9 cells expressing a hH_2R-Gαs fusion protein.[11,36,57] [b]Radioligand competition binding experiments using [^{3}H]UR-DE257 with membrane preparations of *Sf*9 cells expressing a hH_2R-Gαs fusion protein,[43] or [^{125}I]iodoaminopotentidine with membrane preparations of CHO cells expressing the hH_2R.[66-67]

Table 2.3. Potencies (pEC_{50}/pK_b) and efficacies (E_{max}) of ligands at the H_3R explored in the mini-G protein recruitment assay. Data represent mean values ± SEM of at least three independent experiments ($N \geq 3$), each performed in triplicate. Statistical differences (*) of E_{max} > 100% or rather E_{max} < 0% were tested using a one-sample t-test ($\alpha = 0.05$). Functional data obtained in [^{35}S]GTPγS and steady-state GTPase assays and ligand binding affinities (pK_i, pK_d) determined in radioligand competition/saturation binding assays are included for comparison.

	Mini-G Protein Recruitment		GTPγS[a]/GTPase[b]		Competition Binding[c]
Cpd.	pEC_{50}/(pK_b) ± SEM	E_{max} ± SEM [%]	pEC_{50}/(pK_b)	E_{max} [%]	pK_i/(pK_d)[d]
his	6.48 ± 0.04	100	7.3[a,9]	89[a,9]	7.96[c,44]
imet	8.16 ± 0.18	67 ± 2.0	8.6[a,9]	80[a,9]	8.8[c,67]
immep	8.78 ± 0.04	62 ± 0.7	8.8[a,9]	77[a,9]	9.3[c,67]
VUF8430	5.10 ± 0.13	40 ± 3.1			6.0[c,37]
Namh	7.02 ± 0.08	111 ± 1.6*	7.9[a,9]	100[a,9]	8.4[c,67]
4mhis	4.51 ± 0.06	17 ± 1.5			
PI294	8.41 ± 0.06	11 ± 1.1	8.80[b,36]	39[b,36]	(8.96)[d,44]
thio	7.41 ± 0.04 (7.18) ± 0.07	-3 ± 0.4*	6.9[a,9]	−52[a,9]	7.42[c,44]
clob	9.03 ± 0.10 (9.11) ± 0.04	-3 ± 0.2*	9.14[b,10] (9.28)[a,37]	−137[b,10]	9.34[c,44]
JNJ	< 5 (5.44) ± 0.01	-6 ± 0.3*			5.29[c,68]
pito	(8.40) ± 0.05		(9.80)[a,69]		8.57[c,69]

Reference data are taken from (unless otherwise stated, E_{max} values refer to histamine = 100%): [a]functional [^{35}S]GTPγS binding assays using membrane preparations of HEK293 cell expressing the hH_3R (data normalized to (R)-α-methylhistamine (α = 100%) and ABT−239 (α = −100%)),[9] or using membrane preparations of CHO cells expressing the hH_3R.[37,69] [b]functional [^{32}P]GTPase activity assays using membrane preparations of *Sf*9 cells co-expressing hH_3R, $G\alpha i_2$ and $G\beta_1\gamma_2$.[10,36] [c]Radioligand competition binding experiments using [^{3}H]UR-PI294 with membrane preparations of *Sf*9 cells co-expressing hH_3R, $G\alpha i_2$ and $G\beta_1\gamma_2$,[70] [^{3}H]N$^\alpha$-methylhistamine with whole cell homogenates of SK-N-MC cells expressing the hH_3R,[37,67-68] or [^{125}I]iodoproxyfan with whole cell homogenates of CHO cells expressing the hH_3R.[69] [d][^{3}H]UR-PI294 saturation binding assay using membrane preparations of *Sf*9 cells co-expressing hH_3R, $G\alpha i_2$ and $G\beta_1\gamma_2$.[70]

Table 2.4. Potencies (pEC_{50}/pK_b) and efficacies (E_{max}) of ligands at the H_4R explored in the mini-G protein recruitment assay. Data represent mean values ± SEM of at least three independent experiments ($N \geq 3$) each performed in triplicate. Functional data obtained in proximal [^{35}S]GTPγS and steady-state GTPase and ligand binding affinities (pK_i, pK_d) determined in radioligand competition/saturation binding assays are included for comparison.

	Mini-G Protein Recruitment		GTPγS[a]/GTPase[b]		Competition Binding[c]
Cpd.	pEC_{50}/(pK_b) ± SEM	E_{max} ± SEM [%]	pEC_{50}/(pK_b)	E_{max} [%]	pK_i/(pK_d)[d]
his	6.40 ± 0.04	100	7.60[b,71]	100[b,71]	7.8[c,67]
imet	6.97 ± 0.03	48 ± 1.1	8.17[b,65]	69[b,65]	8.2[c,67]
immep	6.76 ± 0.05	68 ± 2.5	7.35[b,65]	68[b,65]	7.7[c,67]
VUF8430	6.84 ± 0.12	58 ± 1.9	7.42[a,8]	84[a,8]	7.5[c,67]
Namh	5.70 ± 0.06	82 ± 1.1			6.5[c,67]
4mhis	6.49 ± 0.05	79 ± 0.3	7.15[b,57]	90[b,57]	7.30[c,67]
PI294	7.73 ± 0.04	85 ± 0.6	8.35[a,8]	102[a,8]	(8.29)[d,44]
clob	7.31 ± 0.06	49 ± 1.8	7.65[a,8]	45[a,8]	7.75[c,44]
thio	6.43 ± 0.22 (6.88) ± 0.03	-8 ± 1.5*	6.58[a,8] (6.83)[a,8]	−139[a,8]	6.9[c,67]
JNJ	n.d. (7.62) ± 0.30	1 ± 0.7	7.10[a,8] (7.60)[a,8]	−39[a,8]	7.52[c,44]
A943931	n.d. (8.43) ± 0.20	-3 ± 1.7	7.3[a,72]	−180[a,72]	8.33[c,73]

Reference data are taken from (unless otherwise stated, E_{max} values refer to histamine = 100%): [a][^{35}S]GTPγS binding assays using membrane preparations of *Sf*9 cells co-expressing hH_4R, $G\alpha i_2$ and $G\beta_1\gamma_2$.[8,72] [b]Steady-state GTPase activity assays using membrane preparations of *Sf*9 cells co-expressing hH_4R, $G\alpha i_2$ and $G\beta_1\gamma_2$ (data normalized to histamine = 100% and thioperamide = −100%[65]).[57,65,71] [c]Radioligand competition binding assays using [^{3}H]histamine either with whole cell homogenates of SK-N-MC cells expressing the hH_4R,[67] or with whole cell homogenates of HEK293 cells expressing the hH_4R,[73] or using [^{3}H]UR-PI294 with membrane preparations of *Sf*9 cells co-expressing hH_4R, $G\alpha i_2$ and $G\beta_1\gamma_2$.[44] [d][^{3}H]UR-PI294 saturation binding assays using membrane preparations of *Sf*9 cells co-expressing hH_4R, $G\alpha i_2$ and $G\beta_1\gamma_2$.[44] n.d. = not detected.

2.3.4. Influence of Mini-G Protein Expression on Agonist Potency and Dynamic Assay Range

Mini-G proteins functionally mimic active Gα subunits, which allows for assuming a mutual cooperativity between mini-G protein and agonist binding to histamine receptors.[23,74] To investigate the influence of mini-G protein expression on agonist potency and the dynamic range of the assay, histamine responses were assessed using HEK293T cells transiently expressing constant receptor and increasing mini-G protein levels subsequent to transient transfection (pcDNA3.1 $H_{1/2/3}$R-NlucC: 1 µg, pIRESpuro3 NlucN-mGsq/-mGs/-mGsi: 0.125, 0.25, 0.5 and 1.0 µg). In all setups, the transfection of increased mini-G protein gene doses correlated with increased expression levels, as demonstrated by Western blots (cf. Appendix, Figure A5). Of note, transient mini-G protein recruitment assays were only performed for $H_{1\text{-}3}$R, but not for H_4R due to its weak transient expression.

In contrast to the presumed cooperativity between G protein expression and agonist binding, pEC_{50} values of histamine were not significantly shifted ($\alpha = 0.05$) by increasing mini-G protein expression levels at $H_{1\text{-}3}$R (Figure 2.3A, 2.3B).[23,74] However, mini-G protein expression levels differently affected the signal amplitudes of the three systems. Specifically, in the case of the H_1R, signal spans obtained were not altered by different mGsq expression levels (Figures 2.3A and 2.3C). On the contrary, the mGsi expression level related to the highest gene dose (1 µg) significantly decreased the dynamic range at the H_3R and, even more striking, rising mGs gene doses led to significantly reduced dynamic ranges at the H_2R ($\alpha = 0.05$). Following the collision coupling model of GPCR – G protein interaction,[19,75] a possible explanation for decreasing signal amplitudes is that a higher mini-G protein expression level increases the basal activity of the system due to a more likely collision of the constitutively active H_2R and mGs. However, because the same gene doses of mini-G protein resulted in different protein expression levels, as determined by Western blots, which were considerably lower, particularly for mGsq (cf. Appendix, Figure A5), one must be cautious in judging the extent of the reduced signal span observed for the H_1R/mGsq, H_2R/mGs, and H_3R/mGsi systems.

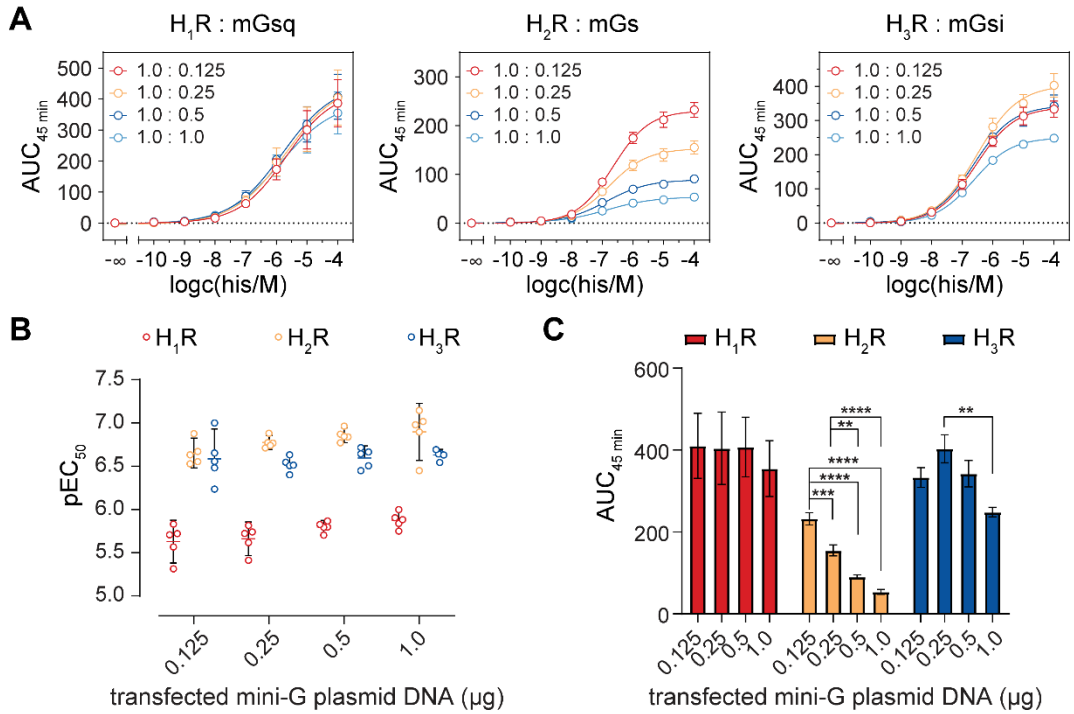

Figure 2.3. Influence of mini-G protein expression levels on agonist potency and dynamic assay signal range. A) Concentration-response curves, B) potencies (pEC_{50}) and C) AUCs of the luminescent traces within 45 min (AUC_{45min}) of histamine obtained in the mini-G protein recruitment assay using HEK293T cells transiently transfected with 1 µg of pcDNA3.1 $H_{1\text{-}3}$R-NlucC plasmids and indicated DNA amounts of pIRESpuro3 NlucN-mGsq/-mGs/-mGsi plasmids. Presented data are from five independent experiments ($N = 5$), each performed in triplicate. Whiskers (B) represent 95% confidential intervals. Significance levels (C) were calculated using one-way ANOVA followed by Tukey's multiple comparison test calculated as **: $p < 0.01$, ***: $p < 0.005$, ****: $p < 0.0001$.

2.3.5. Stabilization of an H_2R High-Affinity State by mGs

To further investigate the assumption that increasing mGs expression levels decrease the H_2R signal amplitude by precoupling to a spontaneously active receptor population, the binding properties of the endogenous agonist histamine and the antagonist famotidine were explored by displacement of [^{3}H]UR-DE257 at HEK293T cells stably expressing NlucN-mGs and H_2R-NlucC fusion proteins (Figure 2.4A; cf. Appendix, Table A2). While the radioligand displacement by famotidine followed a monophasic curve supporting a one-site binding model ($pK_i = 7.68 \pm 0.01$), notably a two-sites binding model was preferred for the agonist histamine ($pK_{i,low} = 3.87 \pm 0.13$; $pK_{i,high} = 6.94 \pm 0.14$). This was in concordance with the formation of a high-affinity binding site at the H_2R as previously described for the ternary H_2R-G protein complex.[66] To correlate the observation to the amount of co-expressed mGs, the binding of histamine to the H_2R was probed by transient transfection of increasing mGs gene doses (from 0 µg to 1 µg of mGs DNA) and a constant gene dose of H_2R (1 µg; Figure 2.4B; cf. Appendix, Table A2). The expression of the H_2R alone (0 µg of mGs DNA) led to a rightward shifted, but monophasic concentration response curve of histamine. In contrast, by increasing mGs gene doses, an extended formation of the high-affinity binding site was observed (Figure 2.4B; cf. Appendix, Table A2).[74] This finding supported that mGs

stabilized an active H_2R conformation in a concentration-dependent manner. Although endogenously expressed G proteins should also stabilize active receptor conformations, we did not detect a high-affinity H_2R binding site using HEK293T cells transiently expressing the H_2R alone, which is presumably due to the extreme stoichiometric discrepancies between the receptor and native G proteins.[74] In addition, mGs constitutes the active GTPase domain of Gαs and therefore should immediately be accessible for binding to the H_2R in active state, whereas endogenous G proteins exist in diverse conformations.[66]

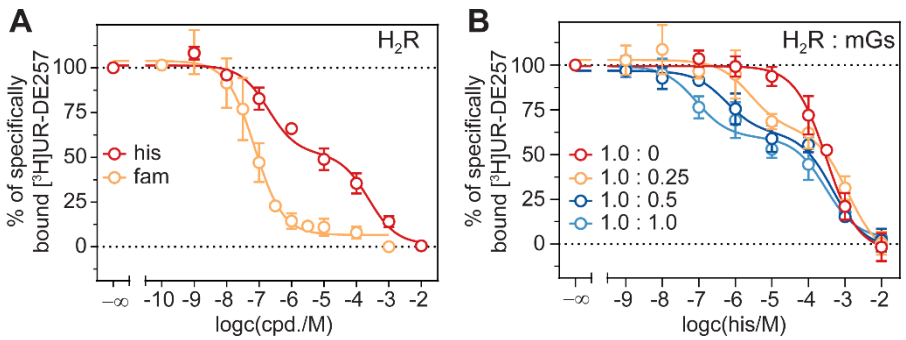

Figure 2.4. Radioligand displacement curves at cells co-expressing the H_2R and mGs. A) [^{3}H]UR-DE257 (50 nM) was displaced by histamine or famotidine. Presented data are means ± SEM of three independent experiments (*N* = 3), each performed in triplicate using HEK293T cells stably co-expressing the H_2R-NlucC and NlucN-mGs constructs. B) Displacement of [^{3}H]UR-DE257 (50 nM) by histamine using HEK293T cells transiently transfected with indicated DNA amounts (in µg) of the H_2R-NlucC and NlucN-mGs constructs 72 h prior to the experiments. Presented data are means ± SEM of three independent experiments (*N* = 3), each performed in duplicate.

2.4. Discussion

Focused on the development of a novel live cell assay that reports on functional properties of histamine receptor ligands at an early stage of signal transduction, split-NanoLuc complementation assays were designed for the four subtypes of the histamine receptor family and mini-G proteins. Overall, excellent signal amplitudes were observed for all receptor subtypes, which was of particular importance for the recombinantly weakly expressed H_4R. Moreover, this study was the first to provide time-resolved courses of agonist-mediated functional responses for an entire receptor family, the subtypes of which couple to three different types of mini-G proteins (mGs, mGsi and mGsq), using mini-G protein sensors based on split-luciferase complementation.

By investigating a large set of standard ligands, we demonstrated the usefulness of mini-G protein sensors to reliably characterize agonists and antagonists. In our system, all four histamine receptor subtypes were constitutively active, although for the H_3R and H_4R to a lesser extent than reported in other recombinant systems.[9-10,64-65] Such occurrence of constitutive receptor activity depends on the expression levels and the stoichiometry of the GPCRs and the G proteins according to the extended ternary complex (ETC) model of GPCR function.[76] In addition, an allosteric binding site for sodium ions from the experimental environment has been reported for several GCPRs including H_1R and H_3R[77-80] affecting agonist affinity and inverse agonism.[81-82] Thus, the applied test system should limit the detectability of constitutive activity and the extent of the inverse efficacy of a ligand.[83] Thus, in future routine characterization of histamine receptor ligands, it will be convenient to introduce a reference ligand that produces inverse deflection of bioluminescence in the mini-G protein recruitment assay, such as diphenhydramine (H_1R), famotidine (H_2R) and thioperamide (H_3R, H_4R).

Since utilized stable transfectants recombinantly expressed receptors and mini-G proteins of unknown stoichiometry, but agonist binding correlates with G protein binding,[74] another focus was to assess the influence of the mini-G protein expression level on assay signals. In the literature, two models of the GPCR-G protein interaction are discussed: A collision coupling, and a precoupled model.[19-20,75] In the case of the H_2R, the lower the gene dose of the mGs, the higher the dynamic range. Further, we observed a high-affinity agonist binding site for histamine subject to the mGs expression level in radioligand competition binding experiments. Both results agreed with the collision coupling model of GPCR-G protein interaction, which supports an increased constitutive activity of GPCRs highly expressed in recombinant systems.[19,75] Because H_1R and H_3R, as well as mGsq, were considerably lower expressed in utilized cells than H_2R or mGs (cf. Appendix, Table A1 and Figure A5), respectively, it was conclusive that such a strong correlation was not observed in these systems between protein expression and the dynamic assay signal range.

Concisely, this study describes the establishment and usefulness of mini-G protein sensors for prospective histamine receptor drug discovery. Due to the homogenous nature and the non-radioactive readout with an excellent dynamic range (Z' factor), the mini-G protein recruitment assay should be automatable, and thus compatible with HTS. With an increasing availability of the mini-G protein sensor concept for numerous GPCRs,[23-31] future studies could assess, on the one hand, the relevance of the different mini-G protein recruitment kinetics observed and, on the other hand, whether information from time-resolved luminescent signals is suitable for complementing ligand binding studies, such as the analysis of association and dissociation rate constants ($k_{on/off}$) and residence time,[48-49] with kinetic functional input. Because mini-G proteins are available from different G protein families, mini-G protein sensors might also be used to study GPCR – G protein coupling profiles, given that mini-G proteins possess coupling specificity equivalent to native G proteins. However, the development of an appropriate assay concept should consider that assay signals may correlate with the mini-G protein expression level, as observed in this study. Thereby, the application of mini-G protein recruitment assays might contribute to an even better pharmacological understanding of ligand-dependent receptor regulation, as well as signal formation and transduction.[84-85]

2.5. References

1. Hamm, H. E., How activated receptors couple to G proteins. *Proc Natl Acad Sci U S A* **2001,** *98* (9), 4819-4821, doi: 10.1073/pnas.011099798.
2. Milligan, G. & Kostenis, E., Heterotrimeric G-proteins: A short history. *Br J Pharmacol* **2006,** *147 Suppl 1*, S46-55, doi: 10.1038/sj.bjp.0706405.
3. Gutowski, S., Smrcka, A., Nowak, L., Wu, D. G., Simon, M. & Sternweis, P. C., Antibodies to the αq subfamily of guanine nucleotide-binding regulatory protein α subunits attenuate activation of phosphatidylinositol 4,5-bisphosphate hydrolysis by hormones. *J Biol Chem* **1991,** *266* (30), 20519-20524.
4. Dowal, L., Provitera, P. & Scarlata, S., Stable association between Gαq and phospholipase Cβ1 in living cells. *J Biol Chem* **2006,** *281* (33), 23999-24014, doi: 10.1074/jbc.M512330200.
5. Sunahara, R. K. & Insel, P. A., The molecular pharmacology of G protein signaling then and now: A tribute to Alfred G. Gilman. *Mol Pharmacol* **2016,** *89* (5), 585-592, doi: 10.1124/mol.116.104216.
6. Lazar, A. M., Irannejad, R., Baldwin, T. A., Sundaram, A. B., Gutkind, J. S., Inoue, A., Dessauer, C. W. & Von Zastrow, M., G protein-regulated endocytic trafficking of adenylyl cyclase type 9. *eLife* **2020,** *9*, e58039, doi: 10.7554/eLife.58039.
7. Hauser, A. S., Attwood, M. M., Rask-Andersen, M., Schioth, H. B. & Gloriam, D. E., Trends in GPCR drug discovery: New agents, targets and indications. *Nat Rev Drug Discov* **2017,** *16* (12), 829-842, doi: 10.1038/nrd.2017.178.
8. Wifling, D., Loffel, K., Nordemann, U., Strasser, A., Bernhardt, G., Dove, S., Seifert, R. & Buschauer, A., Molecular determinants for the high constitutive activity of the human histamine H4 receptor: Functional studies on orthologues and mutants. *Br J Pharmacol* **2015,** *172* (3), 785-798, doi: 10.1111/bph.12801.
9. Bongers, G., Krueger, K. M., Miller, T. R., Baranowski, J. L., Estvander, B. R., Witte, D. G., Strakhova, M. I., van Meer, P., Bakker, R. A., Cowart, M. D., et al., An 80-amino acid deletion in the third intracellular loop of a naturally occurring human histamine H3 isoform confers pharmacological differences and constitutive activity. *J Pharmacol Exp Ther* **2007,** *323* (3), 888-898, doi: 10.1124/jpet.107.127639.
10. Schnell, D., Burleigh, K., Trick, J. & Seifert, R., No evidence for functional selectivity of proxyfan at the human histamine H3 receptor coupled to defined Gi/Go protein heterotrimers. *J Pharmacol Exp Ther* **2010,** *332* (3), 996-1005, doi: 10.1124/jpet.109.162339.
11. Preuss, H., Ghorai, P., Kraus, A., Dove, S., Buschauer, A. & Seifert, R., Constitutive activity and ligand selectivity of human, guinea pig, rat, and canine histamine H2 receptors. *J Pharmacol Exp Ther* **2007,** *321* (3), 983-995, doi: 10.1124/jpet.107.120014.
12. Strasser, A., Striegl, B., Wittmann, H. J. & Seifert, R., Pharmacological profile of histaprodifens at four recombinant histamine H1 receptor species isoforms. *J Pharmacol Exp Ther* **2008,** *324* (1), 60-71, doi: 10.1124/jpet.107.129601.
13. Seifert, R., Wenzel-Seifert, K., Gether, U. & Kobilka, B. K., Functional differences between full and partial agonists: Evidence for ligand-specific receptor conformations. *J Pharmacol Exp Ther* **2001,** *297* (3), 1218-1226.
14. Koval, A., Kopein, D., Purvanov, V. & Katanaev, V. L., Europium-labeled GTP as a general nonradioactive substitute for [35S]GTPγS in high-throughput G protein studies. *Anal Biochem* **2010,** *397* (2), 202-207, doi: 10.1016/j.ab.2009.10.028.
15. Anderson, E. K. & Martin, D. S., A fluorescent GTP analog as a specific, high-precision label of microtubules. *BioTechniques* **2011,** *51* (1), 43-48, doi: 10.2144/000113703.

16. Mondal, S., Hsiao, K. & Goueli, S. A., A homogenous bioluminescent system for measuring GTPase, GTPase activating protein, and guanine nucleotide exchange factor activities. *Assay Drug Dev Technol* **2015,** *13* (8), 444-455, doi: 10.1089/adt.2015.643.

17. Strange, P. G., Use of the GTP γ S ([35S]GTP γ S and Eu-GTP γ S) binding assay for analysis of ligand potency and efficacy at G protein-coupled receptors. *Br J Pharmacol* **2010,** *161* (6), 1238-1249, doi: 10.1111/j.1476-5381.2010.00963.x.

18. Denis, C., Sauliere, A., Galandrin, S., Senard, J. M. & Gales, C., Probing heterotrimeric G protein activation: Applications to biased ligands. *Curr Pharm Des* **2012,** *18* (2), 128-144, doi: 10.2174/138161212799040466.

19. Hein, P., Frank, M., Hoffmann, C., Lohse, M. J. & Bunemann, M., Dynamics of receptor/G protein coupling in living cells. *EMBO J* **2005,** *24* (23), 4106-4114, doi: 10.1038/sj.emboj.7600870.

20. Gales, C., Van Durm, J. J., Schaak, S., Pontier, S., Percherancier, Y., Audet, M., Paris, H. & Bouvier, M., Probing the activation-promoted structural rearrangements in preassembled receptor-G protein complexes. *Nat Struct Mol Biol* **2006,** *13* (9), 778-786, doi: 10.1038/nsmb1134.

21. Mocking, T. A. M., Buzink, M., Leurs, R. & Vischer, H. F., Bioluminescence resonance energy transfer based G protein-activation assay to probe duration of antagonism at the histamine H3 receptor. *Int J Mol Sci* **2019,** *20* (15), doi: 10.3390/ijms20153724.

22. Nehmé, R., Carpenter, B., Singhal, A., Strege, A., Edwards, P. C., White, C. F., Du, H., Grisshammer, R. & Tate, C. G., Mini-G proteins: Novel tools for studying GPCRs in their active conformation. *PLoS One* **2017,** *12* (4), e0175642, doi: 10.1371/journal.pone.0175642.

23. Wan, Q., Okashah, N., Inoue, A., Nehmé, R., Carpenter, B., Tate, C. G. & Lambert, N. A., Mini G protein probes for active G protein-coupled receptors (GPCRs) in live cells. *J Biol Chem* **2018,** *293* (19), 7466-7473, doi: 10.1074/jbc.RA118.001975.

24. Wouters, E., Marin, A. R., Dalton, J. A. R., Giraldo, J. & Stove, C., Distinct dopamine D2 receptor antagonists differentially impact D2 receptor oligomerization. *Int J Mol Sci* **2019,** *20* (7), doi: 10.3390/ijms20071686.

25. Wouters, E., Walraed, J., Robertson, M. J., Meyrath, M., Szpakowska, M., Chevigne, A., Skiniotis, G. & Stove, C., Assessment of biased agonism among distinct synthetic cannabinoid receptor agonist scaffolds. *ACS Pharmacol Transl Sci* **2020,** *3* (2), 285-295, doi: 10.1021/acsptsci.9b00069.

26. Pottie, E., Tosh, D. K., Gao, Z. G., Jacobson, K. A. & Stove, C. P., Assessment of biased agonism at the A3 adenosine receptor using β-arrestin and miniG αi recruitment assays. *Biochem Pharmacol* **2020,** *177*, 113934, doi: 10.1016/j.bcp.2020.113934.

27. Pottie, E., Dedecker, P. & Stove, C. P., Identification of psychedelic new psychoactive substances (NPS) showing biased agonism at the 5-HT2AR through simultaneous use of β-arrestin 2 and miniG αq bioassays. *Biochem Pharmacol* **2020**, 114251, doi: 10.1016/j.bcp.2020.114251.

28. Vasudevan, L., Vandeputte, M., Deventer, M., Wouters, E., Cannaert, A. & Stove, C. P., Assessment of structure-activity relationships and biased agonism at the μ opioid receptor of novel synthetic opioids using a novel, stable bio-assay platform. *Biochem Pharmacol* **2020,** *177*, 113910, doi: 10.1016/j.bcp.2020.113910.

29. Martemyanov, K. A. & Garcia-Marcos, M., Making useful gadgets with miniaturized G proteins. *J Biol Chem* **2018,** *293* (19), 7474-7475, doi: 10.1074/jbc.H118.002879.

30. Bondar, A. & Lazar, J., Optical sensors of heterotrimeric G protein signaling. *The FEBS journal* **2021,** *288* (8), 2570-2584, doi: 10.1111/febs.15655.

31. Jullié, D., Valbret, Z. & Stoeber, M., Optical tools to study the subcellular organization of GPCR neuromodulation. *J Neurosci Methods* **2022,** *366*, 109408, doi: 10.1016/j.jneumeth.2021.109408.

32. Abiuso, A. M. B., Varela, M. L., Haro Durand, L., Besio Moreno, M., Marcos, A., Ponzio, R., Rivarola, M. A., Belgorosky, A., Pignataro, O. P., Berensztein, E., et al., Histamine H4 receptor as a novel therapeutic target for the treatment of Leydig-cell tumours in prepubertal boys. *Eur J Cancer* **2018,** *91*, 125-135, doi: 10.1016/j.ejca.2017.12.003.

33. Dixon, A. S., Schwinn, M. K., Hall, M. P., Zimmerman, K., Otto, P., Lubben, T. H., Butler, B. L., Binkowski, B. F., Machleidt, T., Kirkland, T. A., et al., NanoLuc complementation reporter optimized for accurate measurement of protein interactions in cells. *ACS Chem Biol* **2016,** *11* (2), 400-408, doi: 10.1021/acschembio.5b00753.

34. Elz, S., Kramer, K., Pertz, H. H., Detert, H., ter Laak, A. M., Kuhne, R. & Schunack, W., Histaprodifens: Synthesis, pharmacological in vitro evaluation, and molecular modeling of a new class of highly active and selective histamine H1-receptor agonists. *J Med Chem* **2000,** *43* (6), 1071-1084, doi: 10.1021/jm991056a.

35. Durant, G. J., Ganellin, C. R., Hills, D. W., Miles, P. D., Parsons, M. E., Pepper, E. S. & White, G. R., The histamine H2-receptor agonist impromidine: Synthesis and structure activity considerations. *J Med Chem* **1985,** *28* (10), 1414-1422, doi: 10.1021/jm00148a007.

36. Igel, P., Schneider, E., Schnell, D., Elz, S., Seifert, R. & Buschauer, A., N(G)-acylated imidazolylpropylguanidines as potent histamine H4 receptor agonists: Selectivity by variation of the N(G)-substituent. *J Med Chem* **2009,** *52* (8), 2623-2627, doi: 10.1021/jm9000693.

37. Lim, H. D., Smits, R. A., Bakker, R. A., van Dam, C. M., de Esch, I. J. & Leurs, R., Discovery of S-(2-guanidylethyl)-isothiourea (VUF 8430) as a potent nonimidazole histamine H4 receptor agonist. *J Med Chem* **2006,** *49* (23), 6650-6651, doi: 10.1021/jm060880d.

38. Jablonowski, J. A., Grice, C. A., Chai, W., Dvorak, C. A., Venable, J. D., Kwok, A. K., Ly, K. S., Wei, J., Baker, S. M., Desai, P. J., et al., The first potent and selective non-imidazole human histamine H4 receptor antagonists. *J Med Chem* **2003,** *46* (19), 3957-3960, doi: 10.1021/jm0341047.

39. Littmann, T., Buschauer, A. & Bernhardt, G., Split luciferase-based assay for simultaneous analyses of the ligand concentration- and time-dependent recruitment of β-arrestin2. *Anal Biochem* **2019,** *573*, 8-16, doi: 10.1016/j.ab.2019.02.023.

40. Kim, D. K., Lee, H. J., Kong, J., Cho, H. Y., Kim, S. & Kang, B. S., Structural basis for the dynamics of human methionyl-tRNA synthetase in multi-tRNA synthetase complexes. *Nucl Acids Res* **2021,** *49* (11), 6549-6568, doi: 10.1093/nar/gkab453.

41. Cheng, Y. & Prusoff, W. H., Relationship between the inhibition constant (K1) and the concentration of inhibitor which causes 50 per cent inhibition (I50) of an enzymatic reaction. *Biochem Pharmacol* **1973,** *22* (23), 3099-3108, doi: 10.1016/0006-2952(73)90196-2.

42. Zhang, J. H., Chung, T. D. & Oldenburg, K. R., A simple statistical parameter for use in evaluation and validation of high throughput screening assays. *J Biomol Screen* **1999,** *4* (2), 67-73, doi: 10.1177/108705719900400206.

43. Baumeister, P., Erdmann, D., Biselli, S., Kagermeier, N., Elz, S., Bernhardt, G. & Buschauer, A., [3H]UR-DE257: Development of a tritium-labeled squaramide-type selective histamine H2 receptor antagonist. *ChemMedChem* **2015,** *10* (1), 83-93, doi: 10.1002/cmdc.201402344.

44. Igel, P., Schnell, D., Bernhardt, G., Seifert, R. & Buschauer, A., Tritium-labeled N1-[3-(1H-imidazol-4-yl)propyl]-N2-propionylguanidine ([3H]UR-PI294), a high-affinity histamine H3 and H4 receptor radioligand. *ChemMedChem* **2009,** *4* (2), 225-231, doi: 10.1002/cmdc.200800349.

45. Kagermeier, N., Werner, K., Keller, M., Baumeister, P., Bernhardt, G., Seifert, R. & Buschauer, A., Dimeric carbamoylguanidine-type histamine H2 receptor ligands: A new class of potent and selective agonists. *Bioorg Med Chem* **2015,** *23* (14), 3957-3969, doi: 10.1016/j.bmc.2015.01.012.

46. Ayoub, M. A., Landomiel, F., Gallay, N., Jegot, G., Poupon, A., Crepieux, P. & Reiter, E., Assessing Gonadotropin Receptor Function by Resonance Energy Transfer-Based Assays. *Front Endocrinol (Lausanne)* **2015,** *6*, 130, doi: 10.3389/fendo.2015.00130.

47. Perkovska, S., Mejean, C., Ayoub, M. A., Li, J., Hemery, F., Corbani, M., Laguette, N., Ventura, M. A., Orcel, H., Durroux, T., et al., V1b vasopressin receptor trafficking and signaling: Role of arrestins, G proteins and Src kinase. *Traffic* **2018,** *19* (1), 58-82, doi: 10.1111/tra.12535.

48. Copeland, R. A., The drug-target residence time model: A 10-year retrospective. *Nat Rev Drug Discov* **2016,** *15* (2), 87-95, doi: 10.1038/nrd.2015.18.

49. Hoffmann, C., Castro, M., Rinken, A., Leurs, R., Hill, S. J. & Vischer, H. F., Ligand residence time at G-protein-coupled receptors-why we should take our time to study it. *Mol Pharmacol* **2015,** *88* (3), 552-560, doi: 10.1124/mol.115.099671.

50. Mocking, T. A. M., Verweij, E. W. E., Vischer, H. F. & Leurs, R., Homogeneous, real-time NanoBRET binding assays for the histamine H3 and H4 receptors on living cells. *Mol Pharmacol* **2018,** *94* (6), 1371-1381, doi: 10.1124/mol.118.113373.

51. Bartole, E., Littmann, T., Tanaka, M., Ozawa, T., Buschauer, A. & Bernhardt, G., [3H]UR-DEBa176: A 2,4-diaminopyrimidine-type radioligand enabling binding studies at the human, mouse, and rat histamine H4 receptors. *J Med Chem* **2019,** *62* (17), 8338-8356, doi: 10.1021/acs.jmedchem.9b01342.

52. Schihada, H., Ma, X., Zabel, U., Vischer, H. F., Schulte, G., Leurs, R., Pockes, S. & Lohse, M. J., Development of a conformational histamine H3 receptor biosensor for the synchronous screening of agonists and inverse agonists. *ACS Sens* **2020,** *5* (6), 1734-1742, doi: 10.1021/acssensors.0c00397.

53. Schrage, R., De Min, A., Hochheiser, K., Kostenis, E. & Mohr, K., Superagonism at G protein-coupled receptors and beyond. *Br J Pharmacol* **2016,** *173* (20), 3018-3027, doi: 10.1111/bph.13278.

54. Lieb, S., Littmann, T., Plank, N., Felixberger, J., Tanaka, M., Schafer, T., Krief, S., Elz, S., Friedland, K., Bernhardt, G., et al., Label-free versus conventional cellular assays: Functional investigations on the human histamine H1 receptor. *Pharmacol Res* **2016,** *114*, 13-26, doi: 10.1016/j.phrs.2016.10.010.

55. Strasser, A., Wittmann, H. J., Kunze, M., Elz, S. & Seifert, R., Molecular basis for the selective interaction of synthetic agonists with the human histamine H1-receptor compared with the guinea pig H1-receptor. *Mol Pharmacol* **2009,** *75* (3), 454-465, doi: 10.1124/mol.108.053009.

56. Seifert, R., Wenzel-Seifert, K., Burckstummer, T., Pertz, H. H., Schunack, W., Dove, S., Buschauer, A. & Elz, S., Multiple differences in agonist and antagonist pharmacology between human and guinea pig histamine H1-receptor. *J Pharmacol Exp Ther* **2003,** *305* (3), 1104-1115, doi: 10.1124/jpet.103.049619.

57. Igel, P., Geyer, R., Strasser, A., Dove, S., Seifert, R. & Buschauer, A., Synthesis and structure-activity relationships of cyanoguanidine-type and structurally related histamine H4 receptor agonists. *J Med Chem* **2009,** *52* (20), 6297-6313, doi: 10.1021/jm900526h.

58. Appl, H., Holzammer, T., Dove, S., Haen, E., Strasser, A. & Seifert, R., Interactions of recombinant human histamine H1R, H2R, H3R, and H4R receptors with 34 antidepressants and antipsychotics. *Naunyn Schmiedebergs Arch Pharmacol* **2012,** *385* (2), 145-170, doi: 10.1007/s00210-011-0704-0.

59. Bakker, R. A., Schoonus, S. B., Smit, M. J., Timmerman, H. & Leurs, R., Histamine H1-receptor activation of nuclear factor-κ B: roles for G$\beta\gamma$- and Gαq/11-subunits in constitutive and agonist-mediated signaling. *Mol Pharmacol* **2001,** *60* (5), 1133-1142, doi: 10.1124/mol.60.5.1133.

60. Costa, T. & Herz, A., Antagonists with negative intrinsic activity at δ opioid receptors coupled to GTP-binding proteins. *Proc Natl Acad Sci U S A* **1989,** *86* (19), 7321-7325, doi: 10.1073/pnas.86.19.7321.

61. Smit, M. J., Leurs, R., Alewijnse, A. E., Blauw, J., Van Nieuw Amerongen, G. P., Van De Vrede, Y., Roovers, E. & Timmerman, H., Inverse agonism of histamine H2 antagonist accounts for upregulation of spontaneously active histamine H2 receptors. *Proc Natl Acad Sci U S A* **1996,** *93* (13), 6802-6807, doi: 10.1073/pnas.93.13.6802.

62. Bakker, R. A., Wieland, K., Timmerman, H. & Leurs, R., Constitutive activity of the histamine H1 receptor reveals inverse agonism of histamine H1 receptor antagonists. *Eur J Pharmacol* **2000,** *387* (1), R5-7, doi: 10.1016/s0014-2999(99)00803-1.

63. Diaz Nebreda, A., Zappia, C. D., Rodriguez Gonzalez, A., Sahores, A., Sosa, M., Burghi, V., Monczor, F., Davio, C., Fernandez, N. & Shayo, C., Involvement of histamine H1 and H2 receptor inverse agonists in receptor's crossregulation. *Eur J Pharmacol* **2019,** *847*, 42-52, doi: 10.1016/j.ejphar.2019.01.026.

64. Wifling, D., Bernhardt, G., Dove, S. & Buschauer, A., The extracellular loop 2 (ECL2) of the human histamine H4 receptor substantially contributes to ligand binding and constitutive activity. *PLoS One* **2015,** *10* (1), e0117185, doi: 10.1371/journal.pone.0117185.

65. Schneider, E. H., Schnell, D., Papa, D. & Seifert, R., High constitutive aactivity and a G-protein-independent high-affinity state of the human histamine H4-receptor. *Biochemistry* **2009,** *48* (6), 1424-1438, doi: 10.1021/bi802050d.

66. Leurs, R., Smit, M. J., Menge, W. M. & Timmerman, H., Pharmacological characterization of the human histamine H2 receptor stably expressed in Chinese hamster ovary cells. *Br J Pharmacol* **1994,** *112* (3), 847-854, doi: 10.1111/j.1476-5381.1994.tb13157.x.

67. Lim, H. D., van Rijn, R. M., Ling, P., Bakker, R. A., Thurmond, R. L. & Leurs, R., Evaluation of histamine H1-, H2-, and H3-receptor ligands at the human histamine H4 receptor: Identification of 4-methylhistamine as the first potent and selective H4 receptor agonist. *J Pharmacol Exp Ther* **2005,** *314* (3), 1310-1321, doi: 10.1124/jpet.105.087965.

68. Thurmond, R. L., Desai, P. J., Dunford, P. J., Fung-Leung, W. P., Hofstra, C. L., Jiang, W., Nguyen, S., Riley, J. P., Sun, S., Williams, K. N., et al., A potent and selective histamine H4 receptor antagonist with anti-inflammatory properties. *J Pharmacol Exp Ther* **2004,** *309* (1), 404-413, doi: 10.1124/jpet.103.061754.

69. Ligneau, X., Perrin, D., Landais, L., Camelin, J. C., Calmels, T. P., Berrebi-Bertrand, I., Lecomte, J. M., Parmentier, R., Anaclet, C., Lin, J. S., et al., BF2.649 [1-{3-[3-(4-Chlorophenyl)propoxy]propyl}piperidine, hydrochloride], a nonimidazole inverse agonist/antagonist at the human histamine H3 receptor: Preclinical pharmacology. *J Pharmacol Exp Ther* **2007,** *320* (1), 365-375, doi: 10.1124/jpet.106.111039.

70. Igel, P., Tritium-Labeled N1-[3-(1H-imidazol-4-yl)propyl]-N2propionylguanidine ([3H]UR-PI294), a High-Affinity Histamine H3 and H4 Receptor Radioligand **2009**.

71. Brunskole, I., Strasser, A., Seifert, R. & Buschauer, A., Role of the second and third extracellular loops of the histamine H4 receptor in receptor activation. *Naunyn Schmiedebergs Arch Pharmacol* **2011,** *384* (3), 301-317, doi: 10.1007/s00210-011-0673-3.

72. Nordemann, U., Wifling, D., Schnell, D., Bernhardt, G., Stark, H., Seifert, R. & Buschauer, A., Luciferase reporter gene assay on human, murine and rat histamine H4 receptor orthologs: Correlations and discrepancies between distal and proximal readouts. *PLoS One* **2013,** *8* (9), e73961, doi: 10.1371/journal.pone.0073961.

73. Cowart, M. D., Altenbach, R. J., Liu, H., Hsieh, G. C., Drizin, I., Milicic, I., Miller, T. R., Witte, D. G., Wishart, N., Fix-Stenzel, S. R., et al., Rotationally constrained 2,4-diamino-5,6-disubstituted pyrimidines: A new class of histamine H4 receptor antagonists with improved druglikeness and in vivo efficacy in pain and inflammation models. *J Med Chem* **2008,** *51* (20), 6547-6557, doi: 10.1021/jm800670r.

74. Kenakin, T., Differences between natural and recombinant G protein-coupled receptor systems with varying receptor/G protein stoichiometry. *Trends Pharmacol Sci* **1997,** *18* (12), 456-464, doi: 10.1016/S0165-6147(97)01136-X.

75. Tolkovsky, A. M. & Levitzki, A., Mode of coupling between the β-adrenergic receptor and adenylate cyclase in turkey erythrocytes. *Biochemistry* **1978,** *17* (18), 3795, doi: 10.1021/bi00611a020.

76. Samama, P., Cotecchia, S., Costa, T. & Lefkowitz, R. J., A mutation-induced activated state of the β 2-adrenergic receptor. Extending the ternary complex model. *J Biol Chem* **1993,** *268* (7), 4625-4636.

77. Wittmann, H. J., Seifert, R. & Strasser, A., Mathematical analysis of the sodium sensitivity of the human histamine H3 receptor. *In silico pharmacology* **2014,** *2* (1), 1, doi: 10.1186/s40203-014-0001-y.

78. Schnell, D. & Seifert, R., Modulation of histamine H3 receptor function by monovalent ions. *Neurosci Lett* **2010,** *472* (2), 114-118, doi: 10.1016/j.neulet.2010.01.065.

79. Gibson, W. J., Roques, T. W. & Young, J. M., Modulation of antagonist binding to histamine H1-receptors by sodium ions and by 2-amino-2-hydroxymethyl-propan-1,3-diol HCl. *Br J Pharmacol* **1994,** *111* (4), 1262-1268, doi: 10.1111/j.1476-5381.1994.tb14882.x.

80. Katritch, V., Fenalti, G., Abola, E. E., Roth, B. L., Cherezov, V. & Stevens, R. C., Allosteric sodium in class A GPCR signaling. *Trends Biochem Sci* **2014,** *39* (5), 233-244, doi: 10.1016/j.tibs.2014.03.002.

81. de Ligt, R. A., Kourounakis, A. P. & AP, I. J., Inverse agonism at G protein-coupled receptors: (Patho)physiological relevance and implications for drug discovery. *Br J Pharmacol* **2000,** *130* (1), 1-12, doi: 10.1038/sj.bjp.0703311.

82. Akam, E. & Strange, P. G., Inverse agonist properties of atypical antipsychotic drugs. *Biochem Pharmacol* **2004,** *67* (11), 2039-2045, doi: 10.1016/j.bcp.2004.02.017.

83. Kenakin, T., Efficacy as a vector: the relative prevalence and paucity of inverse agonism. *Mol Pharmacol* **2004,** *65* (1), 2-11, doi: 10.1124/mol.65.1.2.

84. Okashah, N., Wan, Q., Ghosh, S., Sandhu, M., Inoue, A., Vaidehi, N. & Lambert, N. A., Variable G protein determinants of GPCR coupling selectivity. *Proc Natl Acad Sci U S A* **2019,** *116* (24), 12054-12059, doi: 10.1073/pnas.1905993116.

85. Ilyaskina, O. S., Lemoine, H. & Bünemann, M., Lifetime of muscarinic receptor–G-protein complexes determines coupling efficiency and G-protein subtype selectivity. *Proc Natl Acad Sci U S A* **2018,** *115* (19), 5016-5021, doi: 10.1073/pnas.1715751115.

3. Establishment of a Uniform Functional Assay Platform Using Mini-G Protein Sensors

Note: Prior to the submission of this thesis, the development of the NlucN-mGsi/M_2R-NlucC sensor has been published in collaboration with partners:

Weinhart, C. G.; Wifling, D.; Schmidt, M. F.; Neu, E.; Höring, C.; Clark, T.; Gmeiner, P.; Keller, M., Dibenzodiazepinone-type muscarinic receptor antagonists conjugated to basic peptides: Impact of the linker moiety and unnatural amino acids on M_2R selectivity. *Eur J Med Chem* **2021**, 213, 113159, doi: 10.1016/j.ejmech.2021.113159.

The following experimental work was performed by co-workers:

Denise Mönnich:	Molecular cloning of the pcDNA3.1 $D_{1/5}$R-NlucC plasmids and stable expression in parental HEK293T NlucN-mGs cells
Dr. Lukas Grätz:	Molecular cloning of the pcDNA3.1 $M_{1,2,4,5}$R-NlucC, pcDNA3.1 $Y_{1/2/4}$R-NlucC and pcDNA3.1 NTS_1R-NlucC plasmids

3.1. Introduction

As drug targets, G protein-coupled receptors (GPCRs) are a prevalent research topic in medicinal chemistry. In brief, the aim of these studies is to develop molecular tools, such as radio or fluorescent ligands, or potential drug candidates with suitable binding profiles and mechanisms of action.[1-2] GPCRs are heptahelical, membrane-spanning proteins that exist as monomers or (homo-/ hetero-) oligomers.[3-6] As such, GPCRs gate extracellular stimuli into cellular responses via heterotrimeric G protein complexes. These heterotrimers consist of α, β and γ subunits that bind to active GPCRs and then dissociate into the α monomer and $\beta\gamma$ dimer to stimulate or inhibit various intracellular effector molecules.[7-8] To keep pace with the latest advances in drug discovery, available assay methods need to be constantly reconsidered and new functional screens need to be developed when necessary. General conditions include assay homogeneity (helped by assay simplicity), omission of radioactivity, a high signal-to-noise ratio, and suitability for microtiter plates.[9] Another consideration is whether to measure a proximal or distal signaling step. Classically, functional assays can be divided into three levels: First, the receptor level, where GPCR – G protein interactions or other receptor states such as ligand-induced receptor conformations, (hetero)oligomerization and phosphorylation are examined, second, the G protein level, where binding to α subunits or formation of $\beta\gamma$ complexes is explored, and third, the effector level where regulation of effectors by G proteins or G protein-independent signaling is investigated.[2,9] Each of these stages has advantages and disadvantages, so the choice of method is important. In particular, when investigating structure - activity relationships and optimizing ligand scaffolds, measuring events close to GPCR activation is advantageous to reduce the frequency of false positives.[10] However, further along the signal transduction cascade, the signal-to-noise ratio may be increased owing to signal amplification.[9,11]

Recently, a split-luciferase-based mini-G protein recruitment assay has been established for the routine testing of potential histamine receptor ligands (cf. Chapter 2).[12] This novel assay platform fulfilled both a proximal readout and high signal amplitudes, offering the possibility to replace outdated assay concepts with unfavorable conditions, such as distal readouts with long incubation times or low-throughput setups (e.g. cuvettes). In this chapter, the assay concept was applied to additional class A (rhodopsin-like) GPCRs of interest at the institute. Hence, mini-G protein sensors were designed to functionally characterize ligands at dopamine (DR), muscarinic acetylcholine (MR), and neuropeptide Y (YR) receptors, as well as at the neurotensin NTS_1 receptor (NTS_1R) representing aminergic and peptide GPCRs, respectively. In addition, the concept of mini-G protein recruitment was applied to the chemokine receptor subtype CXCR4, a class A protein GPCR, representing the first cell assay for this receptor at the institute.

3.2. Materials and Methods

3.2.1. Materials

Dulbecco's modified Eagle's medium (DMEM) was from Sigma-Aldrich (Taufkirchen, Germany) and Leibovitz' L-15 medium (L-15) from Fisher Scientific (Nidderau, Germany). Fetal calf serum (FCS) and trypsin/EDTA were from Merck Biochrom (Darmstadt, Germany) and furimazine was from Promega (Mannheim, Germany). The pcDNA3.1 vector was from Thermo Scientific (Nidderau, Germany) and the pIRESpuro3 vector was kindly provided by Prof. Dr. Gunter Meister (University of Regensburg, Regensburg, Germany). Plasmids encoding the dopamine D_1 (D_1R) and D_5 (D_5R) receptors were a kind gift of Prof. Dr. Sigurd Elz (University of Regensburg, Regensburg, Germany) and the plasmid encoding the dopamine $D_{2,long}$ (D_2R) was kindly provided by Dr. Harald Hübner (Friedrich Alexander University, Erlangen, Germany). The cDNA encoding muscarinic acetylcholine $M_{1,2,4,5}$ receptors ($M_{1,2,4,5}R$), neuropeptide Y $Y_{1,2,4}$ receptors ($Y_{1,2,4}R$), the neurotensin NTS_1 receptor (NTS_1R) and the chemokine CXCR4 receptor (CXCR4) were purchased from the Missouri cDNA research center (Rolla, MO, USA). Restriction enzymes *Dpn*I, *Hin*dIII, *Xba*I and *Xho*I and the NEBuilder® HiFi DNA Assembly Cloning Kit were from New England Biolabs (Frankfurt am Main, Germany).

Dopamine hydrochloride (dopa), (+)-bromocriptine mesylate (bromo), pramipexole dihydrochloride (prami), (-)-quinpirole dihydrochloride (quin), (+)-butaclamol hydrochloride (buta), spiperone (spip), clozapine (cloz), *R*-(+)-SCH23390 hydrochloride (SCH23390), carbachol chloride (cch), iperoxo iodide (iper), atropine sulfate (atrop), N-methyl-scopolamine bromide (NMS), pirenzepine dihydrochloride (pirenz) and propantheline bromide (propant) were from Sigma Aldrich (Taufkirchen, Germany). *R*-(-)-apomorphine hydrochloride (apo), *R*-(+)-SKF 81297 hydrobromide (SKF81297), oxotremorine sesquifumarate (oxo), CYM 9484 (CYM9484) and SR 142948 (SR142948) were from Tocris Bioscience (Bristol, UK) and aripiprazole (ari) and haloperidol (halo) were from TCI Deutschland (Eschborn, Germany). JNJ 31020028 (JNJ31020028) was from Biomol (Hamburg, Germany) and porcine neuropeptide Y (pNPY), human pancreatic polypeptide (hPP), human peptide YY (hPYY), neurotensin(8-13) (NT(8-13)) and CXC-motif chemokine receptor ligand 12 (CXCL12) were from SynPeptide (Shanghai, China). Xanomeline (xano),[13] BIBO 3304 (BIBO3304),[14] UR-AK95I (AK95I),[15] UR-AK95c (AK95c),[15] UR-MK188 (MK188),[16] and FC 131 (FC131)[17] were synthesized in-house according to published procedures. BIIE 0246 (BIIE0246) was kindly provided by Boehringer Ingelheim (Ingelheim am Rhein, Germany; www.opnme.com). All ligands were dissolved according to their physicochemical properties. For preparing stock solutions, the ligands were preferably dissolved in Millipore water. SKF81297, bromocriptine, aripiprazole, haloperidol, spiperone, clozapine, BIIE0246, JNJ31020028, CYM9484, MK188, SR142948 and FC131 were dissolved in DMSO and pNPY, hPP, hPYY, AK95I and AK95c were dissolved in 10 mM HCl.

Xanomeline and NT(8-13) were dissolved in mixtures of ethanol and 10 mM HCl (50:50 and 30:70, respectively).

3.2.2. Molecular Cloning

The molecular cloning strategy of pIRESpuro3 plasmids encoding either NlucN-mGs, NlucN-mGsi or NlucN-mGsq fusion proteins has been described in Chapter 2 (section 2.2.2). Analogously to histamine $H_{1\text{-}4}$ receptors (cf. Chapter 2), $D_{1,2,5}R$, $M_{1,2,4,5}R$, $Y_{1,2,4}R$, NTS_1R and CXCR4 were subcloned into a linearized pcDNA3.1 NlucC plasmid yielding plasmids encoding $D_{1,2,5}R$-NlucC, $M_{1,2,4,5}R$-NlucC, $Y_{1,2,4}R$-NlucC, NTS_1R-NlucC and CXCR4-NlucC fusion proteins. Specifically, for M_4R, $Y_{1,2,4}R$ and CXCR4, *Hind*III and *Xba*I, and for $M_{1,2,5}R$, *Hin*dIII and *Xho*I were used for restriction digest to subclone the receptor sequences into the pcDNA3.1 NlucC plasmid, whereas for $D_{1,2,5}R$ constructs a Gibson assembly reaction was performed.[18] Therefore, 25 bp overlaps complementary to the desired insertion site of the pcDNA3.1 NlucC vector were added to the receptor cDNA sequences by PCR. Then, the PCR products were digested with *Dpn*I to remove the original template DNA. Using the NEBuilder® HiFi DNA Assembly Cloning Kit, the *Dpn*I digested receptor cDNA and the linearized pcDNA3.1 NlucC plasmid were covalently joined as follows in a one-pot rection: The 5' exonuclease created single-stranded 3' overlap regions (complementary between the vector and the insert cDNA), which facilitated the specifical annealing of both fragments. Then, the DNA polymerase added new nucleotides to possible gaps within the assembled fragments, which were subsequently ligated by the DNA ligase. All plasmid DNA was quantified by UV-Vis absorbance using a NanoDrop spectrophotometer (ThermoFisher, Braunschweig, Germany) and sequences were verified by sequencing performed by Eurofins Genomics (Eurofins Genomics LLC, Ebersberg, Germany).

3.2.3. Cell Culture

HEK293T cells that were a kind gift from Prof. Dr. Wulf Schneider (Institute for Medical Microbiology and Hygiene, Regensburg, Germany), were cultured in DMEM supplemented with 10% FCS (full medium) at 37 °C in a water-saturated atmosphere containing 5% CO_2. The cells were periodically tested negative for mycoplasma contamination using the Venor GeM Mycoplasma Detection Kit (Minerva Biolabs, Berlin, Germany).

3.2.4. Generation of Stable Transfectants

HEK293T cells stably expressing NlucN-mGs, NlucN-mGsi or NlucN-mGsq fusion proteins, the generation of which has been described in Chapter 2 (section 2.2.2), were seeded into a 6-well cell culture plate (Sarstedt, Nümbrecht, Germany) with a cell density of 0.3 x 10^6 cells/mL (2 mL per well) and allowed to attach overnight. The next day, the cells were transfected with 2 µg plasmid DNA encoding GPCR-NlucC constructs using 6 µL of the XtremeGene HP transfection reagent

(Sigma Aldrich, Taufkirchen, Germany; transfection ratio: 1 : 3). More precisely, HEK293T NlucN-mGs cells were transfected with pcDNA3.1 plasmids encoding D_1R-NlucC and D_5R-NlucC constructs, HEK293T NlucN-mGsi cells were transfected with pcDNA3.1 plasmids encoding D_2R-NlucC, M_2R-NlucC, M_4R-NlucC, Y_1R-NlucC, Y_2R-NlucC, Y_4R-NlucC and CXCR4-NlucC constructs and HEK293T NlucN-mGsq cells were transfected with pcDNA3.1 plasmids encoding M_1R-NlucC, M_5R-NlucC and NTS_1R-NlucC constructs. After 48 h, the cells were detached by trypsin treatment and transferred to 25 cm^2 cell culture dishes. Cells were then cultured in DMEM (full medium) under the selective pressure of 1 µg/mL puromycin and 600 µg/mL G418 to maintain the stable integration of NlucN-mini-G protein and GPCR-NlucC sequences into the cells' genome, respectively.

3.2.5. Radioligand Saturation Binding Assays

Radioligand saturation binding experiments were performed using intact HEK293T cells stably co-expressing NlucN-mini-G protein and GPCR-NlucC fusion proteins. Therefore, the following radioligands were used: [^{3}H]SCH23390 ($D_{1,5}$R; α_s = 81 Ci/mmol, Novandi Chemistry AB, Södertälje, Sweden), [^{3}H]N-methyl-spiperone ([^{3}H]NMSP) (D_2R; α_s = 77 Ci/mmol, Novandi Chemistry AB, Södertälje, Sweden), [^{3}H]N-methyl-scopolamine ([^{3}H]NMS; $M_{1,2,4,5}$R; α_s = 75 Ci/mmol, Novandi Chemistry AB, Södertälje, Sweden), [^{3}H]UR-MK299[19] ([^{3}H]MK299; Y_1R; α_s = 48.9 Ci/mmol), [^{3}H]propionyl-pNPY[19] ([^{3}H]propionyl-pNPY; Y_2R; α_s = 37.5 Ci/mmol), [^{3}H]UR-KK200[20] ([^{3}H]KK200; Y_4R; α_s = 26.4 Ci/mmol), [^{3}H]UR-MK300[21] ([^{3}H]MK300; NTS_1R; α_s = 65.0 Ci/mmol). Structures of utilized radioligands are given in the Appendix (Figure A6). The experimental conditions for each cell strain are summarized in Table 3.1. The cells were detached from the cell culture flask by trypsin treatment (0.05% trypsin, 0.02% EDTA in PBS) and centrifuged (700 g, 5 min).

For experiments using adherent cells, the cells were resuspended in DMEM (full medium) and seeded at the indicated cell density (Table 3.1) onto a white 96-well cell culture plate with transparent bottom (Corning Inc., Tewksbury, MA, USA) that previously had been coated using poly-D-lysine hydrobromide (Sigma Aldrich, Taufkirchen, Germany). Thereafter, the cells were incubated overnight to allow them to adhere to the plate at 37 °C under 5% CO_2-control. Prior to the experiment, all (radio)ligands were diluted in assay buffer (10-fold). Then, the cell culture medium was carefully removed from the cells using a multi-channel pipette (Transferpette S-12, Brand, Wertheim, Germany) and the cells were washed once with assay buffer. Then 80 µL assay buffer, 10 µL of the radioligand dilutions and either 10 µL assay buffer (total binding) or 10 µL competitor (non-specific binding) were added to the cells (final volume: 100 µL). After the incubation time given in Table 3.1 at RT, under gentle shaking), the cells were washed twice with

Table 3.1. Experimental conditions for radioligand saturation binding assays using intact HEK293T cells stably co-expressing NlucN-mG /GPCR-NlucC fusion proteins. The number of cells per well was selected according to the binding sites per cell (and thus dpm obtained).

NlucN-mini-G/ GPCR-NlucC	Radioligand	Competitor	Incubation Time [min]	Buffer	Total Volume [µL]	Cells /well	Cell condition
mGs /D_1R	[^{3}H]SCH23390	Buta (4 µM)	60	L-15, 1% BSA	200	40,000	Suspension
mGsi /D_{2L}R	[^{3}H]NMSP	Buta (15 µM)	90	L-15, 1% BSA	200	200,000	Suspension
mGs /D_5R	[^{3}H]SCH23390	Buta (4 µM)	90	L-15, 1% BSA	200	40,000	Suspension
mGsq /M_1R	[^{3}H]NMS	Atrop (3 µM)	180	L-15, 1% BSA	200	40,000	Suspension
mGsi /M_2R	[^{3}H]NMS	Atrop (3 µM)	180	L-15, 1% BSA	200	200,000	Suspension
mGsi /M_4R	[^{3}H]NMS	Atrop (3 µM)	180	L-15, 1% BSA	200	200,000	Suspension
mGsq /M_5R	[^{3}H]NMS	Atrop (3 µM)	180	L-15, 1% BSA	200	200,000	Suspension
mGsi /Y_1R	[^{3}H]MK299	BIBO3304 (2 µM)	90	L-15, 1% BSA	200	200,000	Suspension
mGsi /Y_2R	[^{3}H]propionyl-pNPY	JNJ31020028/CYM 9484 (5 µM each)	120	Buffer 1, 1% BSA, 0.1 µg/mL bacitracin	100	80,000	Adherent
mGsi /Y_4R	[^{3}H]KK200	hPP (5 µM)	90	Buffer 1, 1% BSA, 0.1 µg/mL bacitracin	200	200,000	Suspension
mGsq /NTS_1R	[^{3}H]MK300	NT(8-13) (3 µM)	120	DPBS, 1% BSA, 0.1 µg/mL bacitracin	100	20,000	Adherent

the assay buffer to remove unbound radioligand and treated with 25 µL lysis buffer (8 M urea, 3 M acetic acid and 1% Triton-X in water). The plates were shaken for 20 min and 200 µL of the liquid scintillator (Ultima Gold, Perkin Elmer, Waltham, MA, USA) was added to each well. Then the plates were sealed using a transparent sealing tape (permanent seal for microtiter plates, Perkin Elmer). The next day, the cell-bound radioactivity (dpm) was captured using a Microbeta2 plate counter (Perkin Elmer, Rodgau, Germany).

For experiments using suspended cells, the cells were resuspended in the assay buffer and adjusted to the required cell density (Table 3.1) for direct use. 20 µL of the radioligand dilutions (10-fold concentrated in assay buffer) and either 20 µL assay buffer (total binding) or 20 µL competitor (10-fold concentrated in assay buffer) were pre-casted to a round bottom polypropylene 96-well microtiter plate (Greiner Bio-One, Frickenhausen, Germany) and subsequently, 160 µL of the cell suspension was added (final volume: 200 µL). After the incubation time given in Table 3.1 at RT under gentle shaking, the cell-bound radioactivity was collected by filtration using a 96-well harvester (Brandel Inc., Unterföhring, Germany). The cell-associated radioactivity was measured as described above.

The specific binding of each radioligand was determined by subtracting the nonspecific binding from the corresponding total binding (in dpm) and was plotted against the radioligand concentration. Data were fitted using a hyperbolic function describing a one-site saturation binding model (one site – total and nonspecific binding; one site – specific binding) using the GraphPad Prism9 software (San Diego, CA, USA) yielding K_d and B_{max} values. B_{max} values were used to calculate the number of binding sites per cell as described previously.[21]

3.2.6. Mini-G Protein Recruitment Assays

The day prior to the experiment, HEK293T cells stably expressing NlucN-mini-G protein/GPCR-NlucC fusion proteins were detached using trypsin (0.05% trypsin, 0.02% EDTA in PBS) and centrifuged (700 g, 5 min). Thereafter, the cells were resuspended in L-15 supplemented with 10 mM HEPES (Serva, Heidelberg, Germany) and 5% FCS, and 100,000 cells/well were seeded into a white flat-bottom 96-well microtiter plate (Brand GmbH + CoKG, Wertheim, Germany). The cells were incubated overnight at 37 °C in water-saturated atmosphere without additional CO_2.

Shortly before the experiment, all ligands and the substrate furimazine were diluted in L-15. In the case of $Y_{1,2,4}R$ and NTS_1R ligands, 1% BSA was added to the assay buffer and in the case of CXCR4 ligands, 1% BSA and 100 µg/mL bacitracin were added. Mini-G protein recruitment assays were performed and analyzed as described in Chapter 2 (section 2.2.7). Concentration-response curves were obtained using the area under curve of the luminescence signals within 45 min ($AUC_{45\ min}$), which were normalized to the maximum response of the reference agonist (100%) and L-15 (0%). The logarithmic ligand concentrations were fitted against the normalized intensities with variable slope (log(c) vs. response – variable slope (four parameters)) using the GraphPad Prism9 software yielding pEC_{50} and E_{max} values in the case of agonists and pIC_{50} values in the case of antagonists. The Cheng-Prusoff equation was applied to calculate K_b values from IC_{50} values.[22]

3.3. Results

3.3.1. Receptor Expression in HEK293T Cells Expressing NlucN-mini-G Proteins

To demonstrate the broad applicability of mini-G protein sensors for the routine characterization of potential ligands, the assay concept was applied to several class A (Rhodopsin-like) GPCRs of interest at the institute.

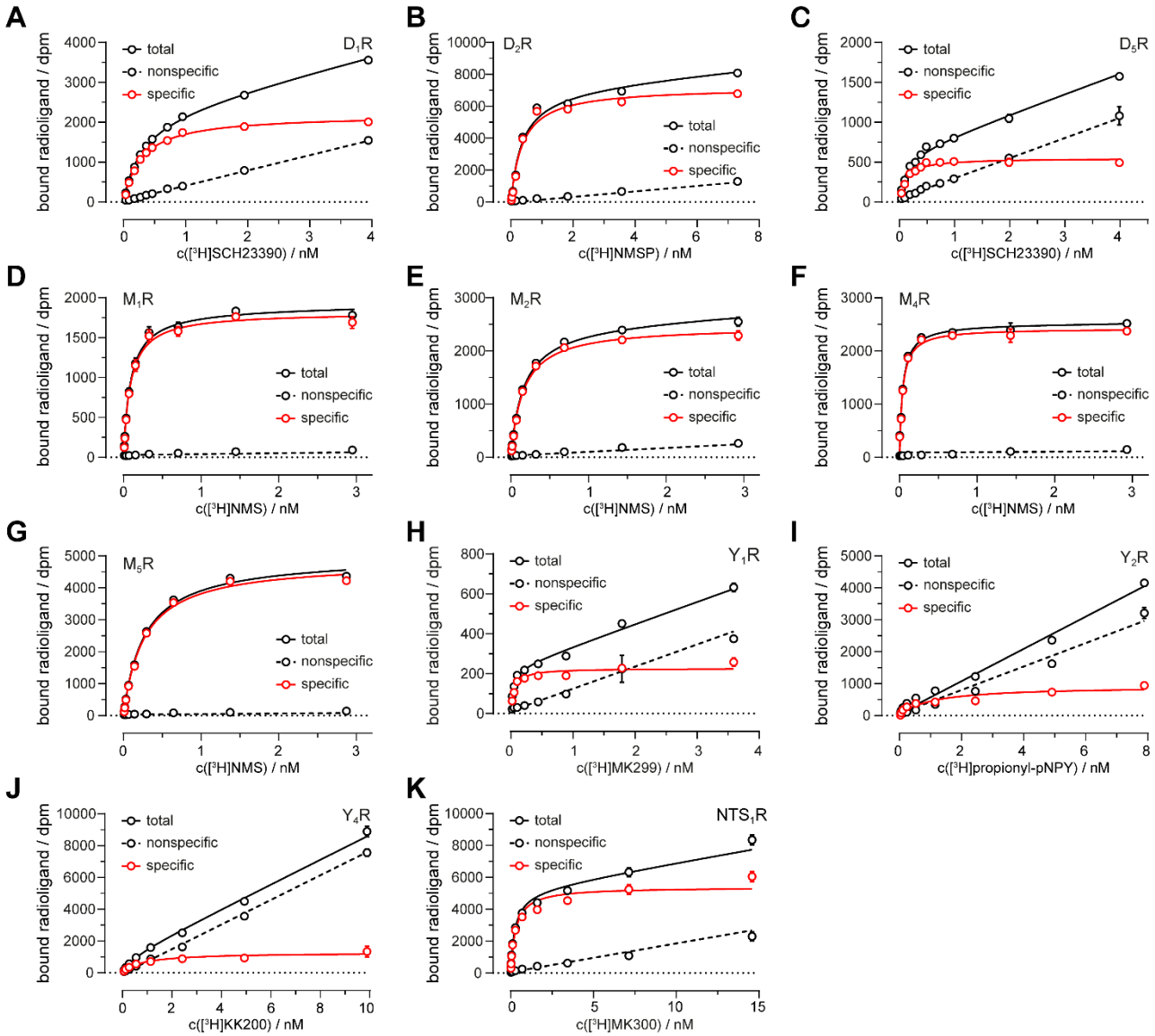

Figure 3.1. Representative binding isotherms of indicated radioligands at HEK293T cells stably co-expressing A) NlucN-mGs/D_1R-NlucC, B) NlucN-mGsi/D_2R-NlucC, C) NlucN-mGs/D_5R-NlucC, D) NlucN-mGsq/M_1R-NlucC, E) NlucN-mGsi/M_2R-NlucC, F) NlucN-mGsi/M_4R-NlucC, G) NlucN-mGsq/M_5R-NlucC, H) NlucN-mGsi/Y_1R-NlucC, I) NlucN-mGsi/Y_2R-NlucC, J) NlucN-mGsi/Y_4R-NlucC or K) NlucN-mGsq/NTS_1R-NlucC fusion proteins. The assay conditions for each cell strain are given in Table 3.1. Structures of utilized (radio)ligands are given in the Appendix (Figures A6, A8, A10-A11, A13-A14).

Stable transfectants of HEK293T cells co-expressing NlucN-mGs in combination with $D_{1/5}$R-NlucC fusion proteins, NlucN-mGsi in combination with D_2R-NlucC, $M_{2/4}$R-NlucC, $Y_{1/2/4}$R-NlucC or CXCR4-NlucC fusion proteins as well as NlucN-mGsq in combination with $M_{1,5}$R-NlucC or NTS_1R-NlucC fusion proteins were generated by antibiotic selection and subsequently tested for receptor expression by specific radioligand saturation binding to the cells (Figure 3.1). It should be mentioned that the receptor expression could not be investigated for the CXCR4, since no radioligand was available in-house. In all cases, the receptor was expressed on the cell surface and pK_d values were in good agreement with literature data (Figure 3.1, Table 3.2). Notably, there was a wide range of the receptor number expressed on the cell surface ranging from 6,169 ± 1,507 (Y_1R) to 1,256,673 ± 164,408 (NTS_1R) binding sites per cell (Table 3.2). In some cases, the non-specific binding of the radioligand to the cell membrane and other components, such as plastic or BSA, exceeded the specific binding isotherm, which correlated with the particularly low receptor expression ($Y_{1/2/4}$R, D_5R).

Table 3.2. Equilibrium dissociation constants (pK_d values) of indicated radioligands determined in radioligand saturation binding assays using HEK293T cells stably co-expressing NlucN-mini-G /GPCR-NlucC fusion proteins. The number of binding sites per cell was calculated using the obtained B_{max} values and the specific activities (α_s) of the radioligands. Presented data are means ± SEM of at least three experiments (N = 3) each performed in triplicate.

		Radioligand Saturation Binding		Literature
NlucN-mini-G / GPCR-NlucC	Radioligand	pK_d ± SEM	Binding Sites / Cell ± SEM	pK_d
mGs /D_1R	[^{3}H]SCH23390	9.53 ± 0.06	160,525 ± 2,7294	9.42[23]
mGsi /D_{2L}R	[^{3}H]NMSP	9.88 ± 0.02	175,228 ± 11,155	10.56[24]
mGs /D_5R	[^{3}H]SCH23390	9.93 ± 0.02	59,097 ± 12,527	9.37[23]
mGsq /M_1R	[^{3}H]NMS	10.12 ± 0.11	122,171 ± 21,428	9.88[25]
mGsi /M_2R	[^{3}H]NMS	9.76 ± 0.05	45,741 ± 586	10.3[25]
mGsi /M_4R	[^{3}H]NMS	10.27 ± 0.08	52,293 ± 11,234	10.5[25]
mGsq /M_5R	[^{3}H]NMS	9.54 ± 0.02	87,576 ± 10,259	9.63[25]
mGsi /Y_1R	[^{3}H]MK299	10.19 ± 0.19	6,169 ± 1,507	10.36[19]
mGsi /Y_2R	[^{3}H]pNPY	8.99 ± 0.10	82,191 ± 3,149	8.85[20]
mGsi /Y_4R	[^{3}H]KK200	9.20 ± 0.08	51,334 ± 7,338	9.17[20]
mGsq /NTS_1R	[^{3}H]MK300	9.54 ± 0.08	1,256,673 ± 164,408	9.29[21]

Reference data are taken from: Radioligand saturation binding assays using COS-7 cells expressing $D_{1,5}$R,[23] HEK293T cells expressing D_{2L}R-ELucC,[24] CHO K9 cells expressing $M_{1,2,4,5}$R,[25] SK-N-MC neuroblastoma cells,[19] CHO-hY_2-G_{qi5}-mtAEQ cells,[20] CHO-hY_4-G_{qi5}-mtAEQ cells,[20] and HT-29 cells.[21]

At this point it should be mentioned that observed receptor densities did not correlate with the assay signal amplitudes of respective reference agonists obtained in mini-G protein recruitment assays that are presented in the next section (cf. Appendix, Figure A7). Presumably an individual mini-G protein turnover at given GPCR or rather the stoichiometry of the GPCR and mini-G protein, as observed for H_2R and mGs in Chapter 2 (section 2.3.4.), are crucial for the signal amplitudes obtained.[26]

3.3.2. Validation of Mini-G Protein Sensors for Selected GPCRs

3.3.2.1. Functional Characterization of Dopamine Receptors

Dopamine receptors are ubiquitously expressed in the periphery and central nervous system (CNS) and respond to the neurotransmitter dopamine.[27] According to their amino acid sequence, expression patterns and pharmacological properties, dopamine receptors are further classified in the Gs-coupled "D_1-like" family comprising D_1R[28-29] and D_5R,[30-31] or the Gi-coupled "D_2-like" family represented by D_2R,[32-33] D_3R[34] and D_4R.[35-36] From a pharmacological perspective, an imbalanced dopaminergic system in the CNS is a key factor in the development of neurological, neurodegenerative, neuropsychiatric disorders as well as of addiction.[37-38]

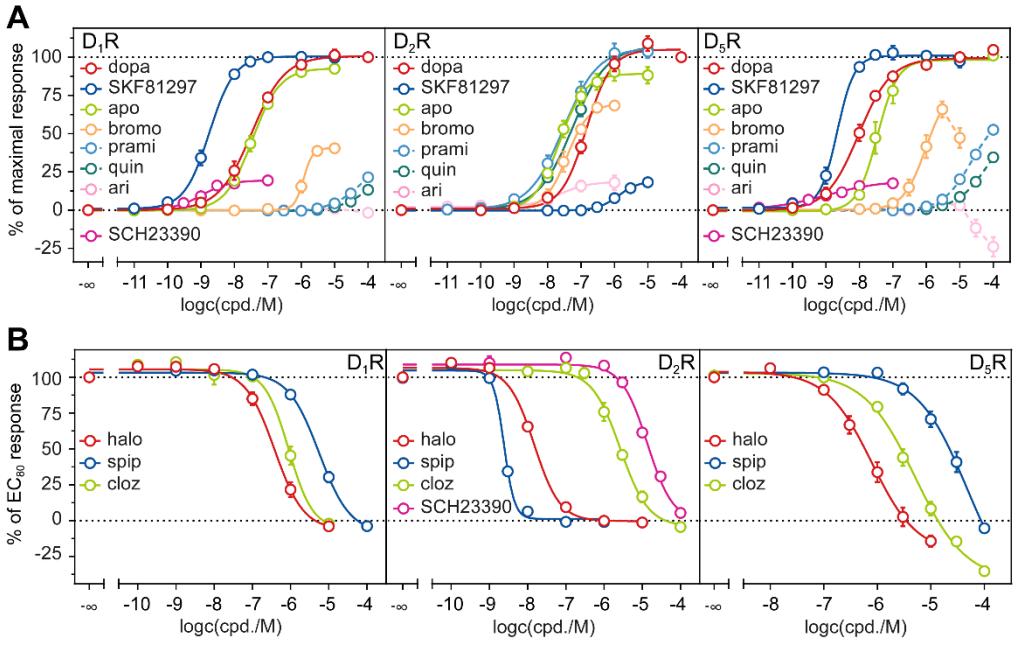

Figure 3.2. Concentration response curves of selected standard A) agonists and B) antagonists obtained in the mini-G protein recruitment assay using HEK293T cells stably co-expressing a combination of NlucN-mGs/D_1R-NlucC, NlucN-mGsi/D_2R-NlucC or NlucN-mGs/D_5R-NlucC fusion proteins. Antagonists were characterized in the presence of 100 nM dopamine. Data were normalized to L-15 as solvent control (0%) and to maximal responses elicited by 100 µM ($D_{1,2}$R) or 10 µM (D_5R) dopamine in the case of agonists and 100 nM dopamine for antagonists (100%). Data represent means ± SEM from at least three independent experiments ($N \geq 3$), each performed in triplicate.

To validate the mini-G protein recruitment assay for dopamine receptors, a set of standard agonists and antagonists that provided receptor subtype selectivity has been analyzed (cf. Appendix, Figure A8). Overall, potencies (pEC_{50}, pK_b) and efficacies (E_{max}) of the ligands were in concordance with reported functional data (Tables 3.3 and 3.4). The endogenous agonist dopamine displayed the renowned increasing potency from D_2R (6.86 ± 0.04) to D_1R (7.52 ± 0.11) and D_5R (8.04 ± 0.11).[30,39-41] Apomorphine was a non-selective, full agonist at $D_{1,2,5}R$ and bromocriptine partially activated all three receptor subtypes with a preference for the D_2R.[42-43] SKF81297, which is known to favor the D_1-like family,[44-45] was a selective full agonist at $D_{1,5}R$ but also partially activated the D_2R (E_{max}: 18 ± 2.4%). In turn, the selective full D_2R agonists, pramipexole and quinpirole, were partial agonists at $D_{1,5}R$, however with very low potency of $pEC_{50} < 5$ in all cases (Figure 3.2, Table 3.3). In addition, the partial D_2R agonist aripiprazole, was silent at the D_1R but decreased the D_5R basal activity thus providing an inverse efficacy of -24 ± 5.2% (Figure 3.2, Table 3.3). Therefore, because the same concentrations of aripiprazole did not affect D_1R activity, the strong decrease in luciferase activity observed for aripiprazole at the D_5R is likely receptor-mediated and not due to the solvent or a direct inhibition of the luciferase.[46]

In the case of investigated antagonists, haloperidol and spiperone were selective for the D_2R and clozapine preferred D_1-like receptors (Table 3.4). Most strikingly, SCH23390 reported as an antagonist at D_1-like receptors, promoted increases in luminescence signals, and thus was characterized as a partial agonist at $D_{1,5}R$ achieving E_{max} values of 19 ± 2.1% and 18 ± 1.0%, respectively (Table 3.3). It is worth mentioning that the investigated antagonists, haloperidol, spiperone and clozapine, significantly decreased the basal $D_{1,5}R$ activity (cf. Appendix, Figure A9A), thus indicating constitutively active systems.

Table 3.3. Potencies (pEC_{50}) and efficacies (E_{max}) of selected standard agonists at dopamine $D_{1,2,5}$ receptors obtained in the mini-G protein recruitment assay. HEK293T cells stably expressing NlucN-mGs and either D_1R-NlucC or D_5R-NlucC as well as NlucN-mGsi and D_2R-NlucC fusion proteins were used. Statistical differences (*) of E_{max} > 100% or E_{max} < 0%, respectively, were tested using a one-sample t-test (α = 0.05). Presented data are of at least three independent experiments (*N* = 3) each performed in triplicate.

		Mini-G Protein Recruitment		Literature		
Subtype	Cpd.	pEC_{50} ± SEM	E_{max} ± SEM [%]	pEC_{50} (pK_b)	E_{max} [%]	pK_i (pIC_{50})
D_1R	Dopa	7.52 ± 0.11	100	6.94[a,39]	98[a,39]	6.92[h,42]
	SKF81297	8.75 ± 0.06	99 ± 0.6	8.40[a,39]	98[a,39]	(7.96)[j,44]
	Apo	7.46 ± 0.04	92 ± 1.6	7.59[a,43]	100[a,43]	7.14[h,42]
	Bromo	5.94 ± 0.07	40 ± 1.8	5.16[b,48]	62[b,48]	5.82[h,48]
	SCH23390	8.93 ± 0.04	19 ± 2.1			8.96[k,49]
	Prami	< 4.5	21 ± 2.5	n.d.[b,48]	18[b,48]	<5[l,40]
	Quin	< 4.5	13 ± 1.5	<5[d,40]		<5[l,40]
	Ari	n.d.	-2 ± 1.1			6.39[h,50]
D_2R	Dopa	6.86 ± 0.04	100	7.78[c,41]	100[c,41]	7.89[o,49]
	SKF81297	5.87 ± 0.1	18 ± 2.4			(5.43)[p,44]
	Apo	7.64 ± 0.01	88 ± 4.4	8.40[d,43]	100[d,43]	7.94[q,42]
	Bromo	7.45 ± 0.11	68 ± 2.1	7.8[c,51]	96.6[c,51]	7.92[r,48]
	Prami	7.52 ± 0.08	104 ± 3.8	8.62[f,48]	108[f,48]	7.64[r,48]
	Quin	7.25 ± 0.06	105 ± 2.9	8.24[c,41]	98[c,41]	8.00[o,49]
	Ari	7.59 ± 0.06	18 ± 3.8	8.0[c,51]	68.5[c,51]	9.28[s,50]
D_5R	Dopa	8.04 ± 0.11	100	8.2[g,40]	100[g,40]	7.5[m,40]
	SKF81297	8.87 ± 0.19	97 ± 3.4	8.7[e,39]	100[e,39]	
	Apo	7.44 ± 0.11	99 ± 2.0	7.9[g,40]	80[g,40]	7.4[m,40]
	Bromo	6.04 ± 0.12	66 ± 4.5			
	SCH23390	9.11 ± 0.27	18 ± 1.0			9.5[m,40]
	Prami	< 5	53 ± 0.9	<5[g,40]	n.d.[g,40]	<5[m,40]
	Quin	< 4.5	35 ± 1.7	<5[g,40]	n.d.[g,40]	<5[m,40]
	Ari	< 5	-24 ± 5.2			5.92[n,50]

Reference data were taken from (unless otherwise stated, E_{max} values refer to dopamine = 100%): Functional cAMP accumulation assays using [a]HEK293 D_1R,[39,43] [b]CHO D_1R,[48] [c]CHO D_{2S}R,[41,51] [d]HEK293 D_2R,[43] or [e]HEK293 D_5R cells,[39] [f]PTX-sensitive [^{3}H]thymidine incorporation mitogenesis assays using CHO D_2R cells (normalized to 0.1 µM quinpirole),[48] or [g]Fluo-4 calcium mobilization assays using cells co-expressing D_5R and Gα15,[40] as well as radioligand displacement experiments using [^{3}H]SCH23390 at membrane preparations/homogenates of [h]CHO D_1R,[42,48,50] [i]rat brain tissues,[44] [k]HEK293 D_1R,[49] [l]LMtk D_1R fibroblasts,[40] [m]D_5R cells,[40] and [n]CHO D_5R cells,[50] [^{3}H]spiperone at homogenates of [o]HEK293 D_2R,[49] and [p]rat brain tissues,[44] [q][^{3}H]raclopride at homogenates of CHO rat D_2R,[42] [r][^{125}I]iodosulpiride at homogenates of CHO D_2R cells,[48] or [s][^{3}H]methylspiperone at homogenates of CHO D_{2S}R.[50]

Table 3.4. Potencies (pK_b) of selected standard antagonists at dopamine $D_{1,2,5}$ receptors obtained in the mini-G protein recruitment assay. HEK293T cells stably expressing NlucN-mGs and either D_1R-NlucC or D_5R-NlucC, as well as NlucN-mGsi and D_2R-NlucC fusion proteins were used. Presented data are of at least three independent experiments (*N* = 3) each performed in triplicate.

		Mini-G Protein Recruitment	Literature
Subtype	Cpd.	pK_b ± SEM	pK_i
D_1R	Halo	7.06 ± 0.07	6.92 [a,49]
	Spip	5.93 ± 0.11	6.33 [a,49]
	Cloza	6.72 ± 0.05	6.70 [a,49]
D_2R	Halo	8.07 ± 0.01	8.68 [c,49]
	SCH23390	5.11 ± 0.03	6.9 [c,40]
	Spip	8.78 ± 0.06	9.89 [c,49]
	Cloza	5.91 ± 0.10	6.62 [c,49]
D_5R	Halo	7.17 ± 0.07	7.31 [b,30]
	Spip	5.38 ± 0.15	5.35 [b,30]
	Cloza	6.37 ± 0.06	6.6 [b,30]

Reference data were taken from: Radioligand displacement assays using [^{3}H]SCH23390 at homogenates/membrane preparations of [a]CHO D_1R cells,[49] or [b]COS-7 D5R cells,[30] and [c][^{3}H]spiperone at homogenates of CHO D_{2L}R cells.[40,49]

3.3.2.2. Functional Characterization of Muscarinic Acetylcholine Receptors

Muscarinic acetylcholine receptors (MR) comprise five receptor subtypes that are further subdivided into Gq/11-coupled M_1R,[52-53] M_3R[54] and M_5R,[55] receptors or Gi/o-coupled M_2R[53] and M_4R.[54,56-57] MRs are widely distributed in the periphery and CNS and, in particular, regulate smooth muscle contraction, glandular secretion, and essential processes in the CNS upon stimulation by the neurotransmitter acetylcholine. Thus, various pathophysiological conditions, such as overactive bladder,[58-59] asthma,[60] Sjögren's[61] or Alzheimer's diseases,[62] schizophrenia[63] and other CNS disorders[57,64] may be compensated by approved or investigational drugs targeting MRs.

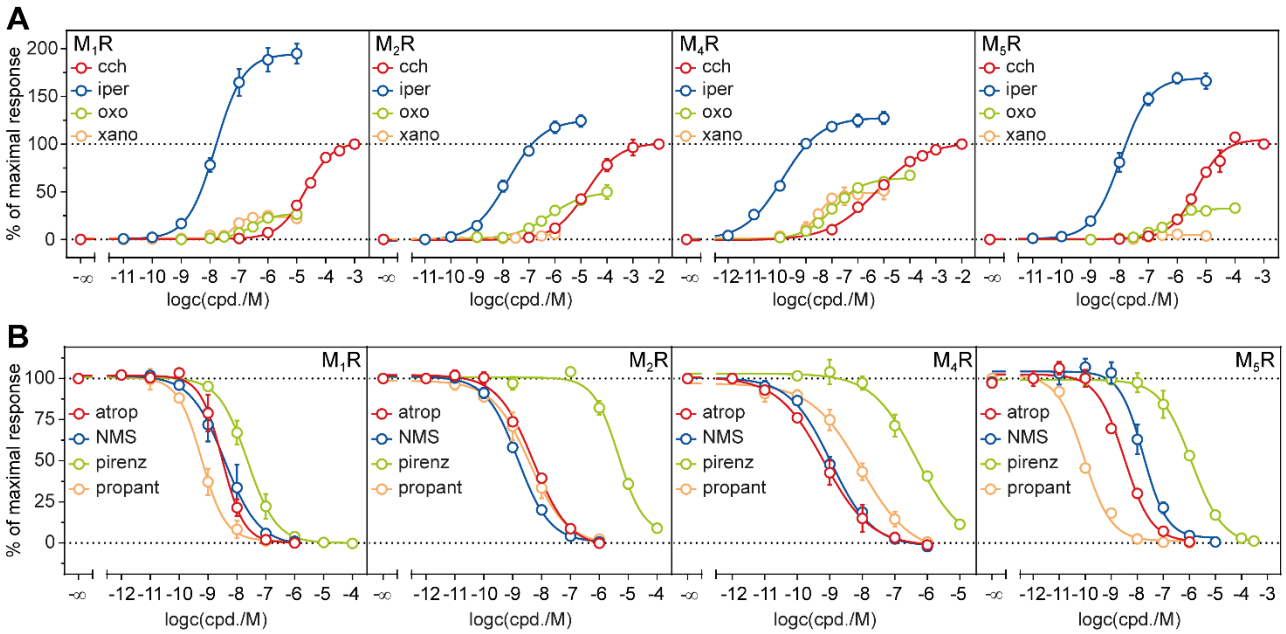

Figure 3.3. Concentration response curves of selected standard A) agonists and B) antagonists obtained in the mini-G protein recruitment assay using HEK293T cells stably co-expressing NlucN-mGsq/M_1R-NlucC, NlucN-mGsi/M_2R-NlucC, NlucN-mGsi/M_4R-NlucC or NlucN-mGsq/M_5R-NlucC fusion proteins. Antagonists were characterized in the presence of 100 µM carbachol. Data were normalized to L-15 as solvent control (%) and to maximal responses elicited by 1 mM ($M_{1,5}$R) or 10 mM ($M_{2,4}$R) carbachol in the case of agonists and 100 µM carbachol for antagonists (100%). Data represent means ± SEM from at least three independent experiments ($N \geq 3$), each performed in triplicate.

In line with the research interest at the institute, this study validated the mini-G protein recruitment assay for the Gq/11-coupled $M_{1,5}R$ and Gi/o-coupled $M_{2,4}R$ using a set of prototypical agonists and antagonists targeting the orthosteric binding site (cf. Appendix, Figure A10).[65-67] Due to the instability of acetylcholine in solution,[68] carbachol was used as a proxy for the endogenous ligand and, thus, its signal served as 100% control in the experiments. In agreement with the literature, the full agonist carbachol and partial agonist oxotremorine were not selective for any of the MR subtypes (Figure 3.3, Table 3.5). In addition, apart from its preference for the M_4R, iperoxo was equipotent at $M_{1,2,5}R$ and provided superagonism at MR with efficacies ranging from 124 ± 5.1% (M_2R) to 204 ± 5.4% (M_1R) (Figure 3.3, Table 3.5), as reported.[69-71] Due a high sequence similarity of the MR orthosteric binding sites (M_2R: 83%; M_4R: 83%; M_5R: 91% compared to the M_1R ligand binding site determined using the GPCRdb web server[72]; www.gpcrdb.org/similaritysearch/referenceselection; access date: 12.05.2022), orthosteric ligands hardly achieve subtype selectivity. However, xanomeline has been reported as a functionally selective, partial agonist at the $M_{1,4}R$ and as nearly mute at $M_{2,5}R$.[73] Likewise, pEC_{50} values of 7.17 ± 0.07 and 7.63 ± 0.13as well as E_{max} values of 22 ± 1.9% and 51 ± 7.4% at the $M_{1,4}R$, respectively, were obtained for xanomeline in mini-G protein recruitment assays (Figure 3.3, Table 3.5).

In addition, following standard antagonists were characterized for assay validation: atropine, N-methyl-scopolamine, pirenzepine and propantheline (Figure 3.3, Table 3.6). Whereas pK_b values of atropine, N-methyl-scopolamine and propantheline were in sub nanomolar range at all MR subtypes, the potency of pirenzepine was considerably weaker (nanomolar range) at these receptors, which agreed with earlier reports (Figure 3.3, Table 3.6).[74-75] Furthermore, the relative subtype selectivity of pirenzepine ($M_1R > M_4R > M_5R > M_2R$), which has been attributed to the orthosteric binding pocket of the Gi-coupled M_4R being more akin to that of the $M_{1,5}R$ (Gq/11-coupled subtype family) than to that of the M_2R (Gi/o-coupled subtype family), was consistent with the literature.[76]

Table 3.5. Potencies (pEC_{50}) and efficacies (E_{max}) of selected standard agonists at muscarinic acetylcholine $M_{1,2,4,5}$ receptors obtained in the mini-G protein recruitment assay. HEK293T cells stably expressing NlucN-mGsq and either M_1R-NlucC or M_5R-NlucC as well as NlucN-mGsi and either M_2R-NlucC or M_4R-NlucC fusion proteins were used. Statistical differences (*) of E_{max} > 100% were tested using a one-sample t-test (α = 0.05). Presented data are of at least three independent experiments (*N* = 3) each performed in triplicate.

		Mini-G Protein Recruitment		Literature		
Subtype	Cpd.	pEC_{50} ± SEM	E_{max} ± SEM [%]	pEC_{50}	E_{max} [%]	pK_i
M_1R	Cch	4.69 ± 0.05	100	6.12 [a,74]	100[a,74]	4.87[k,70]
	Iper	7.80 ± 0.04	204 ± 5.4*	9.42[a,74]	99.8[a,74]	8.35[k,70]
	Oxo	6.53 ± 0.05	26 ± 1.5	7.32[a,74]	83.6[a,74]	6.61[k,70]
	Xan	7.17 ± 0.07	22 ± 1.9	7.19[a,74]	80.6[a,74]	7.29[k,70]
M_2R	Cch	4.74 ± 0.05	100	6.65[c,77]	73[c,77]	4.62[l,70]
	Iper	7.87 ± 0.06	124 ± 5.1	9.80[g,69]	99[g,69]	5.83[l,70]
	Oxo	6.34 ± 0.07	45 ± 5.0	6.88[d,78]	98.9[d,78]	5.70[l,70]
	Xan	n.d.	6 ± 0.8	8.58[h,70]		6.82[l,70]
M_4R	Cch	5.27 ± 0.10	100	6.63e,[77]	88e,[77]	4.68[m,70]
	Iper	8.92 ± 0.12	127 ± 5.6*	8.22[k,70]		5.96[m,70]
	Oxo	6.99 ± 0.02	63 ± 2.7	7.70[f,78]	103[f,78]	5.86[m,70]
	Xan	7.63 ± 0.13	51 ± 7.4	8.86[j,70]		7.04[m,70]
M_5R	Cch	5.30 ± 0.06	100	6.78[b,74]	100[b,74]	4.72[n,70]
	Iper	7.95 ± 0.06	166 ± 7.0*	9.80[b,74]	101.4[b,74]	6.99[n,70]
	Oxo	6.41 ± 0.11	30 ± 2.2	7.19[b,74]	101.4[b,74]	6.16[n,70]
	Xan	7.04 ± 0.04	6 ± 0.3	5.88[b,74]	73.3[b,74]	7.06[n,70]

Reference data were taken from (unless otherwise stated, E_{max} values refer to carbachol = 100%): Functional Gαq-PLC-β3 assay using [a]HEK293T M_1R or [b]HEK293T M_5R cells,[74] cAMP accumulation assays using CHO M_2R cells (normalized to the maximal [c]forskolin or [d]methacholine response) or CHO M_4R cells (normalized to the maximal [e]forskolin or [f]methacholine response),[77-78] [g][^{35}S]GTPγS assay with CHO-K1 cells expressing M_2R,[69] or inositol phosphate accumulation using CHO-K1 cells expressing [h]M_2R-Gα16 [j]M_4R-Gα16 fusion proteins[70] as well as [^{3}H]NMS displacement assays using CHO-K1 cells expressing [k]M_1R-Gα16, [l]M_2R-Gα16 fusion, [m]M_4R-Gα16 or [n]M_5R-Gα16 proteins.[70]

Table 3.6. Potencies (pK_b) of selected standard antagonists at muscarinic acetylcholine $M_{1,2,4,5}$ receptors obtained in the mini-G protein recruitment assay. HEK293T cells stably expressing NlucN-mGsq and either M_1R-NlucC or M_5R-NlucC as well as NlucN-mGsi and either M_2R-NlucC or M_4R-NlucC fusion proteins were used. Presented data are of at least three independent experiments (N = 3) each performed in triplicate.

		Mini-G Protein Recruitment	Literature	
Subtype	Cpd.	pK_b ± SEM	pK_b (pEC_{50})	pK_i, (pK_d)
M_1R	Atrop	9.34 ± 0.12	8.93[a,74]	9.05[g,25]
	NMS	9.18 ± 0.26	9.35[a,74]	(9.88)[l,25]
	Pirenz	8.40 ± 0.15	7.76[a,74]	8.78[g,25]
	Propant	9.95 ± 0.13	9.26[a,74]	9.62[g,25]
M_2R	Atrop	9.11 ± 0.05	(9.94)[c,79]	8.96[h,25]
	NMS	9.63 ± 0.04	(9.41)[c,79]	(10.30)[m,25]
	Pirenz	6.41 ± 0.14	6.2[e,75]	6.60[h,25]
	Propant	9.24 ± 0.16		9.21[h,25]
M_4R	Atrop	10.37 ± 0.24	(9.95)[d,79]	9.22[j,25]
	NMS	10.26 ± 0.06	(9.46)[d,79]	(10.5)[n,25]
	Pirenz	7.55 ± 0.12	7.3[f,75]	7.40[j,25]
	Propant	9.27 ± 0.14		9.60[j,25]
M_5R	Atrop	9.69 ± 0.08	8.66[b,74]	9.29[k,25]
	NMS	9.12 ± 0.10	9.52[b,74]	(9.63)[o,25]
	Pirenz	7.24 ± 0.04	6.65[b,74]	7.10[k,25]
	Propant	11.38 ± 0.04	9.82[b,74]	9.75[k,25]

Reference data were taken from: Functional Gαq-PLC-β3 assays using [a]HEK293T M_1R or [b]HEK293T M_5R cells,[74] [^{3}H]AMP accumulation assays using CHO cells expressing [c]M_2R or [d]M_4R,[79] β-galactosidase activity assay using NIH 3T3 cells co-expressing [e]M_2R or [f]M_4R in combination with G_{qi5},[75] as well as [^{3}H]NMS displacement assays using CHO [g]M_1R, [h]M_2R, [j]M_4R, [k]M_5R cells or [^{3}H]NMS saturation binding experiments using CHO [l]M_1R, [m]M_2R, [n]M_4R, [o]M_5R.[25]

3.3.2.3. Functional Characterization of Neuropeptide Y Receptors

The 36 amino acid peptides NPY, PYY and PP share a high sequence identity up to 70% and bind to a family of Gi/o-coupled class A GPCRs, the NPY receptors. In humans, the NPY receptor family includes four functional subtypes, the Y_1R,[80-81] Y_2R,[82-83] Y_4 R[84-85] and Y_5R.[86,87] Whereas NPY and PYY provide equal affinity for the Y_1R and the Y_2R, PP selectively binds to the Y_4R.[88] NPY receptors are widely expressed across the central and peripheral nervous system and regulate a plethora of physiological processes, such as food intake, blood pressure, anxiety or pain modulation.[89-92] In drug discovery, Y_1R, Y_2R and Y_4R represent potential targets for the pharmacological treatment of depression and obesity.[93-100] Moreover, the development of highly selective Y_1R and Y_2R ligands has contributed to the better understanding of the NPY receptor expression in tumors and the elucidation of NPY-/PYY-mediated effects on tumor cell growth,[89] and labeled Y_1R ligands, such as [^{18}F]BIBP3226 derivatives, are currently being considered as in-vivo imaging agents due to a receptor overexpression in distinct cancers, including breast cancer,[101] renal cell cancer,[102] and ovarian cancer.[103,104-105] In addition, several studies suggested that depending on the tumor type, the use of selective Y_1R agonist or Y_2R antagonists is a promising strategy for medical treatment.[89] For example, Y_1R-mediated signaling in response to PYY was demonstrated to reduce the *in-vitro* tumor cell growth of breast cancer,[106] whereas Y_2R antagonists reduced the vascularization and tumor growth of neuroblastoma cells injected to immune compromised nude mice.[107]

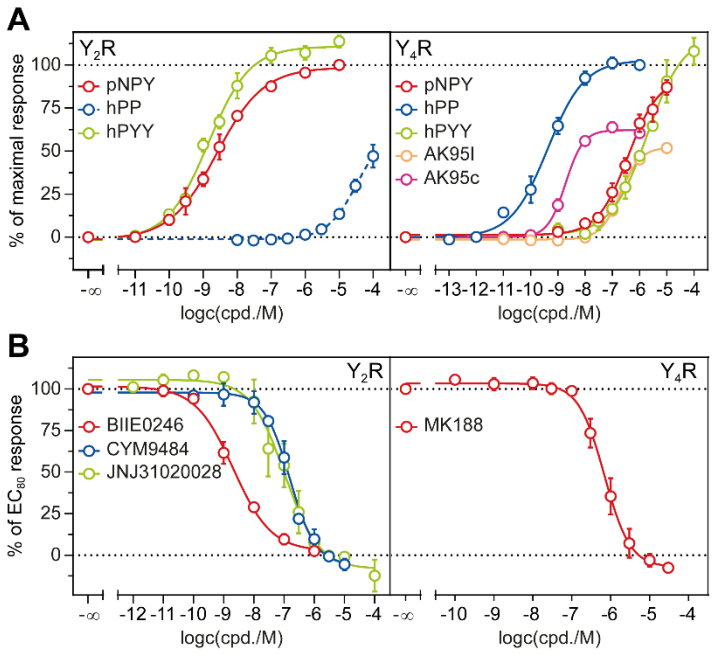

Figure 3.4. Concentration response curves of selected A) agonists and B) antagonists obtained in the mini-G protein recruitment assay using HEK293T cells stably co-expressing NlucN-mGsi and either Y_2R-NlucC or Y_4R-NlucC fusion proteins. Antagonists were characterized in the presence of 50 nM pNPY (Y_2R) or 10 nM hPP (Y_4R). Data were normalized to L-15 as solvent control (0%) and to maximal responses elicited by 10 µM pNPY (Y_2R) or 1 µM hPP (Y_4R) in the case of agonists and 50 nM pNPY (Y_2R) or 10 nM hPP (Y_4R) for antagonists (100%). Data represent means ± SEM from at least three independent experiments ($N \geq 3$), each performed in triplicate.

For mini-G protein recruitment assays, stable transfectants co-expressing the NlucN-mGsi and either Y_2R-NlucC or Y_4R-NlucC fusion proteins were used and developed sensors were validated using a set of standard and in-house developed agonists and antagonists (cf. Appendix, Figure A11). Specifically, the physiological agonists, porcine NPY (pNPY), human PYY (hPYY) and human PP (hPP) were full agonists at the Y_4R, but only pNPY and hPYY fully activated the Y_2R (Figure 3.4, Table 3.7). In agreement to the literature, the Y_2R was selective for pNPY and hPYY, which were nearly equipotent with pEC_{50} values of 8.62 ± 0.08 and 8.80 ± 0.08, respectively.[88] Vice-versa, mGsi recruitment revealed renowned Y_4R preference for hPP by three magnitudes over pNPY and hPYY.[88] When exploring recently published linear and cyclic peptides AK95l and AK95c[15] at the Y_4R, both were characterized as partial agonists with E_{max} values of 52 ± 1.7% and 60 ± 2.0%, respectively. Similar to results obtained in a calcium mobilization assay, the cyclization of the linear peptide AK95l yielding AK95c led to an increase in potency of two magnitudes.[15]

Table 3.7. Potencies (pEC_{50}) and efficacies (E_{max}) of selected standard agonists at neuropeptide $Y_{1,2,4}$ receptors obtained in the mini-G protein recruitment assay. HEK293T cells stably expressing NlucN-mGsi and either Y_1R-NlucC, Y_2R-NlucC or Y_4R-NlucC fusion proteins were used. Statistical differences (*) of E_{max} > 100% were tested using a one-sample t-test (α = 0.05). Presented data are of at least three independent experiments (*N* = 3) each performed in triplicate.

		Mini-G Protein Recruitment		Literature		
Subtype	Cpd.	pEC_{50} ± SEM	E_{max} ± SEM [%]	pEC_{50}	E_{max} [%]	pK_i
Y_1R	pNPY	8.84 ± 0.18	100	9.24[a,108]	100[a,108]	9.3[e,109]
Y_2R	pNPY	8.62 ± 0.08	100	7.93[b,110]	100[b,110]	9.1[f,111]
	hPP	< 4.5	47 ± 5.7			<5.30[f,112]
	hPYY	8.80 ± 0.08	114 ± 2.9	8.12[b,110] (pPYY)	100[b,110] (pPYY)	9.4[f,111]
Y_4R	pNPY	9.21 ± 0.20	100	6.38[c,110]	56[c,110]	6.55[g,112]
	hPP	6.42 ± 0.09	87 ± 3.7	7.96[c,112]	100[c,112]	9.28[g,112]
	hPYY	2.41 ± 2.65	110 ± 4.2	6.40[c,113] (pPYY)	61[c,113] (pPYY)	9.06[h,84]
	AK95l	6.69 ± 0.10	52 ± 1.7	6.98[d,15]	67[d,15]	8.71[j,15]
	AK95c	8.74 ± 0.04	60 ± 2.0	9.00[d,15]	84[d,15]	10.48[j,15]

Reference data ware taken from (unless otherwise stated, E_{max} values refer to pNPY = 100% (Y_1R, Y_2R) or hPP = 100% (Y_4R)): Functional [a]inositol phosphate accumulation assays using HEK293 cells co-expressing Y_1R and $Gaq_{\Delta6i4myr}$,[108] [b][^{35}S]GTPγS binding assays using membrane preparations of *Sf*9 cells expressing Y_2R, $G\alpha_{i2}$, $G\beta_1\gamma_2$ and RGS4,[110] [c][γ^{33}P]GTPase assays using *Sf*9 cell membranes expressing Y_4R, Ga_{i2}, $G\beta_1\gamma_2$ and RGS4,[110,113] [d]calcium aequorin assays using CHO-hY_4R-mAEQ-G_{qi5} cells,[15] as well as flow cytometric fluorescence ligand displacement assays using Cy5-pNPY at [e]HEL-hY_1R,[109] and [f]CHO-hY_2R cells,[111] or [g]Cy5-[K4]hPP at gCHO-hY_4R-G_{qi5}-mtAEQ cells,[112] and radioligand displacement assays using [h][^{125}I]-PYY at membrane preparations of COS-7 Y_4R cells,[84] or [j][^{3}H]KK200 at CHO-hY_4R-mAEQ-G_{qi5} cells.[15]

In addition, pK_b values of selected Y_2R and Y_4R antagonists were determined using described mini-G protein sensors (cf. Appendix, Figure A11B). At the Y_2R, the K_b values of JNJ31020028 and CYM9484 in two-digit nanomolar range agreed with earlier reports, but BIIE0246 was even more potent (sub nanomolar; Table 3.8). The Y_4R antagonist, MK188, revealed a pK_b value of 7.36 ± 0.12 (Table 3.8), which was in good agreement with reported data of a calcium mobilization assay.[16] It is worth mentioning that the basal activity of both, the Y_2R and Y_4R, was not reduced in mini-G protein recruitment assays by investigated antagonists (cf. Appendix, Figure A9), which might be either due to the ligands' mechanism of action or, more likely, due to a lacking constitutive activity of NPY receptors.

In the case of Y_1R, unfortunately, the luminescence signals were too low for a reliable functional characterization of Y_1R ligands (cf. Appendix, Figure A12). This was probably related to the considerably low receptor expression of the utilized HEK293T NlucN-mGsi/Y_1R-NlucC cells, which contained only 6,169 ± 1,507 binding sites per cell determined by [^{3}H]MK299 saturation binding experiments (cf. Table 3.2).

Table 3.8. Potencies (pK_b) of selected standard antagonists at neuropeptide $Y_{2,4}$ receptors obtained in the mini-G protein recruitment assay. HEK293T cells stably expressing NlucN-mGsi and either Y_2R-NlucC or Y_4R-NlucC fusion proteins were used. Presented data are of at least three independent experiments (N = 3) each performed in triplicate.

		Mini-G Protein Recruitment	Literature	
Subtype	Cpd.	pK_b ± SEM	pK_b (pIC_{50})	pK_i (pIC_{50})
Y_2R	BIIE0246	10.05 ± 0.13	7.99[a,113]	(8.07)[e,114]
	JNJ31020028	8.37 ± 0.19	8.04[b,114]	(7.92)[e,114]
	CYM9484	8.07 ± 0.12	(7.72)[c,115]	
Y_4R	MK188	7.36 ± 0.12	7.70[d,16]	6.89[f,16]

Reference data ware taken from: Functional [a][^{35}S]GTPγS binding assays using membrane preparations of *Sf*9 cells expressing Y_2R, $G\alpha_{i2}$, $G\beta_1\gamma_2$ and RGS4,[110] [b]calcium mobilization assays using KAN-Ts cells co-expressing Y_2R and G_{qi9},[114] [c]SAR studies performed at the National Institutes of Health,[115] [d]calcium aequorin assays using CHO-hY_4R-mAEQ-G_{qi5} cells,[15] as well as radioligand displacement assays using [e][^{125}I]PYY at KAN-Ts cells endogenously expressing Y_2R,[114] or [f]fluorescence ligand displacements assays using Cy5-[K^4]hPP at CHO-hY_4R cells.[16]

3.3.2.4. Functional Characterization of the Neurotensin NTS_1 Receptor

Neurotensin receptors comprise three subtypes, two of which, the NTS_1R[116-117] and NTS_2R[118-119] belong to class A GPCRs and primarily couple to Gq proteins.[119-120] In contrast to the NTS_2R, which is mainly found in the CNS, the NTS_1R is more widely expressed the CNS, gastrointestine and liver.[121] The third subtype, the NTS_3R (also: sortilin), constitutes a single transmembrane domain receptor[122] and first has been classified as vascular protein sorting 10 protein (Vps10p).[123] The physiological ligand of the neurotensin receptors is the 13 amino acid neuropeptide neurotensin (NTS).[124] Particularly, the NTS_1R is involved in the development and progression of various malignant tumors, such as breast,[125] lung,[126] pancreas,[127-128] prostate,[129] colon,[130] and gastric cancers,[131] and NTS_1R ligands are currently used as radiopharmaceuticals for the diagnosis of these cancers or to monitor the tumor growth and metastasis. Such radioligands are mainly based on derivatives of the endogenous agonist NTS or on non-peptidic antagonists[132] and incorporate [^{68}Ga]-[128,133-135], or [^{18}F]-labels[134,136] (γ-emitter) for positron emission tomography (PET) imaging, [^{99m}Tc]-,[137-138] or [^{111}In]-labels[133,139] (γ-emitter) for single photon computer tomography (SPET) imaging and scintigraphy, and [^{177}Lu]-,[140] or [^{188}Re]-labels[138] (β-emitter) for endoradiotherapy. A prerequisite prior to the radiolabeling of the ligands is the determination of potent and selective binding to the target site as well as of appropriate functional (agonistic or antagonistic) properties, e.g. in fluorescence ligand competition binding experiments[141] and functional cell assays, such as the presented concept.

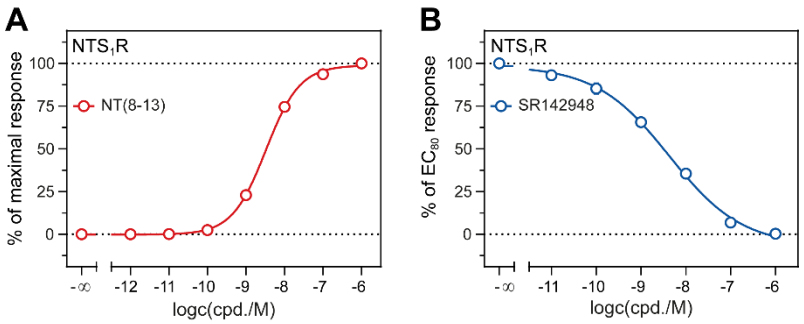

Figure 3.5. Concentration response curves of a selected A) agonist and B) antagonist obtained in the mini-G protein recruitment assay using HEK293T cells stably co-expressing NlucN-mGsq and NTS_1R-NlucC fusion proteins. The antagonist was characterized in the presence of 5 nM NT(8-13). Data were normalized to L-15 as solvent control (0%) and to maximal responses elicited by 1 µM NT(8-13) in the case of agonists and 5 nM NT(8-13) for antagonists (100%). Data represent means ± SEM from at least three independent experiments ($N \geq 3$), each performed in triplicate.

The short analog NT(8-13) constituting the C-terminal hexapeptide of NTS has been reported to fully activate the NTS_1R[142] and was used as reference agonist to characterize HEK293T cells stably co-expressing NlucN-mGsq and NTS_1R-NlucC fusion proteins. In mini-G protein recruitment assays, the agonist NT(8-13) and standard antagonist SR142948 displayed potencies of 8.48 ± 0.046 (pEC_{50}) and 8.78 ± 0.03 (pK_b), respectively (Figure 3.5, Table 3.9 and Appendix, Figure A13). For both, the results were in good agreement with that of a recently published Gαq-PLC-β3 activation sensor.[74] Moreover, no significant changes in the basal relative luminescence of the system (ΔBaseline (%)) were detected upon SR142948 addition (cf. Appendix, Figure A9), which correlated well with the absence of constitutive activity of the wildtype NTS_1R in earlier reports.[143-144]

Table 3.9. Potencies (pEC_{50}, pK_b) and efficacies (E_{max}) of a standard agonist and antagonist at the neurotensin NTS_1 receptor obtained in the mini-G protein recruitment assay. HEK293T cells stably expressing NlucN-mGsq and NTS_1R-NlucC proteins were used. Presented data are of at least three independent experiments (*N* = 3) each performed in triplicate.

		Mini-G Protein Recruitment		Literature		
Subtype	Cpd.	pEC_{50} (pK_b) ± SEM	E_{max} ± SEM [%]	pEC_{50} (pK_b)	E_{max} [%]	pK_i
NTS_1R	NT(8-13)	8.48 ± 0.046	100	8.79[a,74]	100a,[74]	
	SR 142948	(8.78) ± 0.03		(8.20)[a,74]		8.99[b,145]

Reference data were taken from: Functional [a]Gαq-PLC-β3 assays using HEK293T NTS_1R cells,[74] as well as [b][^{125}I-Tyr^3]NT displacement assays using CHO NTS_1R cells.[145]

3.3.2.5. Functional Characterization of the CXC-Motif Chemokine Receptor CXCR4

In the human body, the CXCR4[146-147] is expressed on various cell types of the immune system, such as T cells and macrophages, and acts as a key player in the coordination of cell migration and inflammatory responses regulated by the chemotactic cytokine (chemokine) CXCL12.[148-150] As a co-receptor in host cell infection, the CXCR4 enables the human immunodeficiency virus (HIV) to enter cells upon CD4 receptor binding. At present, the exploration of the CXCR4 relevance in COVID19 diseases is of particular interest. It has been found that COVID19 progression is driven by T cell immunopathogenesis,[151-152] and fatal COVID19 cases were connected to an escalating number of CXCR4 positive T cells in the lung.[153-154] Thus, the development of CXCR4 antagonists is of particular interest to the drug discovery community for a number of reasons: On the one hand, the selective inhibition of CXCR4 is a potential target for the treatment of HIV infection[155-157] or COVID19.[153] On the other hand, patients in the clinics benefit from [^{68}Ga]-, [^{90}Y]-, or [^{177}Lu]-labeled antagonists that are used for in-vivo positron emission tomography (PET) imaging for the diagnosis and monitoring the tumor cell growth and metastasis of, e.g., leukemic blasts,[158] large B cell lymphoma,[159] acute leukemia,[160] or multiple myeloma,[161-162] as well as for the examination of the inflammation infiltration in tissues[163-164] and myocardial infarction.[165-166]

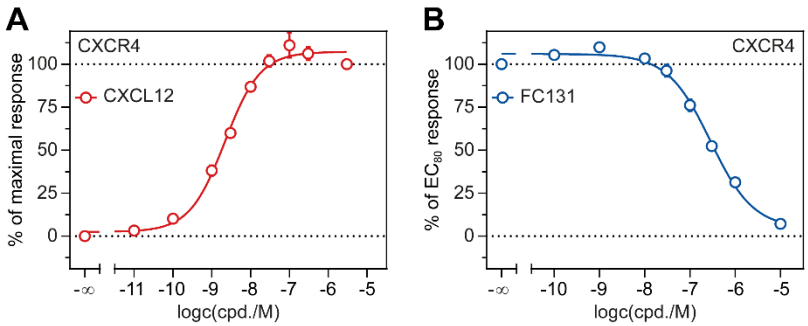

Figure 3.6. Concentration response curves of a selected A) agonist and B) antagonist obtained in the mini-G protein recruitment assay using HEK293T cells stably co-expressing NlucN-mGsi and CXCR4-NlucC fusion proteins. The antagonist was characterized in the presence of 33 nM CXCL12. Data were normalized to L-15 as solvent control (0%) and to maximal responses elicited by 3 µM CXCL12 in the case of agonists and 33 nM CXCL12 for antagonists (100%). Data represent means ± SEM from at least three independent experiments ($N \geq 3$), each performed in triplicate.

The Gi-coupled CXCR4 served as a model for the functional characterization of class A protein GPCRs using mini-G sensors. Using HEK293T cells stably co-expressing NlucN-mGsi and CXCR4-NlucC fusion proteins, we have probed the endogenous agonist CXCL12 and the antagonist FC131 (Figure 3.6, Table 3.10 and Appendix, Figure A14). CXCL12 displayed a potency of 8.68 ± 0.06. For FC131, we obtained a pIC_{50} value of 6.55 ± 0.04 that was converted to a pK_b of 7.77 ± 0.04 using to the Cheng-Prusoff equation.[22] Both the agonist and antagonist potencies were consistent with earlier data accomplished in an inositol phosphate (IP) accumulation assay.[167-168] In the literature some constitutive activity has been reported for the CXCR4, which was predominantly linked to receptor dimerization[169] and could be further increased by point-mutations of Asn-119$^{3.35}$ regulating transmembrane TM3 conformations.[169-170] Other than reported in the study of Isbilir et al. (2020),[169] FC131 did not significantly reduce the basal relative luminescence in the mini-G protein recruitment assay (cf. Appendix, Figure A9). This might be explained by low level receptor expression in the cells, as Isbilir et al. demonstrated a correlation between the receptor expression and dimerization leading to constitutively active CXCR4.[169] Unfortunately, no radioligand has been available at the institute to determine binding sites per cell by radioligand saturation binding in order to evaluate this hypothesis. In future studies, the presented CXCR4/mGsi assay might help to fill this gap as it is the first assay available at the institute to evaluate potential CXCR4 ligands and ultimately to develop a suitable radioligand.

Table 3.10. Potencies (pEC_{50}, pK_b) and efficacies (E_{max}) of a standard agonist and antagonist at the chemokine receptor CXCR4 obtained in the mini-G protein recruitment assay. HEK293T cells stably expressing NlucN-mGsi and CXCR4-NlucC proteins were used. Presented data are of at least three independent experiments (*N* = 3) each performed in triplicate.

		Mini-G Protein Recruitment		Literature		
Subtype	Cpd.	pEC_{50} (pK_b/pIC_{50}) ± SEM	E_{max} ± SEM [%]	pEC_{50} (pIC_{50})	E_{max} [%]	pK_i (pIC_{50})
CXCR4	CXCL12	8.68 ± 0.06	100	8.27[a,168]	100[a,168]	
	FC131	(7.77/6.55) ± 0.04		(6.40)[a,167]		(6.12)[b,167]

Reference data were taken from: Functional [a]IP accumulation assay using COS-7 cells expressing CXCR4-eYFP and $G\alpha_{\Delta 6qi4myr}$,[167-168] as well as [b][^{125}I]12G5 displacement using COS-7 cells expressing the CXCR4.[167]

3.3.3. Verification of Mini-G Protein Sensor Reversibility

Commonly, G protein biosensors, such as FRET-, BRET- or split-luciferase-based sensors, that measure protein - protein interactions deal with the expression of large fluorescent or bioluminescent proteins. Thus, it is a reasonable question to ask how the affinity between such (split-)proteins affects the detection in cell assays.[171] In this study, split-NanoLuc, a split-luciferase with low fragment affinity, was used that should allow for a re-separation of the fragments once they were bound together.[172] At this point, it should be mentioned that maximal stimulation of sensors presented in this chapter and the sensors developed for the histamine receptor family (cf. Chapter 2) revealed different kinetics similar to association exponential kinetics (H_1R, D_1R, D_5R), rise-and-fall-to-steady-state kinetics (H_2R, H_3R, H_4R, D_2R, M_1R, M_4R, M_5R, Y_2R, Y_4R, NTS_1R) or rise-and-fall to baseline kinetics nearly achieved for the CXCR4.[173] Representatively, time-resolved luminescent signals of the different kinetics obtained are depicted in Figure 3.7A, C and E for dopamine at NlucN-mGs/D_5R-NlucC, carbachol at NlucN-mGsq/M_1R-NlucC and CXCL12 at NlucN-mGsi/CXCR4-NlucC, respectively.

To demonstrate the reversibility of all presented mini-G protein sensors, split-luciferase complementation was induced by mini-G protein recruitment in response to reference agonists (~ EC_{80} concentration, respectively) and subsequently reversed by the addition of antagonists at different concentrations (Figure 3.7 and Appendix, Figure A15). Overall, split-NanoLuc complementation of all mini-G protein sensors was reversible after 15 min of agonist stimulation (Figure 3.7 and Appendix, Figure A15). Even in the case of the CXCR4, at which the agonist signal dropped down rapidly (similar to a rise-and-fall to baseline kinetic[173]) the split-luciferase complementation was reversible in a concentration-dependent manner yielding a FC131 pIC_{50} value of 6.73 ± 0.11 (Figures 3.7F and 3.7G). To further evaluate the kinetic differences obtained, in addition to the 15 min agonist incubation, mini-G protein recruitment was terminated after 45 min representatively D_5R and M_1R (Figures 3.7B and 3.7C). In both cases, the displacement of the agonist after different time points led to an antagonist concentration dependent decrease in the relative luminescence. Equivalent pIC_{50} values of 5.68 ± 0.06 (15 min) or 6.05 ± 2.0 (45 min) for haloperidol at the D_5R and of 8.54 ± 0.09 (15 min) or 8.71 ± 0.01 (45 min) for atropine at the M_1R were observed (Figures 3.7A, 3.7B and 3.7D), the differences of which were not statistically significant calculated using a Welch's two-sample t-test for unpaired samples. Interestingly, both the addition of the antagonist and L-15 buffer again triggered signal peaks in systems with rise-and-fall-to-steady-state kinetics, such as for the M_1R, which did not occur in systems with association exponential kinetics, such as for the D_5R (Figure 3.7).[173] It remains unclear, whether this is due to an artificial effect within the recombinant cells, such as ligand binding to the luciferase,[46] or due to an agonist-mediated effect. Hypothetically, agonists might achieve transient receptor conformations

that allow enhanced mini-G protein binding during the displacement process or rather by mechanical stimulation.

Concisely, the split-luciferase complementation of all sensors was fully reversible after different time points and did not correlate with mini-G protein recruitment kinetics. Therefore, obtained luminescence signals should originate from cell surface receptors.

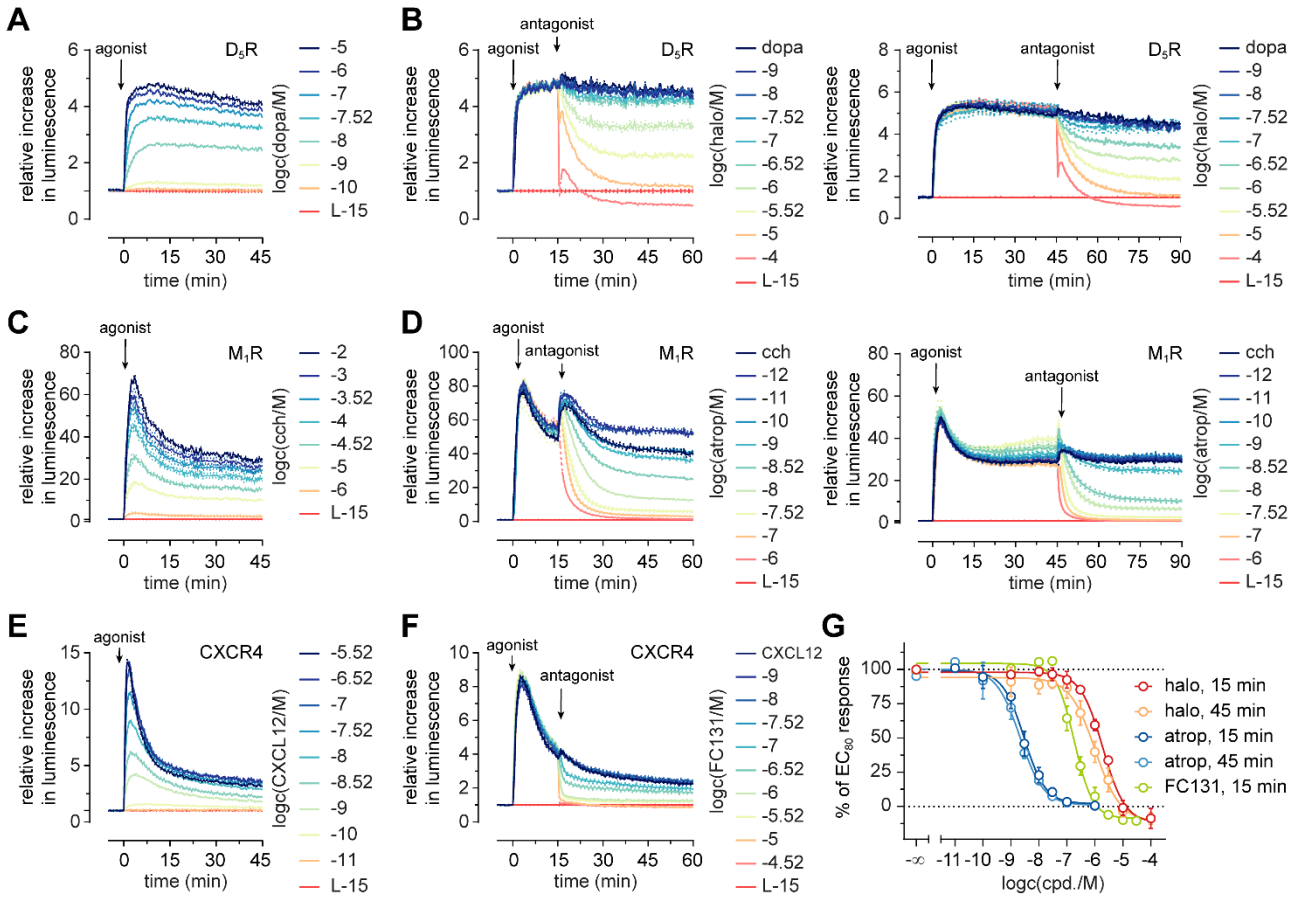

Figure 3.7. Time-resolved luminescent signals and reversibility of mini-G protein sensors with different signaling kinetics representatively shown for HEK293T cells stably co-expressing NlucN-mGs/D_5R-NlucC (A, B), NlucN-mGsq/M_1R-NlucC (C, D) and NlucN-mGsi/CXCR4-NlucC (E, F). Traces in response to reference agonists revealed A) association exponential kinetics for dopa at D_5R, C) rise-and-fall-to-steady-state kinetics for cch at M_1R and nearly E) rise-and-fall to baseline kinetic for CXCL12 at CXCR4. Despite the different kinetics, split-NanoLuc complementation upon stimulation of the B) D_5R with 100 nM dopa, D) M_1R with 100 µM cch and F) CXCR4 with 33 nM CXCL12 was fully reversible after 15 min or 45 min by the addition of indicated antagonists at various concentrations. Presented data show representative luminescent traces of single experiments. G) Concentration response curves of antagonists displacing the respective agonists after 15 min or 45 min were calculated using endpoint values after 45 min incubation upon antagonist addition. Data presented are from at least three independent experiments (*N* = 3), each performed in triplicate.

3.4. Discussion

The aim of this study was to extend mini-G protein sensors to GPCRs relevant for in-house research topics and thus to create a uniform platform for functional assays. Stable transfectants co-expressing NlucN-mini-G protein and GPCR-NlucC fusion proteins were generated, and the receptor expression was verified by radioligand saturation binding experiments except for the CXCR4, for which no radioligand was available in-house. Of note, these experiments revealed that the signal span obtained in mini-G protein recruitment assays did not correlate with receptor expression levels.

Overall, described mini-G protein sensors provided high signal-to-background (S/B) ratios (cf. Appendix, Figure A7) and were fully reversible (Figure 3.7 and Appendix Figure A15). In this study, the assay suitability for the functional characterization of dopamine, muscarinic acetylcholine, neuropeptide Y receptors, NTS_1R and CXCR4 ligands was demonstrated by investigating full and partial agonists as well as antagonists. The agonist iperoxo displayed significantly higher E_{max} values than the reference agonist carbachol at $M_{1,2,4,5}R$ and was therefore classified as superagonist.[174-175] It is widely accepted that activated receptors sequentially activate multiple heterotrimeric G proteins,[176-177] and thus superagonists have been presumed to favor receptor conformations that more efficiently couple the receptor to the G protein activation cycle, resulting in more G proteins being activated than upon binding of the reference agonist.[175] The fact that mini-G proteins represent the active GTPase domain of Gα, and thus the entire protein population should be available for receptor binding independent of the GDP-GTP nucleotide exchange, may explain the strikingly high E_{max} values of up to 204 ± 5.4% observed for iperoxo at M_1R.[178] Unfortunately, at the Y_1R, mini-G protein recruitment signals were unfavorable. Nonetheless, weak mini-G protein recruitment assay signals in line with the low receptor expression proven by radioligand saturation binding suggest that the functional characterization of Y_1R ligands might be achievable by selecting single clones derived from the pooled cell strain or by optimizing the receptor expression or rather the receptor – mGsi stoichiometry.

In recent years, several potent ligands and molecular tools have been developed at the institute that were functionally characterized in calcium mobilization or aequorin assays.[15-16,104,141] Although these assays are suitable for the determination of the ligands' mechanism of action, they also have drawbacks. For instance, the calcium mobilization assay suffers from a low throughput setup in cuvettes and thus higher material costs.[179-180] Unfortunately, the transient calcium flux in cells, which complicates the study of antagonists, has so far prevented the assay format from being adapted to 96-well plates for routine testing. Furthermore, in distal cell assays, the potentiation of agonistic

potencies or efficacies along the signal cascade cannot be precluded, which is a concern in ligand bias studies.[181]

Due to the high signal amplitudes and strong agreement of the pharmacological data obtained for standard ligands with the literature, the described mini-G protein sensors are considered well suited for the future functional characterization of potential ligands and represent an excellent alternative to previously used G protein-dependent assays. In addition, the mGsi recruitment assay is the first CXCR4 cell assay available in-house, thus enabling potent CXCR4 ligands to be developed in upcoming projects, which in turn should support the development of high affinity radio or fluorescent ligands to also establish CXCR4 ligand binding assays.

3.5. References

1. Hauser, A. S., Attwood, M. M., Rask-Andersen, M., Schioth, H. B. & Gloriam, D. E., Trends in GPCR drug discovery: New agents, targets and indications. *Nat Rev Drug Discov* **2017,** *16* (12), 829-842, doi: 10.1038/nrd.2017.178.
2. Zhang, R. & Xie, X., Tools for GPCR drug discovery. *Acta Pharmacol Sin* **2012,** *33* (3), 372-384, doi: 10.1038/aps.2011.173.
3. Faron-Górecka, A., Szlachta, M., Kolasa, M., Solich, J., Górecki, A., Kuśmider, M., Żurawek, D. & Dziedzicka-Wasylewska, M., Understanding GPCR dimerization. *Methods Cell Biol* **2019,** *149*, 155-178, doi: 10.1016/bs.mcb.2018.08.005.
4. Wouters, E., Vasudevan, L., Crans, R. A. J., Saini, D. K. & Stove, C. P., Luminescence- and fluorescence-based complementation assays to screen for GPCR oligomerization: Current state of the art. *Int J Mol Sci* **2019,** *20* (12), doi: 10.3390/ijms20122958.
5. Milligan, G., G protein-coupled receptor dimerisation: Molecular basis and relevance to function. *Biochim Biophys Acta Biomembr* **2007,** *1768* (4), 825-835, doi: 10.1016/j.bbamem.2006.09.021.
6. Dijkman, P. M., Castell, O. K., Goddard, A. D., Munoz-Garcia, J. C., de Graaf, C., Wallace, M. I. & Watts, A., Dynamic tuneable G protein-coupled receptor monomer-dimer populations. *Nat Commun* **2018,** 9 (1), 1710, doi: 10.1038/s41467-018-03727-6.
7. Milligan, G. & Kostenis, E., Heterotrimeric G-proteins: A short history. *Br J Pharmacol* **2006,** *147 Suppl 1*, S46-55, doi: 10.1038/sj.bjp.0706405.
8. Oldham, W. M. & Hamm, H. E., Heterotrimeric G protein activation by G-protein-coupled receptors. *Nat Rev Mol Cell Biol* **2008,** 9 (1), 60-71, doi: 10.1038/nrm2299.
9. Thomsen, W., Frazer, J. & Unett, D., Functional assays for screening GPCR targets. *Curr Opin Biotechnol* **2005,** *16* (6), 655-665, doi: 10.1016/j.copbio.2005.10.008.
10. Milligan, G., Principles: Extending the utility of [35S]GTP γS binding assays. *Trends Pharmacol Sci* **2003,** *24* (2), 87-90, doi: 10.1016/s0165-6147(02)00027-5.
11. Niedernberg, A., Tunaru, S., Blaukat, A., Harris, B. & Kostenis, E., Comparative analysis of functional assays for characterization of agonist ligands at G protein-coupled receptors. *J Biomol Screen* **2003,** *8* (5), 500-510, doi: 10.1177/1087057103257555.
12. Höring, C., Seibel, U., Tropmann, K., Grätz, L., Mönnich, D., Pitzl, S., Bernhardt, G., Pockes, S. & Strasser, A., A dynamic, split-luciferase-based mini-G protein sensor to functionally characterize ligands at all four histamine receptor subtypes. *Int J Mol Sci* **2020,** *21* (22), 8440.
13. Kane, B. E., Grant, M. K., El-Fakahany, E. E. & Ferguson, D. M., Synthesis and evaluation of xanomeline analogs--probing the wash-resistant phenomenon at the M1 muscarinic acetylcholine receptor. *Bioorg Med Chem* **2008,** *16* (3), 1376-1392, doi: 10.1016/j.bmc.2007.10.058.
14. Keller, M., Erdmann, D., Pop, N., Pluym, N., Teng, S., Bernhardt, G. & Buschauer, A., Red-fluorescent argininamide-type NPY Y1 receptor antagonists as pharmacological tools. *Bioorg Med Chem* **2011,** *19* (9), 2859-2878, doi: 10.1016/j.bmc.2011.03.045.
15. Konieczny, A., Conrad, M., Ertl, F. J., Gleixner, J., Gattor, A. O., Grätz, L., Schmidt, M. F., Neu, E., Horn, A. H. C., Wifling, D., et al., N-terminus to arginine side-chain cyclization of linear peptidic neuropeptide Y Y4 receptor ligands results in picomolar binding constants. *J Med Chem* **2021,** *64* (22), 16746-16769, doi: 10.1021/acs.jmedchem.1c01574.
16. Keller, M., Kaske, M., Holzammer, T., Bernhardt, G. & Buschauer, A., Dimeric argininamide-type neuropeptide Y receptor antagonists: Chiral discrimination between Y1 and Y4 receptors. *Bioorg Med Chem* **2013,** *21* (21), 6303-6322, doi: 10.1016/j.bmc.2013.08.065.

17. Fujii, N., Oishi, S., Hiramatsu, K., Araki, T., Ueda, S., Tamamura, H., Otaka, A., Kusano, S., Terakubo, S., Nakashima, H., et al., Molecular-size reduction of a potent CXCR4-chemokine antagonist using orthogonal combination of conformation- and sequence-based libraries. *Angew Chem Int Ed Engl* **2003,** *42* (28), 3251-3253, doi: 10.1002/anie.200351024.

18. Gibson, D. G., Young, L., Chuang, R. Y., Venter, J. C., Hutchison, C. A., 3rd & Smith, H. O., Enzymatic assembly of DNA molecules up to several hundred kilobases. *Nat Methods* **2009,** *6* (5), 343-345, doi: 10.1038/nmeth.1318.

19. Keller, M., Weiss, S., Hutzler, C., Kuhn, K. K., Mollereau, C., Dukorn, S., Schindler, L., Bernhardt, G., Konig, B. & Buschauer, A., N(ω)-carbamoylation of the argininamide moiety: An avenue to insurmountable NPY Y1 receptor antagonists and a radiolabeled selective high-affinity molecular tool ([3H]UR-MK299) with extended residence time. *J Med Chem* **2015,** *58* (22), 8834-8849, doi: 10.1021/acs.jmedchem.5b00925.

20. Kuhn, K. K., Ertl, T., Dukorn, S., Keller, M., Bernhardt, G., Reiser, O. & Buschauer, A., High affinity agonists of the neuropeptide Y (NPY) Y4 receptor derived from the C-terminal pentapeptide of human pancreatic polypeptide (hPP): Synthesis, stereochemical discrimination, and radiolabeling. *J Med Chem* **2016,** *59* (13), 6045-6058, doi: 10.1021/acs.jmedchem.6b00309.

21. Keller, M., Kuhn, K. K., Einsiedel, J., Hübner, H., Biselli, S., Mollereau, C., Wifling, D., Svobodová, J., Bernhardt, G., Cabrele, C., et al., Mimicking of arginine by functionalized N(ω)-carbamoylated arginine as a new broadly applicable approach to labeled bioactive peptides: High affinity angiotensin, neuropeptide Y, neuropeptide FF, and neurotensin receptor ligands as examples. *J Med Chem* **2016,** *59* (5), 1925-1945, doi: 10.1021/acs.jmedchem.5b01495.

22. Cheng, Y. & Prusoff, W. H., Relationship between the inhibition constant (K1) and the concentration of inhibitor which causes 50 per cent inhibition (I50) of an enzymatic reaction. *Biochem Pharmacol* **1973,** *22* (23), 3099-3108, doi: 10.1016/0006-2952(73)90196-2.

23. Demchyshyn, L. L., McConkey, F. & Niznik, H. B., Dopamine D5 receptor agonist high affinity and constitutive activity profile conferred by carboxyl-terminal tail sequence. *J Biol Chem* **2000,** *275* (31), 23446-23455, doi: 10.1074/jbc.M000157200.

24. Forster, L., Grätz, L., Mönnich, D., Bernhardt, G. & Pockes, S., A split luciferase complementation assay for the quantification of β-arrestin2 recruitment to dopamine D2-like receptors. *Int J Mol Sci* **2020,** *21* (17), 6103.

25. Keller, M., Trankle, C., She, X., Pegoli, A., Bernhardt, G., Buschauer, A. & Read, R. W., M2 subtype preferring dibenzodiazepinone-type muscarinic receptor ligands: Effect of chemical homo-dimerization on orthosteric (and allosteric?) binding. *Bioorg Med Chem* **2015,** *23* (14), 3970-3990, doi: 10.1016/j.bmc.2015.01.015.

26. Gurevich, V. V. & Gurevich, E. V., GPCRs and signal transducers: Interaction stoichiometry. *Trends Pharmacol Sci* **2018,** *39* (7), 672-684, doi: 10.1016/j.tips.2018.04.002.

27. Missale, C., Nash, S. R., Robinson, S. W., Jaber, M. & Caron, M. G., Dopamine receptors: From structure to function. *Physiol Rev* **1998,** *78* (1), 189-225, doi: 10.1152/physrev.1998.78.1.189.

28. Dearry, A., Gingrich, J. A., Falardeau, P., Fremeau, R. T., Bates, M. D. & Caron, M. G., Molecular cloning and expression of the gene for a human D1 dopamine receptor. *Nature* **1990,** *347* (6288), 72-76, doi: 10.1038/347072a0.

29. Zhou, Q.-Y., Grandy, D. K., Thambi, L., Kushner, J. A., Tol, H. H. M. V., Cone, R., Pribnow, D., Salon, J., Bunzow, J. R. & Civelli, O., Cloning and expression of human and rat Dt dopamine receptors. *Nature* **1990,** *347* (6288), 76-80, doi: 10.1038/347076a0.

30. Sunahara, R. K., Guan, H.-C., O'Dowd, B. F., Seeman, P., Laurier, L. G., Ng, G., George, S. R., Torchia, J., Van Tol, H. H. M. & Niznik, H. B., Cloning of the gene for a human dopamine D5 receptor with higher affinity for dopamine than D1. *Nature* **1991,** *350* (6319), 614-619, doi: 10.1038/350614a0.

31. Grandy, D. K., Zhang, Y. A., Bouvier, C., Zhou, Q. Y., Johnson, R. A., Allen, L., Buck, K., Bunzow, J. R., Salon, J. & Civelli, O., Multiple human D5 dopamine receptor genes: A functional receptor and two pseudogenes. *Proc Natl Acad Sci U S A* **1991,** *88* (20), 9175-9179, doi: 10.1073/pnas.88.20.9175.

32. Bunzow, J. R., Tol, H. H. M. V., Grandy, D. K., Albert, P., Salon, J., Christie, M., Machida, C. A., Neve, K. A. & Civelli, O., Cloning and expression of a rat D2 dopamine receptor cDNA. *Nature* **1988,** *336* (6201), 783-787, doi: 10.1038/336783a0.

33. Dal Toso, R., Sommer, B., Ewert, M., Herb, A., Pritchett, D. B., Bach, A., Shivers, B. D. & Seeburg, P. H., The dopamine D2 receptor: Two molecular forms generated by alternative splicing. *EMBO J* **1989,** *8* (13), 4025-4034, doi: 10.1002/j.1460-2075.1989.tb08585.x.

34. Sokoloff, P., Giros, B., Martres, M.-P., Bouthenet, M.-L. & Schwartz, J.-C., Molecular cloning and characterization of a novel dopamine receptor (D3) as a target for neuroleptics. *Nature* **1990,** *347* (6289), 146-151, doi: 10.1038/347146a0.

35. Van Tol, H. H. M., Bunzow, J. R., Guan, H.-C., Sunahara, R. K., Seeman, P., Niznik, H. B. & Civelli, O., Cloning of the gene for a human dopamine D4 receptor with high affinity for the antipsychotic clozapine. *Nature* **1991,** *350* (6319), 610-614, doi: 10.1038/350610a0.

36. Tritsch, N. X. & Sabatini, B. L., Dopaminergic modulation of synaptic transmission in cortex and striatum. *Neuron* **2012,** *76* (1), 33-50, doi: 10.1016/j.neuron.2012.09.023.

37. Baik, J.-H., Dopamine signaling in reward-related behaviors. *Front Neural Circuits* **2013,** *7* (152), doi: 10.3389/fncir.2013.00152.

38. Klein, M. O., Battagello, D. S., Cardoso, A. R., Hauser, D. N., Bittencourt, J. C. & Correa, R. G., Dopamine: Functions, signaling, and association with neurological diseases. *Cell Mol Neurobiol* **2019,** *39* (1), 31-59, doi: 10.1007/s10571-018-0632-3.

39. Gray, D. L., Allen, J. A., Mente, S., O'Connor, R. E., DeMarco, G. J., Efremov, I., Tierney, P., Volfson, D., Davoren, J., Guilmette, E., et al., Impaired β-arrestin recruitment and reduced desensitization by non-catechol agonists of the D1 dopamine receptor. *Nat Commun* **2018,** *9* (1), 674, doi: 10.1038/s41467-017-02776-7.

40. Wood, M., Dubois, V., Scheller, D. & Gillard, M., Rotigotine is a potent agonist at dopamine D1 receptors as well as at dopamine D2 and D3 receptors. *Br J Pharmacol* **2015,** *172* (4), 1124-1135, doi: 10.1111/bph.12988.

41. Gardner, B. R., Hall, D. A. & Strange, P. G., Agonist action at D2(short) dopamine receptors determined in ligand binding and functional assays. *J Neurochem* **1997,** *69* (6), 2589-2598, doi: 10.1046/j.1471-4159.1997.69062589.x.

42. Herm, L., Berényi, S., Vonk, A., Rinken, A. & Sipos, A., N-Substituted-2-alkyl- and 2-arylnorapomorphines: Novel, highly active D2 agonists. *Bioorg Med Chem* **2009,** *17* (13), 4756-4762, doi: 10.1016/j.bmc.2009.04.047.

43. Reinart-Okugbeni, R., Vonk, A., Uustare, A., Gyulai, Z., Sipos, A. & Rinken, A., 1-substituted apomorphines as potent dopamine agonists. *Bioorg Med Chem* **2013,** *21* (14), 4143-4150, doi: 10.1016/j.bmc.2013.05.014.

44. Arnt, J., Bøgesø, K. P., Hyttel, J. & Meier, E., Relative dopamine D1 and D2 receptor affinity and efficacy determine whether dopamine agonists induce hyperactivity or oral stereotypy in rats. *Pharmacology & toxicology* **1988,** *62* (3), 121-130, doi: 10.1111/j.1600-0773.1988.tb01859.x.

45. Wang, Q., Jolly, J. P., Surmeier, J. D., Mullah, B. M., Lidow, M. S., Bergson, C. M. & Robishaw, J. D., Differential dependence of the D1 and D5 dopamine receptors on the G protein gamma 7 subunit for activation of adenylylcyclase. *J Biol Chem* **2001,** *276* (42), 39386-39393, doi: 10.1074/jbc.M104981200.

46. Auld, D. S. & Inglese, J., Interferences with luciferase reporter enzymes. In *Assay Guidance Manual*, Markossian, S., Grossman, A., Brimacombe, K., et al., Eds. Eli Lilly & Company and the National Center for Advancing Translational Sciences: Bethesda (MD), 2004.

47. Tauscher, J., Hussain, T., Agid, O., Verhoeff, N. P., Wilson, A. A., Houle, S., Remington, G., Zipursky, R. B. & Kapur, S., Equivalent occupancy of dopamine D1 and D2 receptors with clozapine: differentiation from other atypical antipsychotics. *The American journal of psychiatry* **2004,** *161* (9), 1620-1625, doi: 10.1176/appi.ajp.161.9.1620.

48. Perachon, S., Schwartz, J.-C. & Sokoloff, P., Functional potencies of new antiparkinsonian drugs at recombinant human dopamine D1, D2 and D3 receptors. *Eur J Pharmacol* **1999,** *366* (2), 293-300, doi: 10.1016/S0014-2999(98)00896-6.

49. Kozell, L. B. & Neve, K. A., Constitutive activity of a chimeric D2/D1 dopamine receptor. *Mol Pharmacol* **1997,** *52* (6), 1137-1149, doi: 10.1124/mol.52.6.1137.

50. Lawler, C. P., Prioleau, C., Lewis, M. M., Mak, C., Jiang, D., Schetz, J. A., Gonzalez, A. M., Sibley, D. R. & Mailman, R. B., Interactions of the novel antipsychotic aripiprazole (OPC-14597) with dopamine and serotonin receptor subtypes. *Neuropsychopharmacology : official publication of the American College of Neuropsychopharmacology* **1999,** *20* (6), 612-627, doi: 10.1016/s0893-133x(98)00099-2.

51. Peters, M. F., Knappenberger, K. S., Wilkins, D., Sygowski, L. A., Lazor, L. A., Liu, J. & Scott, C. W., Evaluation of cellular dielectric spectroscopy, a whole-cell, label-free technology for drug discovery on Gi-coupled GPCRs. *J Biomol Screen* **2007,** *12* (3), 312-319, doi: 10.1177/1087057106298637.

52. Allard, W. J., Sigal, I. S. & Dixon, R. A., Sequence of the gene encoding the human M1 muscarinic acetylcholine receptor. *Nucleic Acids Res* **1987,** *15* (24), 10604, doi: 10.1093/nar/15.24.10604.

53. Kubo, T., Maeda, A., Sugimoto, K., Akiba, I., Mikami, A., Takahashi, H., Haga, T., Haga, K., Ichiyama, A., Kangawa, K., et al., Primary structure of porcine cardiac muscarinic acetylcholine receptor deduced from the cDNA sequence. *FEBS Lett* **1986,** *209* (2), 367-372, doi: 10.1016/0014-5793(86)81144-9.

54. Bonner, T. I., Buckley, N. J., Young, A. C. & Brann, M. R., Identification of a family of muscarinic acetylcholine receptor genes. *Science* **1987,** *237* (4814), 527-532.

55. Bonner, T. I., Young, A. C., Brann, M. R. & Buckley, N. J., Cloning and expression of the human and rat M5 muscarinic acetylcholine receptor genes. *Neuron* **1988,** *1* (5), 403-410, doi: 10.1016/0896-6273(88)90190-0.

56. Peralta, E. G., Ashkenazi, A., Winslow, J. W., Ramachandran, J. & Capon, D. J., Differential regulation of PI hydrolysis and adenylyl cyclase by muscarinic receptor subtypes. *Nature* **1988,** *334* (6181), 434-437, doi: 10.1038/334434a0.

57. Kruse, A. C., Kobilka, B. K., Gautam, D., Sexton, P. M., Christopoulos, A. & Wess, J., Muscarinic acetylcholine receptors: novel opportunities for drug development. *Nat Rev Drug Discov* **2014,** *13* (7), 549-560, doi: 10.1038/nrd4295.

58. Athanasopoulos, A. & Giannitsas, K., An overview of the clinical use of antimuscarinics in the treatment of overactive bladder. *Adv Urol* **2011,** *2011*, 820816-820816, doi: 10.1155/2011/820816.

59. Andersson, K.-E., Antimuscarinics for treatment of overactive bladder. *Lancet Neurol* **2004,** *3* (1), 46-53, doi: 10.1016/S1474-4422(03)00622-7.

60. Price, D., Fromer, L., Kaplan, A., van der Molen, T. & Román-Rodríguez, M., Is there a rationale and role for long-acting anticholinergic bronchodilators in asthma? *NPJ Prim Care Respir Med* **2014,** *24* (1), 14023, doi: 10.1038/npjpcrm.2014.23.

61. Fox, R. I., Use of cevimeline, a muscarinic M1 and M3 agonist, in the treatment of Sjögren's syndrome. *Advances in experimental medicine and biology* **2002,** *506* (Pt B), 1107-1116, doi: 10.1007/978-1-4615-0717-8_155.

62. Clader, J. W. & Wang, Y., Muscarinic receptor agonists and antagonists in the treatment of Alzheimer's disease. *Curr Pharm Des* **2005,** *11* (26), 3353-3361, doi: 10.2174/138161205774370762.

63. Shekhar, A., Potter, W. Z., Lightfoot, J., Lienemann, J., Dubé, S., Mallinckrodt, C., Bymaster, F. P., McKinzie, D. L. & Felder, C. C., Selective muscarinic receptor agonist xanomeline as a novel treatment approach for schizophrenia. *The American journal of psychiatry* **2008,** *165* (8), 1033-1039, doi: 10.1176/appi.ajp.2008.06091591.

64. Conn, P. J., Christopoulos, A. & Lindsley, C. W., Allosteric modulators of GPCRs: a novel approach for the treatment of CNS disorders. *Nat Rev Drug Discov* **2009,** *8* (1), 41-54, doi: 10.1038/nrd2760.

65. Gregory, K. J., Hall, N. E., Tobin, A. B., Sexton, P. M. & Christopoulos, A., Identification of orthosteric and allosteric site mutations in M2 muscarinic acetylcholine receptors that contribute to ligand-selective signaling bias. *J Biol Chem* **2010,** *285* (10), 7459-7474, doi: 10.1074/jbc.M109.094011.

66. Langmead, C. J., Fry, V. A., Forbes, I. T., Branch, C. L., Christopoulos, A., Wood, M. D. & Herdon, H. J., Probing the molecular mechanism of interaction between 4-N-butyl-1-[4-(2-methylphenyl)-4-oxo-1-butyl]-piperidine (AC-42) and the muscarinic M1 receptor: Direct pharmacological evidence that AC-42 is an allosteric agonist. *Mol Pharmacol* **2006,** *69* (1), 236-246, doi: 10.1124/mol.105.017814.

67. She, X., Pegoli, A., Mayr, J., Hübner, H., Bernhardt, G., Gmeiner, P. & Keller, M., Heterodimerization of dibenzodiazepinone-type muscarinic acetylcholine receptor ligands leads to increased M2R affinity and selectivity. *ACS Omega* **2017,** *2* (10), 6741-6754, doi: 10.1021/acsomega.7b01085.

68. Sletten, D. M., Nickander, K. K. & Low, P. A., Stability of acetylcholine chloride solution in autonomic testing. *J Neurol Sci* **2005,** *234* (1), 1-3, doi: 10.1016/j.jns.2005.02.007.

69. Schrage, R., Seemann, W. K., Klöckner, J., Dallanoce, C., Racké, K., Kostenis, E., De Amici, M., Holzgrabe, U. & Mohr, K., Agonists with supraphysiological efficacy at the muscarinic M2 ACh receptor. *Br J Pharmacol* **2013,** *169* (2), 357-370, doi: 10.1111/bph.12003.

70. Randáková, A., Nelic, D., Hochmalová, M., Zimčík, P., Mulenga, M. J., Boulos, J. & Jakubík, J., Fusion with promiscuous Gα16 subunit reveals signaling bias at muscarinic receptors. *Int J Mol Sci* **2021,** *22* (18), 10089.

71. Croy, C. H., Schober, D. A., Xiao, H., Quets, A., Christopoulos, A. & Felder, C. C., Characterization of the novel positive allosteric modulator, LY2119620, at the muscarinic M2 and M4 receptors. *Mol Pharmacol* **2014,** *86* (1), 106-115, doi: 10.1124/mol.114.091751.

72. Kooistra, A. J., Mordalski, S., Pándy-Szekeres, G., Esguerra, M., Mamyrbekov, A., Munk, C., Keserű, G. M. & Gloriam, David E., GPCRdb in 2021: Integrating GPCR sequence, structure and function. *Nucleic Acids Res* **2020,** *49* (D1), D335-D343, doi: 10.1093/nar/gkaa1080.

73. Bymaster, F. P., Whitesitt, C. A., Shannon, H. E., DeLapp, N., Ward, J. S., Calligaro, D. O., Shipley, L. A., Buelke-Sam, J. L., Bodick, N. C., Farde, L., et al., Xanomeline: A selective muscarinic agonist for the treatment of Alzheimer's disease. *Drug Dev Res* **1997,** *40* (2), 158-170, doi: 10.1002/(SICI)1098-2299(199702)40:2<158::AID-DDR6>3.0.CO;2-K.

74. Littmann, T., Ozawa, T., Hoffmann, C., Buschauer, A. & Bernhardt, G., A split luciferase-based probe for quantitative proximal determination of Gαq signalling in live cells. *Sci Rep* **2018,** *8* (1), 17179-17179, doi: 10.1038/s41598-018-35615-w.

75. Bräuner-Osborne, H. & Brann, M. R., Pharmacology of muscarinic acetylcholine receptor subtypes (M1–M5): high throughput assays in mammalian cells. *Eur J Pharmacol* **1996,** *295* (1), 93-102, doi: 10.1016/0014-2999(95)00639-7.

76. Thal, D. M., Sun, B., Feng, D., Nawaratne, V., Leach, K., Felder, C. C., Bures, M. G., Evans, D. A., Weis, W. I., Bachhawat, P., et al., Crystal structures of the M1 and M4 muscarinic acetylcholine receptors. *Nature* **2016,** *531* (7594), 335-340, doi: 10.1038/nature17188.

77. Figueroa, K. W., Griffin, M. T. & Ehlert, F. J., Selectivity of agonists for the active state of M1 to M4 muscarinic receptor subtypes. *J Pharmacol Exp Ther* **2009,** *328* (1), 331-342, doi: 10.1124/jpet.108.145219.

78. Mistry, R., Dowling, M. R. & Challiss, R. A., An investigation of whether agonist-selective receptor conformations occur with respect to M2 and M4 muscarinic acetylcholine receptor signalling via Gi/o and Gs proteins. *Br J Pharmacol* **2005,** *144* (4), 566-575, doi: 10.1038/sj.bjp.0706090.

79. Jakubík, J., Bacáková, L., el-Fakahany, E. E. & Tucek, S., Constitutive activity of the M1-M4 subtypes of muscarinic receptors in transfected CHO cells and of muscarinic receptors in the heart cells revealed by negative antagonists. *FEBS Lett* **1995,** *377* (2), 275-279, doi: 10.1016/0014-5793(95)01360-1.

80. Larhammar, D., Blomqvist, A. G., Yee, F., Jazin, E., Yoo, H. & Wahlested, C., Cloning and functional expression of a human neuropeptide Y/peptide YY receptor of the Y1 type. *J Biol Chem* **1992,** *267* (16), 10935-10938.

81. Herzog, H., Hort, Y. J., Ball, H. J., Hayes, G., Shine, J. & Selbie, L. A., Cloned human neuropeptide Y receptor couples to two different second messenger systems. *Proc Natl Acad Sci U S A* **1992,** *89* (13), 5794-5798, doi: 10.1073/pnas.89.13.5794.

82. Gehlert, D. R., Beavers, L. S., Johnson, D., Gackenheimer, S. L., Schober, D. A. & Gadski, R. A., Expression cloning of a human brain neuropeptide Y Y2 receptor. *Mol Pharmacol* **1996,** *49* (2), 224-228.

83. Gerald, C., Walker, M. W., Vaysse, P. J., He, C., Branchek, T. A. & Weinshank, R. L., Expression cloning and pharmacological characterization of a human hippocampal neuropeptide Y/peptide YY Y2 receptor subtype. *J Biol Chem* **1995,** *270* (45), 26758-26761, doi: 10.1074/jbc.270.45.26758.

84. Bard, J. A., Walker, M. W., Branchek, T. A. & Weinshank, R. L., Cloning and functional expression of a human Y4 subtype receptor for pancreatic polypeptide, neuropeptide Y, and peptide YY. *J Biol Chem* **1995,** *270* (45), 26762-26765, doi: 10.1074/jbc.270.45.26762.

85. Lundell, I., Blomqvist, A. G., Berglund, M. M., Schober, D. A., Johnson, D., Statnick, M. A., Gadski, R. A., Gehlert, D. R. & Larhammar, D., Cloning of a human receptor of the NPY receptor family with high affinity for pancreatic polypeptide and peptide YY. *J Biol Chem* **1995,** *270* (49), 29123-29128, doi: 10.1074/jbc.270.49.29123.

86. Gerald, C., Walker, M. W., Criscione, L., Gustafson, E. L., Batzl-Hartmann, C., Smith, K. E., Vaysse, P., Durkin, M. M., Laz, T. M., Linemeyer, D. L., et al., A receptor subtype involved in neuropeptide-Y-induced food intake. *Nature* **1996,** *382* (6587), 168-171, doi: 10.1038/382168a0.

87. Cabrele, C. & Beck-Sickinger, A. G., Molecular characterization of the ligand–receptor interaction of the neuropeptide Y family. *J Pept Sci* **2000,** *6* (3), 97-122, doi: 10.1002/(SICI)1099-1387(200003)6:3<97::AID-PSC236>3.0.CO;2-E.

88. Pedragosa Badia, X., Stichel, J. & Beck-Sickinger, A., Neuropeptide Y receptors: How to get subtype selectivity. *Front Endocrinol* **2013,** *4* (5), doi: 10.3389/fendo.2013.00005.

89. Zhang, L., Bijker, M. S. & Herzog, H., The neuropeptide Y system: Pathophysiological and therapeutic implications in obesity and cancer. *Pharmacol Ther* **2011,** *131* (1), 91-113, doi: 10.1016/j.pharmthera.2011.03.011.

90. Heilig, M., The NPY system in stress, anxiety and depression. *Neuropeptides* **2004,** *38* (4), 213-224, doi: 10.1016/j.npep.2004.05.002.

91. Tan, C. M. J., Green, P., Tapoulal, N., Lewandowski, A. J., Leeson, P. & Herring, N., The role of neuropeptide Y in cardiovascular health and disease. *Front Physiol* **2018,** *9* (1281), doi: 10.3389/fphys.2018.01281.

92. Taylor, B. K., NPY analgesia: Moving from acute to chronic pain. In *The NPY family of peptides in immune disorders, inflammation, angiogenesis and cancer*, Zukowska, Z. & Feuerstein, G. Z., Eds. Birkhäuser Basel: Basel, 2005; pp 135-148.

93. Tasan, R. O., Lin, S., Hetzenauer, A., Singewald, N., Herzog, H. & Sperk, G., Increased novelty-induced motor activity and reduced depression-like behavior in neuropeptide Y (NPY)-Y4 receptor knockout mice. *Neuroscience* **2009,** *158* (4), 1717-1730, doi: 10.1016/j.neuroscience.2008.11.048.

94. Painsipp, E., Wultsch, T., Edelsbrunner, M. E., Tasan, R. O., Singewald, N., Herzog, H. & Holzer, P., Reduced anxiety-like and depression-related behavior in neuropeptide Y Y4 receptor knockout mice. *Genes, brain, and behavior* **2008,** *7* (5), 532-542, doi: 10.1111/j.1601-183X.2008.00389.x.

95. Serova, L., Mulhall, H. & Sabban, E., NPY1 receptor agonist modulates development of depressive-like behavior and gene expression in hypothalamus in SPS rodent PTSD model. *Front Neurosci* **2017,** *11*, 203-203, doi: 10.3389/fnins.2017.00203.

96. Nahvi, R. J., Tanelian, A., Nwokafor, C., Hollander, C. M., Peacock, L. & Sabban, E. L., Intranasal neuropeptide Y as a potential therapeutic for depressive behavior in the rodent single prolonged stress model in females. *Front Behav Neurosci* **2021,** *15* (179), doi: 10.3389/fnbeh.2021.705579.

97. Carvajal, C., Dumont, Y., Herzog, H. & Quirion, R., Emotional behavior in aged neuropeptide Y (NPY) Y2 knockout mice. *J Mol Neurosci* **2006,** *28* (3), 239-245, doi: 10.1385/JMN:28:3:239.

98. Li, J. B., Asakawa, A., Terashi, M., Cheng, K., Chaolu, H., Zoshiki, T., Ushikai, M., Sheriff, S., Balasubramaniam, A. & Inui, A., Regulatory effects of Y4 receptor agonist (BVD-74D) on food intake. *Peptides* **2010,** *31* (9), 1706-1710, doi: 10.1016/j.peptides.2010.06.011.

99. Yan, C., Zeng, T., Lee, K., Nobis, M., Loh, K., Gou, L., Xia, Z., Gao, Z., Bensellam, M., Hughes, W., et al., Peripheral-specific Y1 receptor antagonism increases thermogenesis and protects against diet-induced obesity. *Nat Commun* **2021,** *12* (1), 2622, doi: 10.1038/s41467-021-22925-3.

100. Ailanen, L., Vähätalo, L. H., Salomäki-Myftari, H., Mäkelä, S., Orpana, W., Ruohonen, S. T. & Savontaus, E., Peripherally administered Y2-receptor antagonist BIIE0246 prevents diet-induced obesity in mice with excess neuropeptide Y, but enhances obesity in control mice. *Front Pharmacol* **2018,** 9, 319-319, doi: 10.3389/fphar.2018.00319.

101. Reubi, J. C., Gugger, M., Waser, B. & Schaer, J. C., Y1-mediated effect of neuropeptide Y in cancer: Breast carcinomas as targets. *Cancer research* **2001,** *61* (11), 4636-4641.

102. Körner, M., Waser, B. & Reubi, J. C., Neuropeptide Y receptors in renal cell carcinomas and nephroblastomas. *International journal of cancer* **2005,** *115* (5), 734-741, doi: 10.1002/ijc.20948.

103. Körner, M., Waser, B. & Reubi, J. C., Neuropeptide Y receptor expression in human primary ovarian neoplasms. *Laboratory investigation; a journal of technical methods and pathology* **2004,** *84* (1), 71-80, doi: 10.1038/labinvest.3700009.

104. Buschmann, J., Seiler, T., Bernhardt, G., Keller, M. & Wifling, D., Argininamide-type neuropeptide Y Y1 receptor antagonists: the nature of N(ω)-carbamoyl substituents determines Y1R binding mode and affinity. *RSC Med Chem* **2020,** *11* (2), 274-282, doi: 10.1039/c9md00538b.

105. Maschauer, S., Ott, J. J., Bernhardt, G., Kuwert, T., Keller, M. & Prante, O., 18F-labelled triazolyl-linked argininamides targeting the neuropeptide Y Y1R for PET imaging of mammary carcinoma. *Sci Rep* **2019,** 9 (1), 12990, doi: 10.1038/s41598-019-49399-0.

106. Grisé, K. R., Rongione, A. J., Laird, E. C. & McFadden, D. W., Peptide YY inhibits growth of human breast cancer in vitro and in vivo. *The Journal of surgical research* **1999,** *82* (2), 151-155, doi: 10.1006/jsre.1998.5528.

107. Lu, C., Everhart, L., Tilan, J., Kuo, L., Sun, C. C. J., Munivenkatappa, R. B., Jönsson-Rylander, A. C., Sun, J., Kuan-Celarier, A., Li, L., et al., Neuropeptide Y and its Y2 receptor: Potential targets in neuroblastoma therapy. *Oncogene* **2010,** *29* (41), 5630-5642, doi: 10.1038/onc.2010.301.

108. Kaiser, A., Wanka, L., Ziffert, I. & Beck-Sickinger, A. G., Biased agonists at the human Y1 receptor lead to prolonged membrane residency and extended receptor G protein interaction. *Cell Mol Life Sci* **2020,** *77* (22), 4675-4691, doi: 10.1007/s00018-019-03432-7.

109. Schneider, E., Mayer, M., Ziemek, R., Li, L., Hutzler, C., Bernhardt, G. & Buschauer, A., A simple and powerful flow cytometric method for the simultaneous determination of multiple parameters at G protein-coupled receptor subtypes. *Chembiochem* **2006,** *7* (9), 1400-1409, doi: 10.1002/cbic.200600163.

110. Pop, N., Igel, P., Brennauer, A., Cabrele, C., Bernhardt, G. N., Seifert, R. & Buschauer, A., Functional reconstitution of human neuropeptide Y (NPY) Y2 and Y4 receptors in Sf9 insect cells. *J Recept Signal Transduct Res* **2011,** *31* (4), 271-285, doi: 10.3109/10799893.2011.583253.

111. Ziemek, R., Brennauer, A., Schneider, E., Cabrele, C., Beck-Sickinger, A. G., Bernhardt, G. & Buschauer, A., Fluorescence- and luminescence-based methods for the determination of affinity and activity of neuropeptide Y2 receptor ligands. *Eur J Pharmacol* **2006,** *551* (1-3), 10-18, doi: 10.1016/j.ejphar.2006.08.075.

112. Berlicki, L., Kaske, M., Gutiérrez-Abad, R., Bernhardt, G., Illa, O., Ortuño, R. M., Cabrele, C., Buschauer, A. & Reiser, O., Replacement of Thr32 and Gln34 in the C-terminal neuropeptide Y fragment 25-36 by cis-cyclobutane and cis-cyclopentane β-amino acids shifts selectivity toward the Y4 receptor. *J Med Chem* **2013,** *56* (21), 8422-8431, doi: 10.1021/jm4008505.

113. Pop, N., Development of functional assays for human neuropeptide Y (Y1,2,4,5) receptors exploiting GTPase activity and (bio)luminescence as readout. 2010; 10.5283/epub.16430.

114. Shoblock, J. R., Welty, N., Nepomuceno, D., Lord, B., Aluisio, L., Fraser, I., Motley, S. T., Sutton, S. W., Morton, K., Galici, R., et al., In vitro and in vivo characterization of JNJ-31020028 (N-(4-{4-[2-(diethylamino)-2-oxo-1-phenylethyl]piperazin-1-yl}-3-fluorophenyl)-2-pyridin-3-ylbenzamide), a selective brain penetrant small molecule antagonist of the neuropeptide Y Y(2) receptor. *Psychopharmacology (Berl)* **2010,** *208* (2), 265-277, doi: 10.1007/s00213-009-1726-x.

115. Mittapalli, G. K., Vellucci, D., Yang, J., Toussaint, M., Brothers, S. P., Wahlestedt, C. & Roberts, E., Synthesis and SAR of selective small molecule neuropeptide Y Y2 receptor antagonists. *Bioorg Med Chem* **2012,** *22* (12), 3916-3920, doi: 10.1016/j.bmcl.2012.04.107.

116. Vita, N., Laurent, P., Lefort, S., Chalon, P., Dumont, X., Kaghad, M., Gully, D., Le Fur, G., Ferrara, P. & Caput, D., Cloning and expression of a complementary DNA encoding a high affinity human neurotensin receptor. *FEBS Lett* **1993,** *317* (1-2), 139-142, doi: 10.1016/0014-5793(93)81509-x.

117. Tanaka, K., Masu, M. & Nakanishi, S., Structure and functional expression of the cloned rat neurotensin receptor. *Neuron* **1990,** *4* (6), 847-854, doi: 10.1016/0896-6273(90)90137-5.

118. Chalon, P., Vita, N., Kaghad, M., Guillemot, M., Bonnin, J., Delpech, B., Le Fur, G., Ferrara, P. & Caput, D., Molecular cloning of a levocabastine-sensitive neurotensin binding site. *FEBS Lett* **1996,** *386* (2-3), 91-94, doi: 10.1016/0014-5793(96)00397-3.

119. Mazella, J., Botto, J. M., Guillemare, E., Coppola, T., Sarret, P. & Vincent, J. P., Structure, functional expression, and cerebral localization of the levocabastine-sensitive neurotensin/neuromedin N receptor from mouse brain. *J Neurosci* **1996,** *16* (18), 5613-5620, doi: 10.1523/jneurosci.16-18-05613.1996.

120. Grisshammer, R. & Hermans, E., Functional coupling with Gαq and Gαi1 protein subunits promotes high-affinity agonist binding to the neurotensin receptor NTS1 expressed in Escherichia coli. *FEBS Lett* **2001,** *493* (2-3), 101-105, doi: 10.1016/s0014-5793(01)02281-5.

121. Mustain, W. C., Rychahou, P. G. & Evers, B. M., The role of neurotensin in physiologic and pathologic processes. *Current opinion in endocrinology, diabetes, and obesity* **2011,** *18* (1), 75-82, doi: 10.1097/MED.0b013e3283419052.

122. Mazella, J., Zsürger, N., Navarro, V., Chabry, J., Kaghad, M., Caput, D., Ferrara, P., Vita, N., Gully, D., Maffrand, J. P., et al., The 100-kDa neurotensin receptor is gp95/sortilin, a non-G-protein-coupled receptor. *J Biol Chem* **1998,** *273* (41), 26273-26276, doi: 10.1074/jbc.273.41.26273.

123. Petersen, C. M., Nielsen, M. S., Nykjær, A., Jacobsen, L., Tommerup, N., Rasmussen, H. H., RØigaard, H., Gliemann, J., Madsen, P. & Moestrup, S. K., Molecular identification of a novel candidate sorting receptor purified from human brain by receptor-associated protein affinity chromatography. *J Biol Chem* **1997,** *272* (6), 3599-3605, doi: 10.1074/jbc.272.6.3599.

124. Carraway, R. & Leeman, S. E., The isolation of a new hypotensive peptide, neurotensin, from bovine hypothalami. *J Biol Chem* **1973,** *248* (19), 6854-6861, doi: 10.1016/S0021-9258(19)43429-7.

125. Morgat, C., Brouste, V., Chastel, A., Vélasco, V., Macgrogan, G. & Hindié, E., Expression of neurotensin receptor-1 (NTS1) in primary breast tumors, cellular distribution, and association with clinical and biological factors. *Breast Cancer Res Treat* **2021,** *190* (3), 403-413, doi: 10.1007/s10549-021-06402-5.

126. Younes, M., Wu, Z., Dupouy, S., Mansuet Lupo, A., Mourra, N., Takahashi, T., Flejou, J.-F., Trédaniel, J., Régnard, J. F., Damotte, D., et al., Neurotensin (NTS) and its receptor (NTSR1) causes EGFR, HER2 and HER3 over-expression and their autocrine/paracrine activation in lung tumors, confirming responsiveness to erlotinib. *Oncotarget* **2014,** *5* (18).

127. Körner, M., Waser, B., Strobel, O., Büchler, M. & Reubi, J. C., Neurotensin receptors in pancreatic ductal carcinomas. *EJNMMI Res* **2015,** *5* (1), 17, doi: 10.1186/s13550-015-0094-2.

128. Prignon, A., Provost, C., Alshoukr, F., Wendum, D., Couvelard, A., Barbet, J., Forgez, P., Talbot, J. N. & Gruaz-Guyon, A., Preclinical evaluation of 68Ga-DOTA-NT-20.3: A promising PET imaging probe to discriminate human pancreatic ductal adenocarcinoma from pancreatitis. *Molecular pharmaceutics* **2019,** *16* (6), 2776-2784, doi: 10.1021/acs.molpharmaceut.9b00283.

129. Morgat, C., Chastel, A., Molinie, V., Schollhammer, R., Macgrogan, G., Vélasco, V., Malavaud, B., Fernandez, P. & Hindié, E., Neurotensin receptor-1 expression in human prostate cancer: A pilot study on primary tumors and lymph node metastases. *Int J Mol Sci* **2019,** *20* (7), 1721.

130. Qiu, S., Nikolaou, S., Zhu, J., Jeffery, P., Goldin, R., Kinross, J., Alexander, J. L., Rasheed, S., Tekkis, P. & Kontovounisios, C., Characterisation of the expression of neurotensin and its receptors in human colorectal cancer and its clinical implications. *Biomolecules* **2020,** *10* (8), 1145.

131. Zhou, Z., Xie, J., Cai, Y., Yang, S., Chen, Y. & Wu, H., The significance of NTR1 expression and its correlation with β-catenin and EGFR in gastric cancer. *Diagnostic Pathol* **2015,** *10* (1), 128, doi: 10.1186/s13000-015-0356-3.

132. Maschauer, S. & Prante, O., Radiopharmaceuticals for imaging and endoradiotherapy of neurotensin receptor-positive tumors. *Journal of labelled compounds & radiopharmaceuticals* **2018,** *61* (3), 309-325, doi: 10.1002/jlcr.3581.

133. Alshoukr, F., Prignon, A., Brans, L., Jallane, A., Mendes, S., Talbot, J. N., Tourwé, D., Barbet, J. & Gruaz-Guyon, A., Novel DOTA-neurotensin analogues for 111In scintigraphy and 68Ga PET imaging of neurotensin receptor-positive tumors. *Bioconjug Chem* **2011,** *22* (7), 1374-1385, doi: 10.1021/bc200078p.

134. Maschauer, S., Einsiedel, J., Hübner, H., Gmeiner, P. & Prante, O., 18F- and 68Ga-labeled neurotensin peptides for PET imaging of neurotensin receptor 1. *J Med Chem* **2016,** *59* (13), 6480-6492, doi: 10.1021/acs.jmedchem.6b00675.

135. Renard, E., Moreau, M., Bellaye, P. S., Guillemin, M., Collin, B., Prignon, A., Denat, F. & Goncalves, V., Positron emission tomography imaging of neurotensin receptor-positive tumors with 68Ga-labeled antagonists: The chelate makes the difference again. *J Med Chem* **2021,** *64* (12), 8564-8578, doi: 10.1021/acs.jmedchem.1c00523.

136. Lang, C., Maschauer, S., Hübner, H., Gmeiner, P. & Prante, O., Synthesis and evaluation of a 18F-labeled diarylpyrazole glycoconjugate for the imaging of NTS1-positive tumors. *J Med Chem* **2013,** *56* (22), 9361-9365, doi: 10.1021/jm401491e.

137. García-Garayoa, E., Allemann-Tannahill, L., Bläuenstein, P., Willmann, M., Carrel-Rémy, N., Tourwé, D., Iterbeke, K., Conrath, P. & Schubiger, P. A., In vitro and in vivo evaluation of new radiolabeled neurotensin(8-13) analogues with high affinity for NT1 receptors. *Nuclear medicine and biology* **2001,** *28* (1), 75-84, doi: 10.1016/s0969-8051(00)00190-6.

138. García-Garayoa, E., Bläuenstein, P., Blanc, A., Maes, V., Tourwé, D. & Schubiger, P. A., A stable neurotensin-based radiopharmaceutical for targeted imaging and therapy of neurotensin receptor-positive tumours. *European journal of nuclear medicine and molecular imaging* **2009,** *36* (1), 37-47, doi: 10.1007/s00259-008-0894-y.

139. Schulz, J., Rohracker, M., Stiebler, M., Goldschmidt, J., Grosser, O. S., Osterkamp, F., Pethe, A., Reineke, U., Smerling, C. & Amthauer, H., Comparative evaluation of the biodistribution profiles of a series of nonpeptidic neurotensin receptor-1 antagonists reveals a promising candidate for theranostic applications. *J Nucl Med* **2016,** *57* (7), 1120-1123, doi: 10.2967/jnumed.115.170530.

140. Maschauer, S., Ruckdeschel, T., Tripal, P., Haubner, R., Einsiedel, J., Hübner, H., Gmeiner, P., Kuwert, T. & Prante, O., In vivo monitoring of the antiangiogenic effect of neurotensin receptor-mediated radiotherapy by small-animal positron emission tomography: a pilot study. *Pharmaceuticals (Basel, Switzerland)* **2014,** *7* (4), 464-481, doi: 10.3390/ph7040464.

141. Keller, M., Mahuroof, S. A., Hong Yee, V., Carpenter, J., Schindler, L., Littmann, T., Pegoli, A., Hübner, H., Bernhardt, G., Gmeiner, P., et al., Fluorescence labeling of neurotensin(8–13) via arginine residues gives molecular tools with high receptor affinity. *ACS Med Chem Lett* **2020,** *11* (1), 16-22, doi: 10.1021/acsmedchemlett.9b00462.

142. Granier, C., Van Rietschoten, J., Kitabgi, P., Poustis, C. & Freychet, P., Synthesis and characterization of neurotensin analogues for structure/activity relationship studies. *Eur J Biochem* **1982,** *124* (1), 117-125, doi: 10.1111/j.1432-1033.1982.tb05913.x.

143. Krumm, B. E., Lee, S., Bhattacharya, S., Botos, I., White, C. F., Du, H., Vaidehi, N. & Grisshammer, R., Structure and dynamics of a constitutively active neurotensin receptor. *Sci Rep* **2016,** *6* (1), 38564, doi: 10.1038/srep38564.

144. Barroso, S., Richard, F., Nicolas-Ethève, D., Kitabgi, P. & Labbé-Jullié, C., Constitutive activation of the neurotensin receptor 1 by mutation of Phe(358) in Helix seven. *Br J Pharmacol* **2002,** *135* (4), 997-1002, doi: 10.1038/sj.bjp.0704546.

145. Gully, D., Labeeuw, B., Boigegrain, R., Oury-Donat, F., Bachy, A., Poncelet, M., Steinberg, R., Suaud-Chagny, M. F., Santucci, V., Vita, N., et al., Biochemical and pharmacological activities of SR142948A, a new potent neurotensin receptor antagonist. *J Pharmacol Exp Ther* **1997,** *280* (2), 802-812.

146. Federsppiel, B., Melhado, I. G., Duncan, A. M., Delaney, A., Schappert, K., Clark-Lewis, I. & Jirik, F. R., Molecular cloning of the cDNA and chromosomal localization of the gene for a putative seven-transmembrane segment (7-TMS) receptor isolated from human spleen. *Genomics* **1993,** *16* (3), 707-712, doi: 10.1006/geno.1993.1251.

147. Rimland, J., Xin, W., Sweetnam, P., Saijoh, K., Nestler, E. J. & Duman, R. S., Sequence and expression of a neuropeptide Y receptor cDNA. *Mol Pharmacol* **1991,** *40* (6), 869-875.

148. Bhakta, S., Hong, P. & Koc, O., The surface adhesion molecule CXCR4 stimulates mesenchymal stem cell migration to stromal cell-derived factor-1 in vitro but does not decrease apoptosis under serum deprivation. *Cardiovasc Revasc Med* **2006,** *7* (1), 19-24, doi: 10.1016/j.carrev.2005.10.008.

149. Zlotnik, A. & Yoshie, O., The chemokine superfamily revisited. *Immunity* **2012,** *36* (5), 705-716, doi: 10.1016/j.immuni.2012.05.008.

150. Teixidó, J., Martínez-Moreno, M., Díaz-Martínez, M. & Sevilla-Movilla, S., The good and bad faces of the CXCR4 chemokine receptor. *The international journal of biochemistry & cell biology* **2018,** *95*, 121-131, doi: 10.1016/j.biocel.2017.12.018.

151. Anft, M., Paniskaki, K., Blazquez-Navarro, A., Doevelaar, A., Seibert, F. S., Hoelzer, B., Skrzypczyk, S., Kohut, E., Kurek, J., Zapka, J., et al., COVID-19 progression is potentially driven by T cell immunopathogenesis. *medRxiv* **2020**, 2020.2004.2028.20083089, doi: 10.1101/2020.04.28.20083089.

152. Grifoni, A., Weiskopf, D., Ramirez, S. I., Mateus, J., Dan, J. M., Moderbacher, C. R., Rawlings, S. A., Sutherland, A., Premkumar, L., Jadi, R. S., et al., Targets of T cell responses to SARS-CoV-2 coronavirus in humans with COVID-19 disease and unexposed individuals. *Cell* **2020,** *181* (7), 1489-1501.e1415, doi: 10.1016/j.cell.2020.05.015.

153. Neidleman, J., Luo, X., George, A. F., McGregor, M., Yang, J., Yun, C., Murray, V., Gill, G., Greene, W. C., Vasquez, J., et al., Distinctive features of SARS-CoV-2-specific T cells predict recovery from severe COVID-19. *medRxiv* **2021**, 2021.2001.2022.21250054, doi: 10.1101/2021.01.22.21250054.

154. Lambertini A., H. P., Serfling S., Meybohm P., Schirbel A., Buck A., Gallium-68-CXCR4-PET/CT chemokine receptor-targeting imaging in acute SARS-Cov-2 infection: A case report. *J Nucl Med* **2021,** *60* (02), 1, doi: 10.1055/s-0041-1726735.

155. Tsutsumi, H., Tanaka, T., Ohashi, N., Masuno, H., Tamamura, H., Hiramatsu, K., Araki, T., Ueda, S., Oishi, S. & Fujii, N., Therapeutic potential of the chemokine receptor CXCR4 antagonists as multifunctional agents. *Biopolymers* **2007,** *88* (2), 279-289, doi: 10.1002/bip.20653.

156. Tamamura, H., Araki, T., Ueda, S., Wang, Z., Oishi, S., Esaka, A., Trent, J. O., Nakashima, H., Yamamoto, N., Peiper, S. C., et al., Identification of novel low molecular weight CXCR4 antagonists by structural tuning of cyclic tetrapeptide scaffolds. *J Med Chem* **2005,** *48* (9), 3280-3289, doi: 10.1021/jm050009h.

157. Murakami, T., Nakajima, T., Koyanagi, Y., Tachibana, K., Fujii, N., Tamamura, H., Yoshida, N., Waki, M., Matsumoto, A., Yoshie, O., et al., A small molecule CXCR4 inhibitor that blocks T cell line-tropic HIV-1 infection. *J Exp Med* **1997,** *186* (8), 1389-1393, doi: 10.1084/jem.186.8.1389.

158. Maurer, S., Herhaus, P., Lippenmeyer, R., Hänscheid, H., Kircher, M., Schirbel, A., Maurer, H. C., Buck, A. K., Wester, H. J., Einsele, H., et al., Side effects of CXC-chemokine receptor 4-directed endoradiotherapy with pentixather before hematopoietic stem cell transplantation. *J Nucl Med* **2019,** *60* (10), 1399-1405, doi: 10.2967/jnumed.118.223420.

159. Lapa, C., Hänscheid, H., Kircher, M., Schirbel, A., Wunderlich, G., Werner, R. A., Samnick, S., Kotzerke, J., Einsele, H., Buck, A. K., et al., Feasibility of CXCR4-directed radioligand therapy in advanced diffuse large B-cell lymphoma. *J Nucl Med* **2019,** *60* (1), 60-64, doi: 10.2967/jnumed.118.210997.

160. Habringer, S., Lapa, C., Herhaus, P., Schottelius, M., Istvanffy, R., Steiger, K., Slotta-Huspenina, J., Schirbel, A., Hänscheid, H., Kircher, S., et al., Dual targeting of acute Leukemia and supporting niche by CXCR4-directed theranostics. *Theranostics* **2018,** *8* (2), 369-383, doi: 10.7150/thno.21397.

161. Herrmann, K., Schottelius, M., Lapa, C., Osl, T., Poschenrieder, A., Hänscheid, H., Lückerath, K., Schreder, M., Bluemel, C., Knott, M., et al., First-in-human experience of CXCR4-directed endoradiotherapy with 177Lu- and 90Y-labeled pentixather in advanced-stage multiple myeloma with extensive intra- and extramedullary disease. *J Nucl Med* **2016,** *57* (2), 248-251, doi: 10.2967/jnumed.115.167361.

162. Lapa, C., Herrmann, K., Schirbel, A., Hänscheid, H., Lückerath, K., Schottelius, M., Kircher, M., Werner, R. A., Schreder, M., Samnick, S., et al., CXCR4-directed endoradiotherapy induces high response rates in extramedullary relapsed Multiple Myeloma. *Theranostics* **2017,** *7* (6), 1589-1597, doi: 10.7150/thno.19050.

163. Hyafil, F., Pelisek, J., Laitinen, I., Schottelius, M., Mohring, M., Döring, Y., van der Vorst, E. P., Kallmayer, M., Steiger, K., Poschenrieder, A., et al., Imaging the cytokine receptor CXCR4 in atherosclerotic plaques with the radiotracer 68Ga-pentixafor for PET. *J Nucl Med* **2017,** *58* (3), 499-506, doi: 10.2967/jnumed.116.179663.

164. Derlin, T., Jaeger, B., Jonigk, D., Apel, R. M., Freise, J., Shin, H. O., Weiberg, D., Warnecke, G., Ross, T. L., Wester, H. J., et al., Clinical molecular imaging of pulmonary CXCR4 expression to predict outcome of pirfenidone treatment in idiopathic pulmonary fibrosis. *Chest* **2021,** *159* (3), 1094-1106, doi: 10.1016/j.chest.2020.08.2043.

165. Lapa, C., Reiter, T., Werner, R. A., Ertl, G., Wester, H. J., Buck, A. K., Bauer, W. R. & Herrmann, K., [68Ga]Pentixafor-PET/CT for imaging of chemokine receptor 4 expression after myocardial infarction. *JACC. Cardiovascular imaging* **2015,** *8* (12), 1466-1468, doi: 10.1016/j.jcmg.2015.09.007.

166. Thackeray, J. T., Derlin, T., Haghikia, A., Napp, L. C., Wang, Y., Ross, T. L., Schäfer, A., Tillmanns, J., Wester, H. J., Wollert, K. C., et al., Molecular imaging of the chemokine receptor CXCR4 after acute myocardial infarction. *JACC. Cardiovascular imaging* **2015,** *8* (12), 1417-1426, doi: 10.1016/j.jcmg.2015.09.008.

167. Thiele, S., Mungalpara, J., Steen, A., Rosenkilde, M. M. & Våbenø, J., Determination of the binding mode for the cyclopentapeptide CXCR4 antagonist FC131 using a dual approach of ligand modifications and receptor mutagenesis. *Br J Pharmacol* **2014,** *171* (23), 5313-5329, doi: 10.1111/bph.12842.

168. Spiller, S., Wippold, T., Bellmann-Sickert, K., Franz, S., Saalbach, A., Anderegg, U. & Beck-Sickinger, A. G., Protease-triggered release of stabilized CXCL12 from coated scaffolds in an ex vivo wound model. *Pharmaceutics* **2021,** *13* (10), 1597.

169. Işbilir, A., Möller, J., Arimont, M., Bobkov, V., Perpiñá-Viciano, C., Hoffmann, C., Inoue, A., Heukers, R., de Graaf, C., Smit, M. J., et al., Advanced fluorescence microscopy reveals disruption of dynamic CXCR4 dimerization by subpocket-specific inverse agonists. *Proc Natl Acad Sci U S A* **2020,** *117* (46), 29144-29154, doi: 10.1073/pnas.2013319117.

170. Zhang, W. B., Navenot, J. M., Haribabu, B., Tamamura, H., Hiramatu, K., Omagari, A., Pei, G., Manfredi, J. P., Fujii, N., Broach, J. R., et al., A point mutation that confers constitutive activity to CXCR4 reveals that T140 is an inverse agonist and that AMD3100 and ALX40-4C are weak partial agonists. *J Biol Chem* **2002,** *277* (27), 24515-24521, doi: 10.1074/jbc.M200889200.

171. Milligan, G. & Bouvier, M., Methods to monitor the quaternary structure of G protein-coupled receptors. *The FEBS journal* **2005,** *272* (12), 2914-2925, doi: 10.1111/j.1742-4658.2005.04731.x.

172. Dixon, A. S., Schwinn, M. K., Hall, M. P., Zimmerman, K., Otto, P., Lubben, T. H., Butler, B. L., Binkowski, B. F., Machleidt, T., Kirkland, T. A., et al., NanoLuc complementation reporter optimized for accurate measurement of protein interactions in cells. *ACS Chem Biol* **2016,** *11* (2), 400-408, doi: 10.1021/acschembio.5b00753.

173. Hoare, S. R. J., Tewson, P. H., Quinn, A. M., Hughes, T. E. & Bridge, L. J., Analyzing kinetic signaling data for G-protein-coupled receptors. *Sci Rep* **2020,** *10* (1), 12263, doi: 10.1038/s41598-020-67844-3.

174. Smith, N. J., Bennett, K. A. & Milligan, G., When simple agonism is not enough: emerging modalities of GPCR ligands. *Mol Cell Endocrinol* **2011,** *331* (2), 241-247, doi: 10.1016/j.mce.2010.07.009.

175. Schrage, R., De Min, A., Hochheiser, K., Kostenis, E. & Mohr, K., Superagonism at G protein-coupled receptors and beyond. *Br J Pharmacol* **2016,** *173* (20), 3018-3027, doi: 10.1111/bph.13278.

176. Ross, E. M., G Protein-coupled receptors: Multi-turnover GDP/GTP exchange catalysis on heterotrimeric G proteins. *Cell Logist* **2014,** *4*, e29391-e29391, doi: 10.4161/cl.29391.

177. Ross, E. M., Coordinating speed and amplitude in G-protein signaling. *Curr Biol* **2008,** *18* (17), R777-R783, doi: 10.1016/j.cub.2008.07.035.

178. Nehmé, R., Carpenter, B., Singhal, A., Strege, A., Edwards, P. C., White, C. F., Du, H., Grisshammer, R. & Tate, C. G., Mini-G proteins: Novel tools for studying GPCRs in their active conformation. *PLoS One* **2017,** *12* (4), e0175642, doi: 10.1371/journal.pone.0175642.

179. Müller, M., Knieps, S., Gessele, K., Dove, S., Bernhardt, G. & Buschauer, A., Synthesis and neuropeptide Y Y1 receptor antagonistic activity of N,N-disubstituted ω-guanidino- and ω-aminoalkanoic acid amides. *Arch Pharm (Weinheim)* **1997,** *330* (11), 333-342, doi: 10.1002/ardp.19973301104.

180. Weiss, S., Keller, M., Bernhardt, G., Buschauer, A. & König, B., Modular synthesis of non-peptidic bivalent NPY Y1 receptor antagonists. *Bioorg Med Chem* **2008,** *16* (22), 9858-9866, doi: 10.1016/j.bmc.2008.09.033.

181. Gundry, J., Glenn, R., Alagesan, P. & Rajagopal, S., A practical guide to approaching biased agonism at G protein coupled receptors. *Front Neurosci* **2017,** *11* (17), doi: 10.3389/fnins.2017.00017.

4. Towards the Application of Mini-G Protein Recruitment Assays at the Endogenous Level

Note: The content of this chapter is part of a collaborative project with Dr. Laura Humphrys. While the CRISPR/Cas9 experiments were conceived by Dr. Laura Humphrys, all experimental work, including molecular cloning and cell assays, was performed in equal parts by Carina Höring and Dr. Laura Humphrys.

4.1. Introduction

In G protein-coupled receptor (GPCR) research, the utilization of bioluminescence resonance energy transfer (BRET)- or split luciferase complementation (SLC)-based G protein biosensors has overcome the safety and cost limitations of [^{35}S]GTPγS binding assays traditionally employed for the functional characterization of GPCR ligands.[1-2] Both techniques are commonly used to detect protein - protein interactions in cells and rely on genetically encoded reporter proteins that are conjugated to the proteins of interest, such as the GPCR and G protein.[3-7] While BRET applications use an intact luciferase (donor) to excite a fluorescent protein (acceptor) when both proteins are at a distance < 100 Å, SLC applications use a dissected luciferase.[8-9] Complementation of the luciferase fragments then restores their catalytic activity and promotes the oxidation of a substrate, followed by the release of bioluminescence.[10] In addition to the safety and cost benefits, the homogenous performance of RET- and SLC-based assays allows the observation of G protein activation or rather GPCR – G protein interaction in real-time and in intact cells.[4] However, unlike traditional [^{35}S]GTPγS binding assays, genetically encoded biosensors have only sparsely been applicable at the endogenous receptor level due to the generation of GPCR fusion proteins.[11-12] Considering that overexpression of receptors could lead to a shift in the relative abundance of interacting partners, including potential partners for receptor dimerization, G proteins, or β-arrestins endogenously expressed in cells, receptor expression levels might become critical in terms of receptor reserve and signal amplitudes.[13-14]

In recent years, the modification of endogenous gene loci has been simplified by the discovery of certain endonucleases, such as by zinc-finger nucleases (ZFNs),[15-16] transcription activator-like effector nucleases (TALENs),[17-18] and clustered regularly interspaced short palindromic repeats associated protein (CRISPR/Cas) systems,[19-21] all facilitating programmable site-specific DNA cleavage. Both ZFNs and TALENs consist of a DNA-binding domain, which binds to the gene locus, and an endonuclease domain, which induces double-stranded DNA (dsDNA) breaks upon dimerization.[22] In contrast, Cas endonucleases form a complex with small guide RNA (gRNA), which locates the enzyme to the target site and is particularly easy to design for experiments.[20-21] Therefore, the highly specific and efficient CRISPR/Cas system has become a widely used method for genome editing and has already been used to generate cells endogenously expressing engineered luciferases or fluorescent proteins.[23-26] In particular, the engineered NanoLuc, based on a luciferase from deep-sea shrimp *Oplophorus gracilirostris*, appeared attractive for insertion into cell genomes due to its small size (19 kDa) and bright luminescence.[27] For example, NanoLuc and its dissected variant split NanoLuc[28] have already been integrated into cell genomes allowing the detection of protein up-/downregulation,[29-31] GPCR - β-arrestin interaction[11] and ligand binding to a GPCR[12] under endogenous promotion.

As subject to this thesis, mini-G protein sensors consisted of GPCRs C-terminally fused to the small split-NanoLuc fragment (NlucC) and the corresponding mini-G protein (mGs, mGsi, or mGsq) N-terminally fused to the large fragment (NlucN), and were recombinantly expressed in HEK293T cells (cf. Chapter 2 and 3).[3-4,32-36] Immortalized HEK293 cells are among the most popular human cell lines in GPCR research to exogenously express receptors and other proteins of interest, since they are easy to transfect and provide an appropriate cellular matrix in terms of membrane lipid composition and post-translational modifications,[37-39] greatly influencing receptor conformation, signaling and regulation.[40-42] However, analyses of mRNA expression levels and pharmacological experiments have revealed that HEK293 cells endogenously express certain GPCRs, such as β-adrenoceptors (βAR).[37-38,43] Due to the similarities between the βAR subtypes, there is still uncertainty as to whether HEK293 cells functionally express solely β_2AR or also β_1AR. Although van der Hagen et al. have demonstrated the functional expression of β_1AR in HEK293 cells by mRNA levels and cAMP responses,[43] other studies demonstrated only β_2AR-mediated functional responses, which could not be blocked by β_1-selective antagonist.[44-47]

Therefore, the aim of this study was to investigate, on one hand, whether recently developed SLC-based mini-G protein sensors (cf. Chapter 2 and 3) are useful to detect receptor activation at the endogenous level and, on the other hand, whether only β_2AR or also β_1AR is expressed in HEK293T cells.[3-4,32-36] For this purpose, CRISPR/Cas9 genome editing experiments were designed for both receptor subtypes to generate $\beta_{1,2}$AR-NlucC fusion proteins. To assess whether the receptor expression level affects dynamic and pharmacological aspects of mini-G protein recruitment, mGs sensors were first validated at recombinantly expressed $\beta_{1,2}$AR (overexpressed) using standard agonists and antagonists and then applied to CRISPR/Cas9-modified $\beta_{1,2}$AR to measure receptor activation at the endogenous level.

4.2. Materials and Methods

4.2.1. Materials

Dulbecco's modified Eagle's medium (DMEM) was purchased from Sigma-Aldrich (Taufkirchen, Germany) and Leibovitz' L-15 medium (L-15) from Fisher Scientific (Nidderau, Germany). FCS and trypsin/EDTA were from Merck Biochrom (Darmstadt, Germany) and furimazine was from Promega (Mannheim, Germany). The pcDNA3.1 vector was from Thermo Scientific (Nidderau, Germany) and the pIRESpuro3 vector was a kindly provided by Prof. Dr. Gunter Meister (University of Regensburg, Regensburg, Germany). The pU6-SacB-scRNA-Cas9-T2A-mCherry plasmid was a gift from Kim Failor (Addgene plasmid # 117070 ; www.n2t.net/addgene:117070 ; RRID: Addgene_117070; access date: 12.05.2022) and pFETCh_Donor (EMM0021) was a gift from Eric Mendenhall & Richard M. Myers (Addgene plasmid # 63934 ; www.n2t.net/addgene:63934 ; RRID: Addgene_63934; access date: 12.05.2022). The cDNA encoding the β_1AR was a kind gift from Dr. Ulrike Zabel (University of Würzburg, Würzburg, Germany) and the β_2AR cDNA was purchased from the Missouri cDNA research center (Rolla, MO, USA). Restriction enzymes *Bbs*I and *Bsa*I were from (ThermoFisher, Braunschweig, Germany) and *Dpn*I, *Hin*dIII and *Xba*I as well as the NEBuilder® HiFi DNA Assembly Cloning Kit were from New England Biolabs (New England Biolabs GmbH, Frankfurt a. M., Germany). L-adrenaline (adren), L-noradrenaline tartrate (noradren), isoprenaline hydrochloride (isopren), salbutamol hemisulfate (salbut), carvedilol (carv), ICI 118551 hydrochloride (ICI118551) were from Sigma Aldrich (Taufkirchen, Germany). Xamoterol hemifumarate (xamo) was from Tocris Bioscience (Bristol, UK). For preparation of stock solutions, the ligands were preferably dissolved in Millipore water. Except, adrenaline was dissolved in a mixture of 10 mM HCl and MDSO (50 : 50), and carvedilol was dissolved in DMSO.

4.2.2. Molecular Cloning

4.2.2.1. Isolation of Genomic DNA and RNA

Genomic DNA (gDNA) and RNA were isolated from wildtype or CRISPR/Cas9 genome edited HEK293T cells. For gDNA isolation, the Monarch Genomic DNA Purification kit (New England Biolabs GmbH, Frankfurt a. M., Germany) was utilized using 1-2 x 10^6 cells. RNA was isolated from 1-2 x 10^6 cells using the Jena Bioscience Total RNA Purification kit (Jena Bioscience GmbH, Jena, Germany). Afterwards, co-precipitated DNA was removed by DNAse I (New England Biolabs) digest at 37 °C for 10 min followed by a heat inactivation step at 75 °C for 10 min. Then, RNA was purified from the DNAse reaction mix using the spin column RNA cleanup step of the Qiagen RNeasy Mini kit (Qiagen GmbH, Hilden, Germany) and reversely transcribed into cDNA using the ProtoScript II NEB cDNA synthesis kit (New England Biolabs).

4.2.2.2. Generation of pcDNA3.1 $\beta_{1,2}$AR-NlucC

The molecular cloning strategy of pIRESpuro3 plasmids encoding the NlucN-mGs, fusion protein was described in Chapter 2 (section 2.2.2). For construction of pcDNA3.1 plasmids encoding the β_2AR-NlucC or β_1AR-NlucC fusion protein, a Gibson assembly protocol was performed (cf. Chapter 3, section 3.2.2).[48] Therefore, a pcDNA3.1 encoding the small fragment of the NanoLuc (NlucC) was linearized by restriction digest using *Hin*dIII and *Xba*I and then fused to the *Dpn*I digested PCR product of β_2AR or β_1AR, which contained respective overlaps to the vector backbone, using the NEBuilder® HiFi DNA Assembly Cloning Kit. All plasmid DNA was quantified by UV-Vis absorbance using a NanoDrop spectrophotometer (ThermoFisher, Braunschweig, Germany). All sequences were verified by sequencing performed by Eurofins Genomics (Eurofins Genomics LLC, Ebersberg, Germany).

4.2.2.3. Generation of pU6-gRNA-Cas9-T2A-mCherry Plasmids

To attach NlucC to the C-terminus of endogenously expressed β_2AR and β_1AR, the CRISPR /Cas9 protocol provided by Mendenhall and Myers labs (www.addgene.org/63934/; access date: 12.05.2022) has been used. The utilized CRISPR /Cas9 system consisted of a gRNA attached to a scaffold RNA (scRNA) and Cas9 encoding plasmid (pU6-SacB-scRNA-Cas9-T2A-mCherry) as well as a donor plasmid (pFETCh donor) for homology directed repair (HDR). An overview of primer sequences used for the generation and verification of HEK293T CRISPR $\beta_{1,2}$AR-NlucC cells is given in the Appendix (Table A3). Using the Benchling web server (www.benchling.com; access date: 19.11.2020), oligonucleotides encoding the guide RNA (gRNA oligos; β_1AR: O1/O2, β_2AR: O3/O4; cf. Appendix, Table A3), were selected upstream from the *Streptococcus pyogenes* Cas9 protospacer adjacent motif (PAM; β_1AR-PAM: GGG, β_2AR-PAM: AGG). The gRNA oligos each comprised 20 nucleotides for specific binding to the target site plus four nucleotides forming the corresponding overlap to the *Bbs*I digested vector. The single stranded gRNA oligos were annealed in NEBuffer 2 (New England Biolabs) at 95 °C for 5 min and left to cool down for 1 h. Thereafter, each of the annealed gRNA oligos were subcloned into the pU6-SacB-scRNA-Cas9-mCherry vector using a Golden Gate assembly protocol. In this one-pot reaction, the vector was digested with *Bbs*I at 37 ° for 5 min creating 4-base overlaps. The temperature was adjusted to 22 °C for 10 min to let the T4 DNA ligase (New England Biolabs) form covalent bonds between the vector and gRNA. During another incubation at 37 °C for 30 min, remaining circular vector molecules were completely linearized to reduce false positives after transformation. All enzymes were heat inactivated at 75 °C for 15 min prior to the transformation of TOP10'F *E. coli*. By correct insertion of the gRNA into pU6-SacB-scRNA-Cas9-mCherry yielding pU6-gRNA-Cas9-mCherry plasmids, the SacB gene was destroyed and allowed transformed TOP10'F *E.coli* to grow on LB plates containing

100 µg/mL ampicillin and 5% sucrose, the negative selection marker producing sucrase to convert sucrose into its toxic metabolite.[49]

The ability of selected gRNAs to guide the Cas9 nuclease to $\beta_{1,2}$AR target sites was verified by T7 endonuclease digest recognizing DNA mismatches. For this purpose, 2 µg of the pU6-gRNA-Cas9-T2A-mCherry plasmids were transiently transfected into HEK293T cells using XtremeGene HP (1 : 3 ratio; Merck Biochrom, Darmstadt, Germany). After 48 h at 37 °C in humidified, 5%-CO_2 atmosphere, the transfectants were harvested and gDNA was isolated as described earlier. Diagnostic DNA templates were amplified from gDNA using primer pairs O5/O6 for the β_1AR and O7/O8 for the β_2AR (cf. Appendix, Table A3) and digested using T7 endonuclease I (New England Biolabs GmbH, Frankfurt a. M., Germany) according to the supplier's protocol. Digested PCR products were visually inspected after separation by 0.8% agarose gel electrophoresis and revealed cleaved PCR products, which indicated DNA mismatches caused by Cas9 nuclease cleavage.

4.2.2.4. Generation of Specific pFETCh HOM2-NeoR-P2A-NlucC-HOM1 Plasmids

In a first cloning step, the FLAG sequence of the pFETCh vector was replaced by the NlucC sequence. Primers O9 and O10 were used to linearize the vector and corresponding overlaps were attached to the NlucC sequence using primers O11 and O12 by PCR. The PCR products were digested with *Dpn*I and purified by 0.8% agarose gel electrophoresis and subsequent spin column purification using the Nippon Genetics PCR/Gel electrophoresis purification kit (NIPPON Genetics EUROPE, Düren, Germany). Purified DNA fragments were annealed and ligated using a Gibson assembly protocol yielding pFETCh NeoR-P2A-NlucC. Sequences of the homology arms 1 and 2 (HOM1, HOM2) specific for β_1AR and β_2AR were determined using the Benchling (www.benchling.com) and Ensembl (www.ensembl.org) web servers. Both, HOM1 and HOM2, were designed to include 700 – 800 bp. HOM1 comprised the C-terminal end of either the β_1AR or β_2AR (without stop codon) and HOM2 was selected downstream of the receptor sequence in the genomic DNA. Specifically, homology arm primers were selected to remove the native $\beta_{1,2}$AR stop codon as well as the *Streptococcus pyogenes* Cas9 protospacer adjacent motif (PAM) to prevent further enzymatic cleavage after successful CRISPR/Cas9 reactions (β_1AR-PAM: GGG → GTG, β_2AR-PAM: AGG → AGA). HOM1 and HOM2 were amplified from HEK293T gDNA and overlaps similar to those created by type IIS enzyme digest (*Bsa*I for HOM1 and *Bbs*I for HOM2) were added by PCR. For the β_1AR, the primer pairs O13/O14 and O15/O16, and for the β_2AR the primer pairs O17/O18 and O19/O20 were used to obtain HOM1 and HOM2, respectively (cf. Appendix, Table A3). The pFETCh NeoR-P2A-NlucC plasmid was digested with *Bbs*I and *Bsa*I and annealed with purified HOM1 and HOM2 PCR products in a Gibson assembly reaction yielding pFETCh HOM1-NlucC-P2A-NeoR-HOM2 specific for either β_1AR or β_2AR.

4.2.3. Cell Culture

HEK293T cells that were a kind gift from Prof. Dr. Wulf Schneider (Institute for Medical Microbiology and Hygiene, Regensburg, Germany), were cultured in DMEM supplemented with 10% FCS at 37 °C in humidified, 5% CO_2 atmosphere. The cells were periodically tested negative for mycoplasma contamination using the Venor GeM Mycoplasma Detection Kit (Minerva Biolabs, Berlin, Germany).

4.2.3.1. Generation of Stable Transfectants

To generate HEK293T cells stably co-expressing NlucN-mGs and β_2AR-NlucC or β_1AR-NlucC fusion proteins (overexpressed), the parental HEK293T NlucN-mGs cells (cf. Chapter 2, section 2.2.5) were seeded into a 6-well cell culture plate (Sarstedt, Nümbrecht, Germany) at a cell density of 0.3 x 10^6 cells/mL (2 mL per well) and allowed to attach overnight. The next day, 2 µg of pcDNA3.1 $\beta_{1,2}$AR-NlucC plasmid DNA was transfected to the cells using the XtremeGene HP transfection protocol (ratio 1 µg DNA: 3 µL XtremeGene HP). Finally, the cells were then cultured in DMEM supplemented with 10% FCS, 1 µg/mL puromycin and 600 µg/mL G418 for sustained selection pressure.

To generate genome edited HEK293T cells (HEK293T CRISPR $\beta_{1,2}$AR-NlucC), HEK293T wildtype cells were seeded in a T25 cell culture flask at a cell density of 0.3 x 10^6 cells/mL. After the cells had grown overnight, 2 µg of the pFETCh HOM1-NlucC-P2A-NeoR-HOM2 and 1 µg of the pU6-gRNA-Cas9-T2A-mCherry plasmids, specific for either the β_1AR or β_2AR, were transfected using 12 µL XtremeGene HP transfection reagent (1 : 4 ratio). The pU6-gRNA-Cas9-T2A-mCherry plasmid essentially encoded a β_1AR- or β_2AR-specific guide RNA (gRNA) and the Cas9 endonuclease itself causing DNA double-strand breaks at the target site. The second plasmid, pFETCh donor, contained the "insert" composed of the NlucC sequence, a self-cleaving 2A peptide sequence (P2A), and the neomycin resistance (NeoR) gene flanked by two homology arm sequences selected upstream and downstream of the endogenous receptor stop codon (cf. Figure 4.2A).[50] During homologous recombination of the DNA strands, the insert was integrated in frame to the coding sequence of the $\beta_{1,2}$AR by homology-directed repair (HDR).[50] Through amino acid cleavage and ribosomal skipping at the P2A sequence, transcription and translation of the receptor genes then led to the expression of two individual proteins, $\beta_{1,2}$AR-NlucC and NeoR.[51] After two weeks of antibiotic selection using 1000 µg/mL G418, single clones were isolated from the heterogenous cell population by dilution cloning. Afterwards, single clones were cultured in DMEM (full medium) containing 600 µg/mL G418.

4.2.3.2. Transient Expression of NlucN-mGs in HEK293T CRISPR $\beta_{1,2}$AR-NlucC Cells

To verify successful generation of $\beta_{1,2}$AR-NlucC using CRISPR/Cas9 by mini-G protein recruitment assays, pooled HEK293T CRISPR $\beta_{1,2}$AR-NlucC cells were seeded onto a 6-well cell culture plate at a density of 0.3 x 10^6 cells/mL (2 mL per well) and were transiently transfected the next day with a total amount of 1 µg plasmid DNA using 3 µL XtremeGene HP (1 : 3 ratio). For this purpose, different mixtures were prepared comprising 17 ng, 35 ng, 70 ng, 140 ng, 280 ng or 567 ng of pIRESpuro3 NlucN-mGs plasmid DNA in combination with 983 ng, 965 ng, 930 ng, 860 ng, 720 ng or 433 ng of an empty pIRESpuro3 plasmid (mock DNA), respectively. Transfectants were incubated at 37 °C for 48 h in humidified, 5% CO_2 atmosphere.

To screen single clones isolated from pooled HEK293T CRISPR $\beta_{1,2}$AR-NlucC cells by mini-G protein recruitment assays, the single clones were seeded in duplicate to 96-well cell culture plates at a density of 0.3 x 10^6 cells/mL (100 µL per well) and transiently transfected with pIRESpuro3 NlucN-mGs plasmid DNA using XtremeGene HP transfection reagent (1 : 3 ratio). For this, a transfection mixture was prepared in 250 µL DMEM containing 2600 ng plasmid DNA and 7.8 µL XtremeGene HP, which was of the recommended DNA concentration according to the manufacturers protocol. After 15 min incubation, the transfection mix was diluted to 1000 µL and 100 µL each of the diluted transfection complex were added to the cells in the 96-well plate. Transfectants were incubated at 37 °C for 48 h in humidified, 5% CO_2 atmosphere.

To functionally characterize $\beta_{1,2}$AR ligands in the mini-G protein recruitment assay at the endogenous receptor level, CRISPR/Cas9 positive single clones, HEK293T CRISPR β_1AR-NlucC clone 11 or HEK293T CRISPR β_2AR-NlucC clone 35, were seeded into 6-well cell culture plates at a cell density of 0.3 x 10^6 cells/mL (2 mL per well) and allowed to attach overnight. The next day, the cells were transfected with a total plasmid DNA amount of 1 µg using 3 µL XtremeGeneHP transfection reagent (1 : 3 ratio). For this, 280 ng of pIRESpuro3 NlucN-mGs and 720 ng of empty pIRESpuro3 (mock) plasmid DNA were used. Transfectants were incubated at 37 °C for 48 h in humidified, 5% CO_2 atmosphere.

4.2.4. Mini-G Protein Recruitment Assays

The day prior to the experiment, stable or transient transfectants, except for single clone screens, were detached using trypsin (0.05% trypsin, 0.02% EDTA in PBS) and centrifuged (700 g, 5 min). Thereafter, the cells were resuspended in 2.5 mL L-15 supplemented with 10 mM HEPES (Serva, Heidelberg, Germany) and 5% FCS (assay medium) and 80 µL or 40 µL per well were seeded into white flat-bottom 96- or 384-well microtiter plates (Brand GmbH + CoKG, Wertheim, Germany), respectively. For single clone screens, the cell culture medium (DMEM, full medium) was removed from the cells, which had been transiently transfected in the 96-well plate. Following a washing step, 80 µL of assay medium were added to the cells. All cells were incubated overnight at 37 °C in a water-saturated atmosphere without additional CO_2.

For mini-G protein recruitment assays performed in 96-well plates, the assay protocol was described in Chapter 2, section 2.2.7. When assays were performed in 384-well plates the protocol was adjusted as follows: The furimazine substrate was diluted 1:500 in L-15 and 5 µL were added to the cells (final assay dilution: 1:5000). The plate was transferred to the pre-heated (37 °C) Tecan Infinite 200 Pro plate reader (Tecan Trading, Ltd., Männedorf, Switzerland) and 5 plate repeats of basal luminescence were recorded (~16.5 min). Thereafter, 5 µL of the agonist serial dilutions prepared in L-15 were added to each well (final assay volume: 50 µL) and luminescent signals were recorded for additional 15 plate repeats (~49.5 min). An integration time of 0.2 s per well was used to capture the luminescence and plate repeats lasted 198 s.

Data were analyzed using GraphPad Prism9 software (San Diego, CA, USA). In a first baseline-correction step, the relative luminescence units (RLU) were corrected for slight inter-well variations caused by differences in cell density and substrate concentration by dividing the data of each well by its luminescence prior to the addition of the ligands. In a second baseline-correction step, all data were divided by the mean luminescence of L-15 containing wells giving relative increases in luminescence. For each well, the area under curve (AUC) of the luminescent traces was normalized to the maximum response of the reference agonist (10 µM adren) and L-15 (0% control). For assays performed in 96-well plates using an EnSpire plate reader (Perkin Elmer Inc., Rodgau, Germany), AUCs were calculated of signals within 45 min (90 plate repeats of 30 s length each). For assays performed in 384-well plates, AUCs were calculated of signals within ~49.5 min (15 plate repeats of 198 s length each). Normalized data were then fitted against the logarithmic ligand concentrations with variable slope (log(c) vs. response – variable slope (four parameters)) giving pEC_{50} and E_{max} values.

4.2.5. Calculation of $\Delta\log(E_{max}/EC_{50})$

For each experiment, the efficacy to potency ratio E_{max}/EC_{50} was determined and logarithmically transformed to $\log(E_{max}/EC_{50})$. Subsequently, $\Delta\log(E_{max}/EC_{50})$ for each agonist (A) were calculated using the means ± SEM of single $\log(E_{max}/EC_{50})$ values relative to the reference agonist adrenaline (Ref) as follows:[52-53]

$$\Delta \log\left(\frac{E_{max}}{EC_{50}}\right) = log\left(\frac{E_{max,A}}{EC_{50,A}}\right) - log\left(\frac{E_{max,Ref}}{EC_{50,Ref}}\right)$$

For $\Delta\log(E_{max}/EC_{50})$ values, error propagation was performed according to the following equation:

$$\Delta z = \sqrt{\frac{\sum(x_A - \overline{x}_A)^2}{n_A} + \frac{\sum(x_{Ref} - \overline{x}_{Ref})^2}{n_{Ref}}}$$

where x is the function of $\Delta\log(E_{max}/EC_{50})$ of each agonist (A) and the reference agonist adrenaline (Ref). Consequently, Δz represents the propagated error of z.

4.3. Results

4.3.1. Functional Characterization of $\beta_{1,2}$AR Ligands at Overexpressed Receptors

To validate the applicability of mini-G protein sensors to $\beta_{1,2}$AR, a range of standard agonists and antagonists with different potencies and efficacies were functionally characterized at HEK293T cells recombinantly co-expressing NlucN-mGs and either β_1AR-NlucC or β_2AR-NlucC fusion proteins ("overexpressed"; Figure 4.1, Table 4.1). Structures of the investigated ligands are given in the Appendix (Figure A16). These assays revealed that adrenaline and isoprenaline were full agonists and practically equipotent at both the β_1AR and β_2AR. In contrast, noradrenaline fully activated β_1AR, but only partially activated the β_2AR with an E_{max} of 82 ± 0.4% and a considerably lower potency (pEC_{50}: 6.34 ± 0.05 (β_1AR) vs. 5.15 ± 0.07 (β_2AR)). Vice versa, salbutamol activated the β_2AR to a much stronger extent than the β_1AR with E_{max} of 82 ± 0.8% and 37 ± 1.3%, respectively, and along with this provided a substantially lower potency at the β_1AR (pEC_{50}: 5.4 ± 0.02 (β_1AR) vs. 7.15 ± 0.09 (β_2AR)). In the literature, different modalities ranging from weak partial agonism over silent antagonism to even inverse agonism have been reported for the classical antagonists at $\beta_{1,2}$AR depending on the constitutive activity of the utilized system.[54-60] Using mGs sensors at overexpressed receptors, ICI118,551, xamoterol and carvedilol were silent antagonists at the β_2AR, whereas this was only the case for ICI118,551 at the β_1AR (Figure 4.1B and 4.1D, Table 4.1). Conversely, xamoterol and carvedilol provided weak partial agonism with E_{max} values of 14 ± 0.4% and 7 ± 0.8%, respectively (Figure 4.1A, Table 4.1). For carvedilol, this was particularly striking, especially since the pEC_{50} determined at β_1AR differed from the reported pK_i about two orders of magnitude.[60] In fact, this observation was consistent with previous findings of a second binding site

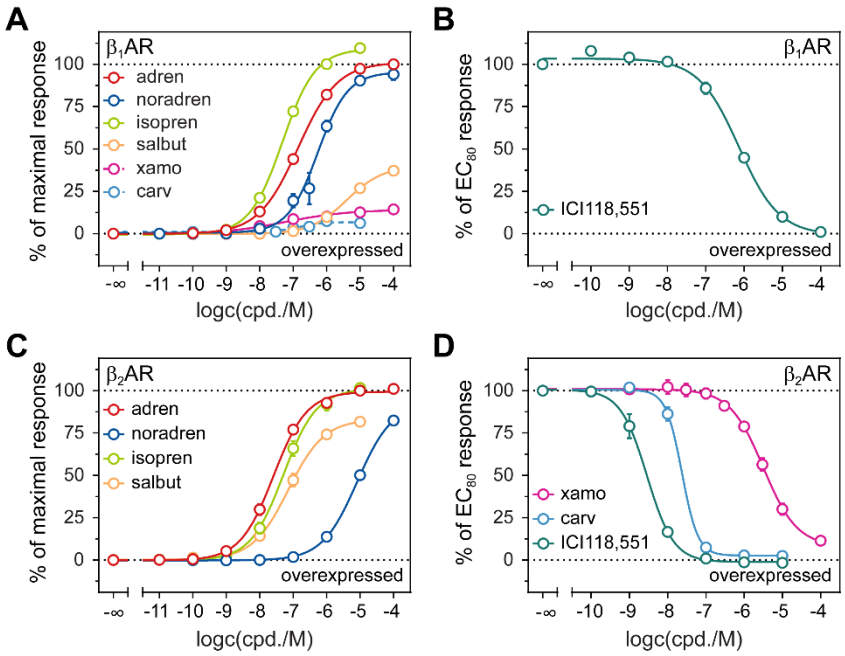

Figure 4.1. Concentration response curves of selected standard agonists (A, C) and antagonists (B, D) obtained in the mini-G protein recruitment assay using HEK293T cells recombinantly co-expressing NlucN-mGs and β_1AR-NlucC (A, B) or β_2AR-NlucC fusion proteins (C, D) were used (overexpressed). Antagonists were characterized in the presence of 100 nM adren. Data were normalized to L-15 as solvent control (0%) and to the maximal response elicited by 100 µM (β_1AR) or 10 µM adren (β_2AR) in the case of agonists or 100 nM adren for antagonists (100%). Data represent means ± SEM from at least three independent experiments ($N \geq 3$) performed in triplicate.

at the β_1AR, to which carvedilol and other antagonists bind with less affinity but increased efficacy.[61-63] Overall, pEC_{50} values obtained by mGs recruitment were between literature pK_i values and pEC_{50} values obtained in cAMP accumulation assays, and E_{max} values obtained by mGs recruitment were lower than cAMP responses for the partial agonists, salbutamol and xamoterol, particularly at the β_1AR. (Table 4.1).[64-65] As with G protein-level functional assays, mGs recruitment assays provided more graded E_{max} values due to a smaller impact of receptor reserve and signal amplification.[66-68] Thus, mini-G protein recruitment assays should constitute a favorable alternative to distal cell assays in the future drug discovery to provide information on structure-activity relationships.

Table 4.1. Potencies (pEC_{50}, pK_b)) and efficacies (E_{max}) of selected standard agonists and antagonists obtained in mini-G protein recruitment assays using HEK293T co-expressing NlucN-mGs and $\beta_{1,2}$AR-NlucC fusion proteins. Responses were normalized to L-15 as solvent control (0%) and to the maximal response elicited by 100 µM (β_1AR) or 10 µM adren (β_2AR) in the case of agonists and 100 nM adren for antagonists (100%). Statistical differences (*) of E_{max} > 100% or rather E_{max} < 0% were tested using a one-sample t-test (α = 0.05). Data represent means ± SEM from at least three independent experiments ($N \geq 3$), performed in triplicate.

		Mini-G Protein Recruitment		cAMP Accumulation		Competition Binding
Subtype	Cpd.	pEC_{50} (pK_b)± SEM	E_{max} ± SEM [%]	pEC_{50}	E_{max} [%]	pK_i
	adren	6.86 ± 0.02	100 ± 0	7.61[a,64]	101.7[a,64]	5.40[c,60]
	noradren	6.34 ± 0.05	94 ± 2.4	7.94[a,64]	102.4[a,64]	5.45[c,60]
	isopren	7.32 ± 0.03	110 ± 0.7*	8.59[a,64]	100[a,64]	6.65[c,60]
β_1AR	salbut	5.4 ± 0.02	37 ± 1.3	6.21[a,64]	103.7[a,64]	5.61[c,60]
	xamo	7.21 ± 0.14	14 ± 0.4*	7.96[a,65]	47.6[a,65]	7.00[e,69]
	ICI118551	(6.38) ± 0.03	n.d.			7.31[c,60]
	carv	6.89 ± 0.07	7 ± 0.8*	7.64[a,62]	10.2[a,62]	9.23[c,60]
	adren	7.59 ± 0.07	100 ± 0	7.93[b,64]	101.9[b,64]	6.13[d,60]
	noradren	5.15 ± 0.07	82 ± 0.4	6.36[b,64]	103.4[b,64]	4.58[d,60]
	isopren	7.3 ± 0.08	101 ± 0.8	8.22[b,64]	100[b,64]	6.34[d,60]
β_2AR	salbut	7.15 ± 0.09	82 ± 0.8	7.72[b,64]	95.8[b,64]	5.66[d,60]
	xamo	(6.19) ± 0.06	n.d.	6.15[b,65]	5.1[b,65]	5.85[f,69]
	ICI118551	(9.24) ± 0.08	n.d.			9.16[d,60]
	carv	(8.32) ± 0.05	n.d.			8.96[d,60]

Reference data were taken from: Functional [^{3}H]cAMP accumulation assays using CHO K1 cells expressing [a]β_1AR or [b]β_2AR (data normalized to maximal responses of isoprenaline)[64-65] and (-)-3-[^{125}I]-iodocyanopindolol displacement assays using CHO cells expressing [c]β_1AR or [d]β_2AR[60] or COS-7 cells expressing [e]β_1AR or [d]β_2AR.[69] n.d. = not detected.

4.3.2. Validation of $\beta_{1,2}$AR-NlucC Fusion Proteins Under Endogenous Promotion

To investigate whether only β_2AR or also β_1AR is expressed in HEK293T cells and whether mGs sensors are useful for detecting $\beta_{1,2}$R activation at the endogenous receptor level, $\beta_{1,2}$AR-NlucC fusion proteins were generated by CRISPR/Cas9 genome editing of HEK293T cells. Essentially, the small split-NanoLuc fragment, NlucC, was inserted into the cell genome by homology directed repair after Cas9-mediated double strand DNA cleavage either in frame with the β_1AR or with the β_2AR (Figure 4.2A). Thereafter, the successful integration of NlucC was verified by mGs recruitment assays upon transient transfection of the heterogenous, CRISPR/Cas9 genome-edited cells (cf. Appendix, Figure A17). To prevent an imbalanced co-expression of $\beta_{1,2}$AR-NlucC and NlucN-mGs proteins from affecting the assay signals, different amounts of pIRESpuro3 NlucN-mGs plasmid DNA were used for transfection (cf. Appendix Figure, A17). In both pooled HEK293T CRISPR $\beta_{1,2}$AR-NlucC cells, mGs recruitment was observed in response to adrenaline, indicating the functional expression of both receptor subtypes, and at the same time, the sufficient $\beta_{1,2}$AR-NlucC expression under endogenous promotion. In addition, converging concentration-response curves in response to different adrenaline concentrations and high assay signals identified the transfection of 280 ng of pIRESpuro3 NlucN-mGs plasmid DNA as well suited for mini-G protein recruitment assays at the endogenous receptor level (cf. Appendix, Figure A17).

However, particularly in the case of β_1AR, overall assay signals were much weaker than in the overexpressed system. Thus, single clones were isolated from the heterogenous cells and clone 11 of HEK293T CRISPR β_1AR-NlucC and clone 35 of HEK293T CRISPR β_2AR-NlucC were selected as CRISPR/Cas9 positives by mGs recruitment in response to 10 µM adrenaline (Figure 4.2.B and 4.2.C, respectively). Nevertheless, it should be kept in mind that immortalized HEK293 cells have an aneuploid chromosome set (pseudo-triploid)[70-71] and that CRISPR/Cas9 reactions might not take place at all chromosomes. To demonstrate this, the CRISPR/Cas9 insert was amplified from genomic DNA isolated from HEK293T CRISPR β_2AR-NlucC clone 35 (Figure 4.2D). For this purpose, primers binding to the regions of the homology arms were used to amplify a 1.3 kb amplicon for non-edited β_2AR DNA and a 2.2 kb amplicon for CRISPR/Cas9-edited β_2AR DNA. To identify the correct bands after gel electrophoresis, gDNA from HEK293T wildtype cells (negative control) and the pFETCh donor plasmid (positive control) were used. Overall, the intensity of the non-edited DNA amplicon was stronger than that of edited DNA amplicon. Thus, qualitatively, HEK293T CRISPR β_2AR-NlucC clone 35 should express native β_2AR in addition to the β_2AR-NlucC fusion protein. However, one should be careful with quantitative statements, i.e., how many chromosomes were modified, since PCR amplicon properties such as the size, GC content and tertiary structure may have a major impact on the amplification efficiency during a PCR, which is also a possible explanation for the multiple amplicons derived from gDNA of CRISPR/Cas9 genome-edited cells (Figure 4.2D).

Unfortunately, it has not been feasible yet to selectively amplify the insert from HEK293T CRISPR β_1AR-NlucC clone 11 by PCR, most likely due to the even higher GC content and nucleotide repeats within the desired amplicon.

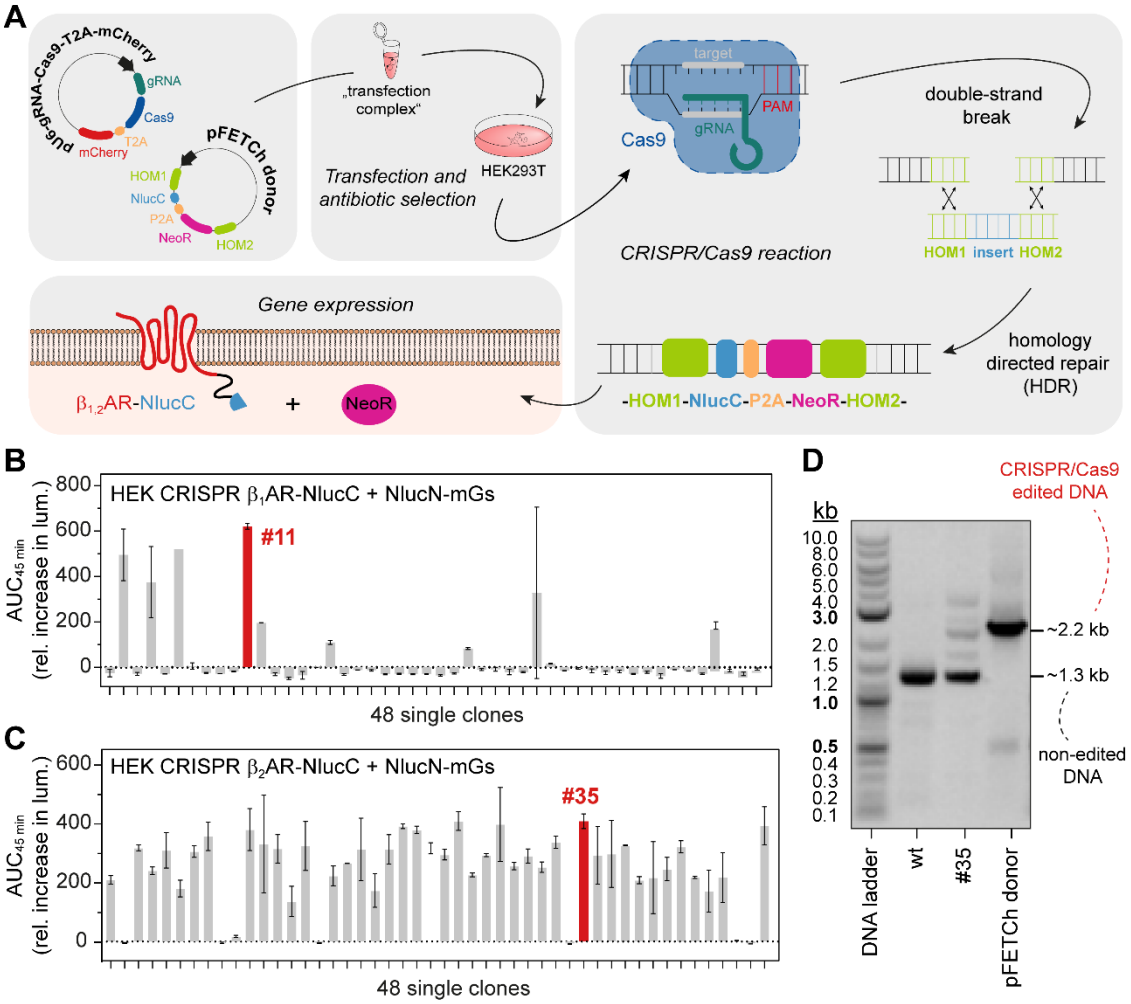

Figure 4.2. Schematic representation of the generation and verification of HEK293T cells expressing $\beta_{1,2}$AR-NlucC fusion proteins at the endogenous level. A) The workflow of the CRISPR/Cas9 experiment included generation of the pFETCh donor and pU6 gRNA-Cas9-T2A-mCherry plasmids, their co-transfection into HEK293T cells, antibiotic selection, and the simultaneous CRISPR/Cas9 reaction in which the insert (NlucC-P2A-NeoR) was integrated into the cell genome by homology directed repair (HDR). Single clones were obtained from genome-edited HEK293T cells and transfected with the pIRESpuro3 plasmid encoding the NlucN-mGs fusion protein. The clones were screened in duplicate for split NanoLuc complementation of either B) β_1AR-NlucC or C) β_2AR-NlucC and NlucN-mGs in response to 10 µM adrenaline. β_1AR-NlucC clone 11 and β_2AR-NlucC clone 35 were selected for further experiments. D) To verify the integration of NlucC-P2A-NeoR into the cell genome, a PCR was performed amplifying the region within HOM1 and HOM2 of the β_2AR using primer pair O21/O22 (cf. Appendix Table A3). The DNA templates were the genomic DNA isolated from HEK293T CRISPR β_2AR-NlucC clone 35 (#35) and HEK293T wildtype cells (wt; negative control) as well as the pFETCh donor plasmid (positive control). PCR products were separated by gel electrophoresis using a 0.8% agarose gel. Unfortunately, it has not been possible to verify β_1AR-NlucC clone 11 by PCR, most likely due to the high GC content and nucleotide repeats within the respective HOM1-HOM2 region.

4.3.3. Mini-G Protein Recruitment Assays at the Endogenous $\beta_{1,2}$AR Level

After the isolation of CRISPR/Cas9 edited positive clones, HEK293T CRISPR β_1AR-NlucC clone 11 and HEK293T CRISPR β_2AR-NlucC clone 35, the suitability of mGs sensors to monitor $\beta_{1,2}$AR activation at the endogenous receptor level was examined. Therefore, functional responses of the full and partial agonists adrenaline, noradrenaline, isoprenaline and salbutamol, were probed after transient expression of the NlucN-mGs fusion protein in HEK293T CRISPR $\beta_{1,2}$AR-NlucC cells. Overall, the traces of mGs recruitment in response to agonists were of similar curve shape at overexpressed and endogenously expressed $\beta_{1,2}$AR, which is representatively depicted for adrenaline at the β_1AR and β_2AR (Figures 4.3A and 4.3D, respectively). However, mGs recruitment to overexpressed $\beta_{1,2}$AR seemed to be modestly faster, most likely due to the higher expression of the biosensor. Moreover, signal-to-background (S/B) ratios were significantly higher at overexpressed β_1AR and β_2AR (Figures 4.3B and 4.3E, respectively).

Overall, agonist properties observed at the endogenous receptor level were consistent with those at overexpressed receptors. Adrenaline and isoprenaline were full agonists at both $\beta_{1,2}$AR, whereas noradrenaline was a full agonist at β_1AR but a partial agonist at β_2AR (Figures 4.3C and 4.3F). In addition, salbutamol partially activated $\beta_{1,2}$AR. However, there were differences in agonist potency and efficacy between overexpressed and endogenous receptors that did not follow a clear trend, although they appeared to be statistically significant. Considering the efficacy of investigated agonists, E_{max} values did not significantly differ between overexpressed and endogenous receptors, except for noradrenaline at β_2AR, (Table 4.2). Nevertheless, considering the potency of investigated agonists, pEC_{50} values were significantly different for salbutamol at β_1AR and adrenaline, noradrenaline and isoprenaline at β_2AR (Table 4.2). Although one could speculate that the observed pEC_{50} rightward shift of the full agonists, adrenaline and isoprenaline at endogenous β_2AR correlated with a decreased mGs sensor sensitivity at lower receptor expression, the leftward shift of pEC_{50} values observed for salbutamol at β_1AR and, particularly noradrenaline at β_2AR were contradictory to this hypothesis. Rather, a correlation between functional properties of agonists and receptor density has been reported in the literature.[52] Thus, dimensionless efficacy to potency ratios relative to the reference agonist adrenaline ($\Delta\log(E_{max}/EC_{50})$) were calculated to prevent a system bias rising from the receptor density (Table 4.2). Statistically significant differences of $\Delta\log(E_{max}/EC_{50})$ values suggested that changes of pEC_{50} and E_{max} were relevant for the partial agonists, salbutamol at $\beta_{1,2}$AR and noradrenaline at β_2AR (Table 4.2). Nevertheless, it remains unclear whether these differences were related to the overall sensor sensitivity, the receptor expression level itself, or potentially the incomplete receptor modification by CRISPR/Cas9 reactions, as demonstrated by PCR for the β_2AR (Figure 4.2D).

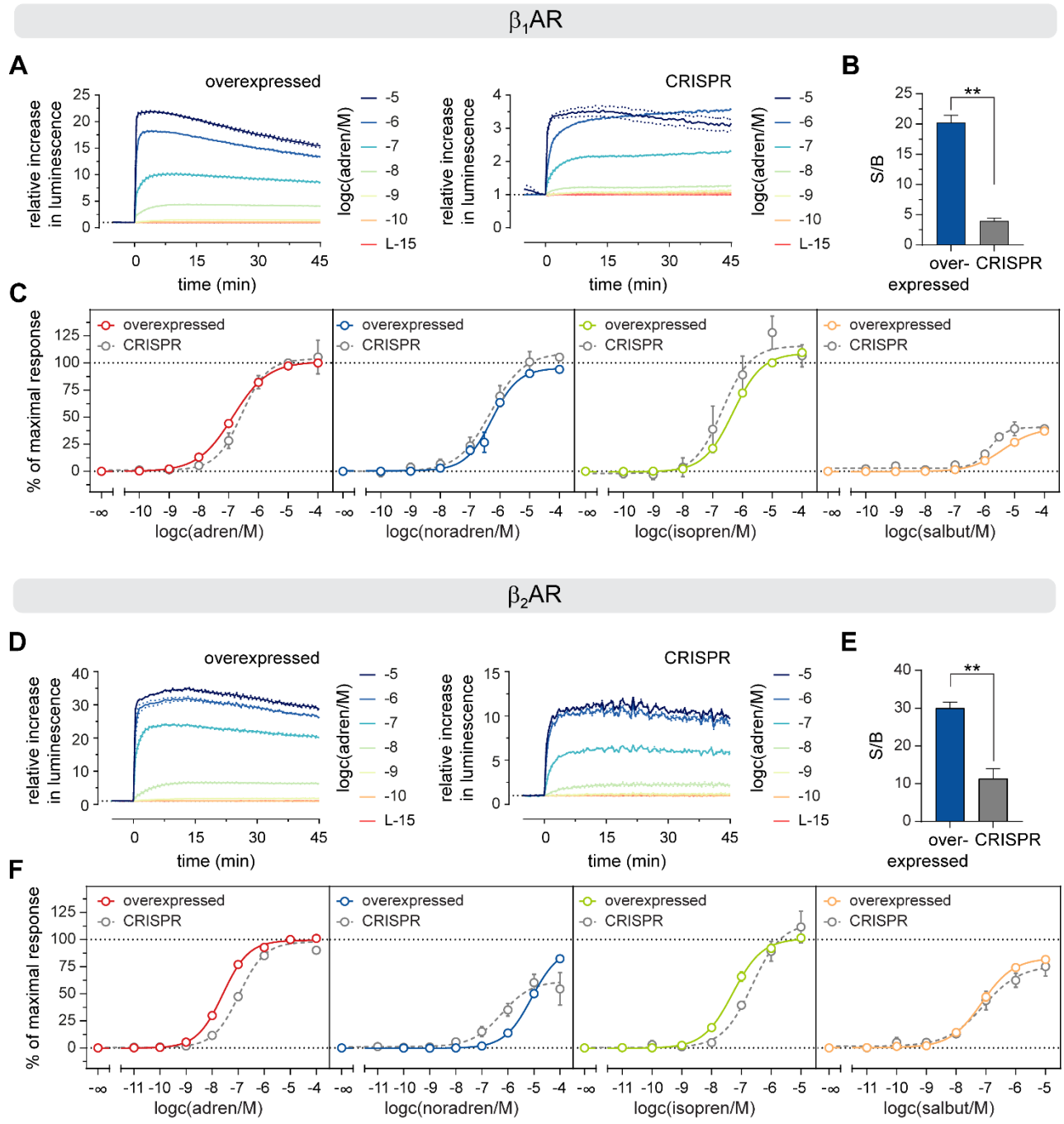

Figure 4.3. Comparison of mGs recruitment to recombinantly (overexpressed) and endogenously (CRISPR) expressed β_1AR (A-C) and β_2AR (D-F). Representative luminescent traces of mGs recruitment (A, D) and overall signal-to-background (S/B) ratios (B, E) obtained for adren are given for overexpressed and CRISPR/Cas9 modified β_1AR and β_2AR (only 96-well assays). Significance of S/B ratios was statistically assessed using a Welch's two-sample t-test (**$p < 0.05$). Agonist concentration response curves were aligned for overexpressed and CRISPR/Cas9 modified β_1AR (C) and β_2AR (F). Mini-G protein recruitment assays were performed using HEK293T cells stably co-expressing NlucN-mGs and $\beta_{1,2}$AR-NlucC fusion proteins or HEK293T CRISPR $\beta_{1,2}$AR-NlucC (clone 11 and 35, respectively) that transiently expressed NlucN-mGs. Data were normalized to L-15 as solvent control (0%) and to the maximal response elicited by 10 µM adren, or 100 µM adren for overexpressed β_1AR. Data represent means ± SEM from at least three independent experiments ($N \geq 3$), performed in triplicate.

Table 4.2. Potencies (pEC_{50}, pK_b), efficacies (E_{max}) and $\Delta\log(E_{max}/EC_{50})$ relative to adrenaline obtained by mGs recruitment. Either HEK293T cells that stably expressed NlucN-mGs and $\beta_{1,2}$AR-NlucC fusion proteins ("overexpressed") or genome edited HEK293T CRISPR $\beta_{1,2}$AR-NlucC cells transiently expressing the NlucN-mGs fusion protein, were used. Agonist responses were normalized to L-15 as solvent control (0%) and to the maximal response elicited by 10 µM adren, or 100 µM adren for overexpressed β_1AR. Data represent means ± SEM from at least three independent experiments ($N \geq 3$), performed in triplicate. Statistical significances of pEC_{50}, E_{max} and $\Delta\log(E_{max}/EC_{50})$ values were assessed using a Welch's two sample t-test comparing data from endogenously expressed to overexpressed $\beta_{1,2}$AR (*: $p < 0.05$, **: $p < 0.01$, ***: $p < 0.005$, ****: $p < 0.001$).

	Overexpressed			CRISPR		
Cpd.	pEC_{50} ± SEM (pK_b) ± SEM	E_{max} ± SEM [%]	$\Delta\log(\frac{E_{max}}{EC_{50}})$ ± SEM	pEC_{50} ± SEM	E_{max} ± SEM [%]	$\Delta\log(\frac{E_{max}}{EC_{50}})$ ± SEM
			β_1AR			
adren	6.86 ± 0.02	100	0	6.6 ± 0.12	100	0
noradren	6.34 ± 0.05	94 ± 2.4	0.50 ± 0.05	6.18 ± 0.20	109 ± 7.3	0.44 ± 0.23
isopren	7.32 ± 0.03	110 ± 0.7	-0.42 ± 0.03	6.61 ± 0.28	107 ± 8.9	0.01 ± 0.29
salbut	5.40 ± 0.02	37 ± 1.3	1.03 ± 0.03	5.76 ± 0.11*	37 ± 5.6	0.37 ± 0.14**
			β_2AR			
adren	7.59 ± 0.07	100	0	6.94 ± 0.07****	100	0
noradren	5.15 ± 0.07	82 ± 0.5	2.44 ± 0.07	6.01 ± 0.19**	61 ± 6.9*	0.69 ± 0.21***
isopren	7.30 ± 0.08	101 ± 0.9	0.30 ± 0.10	6.68 ± 0.07**	112 ± 12.0	0.30 ± 0.14
salbut	7.15 ± 0.09	82 ± 0.8	0.36 ± 0.11	7.15 ± 0.12	67 ± 5.7	-0.39 ± 0.15*

4.4. Discussion

Physiologically, $\beta_{1,2}$AR play a central role in the sympathetic nervous system and, for example, regulate vasodilatation and myocardial contraction.[72-74] From a pharmacological perspective, β-adrenoceptor agonists are the gold standard for the treatment of respiratory disorders, such as asthma,[75-76] whereas antagonists are commonly used in patients with cardiovascular diseases, such as heart failure.[77-78] Beyond clinical applications, the β_2AR has become a role model in structural biology and therefore, represents one of the best studied class A GPCRs.[79-83] To evaluate the mGs sensor suitability for $\beta_{1,2}$AR, standard agonists and antagonists were functionally characterized using HEK293T cells stably co-expressing NlucN-mGs and β_1AR-NlucC or β_2AR-NlucC fusion proteins. Overall, observed potencies were within the range of literature binding affinities (pK_i) determined by radioligand displacement and pEC_{50} values obtained in functional cAMP accumulation assays.[60,64-65,69] However, the tendency was observed that in particular, E_{max} values of the partial agonists were lower in mGs recruitment assays than in the more distal cAMP accumulation assays of the literature. Since the signal amplification along the signaling cascade potentially complicates the discrimination between full and partial agonists in drug discovery by leftward shift of pEC_{50} values and concomitant increase in E_{max}, the presented mGs sensors providing more graded E_{max} values should be an attractive addition to future characterization of $\beta_{1,2}$AR agonists, and thus might prevent overestimation of agonist intrinsic activities.[66-68]

The primary research questions of this project were whether mini-G proteins monitor GPCR activation at the endogenous receptor level and whether β_1AR is functionally expressed in addition to β_2AR in HEK293T cells. This could be confirmed by the generation of CRISPR/Cas9-modified HEK293T cells expressing $\beta_{1,2}$AR-NlucC fusion proteins under endogenous promotion and specific mGs recruitment in response to agonists. Noteworthily, obtained assays signals (S/B) were significantly lower at endogenously expressed $\beta_{1,2}$AR than at overexpressed receptors, but luminescent traces were of similar curve shape (Figure 4.3). Overall, mGs sensors revealed specific agonist modalities and thus should be well suited for the functional characterization of ligands at endogenous receptor density. However, $\Delta\log(E_{max}/EC_{50})$ values significantly differed for partial agonists and further experiments would be needed for explanation. On one hand, larger ligand libraries could be examined to increase the statistical relevance, and on the other hand the impact of the incomplete receptor modification in CRISPR/Cas9 reactions, as demonstrated by PCR for the β_2AR (Figure 4.2D), could be assessed. At low receptor density, the ratio of NlucC-labeled and natively expressed receptors might be relevant, especially for weaker assay responses elicited by partial agonists. Therefore, it might be of interest to quantify the absolute receptor expression, e.g., by radioligand saturation binding, and the number of modified gene loci by quantitative PCR.

4.5. References

1. Strange, P. G., Use of the GTP γ S ([35S]GTP γ S and Eu-GTP γ S) binding assay for analysis of ligand potency and efficacy at G protein-coupled receptors. *Br J Pharmacol* **2010,** *161* (6), 1238-1249, doi: 10.1111/j.1476-5381.2010.00963.x.
2. Milligan, G., Principles: Extending the utility of [35S]GTP γ S binding assays. *Trends Pharmacol Sci* **2003,** *24* (2), 87-90, doi: 10.1016/s0165-6147(02)00027-5.
3. Wan, Q., Okashah, N., Inoue, A., Nehmé, R., Carpenter, B., Tate, C. G. & Lambert, N. A., Mini G protein probes for active G protein-coupled receptors (GPCRs) in live cells. *J Biol Chem* **2018,** *293* (19), 7466-7473, doi: 10.1074/jbc.RA118.001975.
4. Höring, C., Seibel, U., Tropmann, K., Grätz, L., Mönnich, D., Pitzl, S., Bernhardt, G., Pockes, S. & Strasser, A., A dynamic, split-luciferase-based mini-G protein sensor to functionally characterize ligands at all four histamine receptor subtypes. *Int J Mol Sci* **2020,** *21* (22), 8440.
5. Wouters, E., Walraed, J., Robertson, M. J., Meyrath, M., Szpakowska, M., Chevigne, A., Skiniotis, G. & Stove, C., Assessment of biased agonism among distinct synthetic cannabinoid receptor agonist scaffolds. *ACS Pharmacol Transl Sci* **2020,** *3* (2), 285-295, doi: 10.1021/acsptsci.9b00069.
6. Pottie, E., Tosh, D. K., Gao, Z. G., Jacobson, K. A. & Stove, C. P., Assessment of biased agonism at the A3 adenosine receptor using β-arrestin and miniG αi recruitment assays. *Biochem Pharmacol* **2020,** *177*, 113934, doi: 10.1016/j.bcp.2020.113934.
7. Vasudevan, L. & Stove, C. P., A novel nanobody-based bio-assay using functional complementation of a split nanoluciferase to monitor μ-opioid receptor activation. *Anal Bioanal Chem* **2020,** *412* (29), 8015-8022, doi: 10.1007/s00216-020-02945-6.
8. Wouters, E., Vasudevan, L., Crans, R. A. J., Saini, D. K. & Stove, C. P., Luminescence- and fluorescence-based complementation assays to screen for GPCR oligomerization: Current state of the art. *Int J Mol Sci* **2019,** *20* (12), doi: 10.3390/ijms20122958.
9. El Khamlichi, C., Reverchon-Assadi, F., Hervouet-Coste, N., Blot, L., Reiter, E. & Morisset-Lopez, S., Bioluminescence resonance energy transfer as a method to study protein-protein interactions: Application to G protein coupled receptor biology. *Molecules* **2019,** *24* (3), doi: 10.3390/molecules24030537.
10. Hattori, M. & Ozawa, T., Split luciferase complementation for analysis of intracellular signaling. *Anal Sci* **2014,** *30* (5), 539-544, doi: 10.2116/analsci.30.539.
11. White, C. W., Vanyai, H. K., See, H. B., Johnstone, E. K. M. & Pfleger, K. D. G., Using nanoBRET and CRISPR/Cas9 to monitor proximity to a genome-edited protein in real-time. *Sci Rep* **2017,** *7* (1), 3187, doi: 10.1038/s41598-017-03486-2.
12. White, C. W., Johnstone, E. K. M., See, H. B. & Pfleger, K. D. G., NanoBRET ligand binding at a GPCR under endogenous promotion facilitated by CRISPR/Cas9 genome editing. *Cell Signal* **2019,** *54*, 27-34, doi: 10.1016/j.cellsig.2018.11.018.
13. Soave, M., Stoddart, L. A., White, C. W., Kilpatrick, L. E., Goulding, J., Briddon, S. J. & Hill, S. J., Detection of genome-edited and endogenously expressed G protein-coupled receptors. *The FEBS journal* **2021,** *288* (8), 2585-2601, doi: 10.1111/febs.15729.
14. Wacker, D., Stevens, R. C. & Roth, B. L., How ligands illuminate GPCR molecular pharmacology. *Cell* **2017,** *170* (3), 414-427, doi: 10.1016/j.cell.2017.07.009.
15. Miller, J. C., Holmes, M. C., Wang, J., Guschin, D. Y., Lee, Y. L., Rupniewski, I., Beausejour, C. M., Waite, A. J., Wang, N. S., Kim, K. A., et al., An improved zinc-finger nuclease architecture for highly specific genome editing. *Nat Biotechnol* **2007,** *25* (7), 778-785, doi: 10.1038/nbt1319.
16. Urnov, F. D., Rebar, E. J., Holmes, M. C., Zhang, H. S. & Gregory, P. D., Genome editing with engineered zinc finger nucleases. *Nat Rev Genet* **2010,** *11* (9), 636-646, doi: 10.1038/nrg2842.

17. Sanjana, N. E., Cong, L., Zhou, Y., Cunniff, M. M., Feng, G. & Zhang, F., A transcription activator-like effector toolbox for genome engineering. *Nature protocols* **2012,** *7* (1), 171-192, doi: 10.1038/nprot.2011.431.

18. Christian, M., Cermak, T., Doyle, E. L., Schmidt, C., Zhang, F., Hummel, A., Bogdanove, A. J. & Voytas, D. F., Targeting DNA double-strand breaks with TAL effector nucleases. *Genetics* **2010,** *186* (2), 757-761, doi: 10.1534/genetics.110.120717.

19. Horvath, P. & Barrangou, R., CRISPR/Cas, the immune system of bacteria and archaea. *Science* **2010,** *327* (5962), 167-170, doi: 10.1126/science.1179555.

20. Cong, L., Ran, F. A., Cox, D., Lin, S., Barretto, R., Habib, N., Hsu, P. D., Wu, X., Jiang, W., Marraffini, L. A., et al., Multiplex genome engineering using CRISPR/Cas systems. *Science* **2013,** *339* (6121), 819-823, doi: 10.1126/science.1231143.

21. Jinek, M., Chylinski, K., Fonfara, I., Hauer, M., Doudna, J. A. & Charpentier, E., A programmable dual-RNA-guided DNA endonuclease in adaptive bacterial immunity. *Science* **2012,** *337* (6096), 816-821, doi: 10.1126/science.1225829.

22. Wood, A. J., Lo, T. W., Zeitler, B., Pickle, C. S., Ralston, E. J., Lee, A. H., Amora, R., Miller, J. C., Leung, E., Meng, X., et al., Targeted genome editing across species using ZFNs and TALENs. *Science* **2011,** *333* (6040), 307, doi: 10.1126/science.1207773.

23. Rojas-Fernandez, A., Herhaus, L., Macartney, T., Lachaud, C., Hay, R. T. & Sapkota, G. P., Rapid generation of endogenously driven transcriptional reporters in cells through CRISPR/Cas9. *Sci Rep* **2015,** *5*, 9811-9811, doi: 10.1038/srep09811.

24. Kamiyama, D., Sekine, S., Barsi-Rhyne, B., Hu, J., Chen, B., Gilbert, L. A., Ishikawa, H., Leonetti, M. D., Marshall, W. F., Weissman, J. S., et al., Versatile protein tagging in cells with split fluorescent protein. *Nat Commun* **2016,** *7*, 11046, doi: 10.1038/ncomms11046.

25. Ratz, M., Testa, I., Hell, S. W. & Jakobs, S., CRISPR/Cas9-mediated endogenous protein tagging for RESOLFT super-resolution microscopy of living human cells. *Sci Rep* **2015,** *5*, 9592, doi: 10.1038/srep09592.

26. Yang, H., Wang, H., Shivalila, C. S., Cheng, A. W., Shi, L. & Jaenisch, R., One-step generation of mice carrying reporter and conditional alleles by CRISPR/Cas-mediated genome engineering. *Cell* **2013,** *154* (6), 1370-1379, doi: 10.1016/j.cell.2013.08.022.

27. Hall, M. P., Unch, J., Binkowski, B. F., Valley, M. P., Butler, B. L., Wood, M. G., Otto, P., Zimmerman, K., Vidugiris, G., Machleidt, T., et al., Engineered luciferase reporter from a deep sea shrimp utilizing a novel imidazopyrazinone substrate. *ACS Chem Biol* **2012,** *7* (11), 1848-1857, doi: 10.1021/cb3002478.

28. Dixon, A. S., Schwinn, M. K., Hall, M. P., Zimmerman, K., Otto, P., Lubben, T. H., Butler, B. L., Binkowski, B. F., Machleidt, T., Kirkland, T. A., et al., NanoLuc complementation reporter optimized for accurate measurement of protein interactions in cells. *ACS Chem Biol* **2016,** *11* (2), 400-408, doi: 10.1021/acschembio.5b00753.

29. Oh-Hashi, K., Furuta, E., Fujimura, K. & Hirata, Y., Application of a novel HiBiT peptide tag for monitoring ATF4 protein expression in Neuro2a cells. *Biochem Biophys Rep* **2017,** *12*, 40-45, doi: 10.1016/j.bbrep.2017.08.002.

30. Schwinn, M. K., Machleidt, T., Zimmerman, K., Eggers, C. T., Dixon, A. S., Hurst, R., Hall, M. P., Encell, L. P., Binkowski, B. F. & Wood, K. V., CRISPR-mediated tagging of endogenous proteins with a luminescent peptide. *ACS Chem Biol* **2018,** *13* (2), 467-474, doi: 10.1021/acschembio.7b00549.

31. Riching, K. M., Mahan, S. D., Urh, M. & Daniels, D. L., High-throughput cellular profiling of targeted protein degradation compounds using HiBiT CRISPR cell lines. *J Vis Exp* **2020,** (165), doi: 10.3791/61787.

32. Pottie, E., Cannaert, A., Van Uytfanghe, K. & Stove, C. P., Setup of a serotonin 2A receptor (5-HT2AR) bioassay: Demonstration of its applicability to functionally characterize hallucinogenic new psychoactive substances and an explanation why 5-HT2AR bioassays are not suited for universal activity-based screening of biofluids for new psychoactive substances. *Anal Chem* **2019,** *91* (24), 15444-15452, doi: 10.1021/acs.analchem.9b03104.

33. Tropmann, K., Höring, C., Plank, N. & Pockes, S., Discovery of a G protein-biased radioligand for the histamine H2 receptor with reversible binding properties. *J Med Chem* **2020,** *63* (21), 13090-13102, doi: 10.1021/acs.jmedchem.0c01494.

34. Szczepańska, K., Pockes, S., Podlewska, S., Höring, C., Mika, K., Latacz, G., Bednarski, M., Siwek, A., Karcz, T., Nagl, M., et al., Structural modifications in the distal, regulatory region of histamine H3 receptor antagonists leading to the identification of a potent anti-obesity agent. *Eur J Med Chem* **2021,** *213*, 113041, doi: 10.1016/j.ejmech.2020.113041.

35. Gergs, U., Büxel, M. L., Bresinsky, M., Kirchhefer, U., Fehse, C., Höring, C., Hofmann, B., Marušáková, M., Čináková, A., Schwarz, R., et al., Cardiac effects of novel histamine H2 receptor Agonists. *J Pharmacol Exp Ther* **2021,** *379* (3), 223-234, doi: 10.1124/jpet.121.000822.

36. Weinhart, C. G., Wifling, D., Schmidt, M. F., Neu, E., Höring, C., Clark, T., Gmeiner, P. & Keller, M., Dibenzodiazepinone-type muscarinic receptor antagonists conjugated to basic peptides: Impact of the linker moiety and unnatural amino acids on M2R selectivity. *Eur J Med Chem* **2021,** *213*, 113159, doi: 10.1016/j.ejmech.2021.113159.

37. Thomas, P. & Smart, T. G., HEK293 cell line: A vehicle for the expression of recombinant proteins. *J Pharmacol Toxicol Methods* **2005,** *51* (3), 187-200, doi: 10.1016/j.vascn.2004.08.014.

38. Atwood, B. K., Lopez, J., Wager-Miller, J., Mackie, K. & Straiker, A., Expression of G protein-coupled receptors and related proteins in HEK293, AtT20, BV2, and N18 cell lines as revealed by microarray analysis. *BMC genomics* **2011,** *12*, 14, doi: 10.1186/1471-2164-12-14.

39. Wiseman, D. N., Otchere, A., Patel, J. H., Uddin, R., Pollock, N. L., Routledge, S. J., Rothnie, A. J., Slack, C., Poyner, D. R., Bill, R. M., et al., Expression and purification of recombinant G protein-coupled receptors: A review. *Protein Expr Purif* **2020,** *167*, 105524, doi: 10.1016/j.pep.2019.105524.

40. Guixa-Gonzalez, R., Albasanz, J. L., Rodriguez-Espigares, I., Pastor, M., Sanz, F., Marti-Solano, M., Manna, M., Martinez-Seara, H., Hildebrand, P. W., Martin, M., et al., Membrane cholesterol access into a G-protein-coupled receptor. *Nat Commun* **2017,** *8*, 14505, doi: 10.1038/ncomms14505.

41. Jakubik, J. & El-Fakahany, E. E., Allosteric modulation of GPCRs of class A by cholesterol. *Int J Mol Sci* **2021,** *22* (4), doi: 10.3390/ijms22041953.

42. Patwardhan, A., Cheng, N. & Trejo, J., Post-translational modifications of G protein-coupled receptors control cellular signaling dynamics in space and time. *Pharmacol Rev* **2021,** *73* (1), 120-151, doi: 10.1124/pharmrev.120.000082.

43. van der Hagen, E. A. E., Tudpor, K., Verkaart, S., Lavrijsen, M., van der Kemp, A., van Zeeland, F., Bindels, R. J. M. & Hoenderop, J. G. J., β1-Adrenergic receptor signaling activates the epithelial calcium channel, transient receptor potential vanilloid type 5 (TRPV5), via the protein kinase A pathway. *J Biol Chem* **2014,** *289* (26), 18489-18496, doi: 10.1074/jbc.M113.491274.

44. Schmitt, J. M. & Stork, P. J. S., β2-adrenergic receptor activates extracellular signal-regulated kinases (ERKs) via the small G protein Rap1 and the serine/threonine kinase B-Raf. *J Biol Chem* **2000,** *275* (33), 25342-25350, doi: 10.1074/jbc.M003213200.

45. Copik, A. J., Ma, C., Kosaka, A., Sahdeo, S., Trane, A., Ho, H., Dietrich, P. S., Yu, H., Ford, A. P., Button, D., et al., Facilitatory interplay in α1a and β2 adrenoceptor function reveals a non-Gq signaling mode: Implications for diversification of intracellular signal transduction. *Mol Pharmacol* **2009,** *75* (3), 713-728, doi: 10.1124/mol.108.050765.

46. Galaz-Montoya, M., Wright, S. J., Rodriguez, G. J., Lichtarge, O. & Wensel, T. G., β2-Adrenergic receptor activation mobilizes intracellular calcium via a non-canonical cAMP-independent signaling pathway. *J Biol Chem* **2017,** *292* (24), 9967-9974, doi: 10.1074/jbc.M117.787119.

47. Lavoie, C., Mercier, J. F., Salahpour, A., Umapathy, D., Breit, A., Villeneuve, L. R., Zhu, W. Z., Xiao, R. P., Lakatta, E. G., Bouvier, M., et al., β1/β2-adrenergic receptor heterodimerization regulates β2-adrenergic receptor internalization and ERK signaling efficacy. *J Biol Chem* **2002,** *277* (38), 35402-35410, doi: 10.1074/jbc.M204163200.

48. Gibson, D. G., Young, L., Chuang, R. Y., Venter, J. C., Hutchison, C. A., 3rd & Smith, H. O., Enzymatic assembly of DNA molecules up to several hundred kilobases. *Nat Methods* **2009,** *6* (5), 343-345, doi: 10.1038/nmeth.1318.

49. Reyrat, J. M., Pelicic, V., Gicquel, B. & Rappuoli, R., Counterselectable markers: Untapped tools for bacterial genetics and pathogenesis. *Infect Immun* **1998,** *66* (9), 4011-4017, doi: 10.1128/IAI.66.9.4011-4017.1998.

50. Savic, D., Partridge, E. C., Newberry, K. M., Smith, S. B., Meadows, S. K., Roberts, B. S., Mackiewicz, M., Mendenhall, E. M. & Myers, R. M., CETCh-seq: CRISPR epitope tagging ChIP-seq of DNA-binding proteins. *Genome Res* **2015,** *25* (10), 1581-1589, doi: 10.1101/gr.193540.115.

51. Liu, Z., Chen, O., Wall, J. B. J., Zheng, M., Zhou, Y., Wang, L., Ruth Vaseghi, H., Qian, L. & Liu, J., Systematic comparison of 2A peptides for cloning multi-genes in a polycistronic vector. *Sci Rep* **2017,** *7* (1), 2193, doi: 10.1038/s41598-017-02460-2.

52. Kenakin, T., Watson, C., Muniz-Medina, V., Christopoulos, A. & Novick, S., A simple method for quantifying functional selectivity and agonist bias. *ACS chemical neuroscience* **2012,** *3* (3), 193-203, doi: 10.1021/cn200111m.

53. Griffin, M. T., Figueroa, K. W., Liller, S. & Ehlert, F. J., Estimation of agonist activity at G protein-coupled receptors: Analysis of M2 muscarinic receptor signaling through Gi/o, Gs, and G15. *J Pharmacol Exp Ther* **2007,** *321* (3), 1193-1207, doi: 10.1124/jpet.107.120857.

54. Wenzel-Seifert, K., Liu, H. Y. & Seifert, R., Similarities and differences in the coupling of human β1- and β2-adrenoceptors to Gsα splice variants. *Biochem Pharmacol* **2002,** *64* (1), 9-20, doi: 10.1016/s0006-2952(02)00924-3.

55. Varma, D. R., Shen, H., Deng, X. F., Peri, K. G., Chemtob, S. & Mulay, S., Inverse agonist activities of β-adrenoceptor antagonists in rat myocardium. *Br J Pharmacol* **1999,** *127* (4), 895-902, doi: 10.1038/sj.bjp.0702616.

56. Lattion, A., Abuin, L., Nenniger-Tosato, M. & Cotecchia, S., Constitutively active mutants of the β1-adrenergic receptor. *FEBS Lett* **1999,** *457* (3), 302-306, doi: 10.1016/s0014-5793(99)01064-9.

57. Mewes, T., Dutz, S., Ravens, U. & Jakobs, K. H., Activation of calcium currents in cardiac myocytes by empty β-adrenoceptors. *Circulation* **1993,** *88* (6), 2916-2922, doi: doi:10.1161/01.CIR.88.6.2916.

58. Wenzel-Seifert, K. & Seifert, R., Molecular analysis of β2-adrenoceptor coupling to Gs-, Gi-, and Gq-proteins. *Mol Pharmacol* **2000,** *58* (5), 954-966, doi: 10.1124/mol.58.5.954.

59. Wenzel-Seifert, K., Arthur, J. M., Liu, H. Y. & Seifert, R., Quantitative analysis of formyl peptide receptor coupling to Giα1, Giα2, and Giα3. *J Biol Chem* **1999,** *274* (47), 33259-33266, doi: 10.1074/jbc.274.47.33259.

60. Hoffmann, C., Leitz, M. R., Oberdorf-Maass, S., Lohse, M. J. & Klotz, K. N., Comparative pharmacology of human beta-adrenergic receptor subtypes - characterization of stably transfected receptors in CHO cells. *Naunyn Schmiedebergs Arch Pharmacol* **2004,** *369* (2), 151-159, doi: 10.1007/s00210-003-0860-y.

61. Konkar, A. A., Zhu, Z. & Granneman, J. G., Aryloxypropanolamine and catecholamine ligand interactions with the β1-adrenergic receptor: Evidence for interaction with distinct conformations of β1-adrenergic receptors. *J Pharmacol Exp Ther* **2000,** *294* (3), 923-932.

62. Baker, J. G., Hall, I. P. & Hill, S. J., Agonist actions of "β-blockers" provide evidence for two agonist activation sites or conformations of the human beta1-adrenoceptor. *Mol Pharmacol* **2003,** *63* (6), 1312-1321, doi: 10.1124/mol.63.6.1312.

63. Baker, J. G., Proudman, R. G. & Hill, S. J., Impact of polymorphic variants on the molecular pharmacology of the two-agonist conformations of the human β1-adrenoceptor. *PLoS One* **2013,** *8* (11), e77582, doi: 10.1371/journal.pone.0077582.

64. Baker, J. G., The selectivity of β-adrenoceptor agonists at human β1-, β2- and β3-adrenoceptors. *Br J Pharmacol* **2010,** *160* (5), 1048-1061, doi: 10.1111/j.1476-5381.2010.00754.x.

65. Mistry, S. N., Baker, J. G., Fischer, P. M., Hill, S. J., Gardiner, S. M. & Kellam, B., Synthesis and in vitro and in vivo characterization of highly β1-selective β-adrenoceptor partial agonists. *J Med Chem* **2013,** *56* (10), 3852-3865, doi: 10.1021/jm400348g.

66. Kenakin, T. P., Receptor reserve as a tissue misnomer. *Trends Pharmacol Sci* **1986,** *7*, 93-95, doi: 10.1016/0165-6147(86)90271-3.

67. Thomsen, W., Frazer, J. & Unett, D., Functional assays for screening GPCR targets. *Curr Opin Biotechnol* **2005,** *16* (6), 655-665, doi: 10.1016/j.copbio.2005.10.008.

68. Black, J. W. & Leff, P., Operational models of pharmacological agonism. *Proceedings of the Royal Society of London. Series B, Biological sciences* **1983,** *220* (1219), 141-162, doi: 10.1098/rspb.1983.0093.

69. Isogaya, M., Sugimoto, Y., Tanimura, R., Tanaka, R., Kikkawa, H., Nagao, T. & Kurose, H., Binding pockets of the β1- and β2-adrenergic receptors for subtype-selective agonists. *Mol Pharmacol* **1999,** *56* (5), 875-885, doi: 10.1124/mol.56.5.875.

70. Bylund, L., Kytölä, S., Lui, W. O., Larsson, C. & Weber, G., Analysis of the cytogenetic stability of the human embryonal kidney cell line 293 by cytogenetic and STR profiling approaches. *Cytogenetic and genome research* **2004,** *106* (1), 28-32, doi: 10.1159/000078556.

71. Lin, Y.-C., Boone, M., Meuris, L., Lemmens, I., Van Roy, N., Soete, A., Reumers, J., Moisse, M., Plaisance, S., Drmanac, R., et al., Genome dynamics of the human embryonic kidney 293 lineage in response to cell biology manipulations. *Nat Commun* **2014,** *5* (1), 4767, doi: 10.1038/ncomms5767.

72. Yoo, B., Lemaire, A., Mangmool, S., Wolf, M. J., Curcio, A., Mao, L. & Rockman, H. A., β1-adrenergic receptors stimulate cardiac contractility and CaMKII activation in vivo and enhance cardiac dysfunction following myocardial infarction. *American journal of physiology. Heart and circulatory physiology* **2009,** *297* (4), H1377-1386, doi: 10.1152/ajpheart.00504.2009.

73. Milano, C. A., Allen, L. F., Rockman, H. A., Dolber, P. C., McMinn, T. R., Chien, K. R., Johnson, T. D., Bond, R. A. & Lefkowitz, R. J., Enhanced myocardial function in transgenic mice overexpressing the β2-adrenergic receptor. *Science* **1994,** *264* (5158), 582-586, doi: 10.1126/science.8160017.

74. Limberg, J. K., Johansson, R. E., Peltonen, G. L., Harrell, J. W., Kellawan, J. M., Eldridge, M. W., Sebranek, J. J. & Schrage, W. G., β-Adrenergic-mediated vasodilation in young men and women: Cyclooxygenase restrains nitric oxide synthase. *Am J Physiol - Heart Circ Physiol* **2016,** *310* (6), H756-H764, doi: 10.1152/ajpheart.00886.2015.

75. Barisione, G., Baroffio, M., Crimi, E. & Brusasco, V., β-adrenergic agonists. *Pharmaceuticals* **2010,** *3* (4), 1016-1044.

76. Waldeck, B., β-adrenoceptor agonists and asthma - 100 years of development. *Eur J Pharmacol* **2002,** *445* (1-2), 1-12, doi: 10.1016/s0014-2999(02)01728-4.

77. Ripley, T. L. & Saseen, J. J., β-blockers: A review of their pharmacological and physiological diversity in hypertension. *The Annals of pharmacotherapy* **2014,** *48* (6), 723-733, doi: 10.1177/1060028013519591.

78. Ziff, O. J., Samra, M., Howard, J. P., Bromage, D. I., Ruschitzka, F., Francis, D. P. & Kotecha, D., β-blocker efficacy across different cardiovascular indications: An umbrella review and meta-analytic assessment. *BMC Medicine* **2020,** *18* (1), 103, doi: 10.1186/s12916-020-01564-3.

79. Nygaard, R., Zou, Y., Dror, R. O., Mildorf, T. J., Arlow, D. H., Manglik, A., Pan, A. C., Liu, C. W., Fung, J. J., Bokoch, M. P., et al., The dynamic process of β2-adrenergic receptor activation. *Cell* **2013,** *152* (3), 532-542, doi: 10.1016/j.cell.2013.01.008.

80. Manglik, A., Kim, Tae H., Masureel, M., Altenbach, C., Yang, Z., Hilger, D., Lerch, Michael T., Kobilka, Tong S., Thian, Foon S., Hubbell, Wayne L., et al., Structural Insights into the dynamic process of β2-adrenergic receptor signaling. *Cell* **2015,** *161* (5), 1101-1111, doi: 10.1016/j.cell.2015.04.043.

81. Rasmussen, S. G., DeVree, B. T., Zou, Y., Kruse, A. C., Chung, K. Y., Kobilka, T. S., Thian, F. S., Chae, P. S., Pardon, E., Calinski, D., et al., Crystal structure of the β2 adrenergic receptor–Gs protein complex. *Nature* **2011,** *477* (7366), 549-555, doi: 10.1038/nature10361.

82. Hilger, D., Masureel, M. & Kobilka, B. K., Structure and dynamics of GPCR signaling complexes. *Nat Struct Mol Biol* **2018,** *25* (1), 4-12, doi: 10.1038/s41594-017-0011-7.

83. Weis, W. I. & Kobilka, B. K., The molecular basis of G protein-coupled receptor activation. *Annu Rev Biochem* **2018,** *87*, 897-919, doi: 10.1146/annurev-biochem-060614-033910.

5. Towards the Elucidation of GPCR – G Protein Coupling Profiles Using Mini-G Protein Sensors

5.1. Introduction

Cellular communication is an important mechanism for multicellular organisms.[1] Sensory stimuli, such as light, taste and odor[2], or intercellular signals, such as hormones or neurotransmitters,[3-4] are mediated into cellular responses by G protein-coupled receptors (GPCRs), which constitute one of the largest membrane protein families.[5-7] Principally, the activation of a GPCR triggers two major cellular pathways: On the one hand, GPCRs bind to heterotrimeric G proteins composed of α, β, and γ subunits.[8] When a G protein becomes activated, the exchange of GDP by GTP at Gα is facilitated, leading to the dissociation of the GPCR - G protein complex into the GPCR, the Gα monomer and G$\beta\gamma$ dimer.[9-10] The latter G protein constituents are both capable of activating or inhibiting other effectors, such as adenylyl cyclase (AC),[11-14] phospholipase C (PLC),[11,15] or ion channels.[16-17] On the other hand, GPCRs bind to β-arrestins after being phosphorylated by G protein-coupled receptor kinases (GRKs)[18-19] or other kinases,[20-21] which is followed by the internalization of the GPCR - β-arrestin complex assisted by clathrins and other associated proteins.[22-24] In addition to attenuating G protein signaling of GPCRs, diverse signaling mechanisms have been reported for β-arrestins mainly due to scaffolding functions.[25]

With the evidence that agonists can promote different active receptor states and thus discriminate the activation of distinct signaling pathways,[11] the classical concept of 'intrinsic activity' as a system-independent agonistic constant (described by the Black-Leff model of pharmacological agonism[26]) had to be reconsidered.[27-29] Since then, ligands have been studied in terms of their functional selectivity, also referred to as 'biased agonism', in drug discovery.[30-32] Importantly, biased agonists independently activate multiple intracellular signaling pathways, regardless of the strength of the stimulus. This is not to be confused with the fact that highly potent agonists can activate multiple pathways, while a weaker agonist activates only the most efficiently coupled pathway.[30] However, functional selectivity has not only been described to distinguish G protein and other signaling pathways, but also with respect to different Gα proteins.[33-34] Only 21 α isoforms, classified into four major Gα families (Gs, Gi/o, Gq/11, and G12/13),[35-36] filter extracellular stimuli from more than 800 GPCRs resulting in individual G protein signaling patterns.[37] Although the ability to couple to more than one G protein has been described for numerous GPCRs, the exact mechanism remains unclear and the question arises whether G protein subtype selectivity is a druggable target.[38]

A major issue in the determination of G protein subtype selectivity of GPCRs is the evidence of crosstalk in G protein signaling pathways.[39-42] For example, it has been reported that ACs, which are typically stimulated by Gs proteins and inhibited by Gi/o proteins,[14,43] can be regulated by operators of the Gq signaling pathway. Increases in intracellular calcium and activated protein kinase C (PKC), following Gq and PLC activation, are capable of binding to ACs and thus increasing cAMP levels,[44-45] which may be potentiated by direct binding of the Gq-βγ dimer to the AC.[46-47] As a result, interpretation of cell assays that measure functional responses at levels amenable to crosstalk might be difficult, especially when assessing secondary coupling.[48] Therefore, G protein biosensors sensing receptor – G protein interactions or G protein rearrangements upon activation have become useful tools for the determination of functional selectivity of GPCRs without interference from signaling crosstalk.[49-50] Applied in living cells, G protein biosensors typically provide temporal information about cell signaling under physiological conditions.[49-52] In addition, many of these assays can be performed in microtiter plates with simple equipment, increasing throughput.[50]

Recently, mini-G proteins that were developed by the groups of Tate and Lambert[53-54] have become available in BRET- or split-luciferase complementation-based assays for the functional characterization of ligands for a broad range of GPCRs (cf. Chapters 2-4).[55-62] In BRET-based assays, Wan et al. (2018) have demonstrated that these chimeric G protein surrogates maintained appropriate GPCR coupling specificity, which is, e.g., the preferred coupling of Gi/o-coupled GPCRs to mGsi, by probing 12 prototypic receptors.[55] For this purpose, maximal BRET signals were considered but the authors did not specify employed ligands or control mini-G protein expression during the experiments.[55] However, G protein expression levels or rather GPCR – G protein stoichiometry might influence overall assay signal amplitudes, and thus ligand efficacy.[63-64] Therefore, the aim of this study was, on one hand to develop an assay concept using split-NanoLuc-based mini-G protein sensors to control mini-G protein expression levels and, on the other hand, to demonstrate its usefulness of for the investigation of GPCR - G protein coupling profiles. Therefore, the existing assay protocol used for mini-G protein recruitment assays presented in Chapters 2-4 was optimized using Western blots for obtaining equal mini-G protein expression levels and the coupling profiles of overall 22 GPCRs were investigated. Moreover, dimensionless G protein coupling scores were derived that should be less susceptible to varying degrees of signal amplification and, thus should be useful for evaluating functional data obtained in different cell assays and ultimately to assess ligand-dependent G protein bias in future studies.

5.2. Materials and Methods

5.2.1. Materials

Dulbecco's modified Eagle's medium (DMEM) was purchased from Sigma-Aldrich (Taufkirchen, Germany) and Leibovitz' L-15 medium (L-15) from Fisher Scientific (Nidderau, Germany). FCS and trypsin/EDTA were from Merck Biochrom (Darmstadt, Germany) and furimazine was from Promega (Mannheim, Germany). The pcDNA3.1 vector was from Thermo Scientific (Nidderau, Germany) and the pIRESpuro3 vector was kindly provided by Prof. Dr. Gunter Meister (University of Regensburg, Regensburg, Germany). Plasmids encoding the dopamine D_1 and D_5 receptors ($D_{1,5}R$) were a kind gift of Prof. Dr. Sigurd Elz (University of Regensburg, Regensburg, Germany) and the plasmid encoding the dopamine $D_{2,long}$ (D_2R) was kindly provided by Dr. Harald Hübner (Friedrich Alexander University, Erlangen, Germany). The cDNA encoding the α_{2A} and β_2 adrenoceptors ($\alpha_{2A}AR$, β_2AR), histamine $H_{1\text{-}4}$ receptors ($H_{1\text{-}4}R$), serotonin 5-HT_6 receptor (5-HT_6R), muscarinic acetylcholine $M_{1,2,4,5}$ receptors ($M_{1,2,4,5}R$), adenosine $A_{2A,2B}$ receptors ($A_{2A,2B}R$), neuropeptide Y $Y_{1,2,4}$ receptors ($Y_{1,2,4}R$), the neurotensin NTS_1 receptor (NTS_1R) and the chemokine CXCR4 receptor (CXCR4) were purchased from the Missouri cDNA research center (Rolla, MO, USA). The restriction enzymes *Dpn*I, *Hind*III and *Xba*I as well as the NEBuilder® HiFi DNA Assembly Cloning Kit were from New England Biolabs (New England Biolabs GmbH, Frankfurt a. M., Germany).

Histamine dihydrochloride (his) was purchased from Tokyo Chemical Industry (Eschborn, Germany). L-adrenaline (adren), dopamine hydrochloride (dopa), serotonin creatinine sulfate monohydrate (5-HT), iperoxo iodide (iper) and carbachol chloride (cch) were from Sigma Aldrich (Taufkirchen, Germany). 5'-(N-ethylcarboxamido)adenosine (NECA) was from Tocris Bioscience (Bristol, UK). Porcine neuropeptide Y (pNPY), human pancreatic polypeptide (hPP), neurotensin(8-13) (NT(8-13)) and CXC-motif chemokine receptor ligand 12 (CXCL12) were from SynPeptide (Shanghai, China). All ligands were dissolved, according to their physicochemical properties. Preferably, stock solutions were prepared in Millipore distilled water. L-adrenaline, pNPY and hPP were dissolved in 10 mM HCl and NT(8-13) was dissolved in a mixture of ethanol and 10 mM HCl (30:70).

5.2.2. Molecular Cloning

The molecular cloning strategy of pIRESpuro3 plasmids encoding either NlucN-mGs, NlucN-mGsi or NlucN-mGsq fusion proteins and pcDNA3.1 plasmids encoding $H_{1\text{-}3}$R-NlucC constructs has been described in Chapter 2 (section 2.2.2). For pcDNA3.1 plasmids encoding the $D_{1,2,5}$-NlucC, $M_{1,4,5}$R-NlucC, $Y_{1,2,4}$R-NlucC, NTS_1R-NlucC and CXCR4-NlucC fusion proteins, the molecular cloning strategy has been described in Chapter 3 (section 3.2.2). Analogously to pcDNA3.1 $H_{1\text{-}3}$R-NlucC, the CXCR4 and 5-HT_6R were subcloned into a linearized pcDNA3.1 NlucC plasmid using *Hind*III and *Xba*I yielding plasmids encoding CXCR4-NlucC and 5-HT_6R-NlucC constructs. For plasmids encoding α_{2A}AR-NlucC, $\beta_{1,2}$AR-NlucC, 5-HT_7R-NlucC, A_{2A}R-NlucC, A_{2B}R-NlucC, H_4R-NlucC and M_2R-NlucC fusion proteins a Gibson assembly reaction was performed.[65] In the case of the H_4R and M_2R, the sequence encoding the signal peptide of the murine serotonin 5-HT_{3A} receptor (SP; the N-terminal 23 peptide),[662] was N-terminally attached to the receptor by PCR to increase the receptor cell surface expression after transfection.[67-70] Upon translation, signal peptidase complexes (SPases) cleave the SP at the endoplasmatic reticulum (ER) from the receptor.[71] To generate suitable cDNA templates for the Gibson assemblyctions, 25 bp overlaps complementary to the desired insertion site of the pcDNA3.1 NlucC vector were added to the receptor cDNA sequences by PCR. Then, the PCR products were digested with *Dpn*I to remove the original template DNA. Using the NEBuilder® HiFi DNA Assembly Cloning Kit, the *Dpn*I digested receptor cDNA and a linearized pcDNA3.1 NlucC plasmid were covalently joined as described in Chapter 3 (section 3.2.2). Similarly, the Gibson assembly approach was used to generate the pcDNA4 mCherry plasmid encoding the fluorescent protein mCherry.[72] All plasmid DNA was quantified by UV-Vis absorbance using a NanoDrop spectrophotometer (ThermoFisher, Braunschweig, Germany) and verified by sequencing performed by Eurofins Genomics (Eurofins Genomics LLC, Ebersberg, Germany).

5.2.3. Cell Culture

HEK293T cells that were a kind gift from Prof. Dr. Wulf Schneider (Institute for Medical Microbiology and Hygiene, Regensburg, Germany), were cultured in DMEM supplemented with 10% FCS in a humidified 37 °C incubator with *5%* CO_2. The cells were periodically tested negative for mycoplasma contamination using the Venor GeM Mycoplasma Detection Kit (Minerva Biolabs, Berlin, Germany).

5.2.4. Generation of Transient Transfectants

Typically, HEK293T cells were seeded into a 6-well cell culture plate (Sarstedt, Nümbrecht, Germany) at cell density of 0.3 x 10^6 cells/mL (2 mL per well) and allowed to attach overnight. The next day, the cells were transfected using linear polyethyleneimine (PEI, 1 mg/mL in PBS; 1:5 ratio). To allow for an adequate protein expression, the cells were incubated for another 48 h.

For Western blot analysis, a total amount of 2 µg plasmid DNA and 10 µL of PEI in 200 µL DMEM were used for transfection as described in Chapter 2 (section 2.2.5). The plasmid DNA comprised 0.125, 0.25, 0.5 or 1.0 µg of the pIRESpuro3 NlucN-mGs/-mGsi/-mGsq constructs and 1.875, 1.750, 1.5 or 1.0 µg of the empty pIRESpuro3 vector (mock DNA), respectively. For blots designed to monitor the mini-G protein expression level upon transient transfection of the optimized DNA amounts, 0.567 µg of pIRESpuro3 NlucN-mGs, 0.415 µg of pIRESpuro3 NlucN-mGsi or 1.0 µg of pIRESpuro3 NlucN-mGsq plasmids were used in combination with 1.433, 1.585 or 1.0 µg of the empty pIRESpuro3 vector (mock DNA), respectively.

For mini-G protein recruitment assays, a total amount of 3 µg plasmid DNA was used for transfection comprising pcDNA3.1 GPCR-NlucC, pIRESpuro3 NlucN-mini-G protein, the empty pIRESpuro3 and pcDNA4 mCherry plasmids the composition of which is described in Table 5.1. For GPCR-NlucC constructs, a constant amount of 1 µg plasmid DNA was used. For NlucN-mini-G protein constructs, different plasmid DNA amounts were used giving equal protein expression levels of NlucN-mGs, NlucN-mGsi or NlucN-mGsq fusion proteins determined by Western blot analysis beforehand (Figure 5.1). To ensure a uniform transfection efficiency, the empty pIRESpuro3 vector was used as mock DNA to reach a constant DNA amount of 3 µg per well. For transfection control, the transfection mixes were supplemented with 1 µg of the pcDNA4 mCherry plasmid. For this purpose, the red-shifted fluorescent protein mCherry was selected in preference to other fluorescent proteins, such as GFP or mVenus, which emit green or yellow light, respectively, to reduce the spectral overlap with NanoLuc during the assay. For instance, for mVenus, a spectral overlap of 48% has been reported with NanoLuc, whereas mCherry overlap was only 18%.[73]

Table 5.1. Transfection scheme for mini-G protein recruitment assays.

DNA (µg)	mGs	mGsi	mGsq	Control
pcDNA3.1 GPCR-NlucC	1.0	1.0	1.0	-
pIRESpuro3 NlucN-mG	0.567	0.415	1.0	-
pIRESpuro3 (empty)	0.433	0.585	-	-
pcDNA4 mCherry	1.0	1.0	1.0	-
DMEM	300 µL	300 µL	300 µL	300 µL
PEI (1 : 5 ratio)	15 µL	15 µL	15 µL	15 µL

5.2.5. Western Blot Analysis

5.2.5.1. Western Blot Preparation

After 48 h transfection, the cells lysates were prepared as described in Chapter 2 (section 2.2.6). and15 µg lysate protein and 10 µL of the Precision Plus ProteinTM Dual Color Standard (Bio-Rad, Feldkirchen, Germany) were loaded to an 8–16% Novex Tris-glycine polyacrylamide gel (Thermo Scientific). Subsequently, the SDS-page was performed at 225 V for 1 h and blots were developed as described previously (Chapter 2, section 2.2.6).

5.2.5.2. Data Analysis

The NlucN-mini-G protein expression was assessed relative to the housekeeping protein vinculin serving as loading control. Therefore, the absolute luminescent intensities produced by the horseradish peroxidase reaction of the secondary antibody using the Clarity Western ECL substrate (Bio-Rad) obtained for NlucN-mini-G protein fusion proteins were divided by those of vinculin. For each experiment (N = 2), pIRESpuro3 NlucN-mGs/NlucN-mGsi plasmid DNA amounts were calculated to result in the same expression level as NlucN-mGsq after transfecting 1000 ng of pIRESpuro3 NlucN-mGsq. The mean value of the calculated plasmid DNA amounts was considered as the optimized plasmid DNA amounts for transient transfection (pIRESpuro3 NlucN-mGs = 567 ng, pIRESpuro3 NlucN-mGsi = 415 ng, pIRESpuro3 NlucN-mGsq = 1000 ng).

5.2.6. Mini-G Protein Recruitment Assays

The day prior to the experiment, transiently transfected and wildtype HEK293T cells (cf. Table 5.1) were detached using trypsin (0.05% trypsin, 0.02% EDTA in PBS) and centrifuged (700 g, 5 min). The cells were resuspended in 2.5 mL L-15 supplemented with 10 mM HEPES (Serva, Heidelberg, Germany) and 5% FCS, and 80 µL per well were seeded into a white flat-bottom 96-well microtiter plate (Brand GmbH + CoKG, Wertheim, Germany). The cells were incubated overnight at 37 °C in a water-saturated atmosphere without additional CO_2.

The mini-G protein recruitment assay was performed and analyzed as described in Chapter 2 (section 2.2.7) with the following modifications: Shortly before the experiment, the transfection efficiency of the cells was tested for uniformity. For this purpose, the co-expressed fluorescent protein mCherry was excited using an excitation wavelength of λ = 587 nm (E_{ex}) and emission was measured at λ = 610 nm (E_{em}) using an EnSpire plate reader (Perkin Elmer Inc., Rodgau, Germany).[72]

After demonstrating comparable transfection efficiencies of the cells, the furimazine substrate was diluted 1:100 in L-15, and 10 µL were added to the cells (final dilution in the assay: 1:1000). The plate was transferred to the pre-heated (37 °C) EnSpire plate reader and the basal luminescence was recorded for 15 min. Thereafter, 10 µL of the agonist serial dilutions prepared in L-15 were added to each well (final volume: 100 µL) and luminescence traces were recorded for additional 45 min. An integration time of 0.1 s per well was used to capture the luminescence. Data were analyzed using GraphPad Prism9 software (San Diego, CA, USA). The relative luminescence units (RLU) of the GPCR-NlucC/NlucN-mini-G protein expressing cells were corrected for the baseline drift caused by (auto)oxidation of the substrate by dividing all data by the mean luminescence intensity of the HEK293T wildtype control. In a second baseline-correction step, the mean luminescence of L-15 containing wells was subtracted for each cell strain. Concentration-response curves were obtained using the area under curve of the luminescence traces within 45 min ($AUC_{45\ min}$) that were normalized to the maximum response to the utilized agonist of the cells representing the canonical GPCR-G protein pairing (100% control) and L-15 (0% control). The logarithmic ligand concentrations were fitted against the normalized intensities with variable slope (log(c) vs. response–variable slope (four parameters)) yielding pEC_{50} and E_{max} values. To minimize the occurrence of outliers arising from experimental variations and to distinguish from injection preaks, GPCR – mini-G protein coupling was considered valid when, on one hand, concentration-response curves converged, and on the other hand, E_{max} values exceeded a threshold of 5% relative to the canonical system.[74]

5.2.7. Calculation of G Protein Coupling Scores

For each sigmoidal curve obtained in the mini-G protein recruitment assay, the maximal response (E_{max}, as fraction) was divided by the potency (EC_{50} [nM]). The E_{max}/EC_{50} ratio was then logarithmically (base 10) transformed ($\log(E_{max}/EC_{50})$) and normalized to the canonical mini-G protein condition yielding the dimensionless relative G protein score, $\Delta\log(E_{max}/EC_{50})$. Mean $\Delta\log(E_{max}/EC_{50}) \pm$ SEM were calculated using $\Delta\log(E_{max}/EC_{50})$ values of the individual experiments.

5.3. Results

5.3.1. Optimization of Mini-G Protein Expression Levels

Prior to conducting mini-G protein coupling experiments, important considerations were made on the mini-G protein expression levels. It is well accepted that the GPCR – G protein stoichiometry or rather Gα expression levels are decisive for assay signal amplitudes thus influencing ligand efficacy.[63-64] In accordance with this, in Chapter 2 (section 2.3.4), the dynamic range obtained for the H_2R in mini-G protein recruitment assays was sensitive to mGs expression levels. Since the maximal signals (E_{max}) were an important factor in evaluating the coupling efficiency of GPCRs to mini-G proteins, it was crucial that mini-G proteins were consistently expressed. Remarkably, the same mini-G protein gene doses did not result in the same protein expression (cf. Figure 5.1A and Chapter 2, section 2.3.4). Therefore, the amount of transiently transfected mini-G protein plasmid DNA had to be optimized to yield equal mini-G protein expression levels in the cells and thus ensure equal starting conditions for coupling experiments.

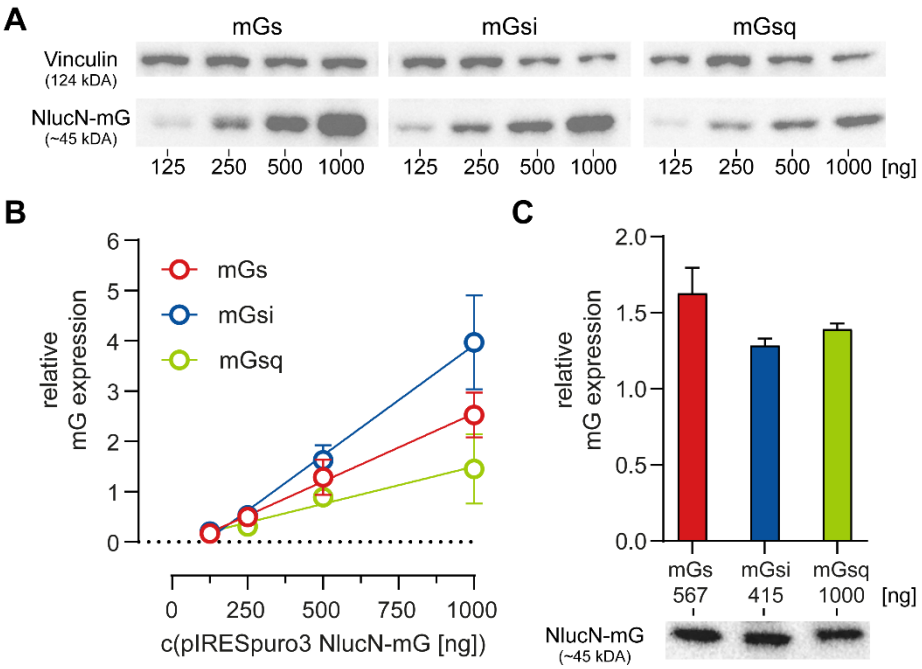

Figure 5.1. Western blot analysis of HEK293T cell lysates expressing the NlucN-mini-G fusion proteins. A) The cells were transiently transfected with indicated pIRESpuro3 plasmid DNA encoding the NlucN-mGs,-mGsi, and -mGsq fusion proteins. For primary staining, α-Nluc (rat; 1:5,000 in PBS-T) and α-vinculin (mouse; 1:500 in PBS-T) antibodies were used. For secondary staining, α-rabbit (HRP-conjugated; 1:10,000 in PBS-T) and α-mouse (HRP-conjugated; 1:100,000 in PBS-T) were used, both raised against IgG. Images were captured using a ChemiDoc MP imager (Bio-Rad). B) Mini-G protein expression levels relative to the housekeeping protein vinculin as loading control were calculated. C) Relative mini-G protein expression levels in HEK293T cells transiently transfected with optimized plasmid DNA amounts. Data represent means ± SD of two independent experiments (*N* = 2).

Therefore, Western blots were performed to determine the mini-G protein expression in cells after transient transfection of different NlucN-mini-G protein plasmid DNA amounts (125-1000 ng, Figure 5.1A). For this purpose, a primary α-NanoLuc (α-Nluc) antibody was used in combination with an HRP-conjugated secondary antibody to detect NlucN-mini-G protein fusion proteins. Of note, 1000 ng of NlucN-mGs and NlucN-mGsi plasmid DNA resulted in approximately 1.7- or 2.7-fold higher protein expression, respectively, than 1000 ng of NlucN-mGsq plasmid DNA (Figure 5.1B). For NlucN-mGs and NlucN-mGsi, the amount of plasmid DNA that should lead to a protein expression comparable to that of 1000 ng of NlucN-mGsq plasmid DNA was calculated giving 567 ng of NlucN-mGs and 415 ng of NlucN-mGsi plasmid DNA. Finally, a control Western blot demonstrated that optimized NlucN-mini-G protein plasmid DNA amounts result in similar protein expression in the cells upon transient transfection (Figure 5.1C).

5.3.2. Determination of GPCR – Mini-G Protein Coupling Profiles

In BRET-based assays, mini-G proteins developed by the groups of Tate and Lambert were demonstrated to maintain appropriate coupling specificity, which is e.g., the preferred coupling of Gi/o-coupled GPCRs to mGsi, by probing 12 prototypic GPCRs.[53-55] For this purpose, maximal BRET signals obtained were considered but the authors did not specify employed ligands or control mini-G protein expression during the experiments.[55] By contrast, the present work aimed at the development of a suitable assay concept, which controls the mini-G protein expression and moreover, allows for the evaluation of GPCR - G protein coupling profiles including both potency and efficacy to minimize false positives. Therefore, a broad series of overall 22 GPCRs was evaluated. This set comprised the Gs-coupled H_2R, D_1R, D_5R, β_1AR and β_2AR, the Gi/o-coupled H_3R, H_4R, D_2R, M_2R, M_4R, Y_1R, Y_2R, Y_4R and CXCR4 and the Gq/11-coupled H_1R, M_1R, M_5R and NTS_1R, which were the subject to the previous Chapters 2-4, as well as additional Gs-coupled 5-HT_6R, $A_{2A}R$ and $A_{2B}R$, and the Gi/o-coupled $\alpha_{2A}AR$.[37] It should be mentioned that some of these receptors were selected to match the study by Wan et al. (2017) allowing for a comparison of the different mini-G protein-based assay setups.

Using the optimized NlucN-mini-G protein and constant GPCR-NlucC plasmid DNA amounts, transiently transfected HEK293T cells were probed for responses to reference agonists in the mini-G protein recruitment assay (Table 5.2, Figure 5.2). For every GPCR investigated, the interaction was strongest with the respective mini-G protein corresponding to the G protein to which it primarily couples according to the IUPHAR/BPS Guide to Pharmacology.[37] Specifically, classically Gs-coupled 5-HT_6R,[75-76] β_1AR,[77] β_2AR,[78-79] D_1R,[80-81] D_5R,[82-83] H_2R,[84-85] $A_{2A}R$,[86-87] and $A_{2B}R$[88] provided the highest potency and efficacy in systems with mGs (Figure 5.2A). The reported Gi/o coupling receptors, $\alpha_{2A}AR$,[89] D_2R,[90-91] H_3R,[92] H_4R,[93-99] M_2R,[100] M_4R,[101] Y_1R,[102-103] Y_2R,[104-105] Y_4R,[106-107] and CXCR4,[108-109] predominantly interacted with mGsi (Figure 5.2B) and canonically Gq/11-coupled

receptors, H_1R,[110-111] M_1R,[100,112] M_5R,[113] and NTS_1R,[114-115] most efficiently recruited mGsq (Figure 5.2C). In conclusion, similar to reported BRET sensors, the split-NanoLuc based mini-G protein sensors provided appropriate specificity for GPCRs.[55]

In addition to suitable primary coupling profiles, individual secondary coupling patterns were obtained for the investigated GPCRs. To prevent false positives, a converging concentration-response curve in combination with an E_{max} of 5% relative to the canonical system was defined as cut-off for mini-G protein coupling. Representative luminescent traces for each GPCR/mini-G protein condition are given in the Appendix (Figures A18-20). Thereby, all Gs- and Gq/11-coupled receptors studied were able to secondarily bind to mGsi, while those receptors classified as Gi-coupled receptors were nearly selective for mGsi. Only $\alpha_{2A}AR$ and D_2R were able to secondarily bind to mGsq (Table 5.2, Figure 5.2B). However, in the case of the D_2R, a Gq-coupling has only been proposed for D_1R-D_2R heteromers.[116-118] In addition to comprehensive mGsi binding, most Gs-coupled receptors, except 5-HT_6R, D_5R and $A_{2A}R$, interacted with mGsq and vice-versa, the Gq/11-coupled M_1R interacted with mGs (in addition to mGsq and mGsi) signifying G protein promiscuity (Table 5.2, Figure 5.2B). Of note, all secondary interactions were of lower potency and efficacy than primary couplings. In summary, observed GPCR coupling profiles to mini-G proteins were in good agreement with that of other G protein biosensors.[55,119] Particular attention should be paid to the pronounced secondary coupling of D_1R to mGsi, $A_{2B}R$ to mGsq, H_1R to mGsi and M_5R to mGsi that were between 64 ± 2.8% ($A_{2B}R$) and 91 ± 4.6% (D_1R), thus suggesting a physiological relevance. As Gs and Gi proteins bind to different sites at ACs, in theory, Gs and Gi proteins could simultaneously bind to AC.[14] Thus, the activation of Gi proteins at high agonist concentrations might terminate or at least attenuate Gs signaling of the D_1R. Earlier, D_1R coupling to Gi proteins was reported to depend on the cellular milieu and thus be tissue-dependent.[120] In the lung, stimulation of Gs-coupled $A_{2B}R$ results in the release of several cytokines promoting inflammatory and fibrotic processes,[121] but the $A_{2B}R$-mediated secretion of interleukin-8 (IL8) has been associated with stimulation of PLC rather than AC.[122] In agreement to prior assumptions, mini-G protein data supported that such PLC stimulation is Gq-mediated,[123] advocating $A_{2B}R$ antagonism as a promising concept for the medical treatment of asthma.[121,124] For H_1R, Gi/o coupling of H_1R has been reported in the literature.[125-126] This can lead to PTX-sensitive production of arachidonic acid in various cell types.[127-128] Surprisingly, at the M_5R, iperoxo elicited a maximal mGsi response of 83 ± 8.5% and was nearly equipotent at M_5R-mGsi and M_5R-mGsq with pEC_{50} values of 8.18 ± 0.16 and 8.35 ± 0.04, respectively. To best of our knowledge, similar results have not been reported before. Compared to other MR subtypes, the M_5R represents an understudied target in the literature.[129-130] Due to missing selectivity of available (radio)ligands, the determination of specific tissue expression or, in general, physiological relevance is a challenge.[130] Thus, there is a need for

the development of selective M_5R ligands to evaluate the physiological relevance of M_5R, including Gi/o coupling.

Table 5.2. Potencies (pEC_{50}) and efficacies (E_{max}) of selected agonists obtained in the mini-G protein recruitment assay. HEK293T cells transiently expressing indicated GPCR-NlucC fusion proteins in combination with either NlucN-mGs, NlucN-mGsi or NlucN-mGsq fusion proteins were used. Presented data are of three independent experiments (*N* = 3) each performed in triplicate (n.d. = not detected).

Subtype	Cpd	mGs		mGsi		mGsq	
		pEC_{50} ± SEM	E_{max} ± SEM [%]	pEC_{50} ± SEM	E_{max} ± SEM [%]	pEC_{50} ± SEM	E_{max} ± SEM [%]
5-HT_6R	5-HT	7.74 ± 0.10	100	7.33 ± 0.06	27 ± 5.9	n.d.	2 ± 0.7
β_1AR	adren	7.37 ± 0.06	100	6.09 ± 0.06	20 ± 1.0	6.10 ± 0.02	6 ± 1.5
β_2AR	adren	8.19 ± 0.13	100	6.89 ± 0.16	38 ± 3.6	6.27 ± 0.06	5 ± 0.7
D_1R	dopa	7.67 ± 0.19	100	6.48 ± 0.04	91 ± 4.6	5.83 ± 0.06	5 ± 0.9
D_5R	dopa	7.72 ± 0.04	100	7.19 ± 0.08	29 ± 10.2	n.d.	-2 ± 0.7
H_2R	his	6.86 ± 0.04	100	5.30 ± 0.06	27 ± 3.5	5.48 ± 0.04	30 ± 3.7
$A_{2A}R$	NECA	7.31 ± 0.07	100	7.13 ± 0.11	12 ± 2.8	n.d.	5 ± 1.2
$A_{2B}R$	NECA	6.92 ± 0.14	100	6.20 ± 0.07	64 ± 2.8	6.10 ± 0.10	16 ± 0.5
α_{2A}AR	adren	n.d.	3 ± 0.9	7.46 ± 0.09	100	6.75 ± 0.06	32 ± 13.5
D_2R	dopa	n.d.	-1 ± 0.4	6.91 ± 0.09	100	6.71 ± 0.11	6 ± 0.8
H_3R	his	n.d.	0 ± 0.7	6.57 ± 0.03	100	n.d.	1 ± 0.3
H_4R	his	n.d.	-14 ± 5.5	6.60 ± 0.10	100	n.d.	13 ± 0.4
M_2R	iper	n.d.	9 ± 0.8	8.41 ± 0.17	100	n.d.	2 ± 0.9
M_4R	iper	n.d.	9 ± 1.5	9.20 ± 0.02	100	n.d.	6 ± 1.8
Y_1R	pNPY	n.d.	0 ± 6.6	9.48 ± 0.09	100	n.d.	-8 ± 7.8
Y_2R	pNPY	n.d.	0 ± 1.0	8.77 ± 0.07	100	n.d.	1 ± 0.2
Y_4R	hPP	n.d.	3 ± 1.8	9.47 ± 0.09	100	n.d.	-1 ± 0.6
CXCR4	CXCL12	n.d.	-5 ± 1.3	8.20 ± 0.57	100	n.d.	0 ± 1.4
H_1R	his	n.d.	17 ± 4.0	5.16 ± 0.10	67 ± 7.0	5.59 ± 0.05	100
M_1R	iper	6.95 ± 0.01	18 ± 9.2	7.37 ± 0.07	29 ± 10.6	7.65 ± 0.09	100
M_5R	iper	n.d.	7 ± 1.1	8.18 ± 0.16	83 ± 8.5	8.35 ± 0.04	100
NTS_1R	NT(8-13)	n.d.	6 ± 2.2	9.26 ± 0.07	30 ± 8.0	8.93 ± 0.01	100

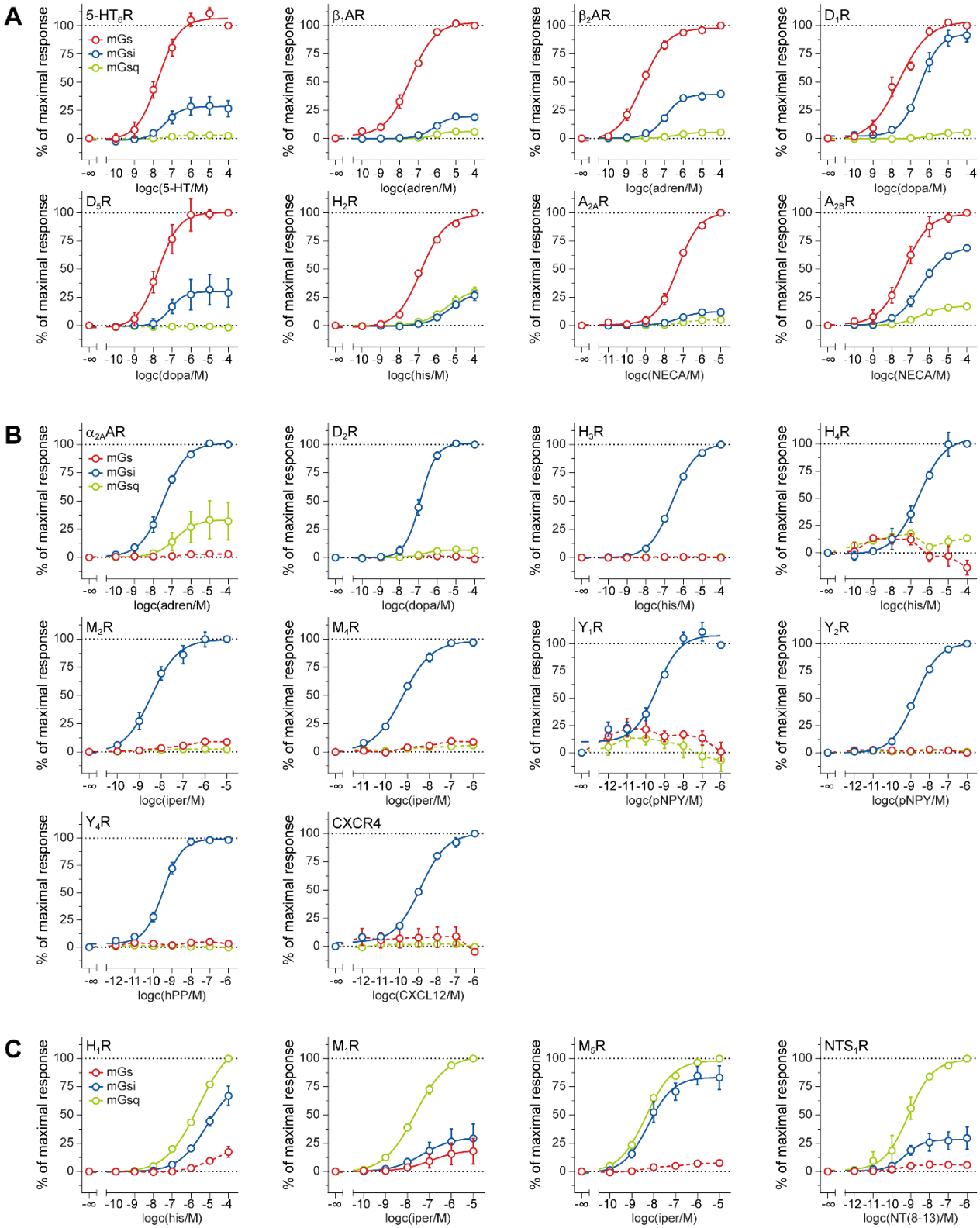

Figure 5.2. Concentration response curves of endogenous/reference agonists at canonically A) Gs-, B) Gi/o- and C) Gq/11-coupling GPCRs obtained in the mini-G protein recruitment assay. HEK293T cells transiently co-expressing GPCR-NlucC and NlucN-mGs, NlucN-mGsi or NlucN-mGsq fusion proteins were used. Presented data are of at least three independent experiments (*N* = 3) each performed in triplicate.

5.3.3. Determination of Dimensionless G Protein Coupling Scores

Lately, different biosensors were applied to G protein assays to study specific interactions with GPCRs.[74,119,131-132] In these studies, GPCR – G protein coupling profiles often were given as heatmaps summarizing potencies or normalized responses of receptor-ligand complexes and transducers similar to Figure 5.3A and 5.3B, respectively, for mini-G protein coupling.[55,119,131-132] However, potencies and efficacies may vary across functional assays due the occurrence of receptor reserve or signal amplification.[133-135] For this, it seems reasonable to define a dimensionless, relative G protein coupling score that includes both efficacy and potency. In drug discovery, the intrinsic relative activity (RA_i), was implemented to quantify the functional selectivity of ligands, which describes the ability to selectively activate different signaling pathways.[28-29,74,136] Classically, these RA_i values are compared for G protein or β-arrestin signaling to determine the functional selectivity of a ligand, also termed bias.[27,57,137] Its analysis relies on the Black-Leff operational model of pharmacological agonism and, in particular, on the transduction coefficient $\log(\tau/K_A)$, where K_A is the equilibrium dissociation constant and τ is the intrinsic activity, which allows for the agonist affinity being dependent on the interaction of the receptor with G proteins or β-arrestins.[26-27,138] The correlation between the transduction coefficient ($\log(\tau/K_A)$) and the ratio of efficacy and potency ($\log(E_{max}/EC_{50})$ of a ligand has been described, enabling the use of curve fit parameters of functional data to determine dimensionless $\Delta\log(E_{max}/EC_{50})$ values that reflect the relative activation of a pathway.[27,29,74,136] Thus, dimensionless G protein coupling scores were calculated for the investigated GPCRs allowing for the classification of $A_{2B}R$, H_1R, M_1R, M_5R and NTS_1R coupling to mGsi as strong secondary coupling defined by $-1 < \Delta\log(E_{max}/EC_{50}) \leq 0$ (Table 5.3, Figure 5.3C).[74]

Moreover, the calculation of $\Delta\log(E_{max}/EC_{50})$ values allowed for comparing the GPCR - G protein coupling profiles obtained by mini-G protein recruitment assays with reference data provided at the G protein database (GproteinDb). GproteinDb integrates data from the research community to curate sequence alignments, structures and mutations from the literature.[139] Another important feature of the database deals with G protein coupling scores of GPCRs.[139-140] Hauser et al. provided $\log(E_{max}/EC_{50})$ to this database generated by using functional data of large G protein studies by the Inoue and Bouvier laboratories.[74,132,140] In these studies, more than 100 GPCRs each were probed for their preferences to bind to G proteins of all four G protein families (Gs, Gi/o, Gq/11 and G12/13) in distal TGF-α shedding assays using chimeric G proteins[74] or proximal G protein-dependent effector membrane translocalization assays (GEMTA).[132] For comparison, available reference $\log(E_{max}/EC_{50})$ values were converted into $\Delta\log(E_{max}/EC_{50})$ values (Table 5.3). It should be mentioned that the studies of Inoue et al. and Avet et al. did not include Y_2R and Y_4R, which selectively bound to mGsi in the mini-G protein recruitment assay (Table 5.3).[74,132] However, in contrast to TGF-α shedding and GEMTA assays, mini-G protein sensors did not detect

GPCR - G protein coupling in the following cases: 5-HT$_6$R-mGsq, D$_5$R-mGsq, A$_{2A}$R-mGsq, α_{2A}AR-mGs, H$_3$R-mGsq, H$_4$R-mGs/-mGsq, M$_2$R-mGs/-mGsq, M$_4$R-mGs, H$_1$R-mGs, M$_5$R-mGs and NTS$_1$R-mGs (Table 5.3).[74,132] And, in return, mini-G protein sensors indicated the following interactions (partially) missing in the literature: β_2AR-mGsi, A$_{2A}$R-mGsi, A$_{2B}$R-mGsi and D$_2$R-mGsq. Overall, this might be attributed to several considerations. On one hand, low signal amplitudes of the presented assay as well as of assays in the literature might mask positive outcomes. E.g., this could be the case for the lacking H$_4$R-mGs interaction, since maximal signal amplitudes were particularly low, even for the H$_4$R-mGsi system (cf. Appendix, Figure 19). On the other hand, different signaling levels might have a major impact on positive outcomes when comparing GPCR – G protein coupling profiles, since signal amplification as well as the occurrence of signaling pathway crosstalk should be pronounced in more distal cell assays, such as in TGF-α shedding assays.[42,48,141-142] E.g., (Gq-like) phosphoinositol production in response to M$_2$R activation was found to originate from the $\beta\gamma$ dimer of the Gi complex activating PLC.[143-144] However, the concept of mini-G protein sensors representing Gα surrogates would not allow for detecting G$\beta\gamma$-mediated responses, which might explain the missing M$_2$R-mGsq interaction. One should also not ignore that other reference agonists were used in the studies by Inoue et al and Avet et al, except for 5-HT$_6$R, D$_{2,5}$R, and H$_{1,3,4}$R, indicating that the ligands might be capable of promoting G protein bias. (cf. Appendix, Table A4).[74,132]

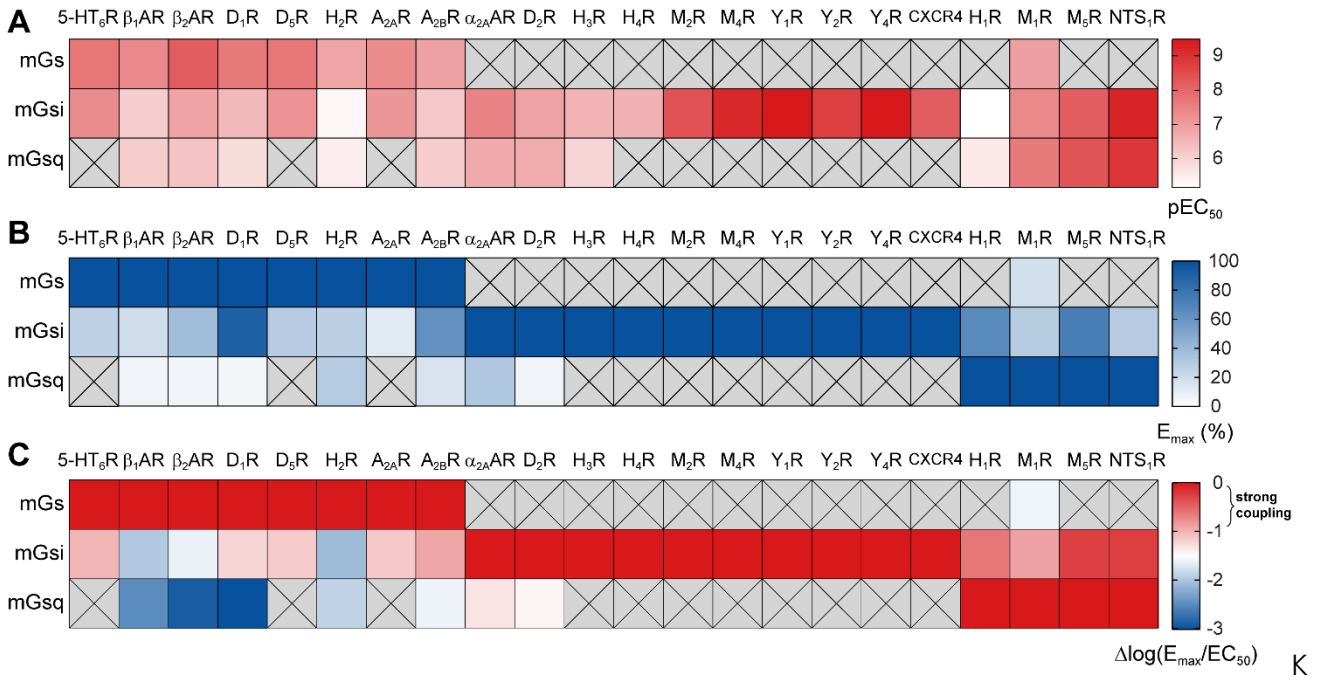

Figure 5.3. Heatmaps illustrating the diversity of receptor-ligand-specific signaling profiles with varying degrees of G protein promiscuity detected by mini-G sensors. Heatmaps were generated using A) potency (pEC$_{50}$) and B) efficacy (E$_{max}$) values of each mini-G protein condition normalized to the maximum response of the primary GPCR-G protein pairing (cf. Table 5.2). C) The Δlog(E$_{max}$/EC$_{50}$) values combine information about potencies and efficacies of receptor-ligand pairs for mini-G protein recruitment. Δlog(E$_{max}$/EC$_{50}$) values were calculated by subtracting log(E$_{max}$/EC$_{50}$) values of the canonical mini-G condition from all log(E$_{max}$/EC$_{50}$) values (cf. Table 5.3). Presented data are of at least three independent experiments (N = 3) each performed in triplicate and GPCR – mini-G protein conditions with no interaction are highlighted by crossed gray boxes.

Table 5.3. Dimensionless G protein coupling scores ($\Delta\log(E_{max}/EC_{50})$) obtained in the mini-G protein recruitment assay. HEK293T cells transiently expressing indicated GPCR-NlucC in combination with either NlucN-mGs, NlucN-mGsi or NlucN-mGsq fusion proteins were used. Presented data are of three independent experiments (*N* = 3) each performed in triplicate.

	$\Delta\log(E_{max}/EC_{50})$ ± SEM			Reference $\Delta\log(E_{max}/EC_{50})$[a]		
Subtype	mGs	mGsi	mGsq	Gs	Gi	Gq
5-HT_6R	0	-1.02 ± 0.12	n.d.	0[c]	0[c]	-0.6[c]
β_1AR	0	-2.01 ± 0.10	-2.59 ± 0.14	0[b≠, c≠]	-3.5[b≠], -1[c≠]	-3.5[b≠], -0.3[c≠]
β_2AR	0	-1.65 ± 0.07	-3.04 ± 0.16	0[b≠, c≠]	n.d.[b≠, c≠]	-1.9[b≠], -0.2[c≠]
D_1R	0	-1.23 ± 0.15	-3.14 ± 0.18	0[b, c]	-3.2[b], 0[c]	-1.2[b], -0.05[c]
D_5R	0	-1.16 ± 0.12	n.d.	0[b, c]	-3.1[b], 0[c]	-0.7[b], -0.05[c]
H_2R	0	-2.15 ± 0.12	-1.92 ± 0.06	0[b, c]	-2.9[b], 0[c]	-0.5[b], -0.71[c]
A_{2A}R	0	-1.15 ± 0.10	n.d.	0[b≠, c≠]	n.d.[b≠, c≠]	-0.2[b≠], -0.1[c≠]
A_{2B}R	0	-0.92 ± 0.07	-1.62 ± 0.25	0[b≠, c≠]	n.d.[b≠, c≠]	0[b≠], -0.6[c≠]
α_{2A}AR	n.d.	0	-1.32 ± 0.16	-3.5[b≠], -2.8[c≠]	0[b≠, c≠]	-3.8[b≠], -2[c≠]
D_2R	n.d.	0	-1.43 ± 0.08	n.d.[b, c]	0[b, c]	n.d.[b, c]
H_3R	n.d.	0	n.d.	n.d.[c]	0[c]	-0.7[c]
H_4R	n.d.	0	n.d.	-1.1[c]	0[c]	-0.6[c]
M_2R	n.d.	0	n.d.	-2.7[b≠], -2.5[c≠]	0[b≠, c≠]	-2.3[b≠], -1.5[c≠]
M_4R	n.d.	0	n.d.	n.d.[b≠, c≠]	0[b≠, c≠]	-2.9[b≠], -1.2[c≠]
Y_1R	n.d.	0	n.d.	n.d.[b≠]	0[b≠]	n.d.[b≠]
Y_2R	n.d.	0	n.d.	n.a.	n.a.	n.a.
Y_4R	n.d.	0	n.d.	n.a.	n.a.	n.a.
CXCR4	n.d.	0	n.d.	n.d.[b]	0[b]	n.d.[b]
H_1R	n.d.	-0.61 ± 0.02	0	-2.3[b], -0.2[c]	-1.36[b], 0[c]	0[b, c]
M_1R	-1.61 ± 0.30	-0.89 ± 0.15	0	-1.9[b≠], -0.9[c≠]	-2.7[b≠], 0[c≠]	0[b≠, c≠]
M_5R	-1.81 ± 0.07	-0.26 ± 0.13	0	-0.8[c≠]	0[c≠]	0[c≠]
NTS_1R	n.d.	-0.25 ± 0.06	0	-1.5[c≠]	0[c≠]	0[c≠]

[a]Rerefence $\Delta\log(E_{max}/EC_{50})$ were assessed using $\log(E_{max}/EC_{50})$ values calculated by Hauser et al. (2021),[140] and provided to the G protein data base GproteinDb (www.gproteindb.org).[139] Original assay data was from proximal [b]G protein dependent effector membrane translocalization assays (GEMTA) by Avet et al. (2020),[132] or from distal [c]TGF-α shedding assays using chimeric G proteins by Inoue et al. (2019),[74] both performed in HEK293 cells. Unless otherwise stated (≠) same ligands were used in these studies. Experimental details of the reference studies are given in the Appendix, Table A4; n.d. = not detected; n.a. = not available.

5.4. Discussion

The aim of this study was to demonstrate the utility of split-NanoLuc-based mini-G protein sensors under equal mini-G protein expression levels for the investigation of GPCR - G protein selectivity. Western blots revealed that NlucN-mGsq gene doses led to a considerably lower protein expression than NlucN-mGs or -mGsi gene doses. Thus, a protocol was designed for the transient transfection of HEK293T cells, which comprised equal GPCR-NlucC (1 µg) and optimized NlucN-mini-G protein gene doses (mGs/mGsi/mGsq: 0.567/0.415/1.0 µg) to minimize misinterpretation of potency and efficacy due to variations in protein expression.[27] Subsequently, the coupling profiles of 22 GPCRs with mini-G proteins were determined using full agonists.

Similar to BRET-based sensors, split-NanoLuc-based mini-G protein sensor maintained appropriate GPCR coupling specificity.[37,55] Moreover, specific secondary coupling profiles were obtained for the GPCRs studied. While 8 out of 22 GPCRs ($H_{3,4}R$, $M_{2,4}R$, $Y_{1,2,4}R$, CXCR4) were observed to exclusively couple to mGsi, none of the GPCRs investigated were restrictive for either mGs or mGsq (Figure 5.4). Rather, all receptors interacted with mGsi, three of which coupled to mGsi/mGs (D_5R, $A_{2A}R$, 5-HT_6R) and 5 of which coupled to mGsi/mGsq (D_2R, $\alpha_{2A}AR$, H_1R, M_5R, NTS_1R). In total, 6 of the 22 GPCRs studied promiscuously bound to all mini-G proteins ($\beta_{1,2}AR$, D_1R, H_2R, $A_{2B}R$, M_1R; Figure 5.4). In the literature, efficacy has often been considered for evidence of the activation of a specific G protein signaling pathway, but this can lead to false positives due to overestimation of weak assay signals, as demonstrated in the present work for the H_4R.[55,119] Since overall signals in the canonical H_4R-mGsi system were particularly low, histamine, e.g., elicited a maximum response of 13 ± 0.4% in the H_4R-mGsq system, even though the concentration response curves did not converge (Table 5.2, Figure 5.2B). Therefore, a cut-off was defined of converging concentration-response curves in combination with an E_{max} of at least 5% relative to the canonical system for evaluating specific GPCR coupling profiles. Another consideration for data evaluation was that ligand potency and efficacy may vary along the signaling cascade due to receptor reserve, general signal amplification, or possible signaling pathway crosstalk, which might complicate the interpretation of functional data obtained at different cellular stages.[42,133-135] Thus, it was a necessity to implement dimensionless G protein coupling scores.

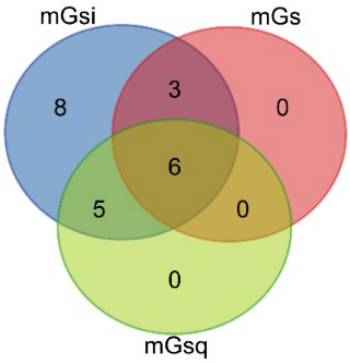

Figure 5.4. Venn diagram summarizing the numbers of investigated GPCRs coupling to mGs, mGsq and mGsi according to $\Delta\log(E_{max}/EC_{50})$ values.

Overall, the calculation of $\Delta\log(E_{max}/EC_{50})$, which has been considered one of the most powerful tools in bias determination,[145] relative to the canonical system has not only allowed to estimate the strength of secondary coupling but also to compare the coupling profiles obtained by mini-G protein sensors with reference data. Of note, the secondary coupling of the $A_{2B}R$, H_1R, M_1R, M_5R and NTS_1R to mGsi was particularly strong demonstrated by $\Delta\log(E_{max}/EC_{50})$ between -1 and 0.[74]

In summary, the presented assay aiming at equal mini-G protein expression levels was suitable for the determination of GPCR - G protein selectivity and offers the potential to assess ligand-dependent G protein bias in future studies.[48,146]

5.5. References

1. Hamm, H. E., The many faces of G protein signaling. *J Biol Chem* **1998,** *273* (2), 669-672, doi: 10.1074/jbc.273.2.669.
2. Dalesio, N. M., Barreto Ortiz, S. F., Pluznick, J. L. & Berkowitz, D. E., Olfactory, taste, and photo sensory receptors in non-sensory organs: It just makes sense. *Front Physiol* **2018,** *9*, doi: 10.3389/fphys.2018.01673.
3. Huang, Y. & Thathiah, A., Regulation of neuronal communication by G protein-coupled receptors. *FEBS Lett* **2015,** *589* (14), 1607-1619, doi: 10.1016/j.febslet.2015.05.007.
4. Culhane, K. J., Liu, Y., Cai, Y. & Yan, E. C. Y., Transmembrane signal transduction by peptide hormones via family B G protein-coupled receptors. *Frontiers in Pharmacology* **2015,** *6*, doi: 10.3389/fphar.2015.00264.
5. Lander, E. S., Linton, L. M., Birren, B., Nusbaum, C., Zody, M. C., Baldwin, J., Devon, K., Dewar, K., Doyle, M., FitzHugh, W., et al., Initial sequencing and analysis of the human genome. *Nature* **2001,** *409* (6822), 860-921, doi: 10.1038/35057062.
6. Venter, J. C., Adams, M. D., Myers, E. W., Li, P. W., Mural, R. J., Sutton, G. G., Smith, H. O., Yandell, M., Evans, C. A., Holt, R. A., et al., The sequence of the human genome. *Science* **2001,** *291* (5507), 1304-1351, doi: 10.1126/science.1058040.
7. Fredriksson, R., Lagerström, M. C., Lundin, L. G. & Schiöth, H. B., The G-protein-coupled receptors in the human genome form five main families. Phylogenetic analysis, paralogon groups, and fingerprints. *Mol Pharmacol* **2003,** *63* (6), 1256-1272, doi: 10.1124/mol.63.6.1256.
8. Milligan, G. & Kostenis, E., Heterotrimeric G-proteins: A short history. *Br J Pharmacol* **2006,** *147 Suppl 1*, S46-55, doi: 10.1038/sj.bjp.0706405.
9. Oldham, W. M. & Hamm, H. E., Heterotrimeric G protein activation by G-protein-coupled receptors. *Nat Rev Mol Cell Biol* **2008,** 9 (1), 60-71, doi: 10.1038/nrm2299.
10. Mahoney, J. P. & Sunahara, R. K., Mechanistic insights into GPCR-G protein interactions. *Curr Opin Struct Biol* **2016,** *41*, 247-254, doi: 10.1016/j.sbi.2016.11.005.
11. Denis, C., Sauliere, A., Galandrin, S., Senard, J. M. & Gales, C., Probing heterotrimeric G protein activation: Applications to biased ligands. *Curr Pharm Des* **2012,** *18* (2), 128-144, doi: 10.2174/138161212799040466.
12. Taussig, R., Tang, W. J., Hepler, J. R. & Gilman, A. G., Distinct patterns of bidirectional regulation of mammalian adenylyl cyclases. *J Biol Chem* **1994,** *269* (8), 6093-6100.
13. Yang, X., Lee Sr, F. Y. G. & Wand, G. S., Increased expression of Gsα enhances activation of the adenylyl cyclase signal transduction cascade. *Mol Endocrinol* **1997,** *11* (8), 1053-1061, doi: 10.1210/mend.11.8.9957.
14. Navarro, G., Cordomí, A., Casadó-Anguera, V., Moreno, E., Cai, N.-S., Cortés, A., Canela, E. I., Dessauer, C. W., Casadó, V., Pardo, L., et al., Evidence for functional pre-coupled complexes of receptor heteromers and adenylyl cyclase. *Nat Commun* **2018,** 9 (1), 1242, doi: 10.1038/s41467-018-03522-3.
15. Harden, T. K., Waldo, G. L., Hicks, S. N. & Sondek, J., Mechanism of activation and inactivation of Gq/phospholipase C-β signaling nodes. *Chem Rev* **2011,** *111* (10), 6120-6129, doi: 10.1021/cr200209p.
16. Dupré, D. J., Robitaille, M., Rebois, R. V. & Hébert, T. E., The role of G$\beta\gamma$ subunits in the organization, assembly, and function of GPCR signaling complexes. *Annu Rev Pharmacol Toxicol* **2009,** *49*, 31-56, doi: 10.1146/annurev-pharmtox-061008-103038.
17. Logothetis, D. E., Kurachi, Y., Galper, J., Neer, E. J. & Clapham, D. E., The $\beta\gamma$ subunits of GTP-binding proteins activate the muscarinic K+ channel in heart. *Nature* **1987,** *325* (6102), 321-326, doi: 10.1038/325321a0.

18. Pitcher, J. A., Freedman, N. J. & Lefkowitz, R. J., G protein-coupled receptor kinases. *Annu Rev Biochem* **1998,** *67*, 653-692, doi: 10.1146/annurev.biochem.67.1.653.

19. Benovic, J. L., Kühn, H., Weyand, I., Codina, J., Caron, M. G. & Lefkowitz, R. J., Functional desensitization of the isolated β-adrenergic receptor by the β-adrenergic receptor kinase: Potential role of an analog of the retinal protein arrestin (48-kDa protein). *Proc Natl Acad Sci U S A* **1987,** *84* (24), 8879-8882, doi: 10.1073/pnas.84.24.8879.

20. Cho, E. Y., Cho, D. I., Park, J. H., Kurose, H., Caron, M. G. & Kim, K. M., Roles of protein kinase C and actin-binding protein 280 in the regulation of intracellular trafficking of dopamine D3 receptor. *Mol Endocrinol* **2007,** *21* (9), 2242-2254, doi: 10.1210/me.2007-0202.

21. Benovic, J. L., Pike, L. J., Cerione, R. A., Staniszewski, C., Yoshimasa, T., Codina, J., Caron, M. G. & Lefkowitz, R. J., Phosphorylation of the mammalian β-adrenergic receptor by cyclic AMP-dependent protein kinase. Regulation of the rate of receptor phosphorylation and dephosphorylation by agonist occupancy and effects on coupling of the receptor to the stimulatory guanine nucleotide regulatory protein. *J Biol Chem* **1985,** *260* (11), 7094-7101.

22. Ferguson, S. S., Downey, W. E., 3rd, Colapietro, A. M., Barak, L. S., Ménard, L. & Caron, M. G., Role of β-arrestin in mediating agonist-promoted G protein-coupled receptor internalization. *Science* **1996,** *271* (5247), 363-366, doi: 10.1126/science.271.5247.363.

23. Goodman, O. B., Jr., Krupnick, J. G., Santini, F., Gurevich, V. V., Penn, R. B., Gagnon, A. W., Keen, J. H. & Benovic, J. L., β-arrestin acts as a clathrin adaptor in endocytosis of the β2-adrenergic receptor. *Nature* **1996,** *383* (6599), 447-450, doi: 10.1038/383447a0.

24. Laporte, S. A., Oakley, R. H., Holt, J. A., Barak, L. S. & Caron, M. G., The interaction of β-arrestin with the AP-2 adaptor is required for the clustering of β2-adrenergic receptor into clathrin-coated pits. *J Biol Chem* **2000,** *275* (30), 23120-23126, doi: 10.1074/jbc.M002581200.

25. Peterson, Y. K. & Luttrell, L. M., The diverse roles of arrestin scaffolds in G protein-coupled receptor signaling. *Pharmacol Rev* **2017,** *69* (3), 256-297, doi: 10.1124/pr.116.013367.

26. Black, J. W. & Leff, P., Operational models of pharmacological agonism. *Proceedings of the Royal Society of London. Series B, Biological sciences* **1983,** *220* (1219), 141-162, doi: 10.1098/rspb.1983.0093.

27. Kenakin, T., Watson, C., Muniz-Medina, V., Christopoulos, A. & Novick, S., A simple method for quantifying functional selectivity and agonist bias. *ACS chemical neuroscience* **2012,** *3* (3), 193-203, doi: 10.1021/cn200111m.

28. Ehlert, F. J., Griffin, M. T., Sawyer, G. W. & Bailon, R., A simple method for estimation of agonist activity at receptor subtypes: Comparison of native and cloned M3 muscarinic receptors in guinea pig ileum and transfected cells. *J Pharmacol Exp Ther* **1999,** *289* (2), 981-992.

29. Griffin, M. T., Figueroa, K. W., Liller, S. & Ehlert, F. J., Estimation of agonist activity at G protein-coupled receptors: Analysis of M2 muscarinic receptor signaling through Gi/o, Gs, and G15. *J Pharmacol Exp Ther* **2007,** *321* (3), 1193-1207, doi: 10.1124/jpet.107.120857.

30. Christopoulos, A. & Kenakin, T., G protein-coupled receptor allosterism and complexing. *Pharmacol Rev* **2002,** *54* (2), 323-374, doi: 10.1124/pr.54.2.323.

31. Kenakin, T., Agonist-receptor efficacy. II. Agonist trafficking of receptor signals. *Trends Pharmacol Sci* **1995,** *16* (7), 232-238, doi: 10.1016/s0165-6147(00)89032-x.

32. Kang, D. S., Tian, X. & Benovic, J. L., Role of β-arrestins and arrestin domain-containing proteins in G protein-coupled receptor trafficking. *Current opinion in cell biology* **2014,** *27*, 63-71, doi: 10.1016/j.ceb.2013.11.005.

33. Milligan, G., Is promiscuity of G protein interaction an issue in the classification of receptors? *Ann N Y Acad Sci* **1997,** *812*, 126-132, doi: 10.1111/j.1749-6632.1997.tb48152.x.

34. Kenakin, T., Are receptors promiscuous? Intrinsic efficacy as a transduction phenomenon. *Life sciences* **1988,** *43* (14), 1095-1101, doi: 10.1016/0024-3205(88)90467-5.

35. Downes, G. B. & Gautam, N., The G protein subunit gene families. *Genomics* **1999,** *62* (3), 544-552, doi: 10.1006/geno.1999.5992.

36. Wettschureck, N. & Offermanns, S., Mammalian G proteins and their cell type specific functions. *Physiol Rev* **2005,** *85* (4), 1159-1204, doi: 10.1152/physrev.00003.2005.

37. Alexander, S. P. H., Christopoulos, A., Davenport, A. P., Kelly, E., Mathie, A., Peters, J. A., Veale, E. L., Armstrong, J. F., Faccenda, E., Harding, S. D., et al., The concise guide to pharmacology 2019/20: G protein-coupled receptors. *Br J Pharmacol* **2019,** *176* (S1), S21-S141, doi: 10.1111/bph.14748.

38. Grisshammer, R., The quest for high-resolution G protein-coupled receptor–G protein structures. *Proc Natl Acad Sci U S A* **2020,** *117* (13), 6971-6973, doi: 10.1073/pnas.2002665117.

39. Meszaros, J. G., Gonzalez, A. M., Endo-Mochizuki, Y., Villegas, S., Villarreal, F. & Brunton, L. L., Identification of G protein-coupled signaling pathways in cardiac fibroblasts: Cross talk between Gq and Gs. *Am J Physiol Cell Physiol* **2000,** *278* (1), C154-C162, doi: 10.1152/ajpcell.2000.278.1.C154.

40. McGraw, D. W., Elwing, J. M., Fogel, K. M., Wang, W. C., Glinka, C. B., Mihlbachler, K. A., Rothenberg, M. E. & Liggett, S. B., Crosstalk between Gi and Gq/Gs pathways in airway smooth muscle regulates bronchial contractility and relaxation. *The Journal of clinical investigation* **2007,** *117* (5), 1391-1398, doi: 10.1172/jci30489.

41. Galaz-Montoya, M., Wright, S. J., Rodriguez, G. J., Lichtarge, O. & Wensel, T. G., β2-Adrenergic receptor activation mobilizes intracellular calcium via a non-canonical cAMP-independent signaling pathway. *J Biol Chem* **2017,** *292* (24), 9967-9974, doi: 10.1074/jbc.M117.787119.

42. Cordeaux, Y. & Hill, S. J., Mechanisms of cross-talk between G-protein-coupled receptors. *Neuro-Signals* **2002,** *11* (1), 45-57, doi: 10.1159/000057321.

43. Simonds, W. F., G protein regulation of adenylate cyclase. *Trends Pharmacol Sci* **1999,** *20* (2), 66-73, doi: 10.1016/s0165-6147(99)01307-3.

44. Wayman, G. A., Impey, S., Wu, Z., Kindsvogel, W., Prichard, L. & Storm, D. R., Synergistic activation of the type I adenylyl cyclase by Ca2+ and Gs-coupled receptors in vivo. *J Biol Chem* **1994,** *269* (41), 25400-25405.

45. Sunahara, R. K., Dessauer, C. W. & Gilman, A. G., Complexity and diversity of mammalian adenylyl cyclases. *Annu Rev Pharmacol Toxicol* **1996,** *36*, 461-480, doi: 10.1146/annurev.pa.36.040196.002333.

46. Schwindinger, W. F. & Robishaw, J. D., Heterotrimeric G-protein $\beta\gamma$-dimers in growth and differentiation. *Oncogene* **2001,** *20* (13), 1653-1660, doi: 10.1038/sj.onc.1204181.

47. Olianas, M. C. & Onali, P., Involvement of $\beta\gamma$ subunits of Gq/11 in muscarinic M1 receptor potentiation of corticotropin-releasing hormone-stimulated adenylyl cyclase activity in rat frontal cortex. *J Neurochem* **2000,** *75* (1), 233-239, doi: 10.1046/j.1471-4159.2000.0750233.x.

48. Lorenzen, E., Ceraudo, E., Berchiche, Y. A., Rico, C. A., Fürstenberg, A., Sakmar, T. P. & Huber, T., G protein subtype-specific signaling bias in a series of CCR5 chemokine analogs. *Science signaling* **2018,** *11* (552), doi: 10.1126/scisignal.aao6152.

49. Wright, S. C. & Bouvier, M., Illuminating the complexity of GPCR pathway selectivity – advances in biosensor development. *Curr Opin Struct Biol* **2021,** *69*, 142-149, doi: 10.1016/j.sbi.2021.04.006.

50. Bondar, A. & Lazar, J., Optical sensors of heterotrimeric G protein signaling. *The FEBS journal* **2021,** *288* (8), 2570-2584, doi: 10.1111/febs.15655.

51. White, C. W., Vanyai, H. K., See, H. B., Johnstone, E. K. M. & Pfleger, K. D. G., Using nanoBRET and CRISPR/Cas9 to monitor proximity to a genome-edited protein in real-time. *Sci Rep* **2017,** *7* (1), 3187, doi: 10.1038/s41598-017-03486-2.

52. White, C. W., Johnstone, E. K. M., See, H. B. & Pfleger, K. D. G., NanoBRET ligand binding at a GPCR under endogenous promotion facilitated by CRISPR/Cas9 genome editing. *Cell Signal* **2019,** *54*, 27-34, doi: 10.1016/j.cellsig.2018.11.018.

53. Carpenter, B. & Tate, C. G., Engineering a minimal G protein to facilitate crystallisation of G protein-coupled receptors in their active conformation. *Protein Eng Des Sel* **2016,** *29* (12), 583-594, doi: 10.1093/protein/gzw049.

54. Nehmé, R., Carpenter, B., Singhal, A., Strege, A., Edwards, P. C., White, C. F., Du, H., Grisshammer, R. & Tate, C. G., Mini-G proteins: Novel tools for studying GPCRs in their active conformation. *PLoS One* **2017,** *12* (4), e0175642, doi: 10.1371/journal.pone.0175642.

55. Wan, Q., Okashah, N., Inoue, A., Nehmé, R., Carpenter, B., Tate, C. G. & Lambert, N. A., Mini G protein probes for active G protein-coupled receptors (GPCRs) in live cells. *J Biol Chem* **2018,** *293* (19), 7466-7473, doi: 10.1074/jbc.RA118.001975.

56. Höring, C., Seibel, U., Tropmann, K., Grätz, L., Mönnich, D., Pitzl, S., Bernhardt, G., Pockes, S. & Strasser, A., A dynamic, split-luciferase-based mini-G protein sensor to functionally characterize ligands at all four histamine receptor subtypes. *Int J Mol Sci* **2020,** *21* (22), 8440.

57. Wouters, E., Walraed, J., Robertson, M. J., Meyrath, M., Szpakowska, M., Chevigne, A., Skiniotis, G. & Stove, C., Assessment of biased agonism among distinct synthetic cannabinoid receptor agonist scaffolds. *ACS Pharmacol Transl Sci* **2020,** *3* (2), 285-295, doi: 10.1021/acsptsci.9b00069.

58. Wouters, E., Marin, A. R., Dalton, J. A. R., Giraldo, J. & Stove, C., Distinct dopamine D2 receptor antagonists differentially impact D2 receptor oligomerization. *Int J Mol Sci* **2019,** *20* (7), doi: 10.3390/ijms20071686.

59. Pottie, E., Tosh, D. K., Gao, Z. G., Jacobson, K. A. & Stove, C. P., Assessment of biased agonism at the A3 adenosine receptor using β-arrestin and miniGαi recruitment assays. *Biochem Pharmacol* **2020,** *177*, 113934, doi: 10.1016/j.bcp.2020.113934.

60. Pottie, E., Dedecker, P. & Stove, C. P., Identification of psychedelic new psychoactive substances (NPS) showing biased agonism at the 5-HT2AR through simultaneous use of β-arrestin 2 and miniG αq bioassays. *Biochem Pharmacol* **2020**, 114251, doi: 10.1016/j.bcp.2020.114251.

61. Tropmann, K., Höring, C., Plank, N. & Pockes, S., Discovery of a G protein-biased radioligand for the histamine H2 receptor with reversible binding properties. *J Med Chem* **2020,** *63* (21), 13090-13102, doi: 10.1021/acs.jmedchem.0c01494.

62. Gruber, C. G., Pegoli, A., Muller, C., Gratz, L., She, X. & Keller, M., Differently fluorescence-labelled dibenzodiazepinone-type muscarinic acetylcholine receptor ligands with high M2R affinity. *RSC Med Chem* **2020,** *11* (7), 823-832, doi: 10.1039/d0md00137f.

63. Kenakin, T., Differences between natural and recombinant G protein-coupled receptor systems with varying receptor/G protein stoichiometry. *Trends Pharmacol Sci* **1997,** *18* (12), 456-464, doi: 10.1016/S0165-6147(97)01136-X.

64. Onfroy, L., Galandrin, S., Pontier, S. M., Seguelas, M. H., N'Guyen, D., Senard, J. M. & Gales, C., G protein stoichiometry dictates biased agonism through distinct receptor-G protein partitioning. *Sci Rep* **2017,** *7* (1), 7885, doi: 10.1038/s41598-017-07392-5.

65. Gibson, D. G., Young, L., Chuang, R. Y., Venter, J. C., Hutchison, C. A., 3rd & Smith, H. O., Enzymatic assembly of DNA molecules up to several hundred kilobases. *Nat Methods* **2009,** *6* (5), 343-345, doi: 10.1038/nmeth.1318.

66. Barnes, N. M., Hales, T. G., Lummis, S. C. & Peters, J. A., The 5-HT3 receptor- the relationship between structure and function. *Neuropharmacology* **2009,** *56* (1), 273-284, doi: 10.1016/j.neuropharm.2008.08.003.

67. Guan, X. M., Kobilka, T. S. & Kobilka, B. K., Enhancement of membrane insertion and function in a type IIIb membrane protein following introduction of a cleavable signal peptide. *J Biol Chem* **1992,** *267* (31), 21995-21998, doi: 10.1016/S0021-9258(18)41623-7.

68. Grunewald, S., Haase, W., Reilander, H. & Michel, H., Glycosylation, palmitoylation, and localization of the human D2S receptor in baculovirus-infected insect cells. *Biochemistry* **1996,** *35* (48), 15149-15161, doi: 10.1021/bi9607564.

69. Kempf, J., Snook, L. A., Vonesch, J.-L., Dahms, T. E. S., Pattus, F. & Massotte, D., Expression of the human μ opioid receptor in a stable Sf9 cell line. *J Biotechnol* **2002,** *95* (2), 181-187, doi: 10.1016/S0168-1656(02)00008-1.

70. Shepard, B. D., Natarajan, N., Protzko, R. J., Acres, O. W. & Pluznick, J. L., A cleavable N-terminal signal peptide promotes widespread olfactory receptor surface expression in HEK293T Cells. *PLOS ONE* **2013,** *8* (7), e68758, doi: 10.1371/journal.pone.0068758.

71. Rutz, C., Klein, W. & Schülein, R., Chapter twelve - N-terminal signal peptides of G protein-coupled receptors: Significance for receptor biosynthesis, trafficking, and signal transduction. In *Prog Mol Biol Transl Sci*, Wu, G., Ed. Academic Press: 2015; Vol. 132, pp 267-287.

72. Shaner, N. C., Campbell, R. E., Steinbach, P. A., Giepmans, B. N., Palmer, A. E. & Tsien, R. Y., Improved monomeric red, orange and yellow fluorescent proteins derived from Discosoma sp. red fluorescent protein. *Nat Biotechnol* **2004,** *22* (12), 1567-1572, doi: 10.1038/nbt1037.

73. Weihs, F., Wang, J., Pfleger, K. D. G. & Dacres, H., Experimental determination of the bioluminescence resonance energy transfer (BRET) Förster distances of NanoBRET and red-shifted BRET pairs. *Anal Chim Acta* **2020,** *6*, 100059, doi: 10.1016/j.acax.2020.100059.

74. Inoue, A., Raimondi, F., Kadji, F. M. N., Singh, G., Kishi, T., Uwamizu, A., Ono, Y., Shinjo, Y., Ishida, S., Arang, N., et al., Illuminating G-protein-coupling selectivity of GPCRs. *Cell* **2019,** *177* (7), 1933-1947 e1925, doi: 10.1016/j.cell.2019.04.044.

75. Kohen, R., Metcalf, M. A., Khan, N., Druck, T., Huebner, K., Lachowicz, J. E., Meltzer, H. Y., Sibley, D. R., Roth, B. L. & Hamblin, M. W., Cloning, characterization, and chromosomal localization of a human 5-HT6 serotonin receptor. *J Neurochem* **1996,** *66* (1), 47-56, doi: 10.1046/j.1471-4159.1996.66010047.x.

76. Monsma, F. J., Jr., Shen, Y., Ward, R. P., Hamblin, M. W. & Sibley, D. R., Cloning and expression of a novel serotonin receptor with high affinity for tricyclic psychotropic drugs. *Mol Pharmacol* **1993,** *43* (3), 320-327.

77. Frielle, T., Collins, S., Daniel, K. W., Caron, M. G., Lefkowitz, R. J. & Kobilka, B. K., Cloning of the cDNA for the human β1-adrenergic receptor. *Proc Natl Acad Sci U S A* **1987,** *84* (22), 7920-7924, doi: 10.1073/pnas.84.22.7920.

78. Dixon, R. A., Kobilka, B. K., Strader, D. J., Benovic, J. L., Dohlman, H. G., Frielle, T., Bolanowski, M. A., Bennett, C. D., Rands, E., Diehl, R. E., et al., Cloning of the gene and cDNA for mammalian β-adrenergic receptor and homology with rhodopsin. *Nature* **1986,** *321* (6065), 75-79, doi: 10.1038/321075a0.

79. Caron, M. G., Kobilka, B. K., Frielle, T., Bolanowski, M. A., Benovic, J. L. & Lefkowitz, R. J., Cloning of the cDNA and genes for the hamster and human β2-adrenergic receptors. *Journal of receptor research* **1988,** *8* (1-4), 7-21, doi: 10.3109/10799898809048975.

80. Dearry, A., Gingrich, J. A., Falardeau, P., Fremeau, R. T., Bates, M. D. & Caron, M. G., Molecular cloning and expression of the gene for a human D1 dopamine receptor. *Nature* **1990,** *347* (6288), 72-76, doi: 10.1038/347072a0.

81. Zhou, Q.-Y., Grandy, D. K., Thambi, L., Kushner, J. A., Tol, H. H. M. V., Cone, R., Pribnow, D., Salon, J., Bunzow, J. R. & Civelli, O., Cloning and expression of human and rat Dt dopamine receptors. *Nature* **1990,** *347* (6288), 76-80, doi: 10.1038/347076a0.

82. Sunahara, R. K., Guan, H.-C., O'Dowd, B. F., Seeman, P., Laurier, L. G., Ng, G., George, S. R., Torchia, J., Van Tol, H. H. M. & Niznik, H. B., Cloning of the gene for a human dopamine D5 receptor with higher affinity for dopamine than D1. *Nature* **1991,** *350* (6319), 614-619, doi: 10.1038/350614a0.

83. Grandy, D. K., Zhang, Y. A., Bouvier, C., Zhou, Q. Y., Johnson, R. A., Allen, L., Buck, K., Bunzow, J. R., Salon, J. & Civelli, O., Multiple human D5 dopamine receptor genes: A functional receptor and two pseudogenes. *Proc Natl Acad Sci U S A* **1991,** *88* (20), 9175-9179, doi: 10.1073/pnas.88.20.9175.

84. Gantz, I., Munzert, G., Tashiro, T., Schäffer, M., Wang, L., DelValle, J. & Yamada, T., Molecular cloning of the human histamine H2 receptor. *Biochem Biophys Res Commun* **1991,** *178* (3), 1386-1392, doi: 10.1016/0006-291x(91)91047-g.

85. Gantz, I., Schaffer, M., DelValle, J., Logsdon, C., Campbell, V., Uhler, M. & Yamada, T., Molecular cloning of a gene encoding the histamine H2 receptor. *Proc Natl Acad Sci U S A* **1991,** *88* (13), 5937.

86. Le, F., Townsend-Nicholson, A., Baker, E., Sutherland, G. R. & Schofield, P. R., Characterization and chromosomal localization of the human A2a adenosine receptor gene: ADORA2A. *Biochem Biophys Res Commun* **1996,** *223* (2), 461-467, doi: 10.1006/bbrc.1996.0916.

87. Furlong, T. J., Pierce, K. D., Selbie, L. A. & Shine, J., Molecular characterization of a human brain adenosine A2 receptor. *Brain research. Molecular brain research* **1992,** *15* (1-2), 62-66, doi: 10.1016/0169-328x(92)90152-2.

88. Pierce, K. D., Furlong, T. J., Selbie, L. A. & Shine, J., Molecular cloning and expression of an adenosine A2B receptor from human brain. *Biochem Biophys Res Commun* **1992,** *187* (1), 86-93, doi: 10.1016/s0006-291x(05)81462-7.

89. Kobilka, B. K., Matsui, H., Kobilka, T. S., Yang-Feng, T. L., Francke, U., Caron, M. G., Lefkowitz, R. J. & Regan, J. W., Cloning, sequencing, and expression of the gene coding for the human platelet α 2-adrenergic receptor. *Science* **1987,** *238* (4827), 650-656, doi: 10.1126/science.2823383.

90. Bunzow, J. R., Tol, H. H. M. V., Grandy, D. K., Albert, P., Salon, J., Christie, M., Machida, C. A., Neve, K. A. & Civelli, O., Cloning and expression of a rat D2 dopamine receptor cDNA. *Nature* **1988,** *336* (6201), 783-787, doi: 10.1038/336783a0.

91. Dal Toso, R., Sommer, B., Ewert, M., Herb, A., Pritchett, D. B., Bach, A., Shivers, B. D. & Seeburg, P. H., The dopamine D2 receptor: Two molecular forms generated by alternative splicing. *EMBO J* **1989,** *8* (13), 4025-4034, doi: 10.1002/j.1460-2075.1989.tb08585.x.

92. Lovenberg, T. W., Roland, B. L., Wilson, S. J., Jiang, X., Pyati, J., Huvar, A., Jackson, M. R. & Erlander, M. G., Cloning and functional expression of the human histamine H3 receptor. *Mol Pharmacol* **1999,** *55* (6), 1101-1107.

93. Nakamura, T., Itadani, H., Hidaka, Y., Ohta, M. & Tanaka, K., Molecular cloning and characterization of a new human histamine Receptor, HH4R. *Biochem Biophys Res Commun* **2000,** *279* (2), 615-620, doi: 10.1006/bbrc.2000.4008.

94. Oda, T., Morikawa, N., Saito, Y., Masuho, Y. & Matsumoto, S., Molecular cloning and characterization of a novel type of histamine receptor preferentially expressed in leukocytes. *J Biol Chem* **2000,** *275* (47), 36781-36786, doi: 10.1074/jbc.M006480200.

95. Liu, C., Ma, X., Jiang, X., Wilson, S. J., Hofstra, C. L., Blevitt, J., Pyati, J., Li, X., Chai, W., Carruthers, N., et al., Cloning and pharmacological characterization of a fourth histamine receptor (H4) expressed in bone marrow. *Mol Pharmacol* **2001,** *59* (3), 420-426, doi: 10.1124/mol.59.3.420.

96. Morse, K. L., Behan, J., Laz, T. M., West, R. E., Greenfeder, S. A., Anthes, J. C., Umland, S., Wan, Y., Hipkin, R. W., Gonsiorek, W., et al., Cloning and characterization of a novel human histamine receptor. *J Pharmacol Exp Ther* **2001,** *296* (3), 1058-1066.

97. Nguyen, T., Shapiro, D. A., George, S. R., Setola, V., Lee, D. K., Cheng, R., Rauser, L., Lee, S. P., Lynch, K. R., Roth, B. L., et al., Discovery of a novel member of the histamine receptor family. *Mol Pharmacol* **2001,** *59* (3), 427-433, doi: 10.1124/mol.59.3.427.

98. Zhu, Y., Michalovich, D., Wu, H., Tan, K. B., Dytko, G. M., Mannan, I. J., Boyce, R., Alston, J., Tierney, L. A., Li, X., et al., Cloning, expression, and pharmacological characterization of a novel human histamine receptor. *Mol Pharmacol* **2001,** *59* (3), 434-441, doi: 10.1124/mol.59.3.434.

99. O'Reilly, M., Alpert, R., Jenkinson, S., Gladue, R. P., Foo, S., Trim, S., Peter, B., Trevethick, M. & Fidock, M., Identification of a histamine H4 receptor on human eosinophils- role in eosinophil chemotaxis. *J Recept Signal Transduct Res* **2002,** *22* (1-4), 431-448, doi: 10.1081/rrs-120014612.

100. Kubo, T., Maeda, A., Sugimoto, K., Akiba, I., Mikami, A., Takahashi, H., Haga, T., Haga, K., Ichiyama, A., Kangawa, K., et al., Primary structure of porcine cardiac muscarinic acetylcholine receptor deduced from the cDNA sequence. *FEBS Lett* **1986,** *209* (2), 367-372, doi: 10.1016/0014-5793(86)81144-9.

101. Bonner, T. I., Buckley, N. J., Young, A. C. & Brann, M. R., Identification of a family of muscarinic acetylcholine receptor genes. *Science* **1987,** *237* (4814), 527-532.

102. Larhammar, D., Blomqvist, A. G., Yee, F., Jazin, E., Yoo, H. & Wahlested, C., Cloning and functional expression of a human neuropeptide Y/peptide YY receptor of the Y1 type. *J Biol Chem* **1992,** *267* (16), 10935-10938.

103. Herzog, H., Hort, Y. J., Ball, H. J., Hayes, G., Shine, J. & Selbie, L. A., Cloned human neuropeptide Y receptor couples to two different second messenger systems. *Proc Natl Acad Sci U S A* **1992,** *89* (13), 5794-5798, doi: 10.1073/pnas.89.13.5794.

104. Gehlert, D. R., Beavers, L. S., Johnson, D., Gackenheimer, S. L., Schober, D. A. & Gadski, R. A., Expression cloning of a human brain neuropeptide Y Y2 receptor. *Mol Pharmacol* **1996,** *49* (2), 224-228.

105. Gerald, C., Walker, M. W., Vaysse, P. J., He, C., Branchek, T. A. & Weinshank, R. L., Expression cloning and pharmacological characterization of a human hippocampal neuropeptide Y/peptide YY Y2 receptor subtype. *J Biol Chem* **1995,** *270* (45), 26758-26761, doi: 10.1074/jbc.270.45.26758.

106. Bard, J. A., Walker, M. W., Branchek, T. A. & Weinshank, R. L., Cloning and functional expression of a human Y4 subtype receptor for pancreatic polypeptide, neuropeptide Y, and peptide YY. *J Biol Chem* **1995,** *270* (45), 26762-26765, doi: 10.1074/jbc.270.45.26762.

107. Lundell, I., Blomqvist, A. G., Berglund, M. M., Schober, D. A., Johnson, D., Statnick, M. A., Gadski, R. A., Gehlert, D. R. & Larhammar, D., Cloning of a human receptor of the NPY receptor family with high affinity for pancreatic polypeptide and peptide YY. *J Biol Chem* **1995,** *270* (49), 29123-29128, doi: 10.1074/jbc.270.49.29123.

108. Federsppiel, B., Melhado, I. G., Duncan, A. M., Delaney, A., Schappert, K., Clark-Lewis, I. & Jirik, F. R., Molecular cloning of the cDNA and chromosomal localization of the gene for a putative seven-transmembrane segment (7-TMS) receptor isolated from human spleen. *Genomics* **1993,** *16* (3), 707-712, doi: 10.1006/geno.1993.1251.

109. Rimland, J., Xin, W., Sweetnam, P., Saijoh, K., Nestler, E. J. & Duman, R. S., Sequence and expression of a neuropeptide Y receptor cDNA. *Mol Pharmacol* **1991,** *40* (6), 869-875.

110. Yamashita, M., Fukui, H., Sugama, K., Horio, Y., Ito, S., Mizuguchi, H. & Wada, H., Expression cloning of a cDNA encoding the bovine histamine H1 receptor. *Proc Natl Acad Sci U S A* **1991,** *88* (24), 11515-11519, doi: 10.1073/pnas.88.24.11515.

111. Fukui, H., Fujimoto, K., Mizuguchi, H., Sakamoto, K., Horio, Y., Takai, S., Yamada, K. & Ito, S., Molecular cloning of the human histamine H1 receptor gene. *Biochem Biophys Res Commun* **1994,** *201* (2), 894-901, doi: 10.1006/bbrc.1994.1786.

112. Allard, W. J., Sigal, I. S. & Dixon, R. A., Sequence of the gene encoding the human M1 muscarinic acetylcholine receptor. *Nucleic Acids Res* **1987,** *15* (24), 10604, doi: 10.1093/nar/15.24.10604.

113. Bonner, T. I., Young, A. C., Brann, M. R. & Buckley, N. J., Cloning and expression of the human and rat M5 muscarinic acetylcholine receptor genes. *Neuron* **1988,** *1* (5), 403-410, doi: 10.1016/0896-6273(88)90190-0.

114. Vita, N., Laurent, P., Lefort, S., Chalon, P., Dumont, X., Kaghad, M., Gully, D., Le Fur, G., Ferrara, P. & Caput, D., Cloning and expression of a complementary DNA encoding a high affinity human neurotensin receptor. *FEBS Lett* **1993,** *317* (1-2), 139-142, doi: 10.1016/0014-5793(93)81509-x.

115. Tanaka, K., Masu, M. & Nakanishi, S., Structure and functional expression of the cloned rat neurotensin receptor. *Neuron* **1990,** *4* (6), 847-854, doi: 10.1016/0896-6273(90)90137-5.

116. Rashid, A. J., O'Dowd, B. F., Verma, V. & George, S. R., Neuronal Gq/11-coupled dopamine receptors: An uncharted role for dopamine. *Trends Pharmacol Sci* **2007,** *28* (11), 551-555, doi: 10.1016/j.tips.2007.10.001.

117. Hasbi, A., O'Dowd, B. F. & George, S. R., Dopamine D1-D2 receptor heteromer signaling pathway in the brain: emerging physiological relevance. *Mol Brain* **2011,** *4* (1), 26, doi: 10.1186/1756-6606-4-26.

118. Lee, S. P., So, C. H., Rashid, A. J., Varghese, G., Cheng, R., Lança, A. J., O'Dowd, B. F. & George, S. R., Dopamine D1 and D2 receptor co-activation generates a novel phospholipase C-mediated calcium signal. *J Biol Chem* **2004,** *279* (34), 35671-35678, doi: 10.1074/jbc.M401923200.

119. Okashah, N., Wan, Q., Ghosh, S., Sandhu, M., Inoue, A., Vaidehi, N. & Lambert, N. A., Variable G protein determinants of GPCR coupling selectivity. *Proc Natl Acad Sci U S A* **2019,** *116* (24), 12054-12059, doi: 10.1073/pnas.1905993116.

120. Sidhu, A. & Niznik, H. B., Coupling of dopamine receptor subtypes to multiple and diverse G proteins. *International journal of developmental neuroscience : the official journal of the International Society for Developmental Neuroscience* **2000,** *18* (7), 669-677, doi: 10.1016/s0736-5748(00)00033-2.

121. Della Latta, V., Cabiati, M., Rocchiccioli, S., Del Ry, S. & Morales, M. A., The role of the adenosinergic system in lung fibrosis. *Pharmacol Res* **2013,** *76*, 182-189, doi: 10.1016/j.phrs.2013.08.004.

122. Feoktistov, I. & Biaggioni, I., Adenosine A2b receptors evoke interleukin-8 secretion in human mast cells. An enprofylline-sensitive mechanism with implications for asthma. *The Journal of clinical investigation* **1995,** *96* (4), 1979-1986, doi: 10.1172/jci118245.

123. Linden, J., Thai, T., Figler, H., Jin, X. & Robeva, A. S., Characterization of human A2B adenosine receptors: Radioligand binding, western blotting, and coupling to Gq in human embryonic kidney 293 cells and HMC-1 mast cells. *Mol Pharmacol* **1999,** *56* (4), 705-713.

124. Brown, R. A., Spina, D. & Page, C. P., Adenosine receptors and asthma. *Br J Pharmacol* **2008,** *153 Suppl 1* (Suppl 1), S446-456, doi: 10.1038/bjp.2008.22.

125. Wang, Y. X. & Kotlikoff, M. I., Signalling pathway for histamine activation of non-selective cation channels in equine tracheal myocytes. *J Physiol* **2000,** *523 Pt 1* (Pt 1), 131-138, doi: 10.1111/j.1469-7793.2000.t01-3-00131.x.

126. Seifert, R., Grunbaum, L. & Schultz, G., Histamine H1-receptors in HL-60 monocytes are coupled to Gi-proteins and pertussis toxin-insensitive G-proteins and mediate activation of Ca2+ influx without concomitant Ca2+ mobilization from intracellular stores. *Naunyn Schmiedebergs Arch Pharmacol* **1994,** *349* (4), 355-361, doi: 10.1007/BF00170880.

127. Leurs, R., Traiffort, E., Arrang, J. M., Tardivel-Lacombe, J., Ruat, M. & Schwartz, J. C., Guinea pig histamine H1 receptor. II. Stable expression in Chinese hamster ovary cells reveals the interaction with three major signal transduction pathways. *J Neurochem* **1994,** *62* (2), 519-527, doi: 10.1046/j.1471-4159.1994.62020519.x.

128. Murayama, T., Kajiyama, Y. & Nomura, Y., Histamine-stimulated and GTP-binding proteins-mediated phospholipase A2 activation in rabbit platelets. *J Biol Chem* **1990,** *265* (8), 4290-4295.

129. Bender, A. M., Garrison, A. T. & Lindsley, C. W., The muscarinic acetylcholine receptor M5: Therapeutic implications and allosteric modulation. *ACS chemical neuroscience* **2019,** *10* (3), 1025-1034, doi: 10.1021/acschemneuro.8b00481.

130. Eglen, R. M. & Nahorski, S. R., The muscarinic M5 receptor: A silent or emerging subtype? *Br J Pharmacol* **2000,** *130* (1), 13-21, doi: 10.1038/sj.bjp.0703276.

131. Olsen, R. H. J., DiBerto, J. F., English, J. G., Glaudin, A. M., Krumm, B. E., Slocum, S. T., Che, T., Gavin, A. C., McCorvy, J. D., Roth, B. L., et al., TRUPATH, an open-source biosensor platform for interrogating the GPCR transducerome. *Nat Chem Biol* **2020,** *16* (8), 841-849, doi: 10.1038/s41589-020-0535-8.

132. Avet, C., Mancini, A., Breton, B., Le Gouill, C., Hauser, A. S., Normand, C., Kobayashi, H., Gross, F., Hogue, M., Lukasheva, V., et al., Selectivity landscape of 100 therapeutically relevant GPCR profiled by an effector translocation-based BRET platform. *bioRxiv* **2020**, 2020.2004.2020.052027, doi: 10.1101/2020.04.20.052027.

133. Kenakin, T. P., Receptor reserve as a tissue misnomer. *Trends Pharmacol Sci* **1986,** *7*, 93-95, doi: 10.1016/0165-6147(86)90271-3.

134. Ross, E. M., Signal sorting and amplification through G protein-coupled receptors. *Neuron* **1989,** *3* (2), 141-152, doi: 10.1016/0896-6273(89)90027-5.

135. Ross, E. M., G Protein-coupled receptors: Multi-turnover GDP/GTP exchange catalysis on heterotrimeric G proteins. *Cell Logist* **2014,** *4*, e29391-e29391, doi: 10.4161/cl.29391.

136. Figueroa, K. W., Griffin, M. T. & Ehlert, F. J., Selectivity of agonists for the active state of M1 to M4 muscarinic receptor subtypes. *J Pharmacol Exp Ther* **2009,** *328* (1), 331-342, doi: 10.1124/jpet.108.145219.

137. Vasudevan, L., Vandeputte, M., Deventer, M., Wouters, E., Cannaert, A. & Stove, C. P., Assessment of structure-activity relationships and biased agonism at the μ opioid receptor of novel synthetic opioids using a novel, stable bio-assay platform. *Biochem Pharmacol* **2020,** *177*, 113910, doi: 10.1016/j.bcp.2020.113910.

138. Black, J. W., Leff, P., Shankley, N. P. & Wood, J., An operational model of pharmacological agonism: the effect of E/[A] curve shape on agonist dissociation constant estimation. *Br J Pharmacol* **1985,** *84* (2), 561-571, doi: 10.1111/j.1476-5381.1985.tb12941.x.

139. Pándy-Szekeres, G., Esguerra, M., Hauser, A. S., Caroli, J., Munk, C., Pilger, S., Keserű, György M., Kooistra, Albert J. & Gloriam, David E., The G protein database, GproteinDb. *Nucleic Acids Res* **2022,** *50* (D1), D518-D525, doi: 10.1093/nar/gkab852.

140. Hauser, A. S., Avet, C., Normand, C., Mancini, A., Inoue, A., Bouvier, M. & Gloriam, D. E., GPCR-G protein selectivity – a unified meta-analysis. *bioRxiv* **2021**, 2021.2009.2007.459250, doi: 10.1101/2021.09.07.459250.

141. Niedernberg, A., Tunaru, S., Blaukat, A., Harris, B. & Kostenis, E., Comparative analysis of functional assays for characterization of agonist ligands at G protein-coupled receptors. *J Biomol Screen* **2003,** *8* (5), 500-510, doi: 10.1177/1087057103257555.

142. Kostenis, E., Potentiation of GPCR-signaling via membrane targeting of G protein α subunits. *J Recept Signal Transduct Res* **2002,** *22* (1-4), 267-281, doi: 10.1081/rrs-120014601.

143. Ashkenazi, A., Winslow, J. W., Peralta, E. G., Peterson, G. L., Schimerlik, M. I., Capon, D. J. & Ramachandran, J., An M2 muscarinic receptor subtype coupled to both adenylyl cyclase and phosphoinositide turnover. *Science* **1987,** *238* (4827), 672-675, doi: 10.1126/science.2823384.

144. Zhu, X. & Birnbaumer, L., G protein subunits and the stimulation of phospholipase C by Gs-and Gi-coupled receptors: Lack of receptor selectivity of Gα16 and evidence for a synergic interaction between Gbeta gamma and the alpha subunit of a receptor activated G protein. *Proc Natl Acad Sci U S A* **1996,** *93* (7), 2827-2831, doi: 10.1073/pnas.93.7.2827.

145. Winpenny, D., Clark, M. & Cawkill, D., Biased ligand quantification in drug discovery: from theory to high throughput screening to identify new biased μ opioid receptor agonists. *Br J Pharmacol* **2016,** *173* (8), 1393-1403, doi: 10.1111/bph.13441.

146. Yang, Y., Functional selectivity of dopamine D1 receptor signaling: Retrospect and prospect. *Int J Mol Sci* **2021,** *22* (21), 11914.

6. Specific Engineered G Protein Coupling to Histamine Receptors Revealed from Cellular Assay Experiments and Accelerated Molecular Dynamics Simulations

Note: Prior to the submission of this thesis, the content of this chapter, except for minor changes, has been published in collaboration with partners:

Höring, C.; Conrad, M.; Söldner, C.A.; Wang, J.; Sticht, H.; Strasser, A.; Miao, Y. Specific engineered G protein coupling to histamine receptors revealed from cellular assay experiments and accelerated molecular dynamics simulations. *Int J Mol Sci* **2021**, *22*, 10047, doi: 10.3390/ijms221810047.

6.1. Introduction

In the human body, the neurotransmitter histamine interacts with four subtypes of histamine receptors ($H_{1-4}R$) that are all classified as rhodopsin-like class A G protein-coupled receptors (GPCRs).[1] As the largest membrane protein superfamily,[2-3] GPCRs have been intensively studied as important drug targets over the past decades, leading to more than 30% of approved drugs binding to GPCRs.[4] In the 1970s, H_2R antagonists, such as cimetidine and ranitidine, were among the blockbuster drugs on the market, reducing gastric acid secretion.[5] In addition to the expression in gastric parietal cells, the H_2R is also widely found in smooth muscle cells, chondrocytes, endothelial and epithelial cells, dendritic cells, and macrophages as well as T and B cells.[1] Currently, the H_2R function in the central nervous system (CNS) is investigated with CNS-penetrating agonists.[6-7] In contrast, no substance has yet been approved for medical treatment related to the Gi-coupled H_4R. However, the involvement of the H_4R in allergic and inflammatory processes is undisputed due to its expression in immune cells, mast cells, and eosinophils,[8-13] which has raised the H_4R as a potential target for the treatment of atopic dermatitis.[14-15] And, currently, the first antagonist, ZPL-3893787, is being considered for use in patients.[16]

One of the key events in GPCR signaling is the activation of heterotrimeric G proteins consisting of the α, β, and γ subunits.[17-19] Today, more than 800 GPCRs and 16 G proteins have been identified in the human genome.[20-21] There is evidence that GPCRs interact with multiple intracellular G proteins, giving unique coupling profiles with multidimensional cellular effects.[22-26] In the 1990s, the human H_2R was cloned and demonstrated to couple to Gs due to the increasing cAMP level upon receptor activation.[27] Kühn et al. reported an H_2R interaction with Gq by immunoprecipitation of H_2R-Gq assemblies and by inositol phosphate accumulation when the H_2R was co-expressed with Gq family members $G\alpha q$, $G\alpha 11$, $G\alpha 14$, and $G\alpha 15$.[28] Around the millennium, the human H_4R was cloned by several groups, and Gi/o coupling has been proven by the inhibition of forskolin-induced cAMP accumulation.[29-35] In addition, an increase in intracellular Ca^{2+} has been reported in eosinophils,[36] monocytes,[37] and mast cells upon H_4R activation,[11,38] which was initially discussed as a $\beta\gamma$ signal activating phospholipase C[11] (PLC) but later was identified as an H_1R-mediated response.[38] In terms of $G\alpha$ subtype selectivity, a preference of $G\alpha i_2$ over $G\alpha i_1$, $G\alpha i_3$, and $G\alpha o$ proteins was reported for the H_4R in a [^{35}S]GTPγS binding assay, in which the amount of the non-hydrolysable guanine nucleotide analog bound to the H_4R-$G\alpha$ complex was quantified.[39]

Nowadays, several assay techniques have facilitated the analysis of GPCR G protein interactions, such as BRET-based heterotrimeric G protein biosensors either detecting the dissociation of the heterotrimeric G protein into an α monomer and a $\beta\gamma$ dimer[40] or the dissociation of the $\beta\gamma$ dimer from the receptor[41] as well as the BRET-based effector membrane translocation assay (EMTA)

monitoring the activation of Gα proteins by the recruitment of specific G protein effector molecules.[42] Another prominent technique to study GPCR – G protein interactions is the application of chimeric G proteins, essentially consisting of the α5 helix of a G protein subtype and a specific G protein core.[43] The α5 helix was reported to account for more than 70% of the contact area between a GPCR and G protein, thus dictating successful interaction.[41,44-45] In contrast, the G protein core can be used to redirect signals into a specific readout. For instance, Inoue et al. applied 11 chimeric G proteins from all major G protein families to demonstrate the coupling behavior of 148 GPCRs by redirecting all signals into TGF-α shedding.[46] A similar approach has been used in the development of genetically engineered minimal G (mini-G) proteins consisting of the GTPase domain of Gαs and respective α5 helices of G proteins from each G protein family (Gs, Gi/o, Gq/11, and G12/13).[47-49] Combined with BRET or split-luciferase complementation techniques, mini-G proteins are suitable for ligand characterization in cell-based assays.[49-54] Moreover, since these proteins were originally designed to stabilize GPCRs in their active state to enable the elucidation of GPCR – G protein complexes by X-ray and cryo-electron microscopy (cryo-EM), structures have become available in complex with the adenosine A_{2A} ($A_{2A}R$),[55] dopamine D_1 (D_1R),[56] GPR52,[57] serotonin 5-HT_{1B} (5-$HT_{1B}R$),[58] and 5-HT_{2A} (5-$HT_{2A}R$)[59] receptors so far.

Recent years have seen remarkable advances in the structural determination of GPCR – G protein complexes.[60-61] In 2020 alone, new structures of 34 GPCR–Gs complexes, 19 GPCR-Gi/o complexes, and the first GPCR-Gq/11 complex were published (www.gpcrdb.org, access date: 08.10.2021), providing valuable atomic-level insights into the binding interface of GPCRs with G proteins from different major families.[60] Another milestone in histamine receptor research was the resolution of the first active structure of the histamine H_1 receptor in complex with Gq in 2021.[62] Nevertheless, static structures alone do not allow us to map the dynamics of a GPCR – G protein interaction, and only complexes of primary coupling GPCRs and G proteins are available so far. Thus, the dynamic mechanism of specific GPCR–G protein interactions remains poorly understood. To fill this gap, computational approaches were developed to model the dynamic GPCR – G protein interactions.[63-64] For instance, Flock et al. provided a bioinformatics approach to determine a selectivity barcode (patterns of amino acids) of GPCR − G protein coupling.[44] More commonly, molecular dynamics (MD) simulations have been used to explore the conformational changes and free energy landscapes of GPCR – G protein interactions, ideally combined with complementary experiments.[65-67] However, conventional MD (cMD) simulations often suffer from insufficient sampling of GPCR – G protein interactions due to limited simulation time-scales. Thus, enhanced sampling methods have been applied to improve the simulations of GPCR – G protein interactions.[64,68] Among these methods, Gaussian accelerated molecular dynamics (GaMD) is a robust method that allows for unconstrained enhanced sampling and free energy calculations of large biomolecules.[69-72] GaMD has been applied to successfully simulate protein folding,[70,73]

protein-ligand binding and unbinding,[69-70,74] GPCR activation,[74] and binding to a G protein mimetic nanobody.[75] In the latter study, the nanobody binding pathway to the muscarinic acetylcholine M_2 (M_2R) receptor has been investigated, demonstrating that the intracellular loops play a key role in nanobody recognition and binding.[75] Moreover, GaMD has been used to identify the coupling mechanisms of adenosine A_1 (A_1R) and A_{2A} ($A_{2A}R$) receptors to Gs and Gi proteins.[76] Protein flexibility and complementary residue interactions at the protein interface have revealed that the A_1R preferred Gi coupling and the $A_{2A}R$ coupled to Gs and Gi.[76]

In the present study, cellular assay experiments and GaMD-enhanced sampling simulations were combined to investigate the G protein coupling profiles of the H_2R and H_4R. Three types of engineered G proteins, mGs, mGsi, and mGsq, were used to characterize the coupling profiles of each receptor. For both receptors, the interaction with mini-G proteins upon receptor activation in response to the endogenous ligand histamine was explored using a recently published mini-G protein recruitment assay.[54] Furthermore, all-atom GaMD simulations were performed on the $H_{2,4}R$ in complex with mGs, mGsi, and mGsq in explicit lipids and solvent. In all six systems, the endogenous ligand histamine was bound to the $H_{2,4}R$. Thereby, GaMD simulations allowed for characterizing the structural flexibility and low-energy conformations of $H_{2,4}R$ in complex with mGs, mGsi, and mGsq. Overall, the combination of cellular experiments and GaMD simulations provided important mechanistic insights into the selective coupling of engineered G proteins to the $H_{2,4}Rs$

6.2. Materials and Methods

6.2.1. Generation of Transient Transfectants

The day prior to the transfection, HEK293T were seeded into a 6-well cell culture plate (Sarstedt, Nümbrecht, Germany) at a density of 0.3 × 106 cells/mL. The cells were transiently transfected with a total amount of 3 µg plasmid DNA using linear polyethyleneimine (PEI, 1 mg/mL in PBS, transfection ratio 1:5; 3 µg DNA + 15 µL PEI). Therefore, combinations of the following plasmids the construction of which has been described in Chapter 2 (section 2.2.2) were used: pcDNA3.1 H_2R–NlucC, pcDNA3.1 H_4R–NlucC, pIRESpuro3 NlucN–mGs, pIRESpuro3 NlucN–mGsi, and pIRESpuro3 NlucN–mGsq. The cells were incubated for 48 h to allow for an adequate protein expression.

6.2.2. Mini-G Protein Recruitment Assays

Mini-G protein recruitment assays were performed as described in Chapter 5 (section 5.2.6). Data were analyzed using GraphPad Prism9 software (San Diego, CA, USA). The relative luminescence units (RLU) were corrected for the baseline drift caused by autooxidation of the substrate by dividing all data by the mean luminescence intensity of the HEK293T wild-type control. Thereafter, the baseline luminescence of the respective L-15 control was subtracted. The area under the curve (AUC) of each concentration was normalized to the AUC of 100 µM histamine (100%) obtained in the canonical system (H_2R-mGs or H_4R-mGsi, respectively) and L-15 (0%). The logarithmic histamine concentrations were fitted against the normalized AUCs with variable slope (log(c) vs. response - variable slope (four parameters) yielding pEC_{50} and E_{max} values.

6.2.3. Preparation of the $H_{2,4}R$-Mini-G Protein Complexes

To obtain the H_2R complexes, the H_2R–Gs structure that has been published by Conrad et al. was used as template containing the coordinates of the H_2R (residues 15–304) and the ligand histamine.[77] To obtain the mini-G protein structures mGs, mGsi, and mGsq (according to mGs393, mGsi43, and mGsq71[48]), homology modeling was performed on the Gs structure using Modeller 9.16.[78] To avoid artificial charges at the termini of the H_2R, N-terminal acetyl and C-terminal N-methyl capping groups were added to the structure using Sybyl7.3 (Tripos International, St. Louis, MO, USA (2006)). The setup of the complexes for subsequent Gaussian accelerated MD simulations was performed as described previously.[79] During the setup, missing hydrogen atoms were added and *f99SB* force field[80] parameters were assigned to the complexes, and the H_2R disulfide bond C91–C174 was created using tleap. The energy minimization and equilibration steps were essentially performed as described before using Amber17[81] (San Franscicso, CA, USA) and Gromacs 2016.5.[79,82] In order to embed the H_2R into a membrane, the structure was overlaid with a pre-equilibrated dioleylphosphatidylcholine (DOPC) bilayer (*gaff* force field[83]) and solvated with SPC water.[84] Therefore, the pseudo-atom entries of the 3SN6 structure (β_2AR-Gs complex) from the

Orientations of Proteins in Membranes (OPM) database have been used containing the position of extracellular and intracellular membrane layer.

The H_4R systems were obtained using the homology model of the receptor provided by GPCRdb (www.gpcrdb.org, version: 03.09.2019, mainly based on M_2R structure; pdb-id: 4MQT) as template.[85] The utilized model comprised residues 6–380, but due to the lack of an appropriate ICL3 model, the native 82 amino acid-sized ICL3 of the H_4R was truncated (69 total missing amino acids) and only consisted of the first 8 (-CQSHPGLT-) and last 5 residues (-LHQRE-). Amber coordinates and topology files were generated for the downloaded pdb file using ambpdb, and the disulfide bond C87–C164 was created using tleap. Initially, the structure was solvated in a TIP3 waterbox with Cl^- as counter ions and minimized as performed for the H_2R structures. To set up H_4R–mini-G protein complexes, a loop refinement of the ICL3 was performed using the ModLoop[86-87] web server (www.modbase.compbio.ucsf.edu/modloop, access date: 08.10.2021) to avoid clashes between the receptor and mini-G protein structures. The refined H_4R structure and the mini-G protein homology models that have been generated in complex with the H_2R were aligned to the M_2R structure in complex with Gi (pdb-id.: 6OIK) to extract appropriate coordinates. Thereafter, similar protocols as for the H_2R complexes were performed to prepare the H_4R systems (H_4R-mGs, H_4R-mGsi and H_4R–mGsq) with the ligand histamine. A computational model of GaMD simulation systems and sequence alignments of the $H_{2,4}R$ as well as of the G protein chimeras and the "parental" G protein subunit Gαs are provided in the Appendix (Figures A21, A22 and A23, respectively).

6.2.4. Gaussian Accelerated Molecular Dynamics (GaMD) Simulations

In GaMD, a harmonic, Gaussian-distributed boost potential is applied to biomolecules to smooth the potential energy surface and reduce energy barriers.[69] When the system potential $V(\vec{r})$ is lower than a reference energy E, the modified potential $V^*(\vec{r})$ is calculated as:

$$V^*(\vec{r}) = V(\vec{r}) + \Delta V(\vec{r})$$
$$\Delta V(\vec{r}) = \begin{cases} \frac{1}{2}k\left(E - V(\vec{r})\right)^2, V(\vec{r}) < E \\ 0, V(\vec{r}) \geq E, \end{cases} \quad (1)$$

where k is the harmonic force constant. The two adjustable parameters E and k are automatically determined on three enhanced sampling principles as described before.[69] In summary, E needs to be in the range:

$$V_{max} \leq E \leq V_{min} + \frac{1}{k'} \quad (2)$$

where V_{min} and V_{max} are the minimum and maximum potential energies of the system. To ensure that equation (2) is valid, k is defined as $k = k_0 \cdot 1/(V_{max} - V_{min})$ and thus $0 < k_0 \leq 1$. To enable an accurate energetic reweighting using cumulant expansion to the second order, the third standard deviation of ΔV needs to be small enough: $\sigma_{\Delta V} = k\left(E - V_{avg}\right)\sigma_V \leq \sigma_0$, where V_{avg} and σ_V are the average and standard deviation of the system potential energies and $\sigma_{\Delta V}$ is the standard deviation of ΔV with σ_0 as a user-specified upper limit for accurate reweighting. When E is set to the lower bound $E = V_{max}$, according to Equation (2), k_0 can be calculated as:

$$k_0 = \min(1.0, k_0') = min\left(1.0, \frac{\sigma_0}{\sigma_V} \cdot \frac{V_{max} - V_{min}}{V_{max} - V_{avg}}\right), \quad (3)$$

Alternatively, when the threshold energy E is set to its upper bound $E = V_{min} + 1/k$, k_0 is set to:

$$k_0 = k_0'' \equiv \left(1 - \frac{\sigma_0}{\sigma_V}\right) \cdot \frac{V_{max} - V_{min}}{V_{avg} - V_{min}}, \quad (4)$$

if k_0'' is found between 0 and 1. Otherwise, k_0 is calculated using equation (3).

6.2.5. Energetic Reweighting of GaMD Simulations

To calculate the potential of the mean force (PMF) and energetically reweight GaMD simulations, the probability distribution along a reaction coordinate is written as $p^*(A)$. Given the boost potential $\Delta V(r)$ of each frame, $p^*(A)$ can be reweighted to recover the canonical ensemble distribution $p(A)$, as:

$$p(A_j) = p^*(A_j)\frac{\langle e^{\beta\Delta V(r)}\rangle_j}{\sum_{i=1}^{M}\langle p^*(A_i)e^{\beta\Delta V(r)}\rangle_i}, j = 1, \dots, M, \quad (5)$$

where M is the number of bins, $\beta = k_B T$, and $\langle e^{\beta\Delta V(r)}\rangle_j$ is the ensemble-averaged Boltzmann factor of $\Delta V(r)$ for simulation frames found in the j^{th} bin. The ensemble-averaged reweighting factor can be approximated using cumulant expansion:

$$\langle e^{\beta\Delta V(r)}\rangle = exp\left\{\sum_{k=1}^{\infty}\frac{\beta^k}{k!}C_k\right\}, \quad (6)$$

where the first two cumulants are given by:

$$\begin{aligned} C_1 &= \langle\Delta V\rangle, \\ C_2 &= \langle\Delta V^2\rangle - \langle\Delta V\rangle^2 = \sigma_v^2 \end{aligned} \quad (7)$$

The boost potential obtained from GaMD simulations usually follows near-Gaussian distribution.[71-72] Thus, the cumulant expansion to the second order provides a good approximation for computing the reweighting factor.[69,88] The reweighted free energy $F(A) = -k_B T \ln p(A)$ is calculated as:

$$F(A) = F^*(A) - \sum_{k=1}^{2}\frac{\beta^k}{k!}C_k + F_c, \quad (8)$$

where $F^*(A) = -k_B T \ln p^*(A)$ is the modified free energy obtained from GaMD simulation and F_c is a constant.

6.2.6. Simulation Protocol

GaMD has been implemented in the AMBER software package, so that all molecular dynamics (MD) simulations could be performed using *Amber18*[89] (San Franscicso, CA, USA). During the simulations, periodic boundary conditions were given. The *SHAKE* algorithm was applied to remove the bond stretching freedom of all hydrogen-containing bonds. The GaMD simulations were preceded by a short conventional MD (cMD) simulation of 10.4 ns for the statistical collection of boost parameters (V_{max}, V_{min}, V_{avg}, and σ_V), which was followed by 32 ns "dual-boosted" MD simulations using the calculated parameters (2 fs time steps), in which boost parameters were imposed on the total potential energy and the dihedral energy terms.

Table 6.1. Summary of the boost potentials applied in the Gaussian accelerated molecular dynamics (GaMD) simulations. In all GaMD simulations, the total potential energy (E_{pot}) and the dihedral energy ($E_{dihedral}$) were boosted ("dual-boost"). Average ± SD of the corresponding boost potentials (ΔV_{pot} and $\Delta V_{dihedral}$) are given for the different simulations of the H_2R and H_4R systems.

System	N_{atoms}	Simulation	Length (ns)	ΔV_{pot} (kcal/mol)	$\Delta V_{dihedral}$ (kcal/mol)
H_2R–mGs	128,856	GaMD1	1000	7.53 ± 3.15	6.40 ± 2.65
		GaMD2	1000	7.50 ± 3.15	6.50 ± 2.68
		GaMD3	1000	7.53 ± 3.16	6.36 ± 2.64
H_2R–mGsi	128,819	GaMD1	1000	7.87 ± 3.23	5.93 ± 2.55
		GaMD2	1000	7.86 ± 3.23	5.88 ± 2.54
		GaMD3	1000	7.85 ± 3.22	5.98 ± 2.56
H_2R–mGsq	128,864	GaMD1	1000	7.39 ± 3.13	6.32 ± 2.63
		GaMD2	1000	7.36 ± 3.13	6.34 ± 2.64
		GaMD3	1000	7.37 ± 3.13	6.52 ± 2.68
H_4R–mGs	129,747	GaMD1	1000	7.87 ± 3.23	6.25 ± 2.62
		GaMD2	1000	7.86 ± 3.23	6.08 ± 2.58
		GaMD3	1000	7.84 ± 3.23	6.45 ± 2.66
H_4R–mGsi	129,737	GaMD1	1000	8.05 ± 3.26	6.03 ± 2.57
		GaMD2	1000	8.02 ± 3.25	6.42 ± 2.65
		GaMD3	1000	8.04 ± 3.26	6.19 ± 2.60
H_4R–mGsq	129,788	GaMD1	1000	8.09 ± 3.27	6.55 ± 2.68
		GaMD2	1000	8.21 ± 3.29	6.57 ± 2.68
		GaMD3	1000	8.22 ± 3.30	6.43 ± 2.65

The reference energy was set to the lower bound ($E = V_{max}$), and the boost parameters were updated every 400,000 steps (800 ps). The upper limit of the standard deviation of the boost potential, of the total potential energy, and of the dihedral energy was restrained to $\sigma_{OP} = \sigma_{OD} = 6.0$ kcal/mol. After the preparatory stage, 3 × 1000 ns of GaMD production runs were performed for the H_2R and H_4R systems. Table 6.1 gives an overview of the average boost potentials that have been applied for the different systems and simulation runs.

6.2.7. Structural Analysis

For subsequent analysis, periodic boundaries were removed from the trajectories, and all atoms were imaged to the receptors' transmembrane domains using *cpptraj* of *Amber18* software (San Franscicso, CA, USA).[89] Furthermore, *cpptraj* was used for the structural analysis of all distances and angles. Contacts between the $H_{2,4}R$ and mini-G proteins were assessed using the *nativecontacts* command with a distance cut-off of 5 Å. Binding energies of the ligand histamine were determined using the *mm_pbsa.pl* script using IGB = 2 and further parameters in default option according to the MM/GBSA method.[90-92] Plots were created using GraphPad Prism9 (GraphPad Software, San Diego, CA, USA), Cytoscape[93] and Origin2021 (OriginLab Corporation, Northampton, MA, USA), and the structural visualization was performed using *pymol* (The PyMOL Molecular Graphics System, Version 2.0 Schrödinger, LLC, New York, NY, USA).

Important reaction coordinates were identified from the simulation trajectories to reveal the dynamic regions of the systems and were used to differentiate conformational states of the $H_{2,4}R$–mini-G protein complexes. The observed dynamic regions included the ligand histamine, the receptor TM6 helix, and the C terminus of the mini-G protein α5 helix. Therefore, the distance between the charged amine group of histamine and the highly conserved $D^{3.32}$ and the receptor TM3 and TM6 intracellular ends were selected as reaction coordinates. The distance between the conserved NPxxY motif in the TM7 intracellular end of the receptors and the C terminus of the mini-G protein α5 helix (α5 hook) was used to characterize the $H_{2,4}R$–mini-G protein interactions. Furthermore, the TM2–α5 distance was calculated to estimate the α5 hook orientation inside the binding cavity. Specifically, distances were calculated between the backbone (Cα, C, and N) atoms using the center of mass of the following residues. For the TM3–TM6 distance, residues $R^{3.50}$ and $E/A^{6.30}$, and for the NPxxY–α5 distance, residues $N^{7.49}$, $P^{7.50}$, and $Y^{7.53}$ as well as the last five residues of the mini-G protein α5 helix were used. To calculate the α5–TM2 distance, the last five residues of the α5 helix and $T/S^{2.39}$ were used. The time courses of these reaction coordinates for the H_2R and H_4R systems were plotted in the Appendix (Figures A24 and A25, respectively). Root-mean-square fluctuations (RMSFs) were calculated for the protein residues and histamine, averaged over three independent GaMD simulations, and color coded for the schematic representation of each complex system (cf. Appendix, Figure A26).

The representative low-energy conformations of the $H_{2,4}$R–mini-G protein complexes were used to compute their residue contact network at the binding interface of the proteins using the *nativecontacts* command of *cpptraj* with a distance cut-off of 4 Å.

To recover the original free energy or potential of mean force (PMF) profiles of the six $H_{2,4}$R–mini-G protein systems, GaMD simulations were reweighted using the PyReweighting toolkit as described in section 6.2.5.[88] PMF profiles were computed using the combined trajectories from all three independent GaMD simulations (3 × 1000 ns length) for each system. For 2D PMF calculations, a bin size of 1.0 Å was used, and the cut-off was set to 500 frames The 2D PMF profiles were obtained for each simulation system regarding $D^{3.32}$–histamine distance in combination with the TM3–TM6 distance, the NPxxY–α5 distance, and the TM2–α5 distance.

6.3. Results

6.3.1. Functional Characterization of $H_{2,4}R$–Mini-G Protein Complexes

Recently, a dynamic split-luciferase based mini-G protein recruitment assay was developed for the histamine receptor family[54] meeting the requirements of a proximal readout as well as a simple, robust, non-radioactive and homogenous performance.[94] In this assay, HEK293T cells express $H_{2,4}R$ subtypes that are C-terminally fused to the small fragment of the NanoLuc (NlucC) and mini-G proteins N-terminally attached to the large fragment (NlucN). The complementation of the NanoLuc, and thus signal output, is enabled by the recruitment of the mini-G protein to the receptor upon activation by a ligand. In the present study, the same concept was applied to investigate the coupling profiles of the H_2R and H_4R to engineered G proteins. Therefore, transfectants expressing $H_{2,4}R$-NlucC in combinations with NlucN-mGs, NlucN-mGsi and NlucN-mGsq were used to probe the functional responses of histamine in the different cell systems. The H_2R was observed to interact with mGs, mGsi, and mGsq, whereas the H_4R was selective for binding to mGsi (Figure 6.1A and 6.1B).

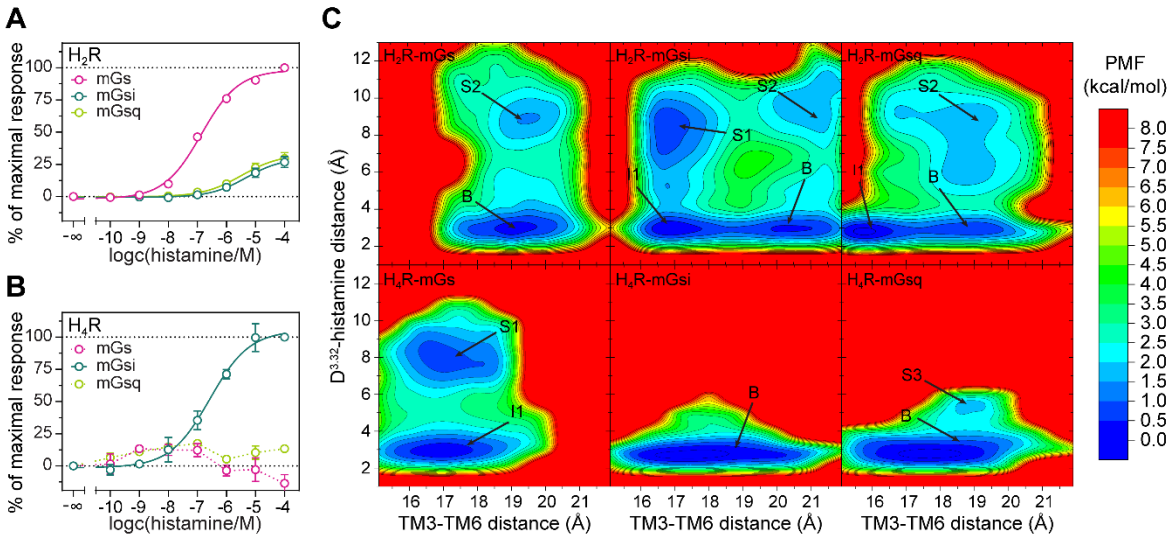

Figure 6.1. Concentration–response curves of histamine obtained in split-NanoLuc complementation-based mini-G protein recruitment assays using HEK293T cells transiently expressing either A) H_2R-NlucC or B) H_4R-NlucC fusion proteins in combination with NlucN-mGs, NlucN-mGsi, or NlucN-mGsq. Presented data are of three independent experiments ($N = 3$), each performed in triplicate. C) Free energy profiles of GaMD simulations with complexes containing either the H_2R or the H_4R in combination with mGs, mGsi, or mGsq. Distances of the $D^{3.32}$ (Cγ atom) and the amino group of histamine (Nα atom) as well as of the intracellular ends of TM3 and TM6 were used as reaction coordinates. TM3–TM6 distances were calculated using Cα, C, and N atoms of $R^{3.50}$ and $E/A^{6.30}$. For each system, three independent GaMD simulations were used for analysis (cf. Appendix, Figures A24 and A25). (Labels: "B" = "Bound", low-energy wells of fully active receptors bound to histamine; "I1" = "Intermediate", low-energy wells of receptor conformations with smaller or larger TM3–TM6 spacings. "S1", "S2", and "S3" = "Separated", low-energy states with different TM3–TM6 distances, in which histamine was separated from the conserved receptor residue $D^{3.32}$).

Notably, histamine was less potent (pEC_{50}) and effective (E_{max}) in H_2R-mGsi (pEC_{50} = 5.30 ± 0.06; E_{max} = 27 ± 3.5%) and H_2R-mGsq (pEC_{50} = 5.48 ± 0.04; E_{max} = 30 ± 3.7%) systems than in the H_2R-mGs system (pEC_{50} = 6.86 ± 0.04; E_{max} = 100%) that represents the canonical system (Table 6.2). In other words, a stronger binding of the H_2R to mGs than to mGsi and mGsq was observed. These observations were consistent with prior findings for the H_2R by Okashah et al. using BRET-based heterotrimeric G protein sensors and by Inoue et al. using chimeric G proteins.[41,46] In the cell assays, the H_4R bound selectively to mGsi yielding a pEC_{50} of 6.60 ± 0.10 and an E_{max} of 100% for the endogenous ligand histamine (per definition). Similar results were reported in a previous study using another chimeric G protein approach, in which the H_4R selectively coupled to members of the Gi family and only slightly to Gα16 of the Gq family.[46]

Table 6.2. Comparison of biochemical and computational ligand binding data. Potencies (pEC_{50}) and efficacies (E_{max}) of histamine obtained in split-NanoLuc complementation-based mini-G protein recruitment assays using HEK293T cells transiently expressing $H_{2,4}R$-NlucC in combination with NlucN-mGs, NlucNmGsi, or NlucN-mGsq. Presented data are of three independent experiments (*N* = 3) each performed in triplicate. Binding energies (kcal/mol) of histamine obtained in the given complexes applying the MM/GBSA method to the GaMD trajectories. For each system, 60,000 frames of the top histamine cluster were analyzed. Averages ± SD are given.

	Mini-G Protein Recruitment		MM/GBSA
	pEC_{50} ± SEM	E_{max} ± SEM [%]	Binding Energy ± SD [kcal/mol]
H_2R–mGs	6.86 ± 0.04	100	−17.23 ± 3.44
H_2R–mGsi	5.30 ± 0.06	27 ± 3.5	−16.57 ± 3.81
H_2R–mGsq	5.48 ± 0.04	30 ± 3.7	−16.25 ± 6.35
H_4R–mGs	n.d.	−14 ± 5.5	−20.03 ± 5.44
H_4R–mGsi	6.60 ± 0.10	100	−27.91 ± 4.69
H_4R–mGsq	n.d.	14 ± 0.3	−20.49 ± 6.78

6.3.2. Free Energy Profiles of $H_{2,4}R$ – Mini-G Protein Complexes in GaMD Simulations

In the absence of experimental structures, homology models were built in this study to generate initial complexes of the H_2R and H_4R with the mGs, mGsi, and mGsq proteins. A model recently published by Conrad et al.[77] and a model provided by GPCRdb[85] (www.gpcrdb.prg, access date: 08.10.2021) were used as simulation starting structures for the H_2R and the H_4R, respectively. A computational model of GaMD simulation systems is provided in the Appendix (Figure A21). For each of the six systems, three GaMD production runs, each of 1000 ns length and with individual boost parameters were performed (Table 6.1). Overall, the H_2R and H_4R remained in complex with the ligand histamine and their respective mini-G proteins during the simulations and similar regions of the complexes were identified as structurally flexible (cf. Appendix, Figure A26). Specifically, except for the respective α5 helix of the mini-G proteins, which were bound to the intracellular $H_{2,4}R$

binding cavity, mGs, mGsi, and mGsq were structurally more flexible than the membrane-bound H_2R and H_4R (cf. Appendix, Figure A26). For the receptors, the largest flexible regions were located at the N- and C-terminal ends and the extracellular loop (ECL) 2. In contrast to the H_2R, a higher flexibility of the intracellular loop (ICL) 3, ECL2, and ECL3 was observed in addition for the H_4R complexes (cf. Appendix, Figure A26). In all H_2R and H_4R complexes, the histamine ligand was inside the orthosteric binding pocket but had flexible orientation according to its root-mean-square fluctuation (RMSF), in particular for H_2R-mGsi and H_4R-mGs systems. Overall, both protein complex RMSF and histamine RMSF were lowest in the systems corresponding to the natural complexes (H_2R-mGs and H_4R-mGsi), indicating that these systems were energetically most favorable (cf. Appendix, Figure A26). In the H_2R systems, the replacement of mGs with mGsi and mGsq in the H_2R systems resulted in a higher structural flexibility of the mini-G protein binding surface (TM5, TM6, H8, and ICLs). In contrast, in the H_4R complexes, the structural variability at the binding surface was comparatively low when mGsi was replaced by mGs or mGsq. Only in H_4R–mGs higher fluctuations were observed at the intracellular ends of TM5, TM6 (kinked TM6, Figure 6.3F), ICL2, and ICL3. More characteristic for the H_4R–mGs and H_4R–mGsq complexes was the structural flexibility of the extracellular TM ends, which might be related to the structural flexibility of the histamine ligand. In combination with the results obtained in the cell assay, one could conclude that the flexibility of the H_2R intracellular surface has a positive effect on G protein binding, thus allowing the H_2R to interact with mGs, mGsi, and mGsq. In contrast, the complex formation of the H_4R-mGs and H_4R-mGsq seems to be unfavorable in view of the increased structural flexibility of the orthosteric binding pocket and thus decreased conformational stability.

In the starting structures of the simulations, histamine formed a salt bridge by its charged amino group with the conserved residue $D^{3.32}$ in the orthosteric binding pocket, similarly as postulated in the literature for the entire histamine receptor family.[95] During the simulations, this interaction performed different dynamics in the H_2R and H_4R systems. Whereas histamine was permanently bound to $D^{3.32}$ in the H_4R–mGsi and H_4R–mGsq complexes, histamine was observed to disengage this bond in all H_2R complexes and the H_4R-mGs complex, however, to distinct extent (cf. time courses and schematic illustration of the reaction coordinates in the Appendix, (Figures A24, A25 and A27, respectively). The lower abundance of the salt bridge in the H_2R complexes was in good agreement with the generally lower binding affinity of histamine to H_2R than to the H_4R.[6] To investigate whether the presence of the salt bridge was related to the activation state of the receptors, we used the distance between the charge centers of the amino group in histamine and the conserved receptor aspartate $D^{3.32}$ (denoted as $D^{3.32}$–histamine distance) as well as the receptor TM3–TM6 distance (measured between the Cα, C, and N atoms of residues $R^{3.50}$ and $E/A^{6.30}$) as reaction coordinates to calculate the free energy profiles (Figure 6.1C). The outward

movement of TM6 resulting in larger TM3–TM6 spacings is one of the key features of GPCR activation and is also suggested to determine G protein selectivity of Gs- and Gi-coupling GPCRs.[96-97] In all systems, the global minima were found for the fully histamine-bound states ($D^{3.32}$–histamine distance of ~3 Å). In the H_2R–mGs system, the global minimum was at a TM3–TM6 distance of ~19 Å (denoted as "B") (Figures 6.1C and 6.2E). In the H_2R–mGsi and H_2R–mGsq complexes, energetic minima at similar TM3–TM6 spacings were present (20 and 19 Å, respectively) (Figures 6.1C and 6.2E). However, the global minima of these complexes were located at a slightly smaller TM3–TM6 distance of ~17 Å (denoted as "I1") (Figures 6.1C and 6.2F). The lower capacity of mGsi and mGsq to stabilize the fully active H_2R conformation was in concordance with the lower E_{max} values (~25–30%) in the mini-G protein recruitment assay (Table 6.2). The global minimum of the canonical H_4R system, H_4R–mGsi as well as of H_4R–mGsq were observed at a TM3–TM6 distance of ~18 Å (Figures 6.1C and 6.3E). Smaller TM3–TM6 distances in Gi- compared to Gs-coupled GPCRs are related to the smaller α5 helix volume of Gi that requires less three-dimensional space.[98] Interestingly, in the H_4R–mGs system, the TM3–TM6 distances was even smaller ("I1" state in Figure 6.3E). Strikingly, this could be attributed to a kinked TM6 helix indicating an unfavorable interaction between the H_4R and mGs (Figure 6.3F).

6.3.3. Different Binding Affinities and Conformations of Histamine in $H_{2,4}R$-Complexes

As described, potencies (pEC_{50}) and efficacies (E_{max}) of histamine at the different complexes were determined in mini-G protein recruitment assays. It is worth mentioning that complicated relationships might exist between ligand binding affinity and efficiency,[99] and thus it was of interest whether the experimentally determined pEC_{50} values of histamine would correlate with its binding affinities in the respective $H_{2,4}R$ complexes. Therefore, the binding energy of histamine was calculated in all six complexes using the molecular mechanics generalized Born surface area (MM/GBSA) approach.[90-92] Since differences in the histamine orientation to $D^{3.32}$ within the orthosteric binding pocket were observed (Figure 6.1), histamine coordinates obtained during the GaMD simulations were clustered in 10 groups and only the frames of the first cluster were used to determine the binding energies. In the H_2R–mGs complex, histamine was bound ~1.0 kcal/mol stronger than in the H_2R–mGsi and H_2R–mGsq systems (Table 6.2). This trend was in concordance with the pEC_{50} values of the live cell assay (Table 6.2). In the H_4R systems, histamine was most effectively bound to the H_4R–mGsi complex with a difference of 7.88 kcal/mol or 7.42 kcal/mol compared to the systems containing mGs or mGsq, respectively (Table 6.2). Although the computational approach gave more pronounced differences in the binding energies of histamine at the H_2R–mGs and H_4R–mGsi complexes than the pEC_{50} values obtained in the live cell assay, the calculated binding energies seemed to be consistent with the general dynamics of the systems. In the four complexes with weaker histamine binding (H_2R–mGs, H_2R–mGsi, H_2R–mGsq, and H_4R–mGs),

the disengagement of histamine from $D^{3.32}$ could be detected (Figure 6.1C). Combined with the lacking interaction in the live cell assay, the more pronounced difference in histamine binding energies might serve as an indicator that the H_4R is difficult to couple with Gs and Gq proteins.

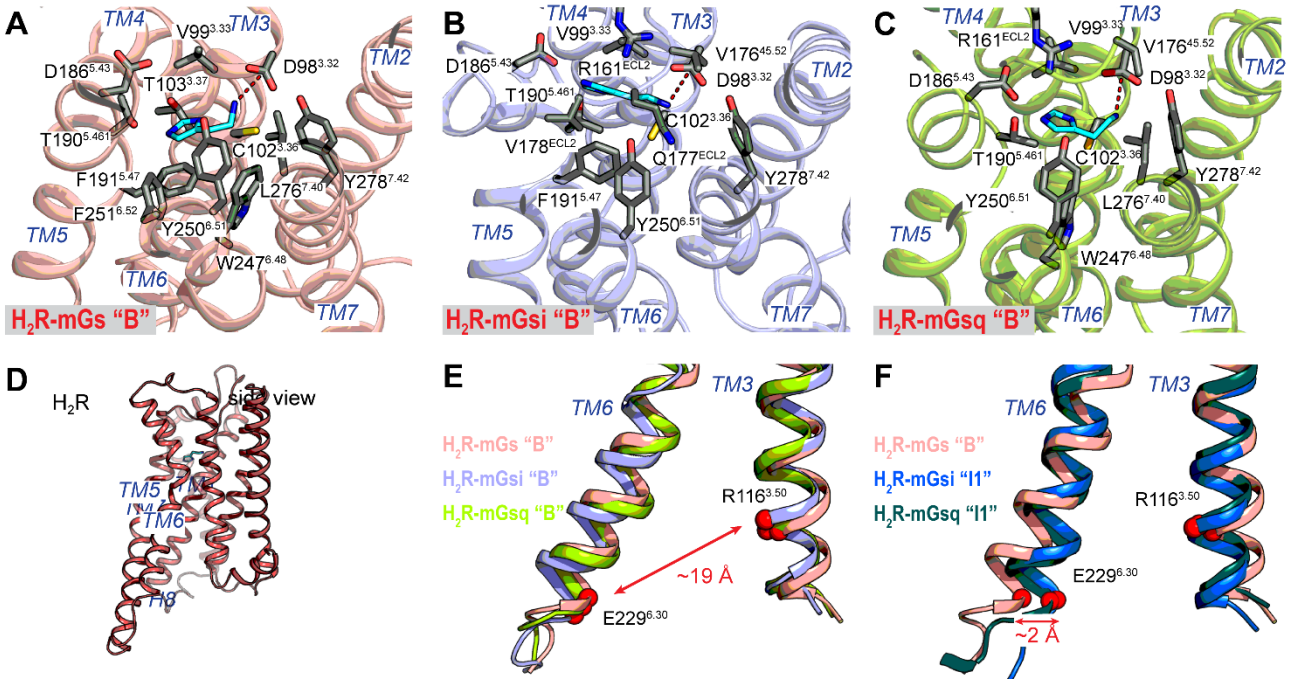

Figure 6.2. Binding modes of histamine (light blue) within the orthosteric binding pocket of the A) H_2R–mGs, B) H_2R–mGsi, and C) H_2R–mGsq complexes. Structures represent the fully bound state "B" (cf. Figure 6.1). Contact residues within 4 Å of the ligand are highlighted as sticks (dark gray). The conserved salt bridge between the amino group of histamine and $D^{3.32}$ is given as a red, dashed line. D) Side view of the H_2R (pink). E) TM3–TM6 distance of the "B" (fully active histamine-bound receptor) states of the H_2R–mGs (salmon), H_2R–mGsi (purple), and H_2R–mGsq (green). F) TM3–TM6 distance of the "B" state of the H_2R–mGs (salmon) and the "I1" intermediate states of the H_2R–mGsi (dark green), and H_2R–mGsq (blue). Residues $R^{3.50}$ and $E^{6.30}$ were used to calculate the TM3–TM6 distance and are given as red spheres.

Recently, the first structure of a histamine receptor subtype in an active conformation, the H_1R, was resolved using cryo-EM, providing insights at the molecular level into the binding mode of the endogenous agonist histamine.[62] The polar interactions at positions 3.32, 3.37, 5.46 and 6.51 postulated for the entire histamine receptor family were confirmed in this structure. Generally, we observed similar binding modes, with only slight differences, for histamine in the representative structures of the "Bound" low-energy states of the H_2R and H_4R complexes as in the H_1R structure. In the H_2R systems, the orthosteric binding pocket was formed by polar residues $D^{3.32}$, $C^{3.36}$, $T^{3.37}$, $D^{5.43}$, $T^{5.461}$, $Y^{6.51}$, and $Y^{7.42}$ and hydrophobic residues $V^{3.33}$, $F^{5.47}$, $F^{6.42}$, $W^{6.48}$, and $L^{7.40}$ (Figures 6.2A–6.2C). In all three H_2R complexes, a salt bridge of the histamine primary amine group with $D^{3.32}$ was formed. The imidazole ring was stabilized by the polar residues $D^{5.43}$ and $T^{5.461}$. In addition, $T^{3.37}$ is further involved in the latter in the H_2R–mGs system (Figure 6.2A). Unlike in the H_1R structure, the sidechain of histamine in the H_2R–mGs and H_2R–mGsq complexes is directed toward the hydrophobic residues $W^{6.48}$ and $L^{7.40}$. In the H_2R–mGsi complex, the histamine sidechain was more likely to be attracted by the backbone of ECL2 residues ($V^{45.52}$, Q177, and V178) (Figure 6.2B). In

the H_4R systems, the orthosteric binding pocket was surrounded by the polar residues $D^{3.32}$, $Y^{3.33}$, $T^{3.37}$, $E^{5.461}$, $Y^{5.51}$, $Q^{7.41}$, and the hydrophobic residues $W^{6.48}$, $F^{7.38}$, and $W^{7.42}$ (Figure 6.3A–C). As in the H_2R complexes, $D^{3.32}$ formed a salt bridge with the primary amine of histamine. The imidazole ring was bound by polar residues $Y^{3.33}$, $T^{3.37}$, and $E^{5.461}$. The structural details of the separated histamine states "S1" and "S2" of the H_2R complexes and the H_4R–mGs complex (Figure 6.1C) were provided in the Appendix (Figure A28).

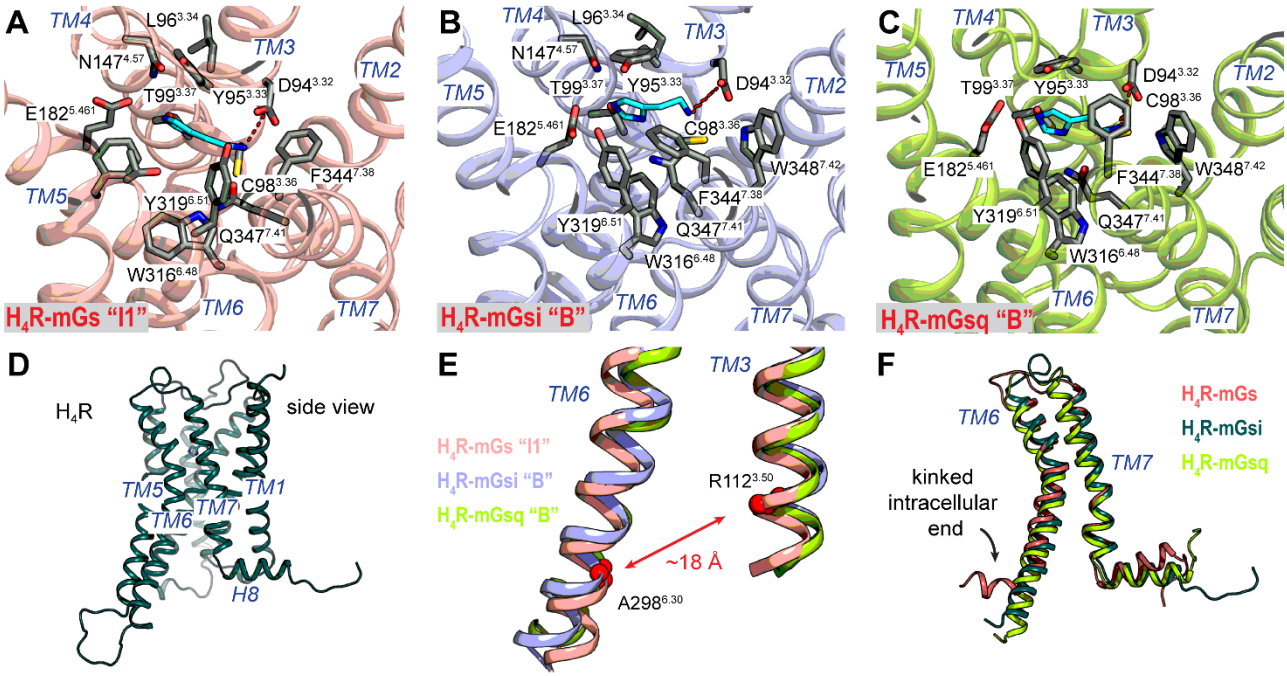

Figure 6.3. Binding modes of histamine (light blue) within the orthosteric binding pocket of the A) H_4R–mGs, B) H_4R–mGsi and C) H_4R–mGsq complexes. Representative structures of the intermediate "I1" H_4R–mGs state and of the fully bound "B" H_4R–mGsi and H_4R–mGsq states are shown (cf. Figure 6.1). Contact residues within 4 Å of the ligand are highlighted in sticks (dark gray). The conserved salt bridge between the amino group of histamine and $D^{3.32}$ is highlighted as a red dashed line. D) Side view of the H_4R (purple). E) TM3–TM6 distances in the in the intermediate state "I1" of H_4R-mGs (salmon) and the fully bound "B" states of the H_4R–mGsi (purple) and H_4R–mGsq (green) complexes. F) Side view of TM6 and TM7 of representative H_4R–mGs (pink), the H_4R–mGsi (dark green), and H_4R–mGsq (green) structures.

6.3.4. Residue Contacts at the Protein Binding Interface in $H_{2,4}R$ Systems

To examine the coupling profiles of the H_2R and H_4R, residue contact networks for the representative structures of the receptor–mini-G protein complexes were extracted from GaMD simulations (Figures 6.4 and 6.5). It should be noted at the outset of this section that the quantitative number of contacts at the protein interface is not necessarily decisive, since different residue volumes should result in different contact areas of the mini-G protein α5 helices. For example, the mGsi α5 helix generally formed smaller number of contacts than mGs and mGsq, even in the canonical H_4R–mGsi system. Thus, the protein binding interface should also be qualitatively evaluated, and thus include the types of residue contacts.

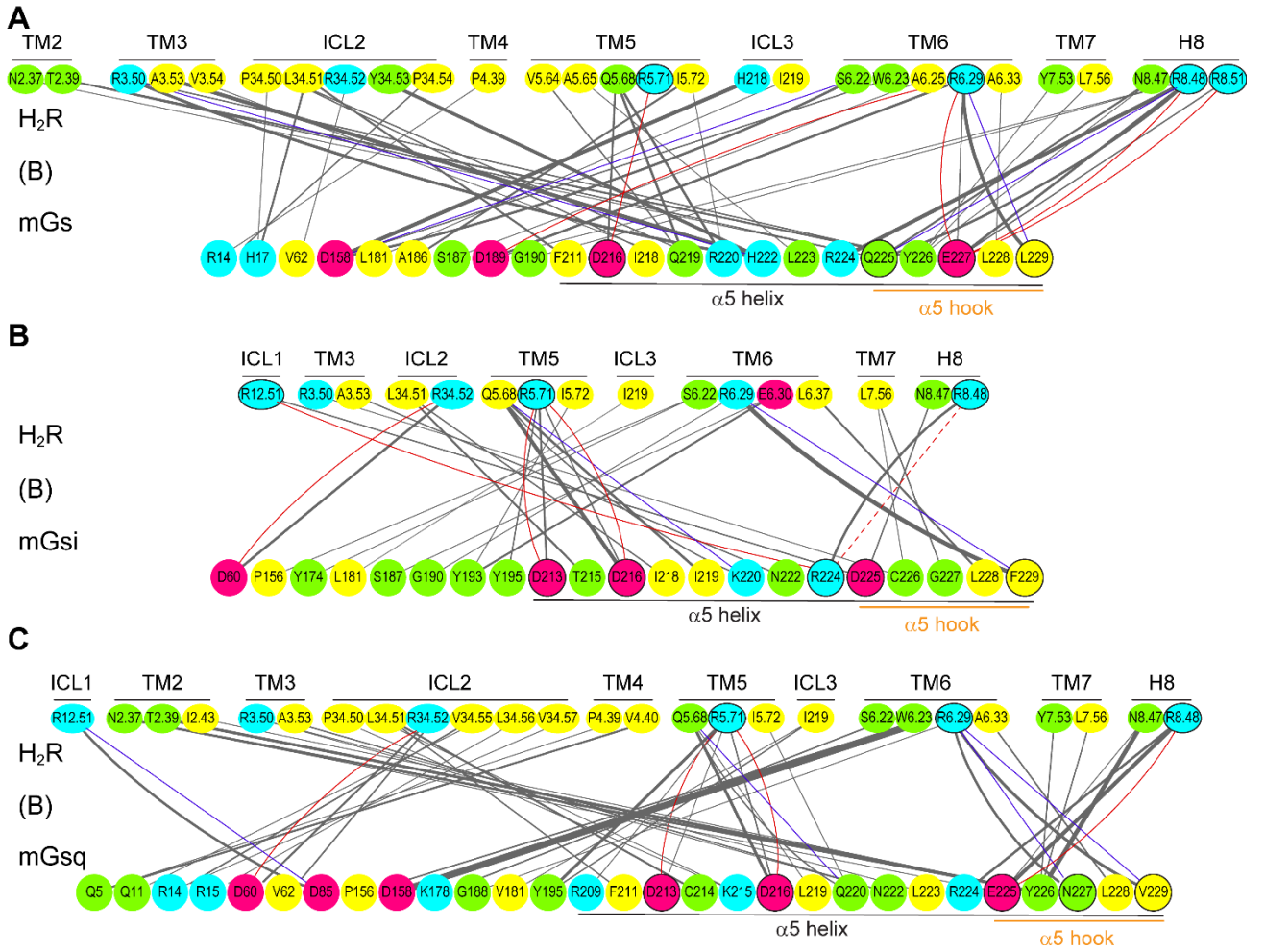

Figure 6.4. Quantitative residue interactions at the protein interface in the A) H_2R–mGs, B) H_2R–mGsi, and C) H_2R–mGsq (fully active histamine-bound receptor conformations) complexes. The interaction contacts were calculated using the representative low-energy conformation of the systems. Van der Waals, hydrogen bond, and salt bridge interactions are colored in gray, blue, and red, respectively. The line thickness is proportional to the number of contacts of the residue pairs. Hydrophobic, polar, basic, and acidic residues are colored in yellow, green, light blue, and pink, respectively. The red dashed line highlights a parallel guanidinium cation orientation of arginine residues. Important amino acids responsible for polar contacts at the binding interface were highlighted by black circles. For the H_2R, the GPCRdb numbers based on BW nomenclature are used for TM helices and ICL1/2. For ICL3, original index numbers are given. For the mini-G proteins, the original index numbers are given. For two-dimensional visualization of the residue contact network, the Cytoscape[93] software was used.

The protein contact areas were very similar in the H_2R complexes but rather different in the H_4R complexes. The main contacts of the H_2R with mGs, mGsi, and mGsq involved the receptors ICL2, TM3, TM5, TM6, and H8 (Figure 6.4). In particular, the negatively charged residues of the mini-G protein α5 helices ($D213^{mini\text{-}G}$, $D216^{mini\text{-}G}$, $D225^{mGsi}$/$E225^{mGsq}$, and $E227^{mGs}$) formed salt bridges with following H_2R residues leading to comparable mini-G protein binding positions. Specifically, $R^{5.71}$ (TM5) formed salt bridges with the conserved residues $D213^{mini\text{-}G}$ and $D216^{mini\text{-}G}$ of the α5 helices in the mGs, mGsi, and mGsq (Figure 6.4). In addition, the α5 hook of the mini-G proteins was also stabilized by salt bridges in the binding pocket. Accordingly, $E227^{mGs}$ formed three salt bridges with receptor $R^{6.29}$ (TM6), $R^{8.48}$, and $R^{8.51}$ (H8), and $E225^{mGsq}$ formed a single salt bridge with receptor $R^{8.48}$ (Figure 6.4A and 6.4C). In addition to a salt bridge between $D225^{mGsi}$ and $R^{12.51}$ (ICL1), the α5 hook

of mGsi was stabilized in the receptor binding cavity by essentially the same H_2R residues that also interacted with mGs and mGsq: $R^{6.29}$ and $R^{8.48}$ (Figure 6.4). More specifically, a hydrogen bond was formed between $F229^{mGsi}$ and $R^{6.29}$ and arginines $R224^{mGsi}$ and $R^{8.48}$ were stacked. Despite the repulsive forces of arginine guanidinium cations, arginine parings in parallel orientation have been frequently reported at protein – protein interfaces, and rather are considered as driving force for protein – protein interaction in terms of charge distribution and solvent exclusion free energy.[100-101]

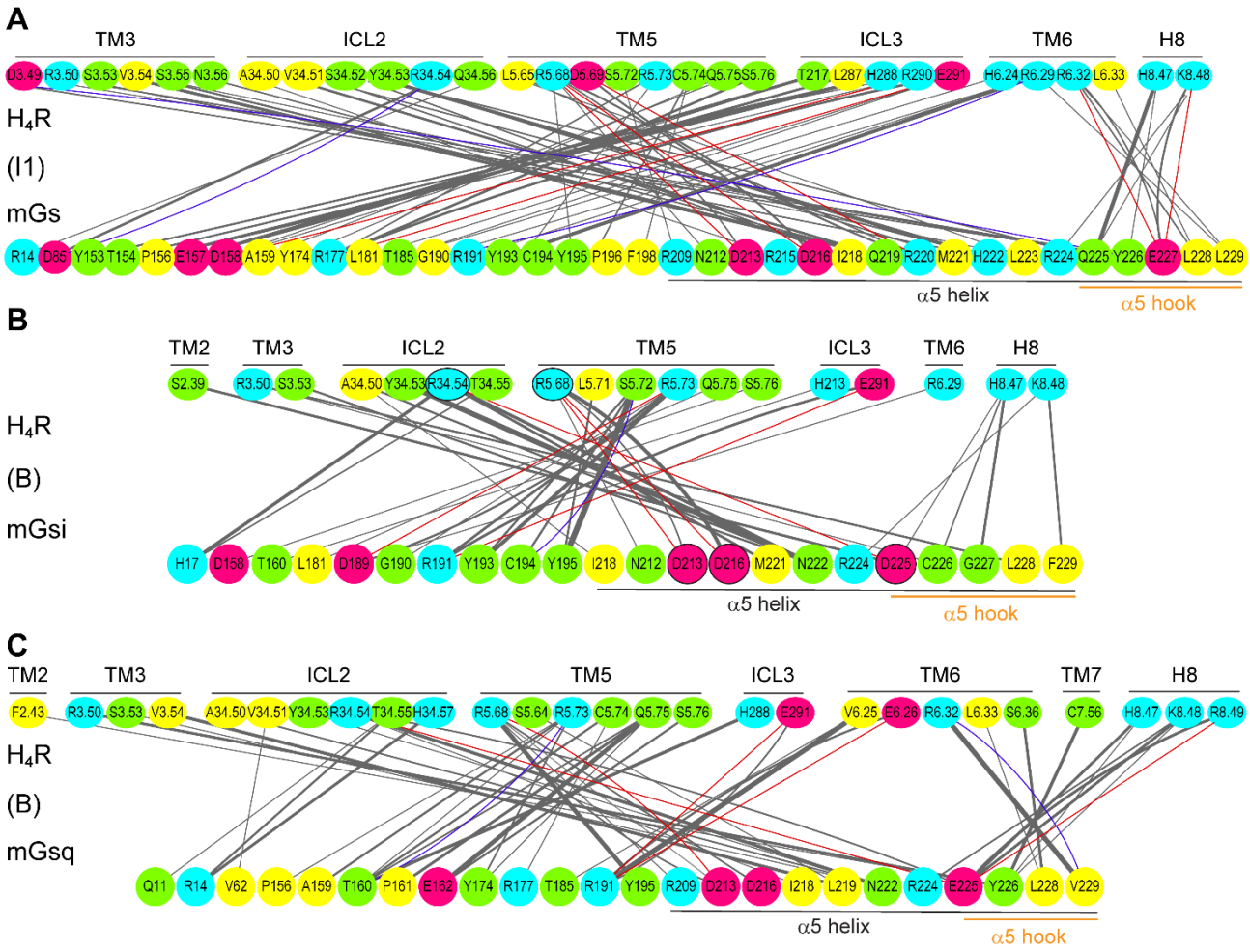

Figure 6.5. Quantitative residue interactions at the protein interface in the A) H_4R–mGs, B) H_4R–mGsi, and C) H_4R–mGsq (histamine-bound receptor conformations) complexes. The interaction contacts were calculated using the representative low-energy conformation of the systems. Van der Waals, hydrogen bond, and salt bridge interactions are colored in gray, blue, and red, respectively. The line thickness is proportional to the number of contacts of the residue pairs. Hydrophobic, polar, basic, and acidic residues are colored in yellow, green, light blue, and pink, respectively. Important amino acids responsible for polar contacts at the binding interface in the canonical H_4R–mGsi complex were highlighted by black circles. For the H_4R, the GPCRdb numbers based on BW nomenclature are used for TM helices and ICL1/2. For ICL3, original index numbers are given. For the mini-G proteins, the original index numbers are given. For two-dimensional visualization of the residue contact network, the Cytoscape[93] software was used.

In contrast to the H_2R systems, the contact surface in the H_4R complexes were more versatile. In the canonical system, H_4R–mGsi, a different contact network was present compared with that in the H_2R complexes (Figures 6.4B and 6.5B). For the H_4R, residues of ICL2 and TM5 contributed the main interactions with the mGsi. Like the H_2R systems, mGsi residues $D213^{mGsi}$ and $D216^{mGsi}$ formed salt bridges with a receptor residue in TM5, $R^{5.68}$. In addition, $D225^{mGsi}$ of the $\alpha5$ hook formed a salt bridge with $R^{34.54}$ of ICL2. Unlike in the H_2R complexes, the $\alpha5$ hook formed few contacts. Notably, it lacked strong interactions with TM6 and H8. In the H_4R–mGsq complex, a comparable contact network as in the H_2R–mGsq complex was detected with the main contacts rising from ICL2, TM5, TM6, and H8 (Figure 6.5C). In this system, the conserved mini-G protein residue $D213^{mGsq}$ formed a salt bridge with $R^{5.68}$ of the H_4R. The $\alpha5$ hook was further closely bound to the H_4R via the two salt bridges $E225^{mGsq}$–$R^{34.54}$ (ICL2) and $E225^{mGsq}$–$R^{8.49}$ (H8) and by means of a hydrogen bond between $V229^{mGsq}$ and $R^{6.32}$. By contrast, in the H_4R–mGs complex only fewer interactions were formed between the $\alpha5$ hook and the receptor comprising hydrophobic interactions and two salt bridges between $E227^{mGs}$ and $R^{6.32}$ of TM6 as well as $K^{8.48}$ of H8 (Figure 6.5A). Rather, this system contained an extremely high number of hydrophobic contacts with TM3, ICL2, TM5, and ICL3, which was particularly striking, since no H_4R-mGs interaction was observed in mini-G protein recruitment assays (Figure 6.1B). However, visual analysis of the trajectories supported that mGs rather stuck to the H_4R by the large hydrophobic contacts than specifically interacted with the receptor. Thus, it is possible that the H_4R and mGs only stayed in the complex generated for GaMD simulations because of predefined spatial restrictions (e.g., the box size), and the H_4R-mGs complex would not occur in cell assays.

6.3.5. $\alpha5$ Hook Orientation at the Binding Interface of $H_{2,4}R$ Complexes

To further characterize the mini-G protein binding in the H_2R and H_4R complexes, specific $\alpha5$ hook positions within the receptor binding cavity were analyzed by the $\alpha5$–NPxxY distance (cf. Appendix, Figure A29) and the sideward orientation of the $\alpha5$ helix (Figure 6.6). In the literature, it has been described that the penetration depth of G protein $\alpha5$ helices is characteristic for the G protein families, which is often described by the distance of the $\alpha5$ to the conserved NPxxY motif ($N^{7.49}$, $P^{7.50}$, $Y^{7.53}$). Commonly, larger outward movements of TM6 in Gs- and Gq-coupled GPCRs move the $\alpha5$ helix further away from TM7 and thus NPxxY.[98] Accordingly, the mGsi protein was ~1–2 Å closer to the H_2R-NPxxY and H_4R–NPxxY motifs than mGs and mGsq (cf. Appendix, Figure A29).

More decisively, differences were detected in the sideward orientation of the α5 helices in the H_2R and H_4R systems. In the H_2R systems, the last five residues of the α5 helices (hook) of mGs, mGsi, and mGsq were in equal position, which was identified as a Gs-like position considering available GPCR–Gs complexes as reference (cf. Appendix, Figure A30A and A30D). It should not be disregarded that this might be related to the utilized receptor model, which was based on a H_2R-Gs structure,[77] and thus to a predefined the α5 position. Nevertheless, the α5 hook of mGsi was able to adopt a Gi-like orientation in the H_4R systems, which was not achieved by mGs and mGsq (cf. Appendix, Figures A30B, A30E, A30F). In all systems, a single low-energy well was identified from the free energy profiles calculated using the $D^{3.32}$–histamine distance and α5–TM2 distance as reaction coordinates (Figure 6.6).

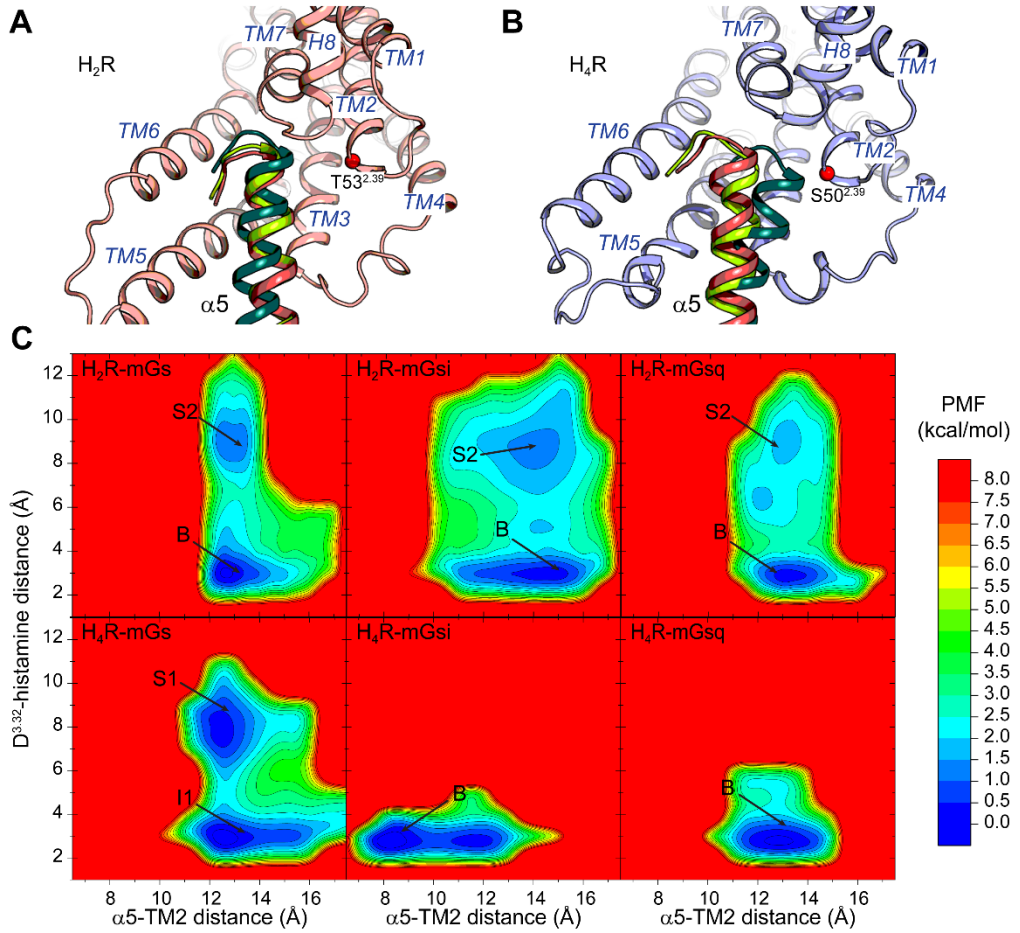

Figure 6.6. Orientation of the α5 helices of mGs, mGsi, and mGsq in the A) H_2R complexes and B) H_4R complexes. The last five residues of α5 helix and residue $T/S^{2.39}$ were used to determine the α5–TM2 distance in the H_2R and H_4R complexes, respectively. $T/S^{2.39}$ is shown as red spheres. The H_2R is depicted in salmon, the H_4R is depicted in purple, mGs in pink, mGsi in dark green, and mGsq in green, respectively. C) Free energy profiles of GaMD simulations with complexes of either the H_2R or the H_4R in combination with mGs, mGsi, or mGsq. Distances of $D^{3.32}$ (Cγ atom) and the amino group of histamine (Nα atom) as well as of the α5 helix and TM2 were used as reaction coordinates. The α5–TM2 distances were calculated using the geometric center of Cα, C, and N atoms of the last five residues of the mini-G protein α5 helix and $T/S^{2.39}$. For each system, three independent GaMD simulations were used for analysis. (Labels: "B" indicates representative low-energy wells of fully active receptors bound to histamine, "I1" indicates low-energy wells of intermediate receptor conformation bound to histamine. "S1" and "S2" indicate low-energy wells containing conformations with histamine separated from $D^{3.32}$, cf. Figure 6.1C).

Specifically, the α5 helix in all H_2R systems as well as in H_4R–mGs and H_4R–mGsq systems was oriented toward TM6, giving α5–TM2 distances in the range of ~14 Å. In the H_4R–mGsi complex, the global minimum was at an essentially lower α5–TM2 distance of ~8 Å. Notably, the findings that the α5 helices of all mini-G proteins were in the Gs-like orientation toward TM6 in the H_2R complexes but only the α5 helix of mGsi was in the Gi-like orientation toward TM2 in H_4R complexes were consistent with the results obtained in the live cell assay: Histamine elicited the recruitment of mGs, mGsi, and mGsq to the H_2R but only of mGsi to the H_4R (Figure 6.1). In combination with the observed increased structural flexibility of the intracellular H_2R side in contrast to the H_4R (cf. Appendix, Figure A26), it seemed likely that the ability of the H_2R or rather the inability of the H_4R to direct the α5 helix to a precise Gs- or Gi-like position contributed to the promiscuous coupling of the H_2R to mGs, mGsi, and mGsq and the selective H_4R binding to mGsi.

6.4. Discussion

In this study, the H_2R and H_4R were investigated in complex with three types of mini-G proteins, mGs, mGsi, and mGsq, respectively. The results obtained in cellular experiments and GaMD simulations were in good agreement providing important insights into the mechanism of engineered G protein coupling to both receptors. Mini-G protein recruitment assays were performed using HEK293T cells transiently co-expressing combinations of either the H_2R-NlucC or the H_4R-NlucC and NlucN-mGs, NlucN-mGsi, and NlucN-mGsq fusion proteins (Figure 6.1A and 6.1B). For the H_2R, a promiscuous coupling pattern to mGs, mGsi, and mGsq was observed upon activation by the endogenous ligand histamine. Regardless, the H_2R preferred mGs binding over mGsi or mGsq binding revealed by pEC_{50} and E_{max} values (Figure 6.1A, Table 6.2). In contrast, the H_4R selectively bound to mGsi.

To obtain dynamic insight at the molecular level, 3D complexes of the $H_{2,4}R$ and mGs, mGsi and mGsq bound to histamine were generated and GaMD simulations were performed. Although the salt bridge between Nα of histamine and $D^{3.32}$, which is conserved among histamine receptor subtypes,[62,95] was present in the starting structures, this bond tended to disengage during the simulations. When considering only bound conformations, stronger histamine binding energies were determined by MM/GBSA for H_4R complexes than H_2R complexes (Table 6.2), which was in concordance with the higher binding affinity of histamine to the H_4R reported.[102-103] In addition, for H_2R complexes, the trend of histamine binding energies was consistent with histamine pEC_{50} values obtained in mini-G protein recruitment assays (mGs < mGsi ≈ mGsq; Table 6.2).

As a general observation, H_2R complexes were more dynamic than H_4R complexes (cf. Appendix, Figure A26) and revealed larger fluctuations in the TM3–TM6 distances, in particular for H_2R–mGsi and H_2R–mGsq complexes (Figure 6.1C), which is commonly considered an indicator for GPCR activation.[96,104] In agreement with lower potencies and efficacies obtained in mini-G protein recruitment assays, mGsi and mGsq were less able to stabilize the fully active H_2R conformation (TM3–TM6 distance of ~19–20 Å) in GaMD simulations, and the systems also visited conformations with a smaller TM3–TM6 spacing (Figure 6.1C). As observed for many Gi-coupling GPCRs, the TM3–TM6 distance of the fully active H_4R in the H_4R–mGsi complex was lower (~18 Å) compared to the primarily Gs-coupling H_2R. Strikingly, the overall TM3–TM6 distance in the H_4R-mGs complex ("I1" state) was even lower than in the H_4R–mGsi ("B" state), however most likely due to an unnaturally kinked TM6. Concisely, compared to the other H_2R and H_4R systems, the lowest structural fluctuations (cf. Appendix, Figure A26) and strongest histamine binding energies (Table 6.2) were observed for H_2R-mGs and H_4R-mGsi systems, respectively, thus reflecting the primary coupling pattern of the receptors obtained in mini-G protein recruitment assays.

However, it should be mentioned that GaMD alone did not clearly indicate that the H_4R would not couple to mGs and mGsq since the proteins remained in the preformed complexes during the simulations. Rather, mini-G protein recruitment assays helped to evaluate several small indicators that H_4R-mGs and H_4R-mGsq complexes were unfavorable, including large fluctuations in the orthosteric binding pocket (see Appendix, Figure A26) and related, considerably lower histamine binding energies compared to the H_4R-mGsi complex (Table 6. 2). Moreover, the detailed inspection of the protein interface revealed a strikingly high number of hydrophobic interactions at the H_4R-mGs binding interface, which was interpreted as sticking rather than specific interaction by visual inspection of the trajectories (Figure 6.5).

While the contact network in H_4R complexes was more divergent, mGs, mGsi, and mGsq revealed similar residue contributions and binding orientations in the H_2R binding cavity. Specifically, all α5 helices were in Gs-like orientation (toward TM6), which was stabilized by specific polar interactions of the α5 hook with TM6 and H8 (Figures 6.4 and 6.6). In contrast, only few contacts of the α5 hook and the receptor but rather specific α5 helix interactions with TM5 and ICL2 most likely led to the Gi-like orientation (toward TM2) of mGsi in the H_4R complex (Figures 6.5 and 6.6). It was particularly striking that mGs and mGsq, which did not couple to H_4R in the live cell assay, did not adopt Gi-like orientations in H_4R complexes but instead were in the same position as in the H_2R complexes, the Gs-like orientation (Figure 6.6). Thus, in combination with the observed increased flexibility of the intracellular side of the H_2R (cf. Appendix, Figure A26), the ability to accommodate G proteins at a (receptor-)specific position was suggested to determine the coupling profile of a receptor.

In summary, this study provided comprehensive insight into the coupling profiles of $H_{2,4}R$ to engineered G proteins by the combination of biochemical as well as computational experiments and supported the following: The H_2R promiscuously binds to mGs, mGsi, and mGsq, whereas the H_4R selectively binds to mGsi. However, the $H_{2,4}R$ coupling profiles obtained should not be generalized to entire G protein classes, since mini-G proteins are chimeric G proteins comprising α5 helices of Gαs, Gαi_1, and Gαq. Thus, it remains unclear whether or in which way $H_{2,4}R$ would form complexes with Gi/o family members Gαi_3 and Gαo or to Gα14 and Gα15 of the Gq/11 family having diverse α5 helices within the Gα classes. For example, a H_4R-Gα15 interaction was demonstrated by Inoue et al.,[46] which was consistent with Ca^{2+} signals obtained earlier using cells co-expressing the H_4R and Gα15[32] but were missing in HEK cells recombinantly expressing the H_4R alone.[29] Furthermore, the hypothesis that the flexibility of the intracellular receptor side might allow or not allow the accommodation of the α5 hook in a precise position (e.g., Gs-like or Gi-like), thereby determining to the coupling profiles of GPCRs, should be explored more in detail. Thus, it would be useful to apply site-directed mutagenesis in future studies to unravel which $H_{2,4}R$ residues determine their coupling preference.

6.5. References

1. Panula, P., Chazot, P. L., Cowart, M., Gutzmer, R., Leurs, R., Liu, W. L., Stark, H., Thurmond, R. L. & Haas, H. L., International Union of Basic and Clinical Pharmacology. XCVIII. Histamine receptors. *Pharmacol Rev* **2015,** *67* (3), 601-655, doi: 10.1124/pr.114.010249.
2. Jacoby, E., Bouhelal, R., Gerspacher, M. & Seuwen, K., The 7 TM G-protein-coupled receptor target family. *ChemMedChem* **2006,** *1* (8), 761-782, doi: 10.1002/cmdc.200600134.
3. Lagerstrom, M. C. & Schioth, H. B., Structural diversity of G protein-coupled receptors and significance for drug discovery. *Nat Rev Drug Discov* **2008,** *7* (4), 339-357, doi: 10.1038/nrd2518.
4. Hauser, A. S., Attwood, M. M., Rask-Andersen, M., Schioth, H. B. & Gloriam, D. E., Trends in GPCR drug discovery: New agents, targets and indications. *Nat Rev Drug Discov* **2017,** *16* (12), 829-842, doi: 10.1038/nrd.2017.178.
5. van der Goot, H. & Timmerman, H., Selective ligands as tools to study histamine receptors. *Eur J Med Chem* **2000,** *35* (1), 5-20, doi: 10.1016/s0223-5234(00)00101-x.
6. Pockes, S., Wifling, D., Keller, M., Buschauer, A. & Elz, S., Highly potent, stable, and selective dimeric hetarylpropylguanidine-type histamine H2 receptor agonists. *ACS Omega* **2018,** *3* (3), 2865-2882, doi: 10.1021/acsomega.8b00128.
7. Tropmann, K., Bresinsky, M., Forster, L., Monnich, D., Buschauer, A., Wittmann, H. J., Hubner, H., Gmeiner, P., Pockes, S. & Strasser, A., Abolishing dopamine D2long/D3 receptor affinity of subtype-selective carbamoylguanidine-type histamine H2 receptor agonists. *J Med Chem* **2021,** *64* (12), 8684-8709, doi: 10.1021/acs.jmedchem.1c00692.
8. Hirasawa, N., Ohsawa, Y., Katoh, G., Shibata, K., Ishihara, K., Seyama, T., Tamura, S., Hong, J. & Ohuchi, K., Modification of the picryl chloride-induced allergic dermatitis model in mouse ear lobes by 12-O-tetradecanoylphorbol 13-acetate, and analysis of the role of histamine in the modified model. *Int Arch Allergy Immunol* **2009,** *148* (4), 279-288, doi: 10.1159/000170381.
9. Zampeli, E. & Tiligada, E., The role of histamine H4 receptor in immune and inflammatory disorders. *Br J Pharmacol* **2009,** *157* (1), 24-33, doi: 10.1111/j.1476-5381.2009.00151.x.
10. Cowden, J. M., Riley, J. P., Ma, J. Y., Thurmond, R. L. & Dunford, P. J., Histamine H4 receptor antagonism diminishes existing airway inflammation and dysfunction via modulation of Th2 cytokines. *Respir Res* **2010,** *11*, 86, doi: 10.1186/1465-9921-11-86.
11. Hofstra, C. L., Desai, P. J., Thurmond, R. L. & Fung-Leung, W. P., Histamine H4 receptor mediates chemotaxis and calcium mobilization of mast cells. *J Pharmacol Exp Ther* **2003,** *305* (3), 1212-1221, doi: 10.1124/jpet.102.046581.
12. Ling, P., Ngo, K., Nguyen, S., Thurmond, R. L., Edwards, J. P., Karlsson, L. & Fung-Leung, W. P., Histamine H4 receptor mediates eosinophil chemotaxis with cell shape change and adhesion molecule upregulation. *Br J Pharmacol* **2004,** *142* (1), 161-171, doi: 10.1038/sj.bjp.0705729.
13. Gutzmer, R., Mommert, S., Gschwandtner, M., Zwingmann, K., Stark, H. & Werfel, T., The histamine H4 receptor is functionally expressed on TH2 cells. *J Allergy Clin Immunol* **2009,** *123* (3), 619-625, doi: 10.1016/j.jaci.2008.12.1110.
14. Simon, D., Braathen, L. R. & Simon, H. U., Eosinophils and atopic dermatitis. *Allergy* **2004,** *59* (6), 561-570, doi: 10.1111/j.1398-9995.2004.00476.x.
15. Liu, F. T., Goodarzi, H. & Chen, H. Y., IgE, mast cells, and eosinophils in atopic dermatitis. *Clin Rev Allergy Immunol* **2011,** *41* (3), 298-310, doi: 10.1007/s12016-011-8252-4.
16. Werfel, T., Layton, G., Yeadon, M., Whitlock, L., Osterloh, I., Jimenez, P., Liu, W., Lynch, V., Asher, A., Tsianakas, A., et al., Efficacy and safety of the histamine H4 receptor antagonist ZPL-3893787 in patients with atopic dermatitis. *J Allergy Clin Immunol* **2019,** *143* (5), 1830-1837.e1834, doi: 10.1016/j.jaci.2018.07.047.

17. Milligan, G. & Kostenis, E., Heterotrimeric G-proteins: A short history. *Br J Pharmacol* **2006,** *147 Suppl 1*, S46-55, doi: 10.1038/sj.bjp.0706405.

18. Wettschureck, N. & Offermanns, S., Mammalian G proteins and their cell type specific functions. *Physiol Rev* **2005,** *85* (4), 1159-1204, doi: 10.1152/physrev.00003.2005.

19. Lefkowitz, R. J., Seven transmembrane receptors: a brief personal retrospective. *Biochim Biophys Acta* **2007,** *1768* (4), 748-755, doi: 10.1016/j.bbamem.2006.11.001.

20. Fredriksson, R., Lagerström, M. C., Lundin, L. G. & Schiöth, H. B., The G-protein-coupled receptors in the human genome form five main families. Phylogenetic analysis, paralogon groups, and fingerprints. *Mol Pharmacol* **2003,** *63* (6), 1256-1272, doi: 10.1124/mol.63.6.1256.

21. Simon, M. I., Strathmann, M. P. & Gautam, N., Diversity of G proteins in signal transduction. *Science* **1991,** *252* (5007), 802-808, doi: 10.1126/science.1902986.

22. Milligan, G., Is promiscuity of G protein interaction an issue in the classification of receptors? *Ann N Y Acad Sci* **1997,** *812*, 126-132, doi: 10.1111/j.1749-6632.1997.tb48152.x.

23. Albert, P. R. & Robillard, L., G protein specificity: Traffic direction required. *Cell Signal* **2002,** *14* (5), 407-418, doi: 10.1016/s0898-6568(01)00259-5.

24. Harding, S. D., Sharman, J. L., Faccenda, E., Southan, C., Pawson, A. J., Ireland, S., Gray, A. J. G., Bruce, L., Alexander, S. P. H., Anderton, S., et al., The IUPHAR/BPS Guide to pharmacology in 2018: updates and expansion to encompass the new guide to immunopharmacology. *Nucleic Acids Res* **2018,** *46* (D1), D1091-d1106, doi: 10.1093/nar/gkx1121.

25. Alexander, S. P. H., Christopoulos, A., Davenport, A. P., Kelly, E., Mathie, A., Peters, J. A., Veale, E. L., Armstrong, J. F., Faccenda, E., Harding, S. D., et al., The concise guide to pharmacology 2019/20: G protein-coupled receptors. *Br J Pharmacol* **2019,** *176* (S1), S21-S141, doi: 10.1111/bph.14748.

26. Woehler, A. & Ponimaskin, E. G., G protein-mediated signaling: Same receptor, multiple effectors. *Curr Mol Pharmacol* **2009,** *2* (3), 237-248, doi: 10.2174/1874467210902030237.

27. Gantz, I., Munzert, G., Tashiro, T., Schäffer, M., Wang, L., DelValle, J. & Yamada, T., Molecular cloning of the human histamine H2 receptor. *Biochem Biophys Res Commun* **1991,** *178* (3), 1386-1392, doi: 10.1016/0006-291x(91)91047-g.

28. Kühn, B., Schmid, A., Harteneck, C., Gudermann, T. & Schultz, G., G proteins of the Gq family couple the H2 histamine receptor to phospholipase C. *Mol Endocrinol* **1996,** *10* (12), 1697-1707, doi: 10.1210/mend.10.12.8961278.

29. Nakamura, T., Itadani, H., Hidaka, Y., Ohta, M. & Tanaka, K., Molecular cloning and characterization of a new human histamine Receptor, HH4R. *Biochem Biophys Res Commun* **2000,** *279* (2), 615-620, doi: 10.1006/bbrc.2000.4008.

30. Liu, C., Ma, X., Jiang, X., Wilson, S. J., Hofstra, C. L., Blevitt, J., Pyati, J., Li, X., Chai, W., Carruthers, N., et al., Cloning and pharmacological characterization of a fourth histamine receptor (H4) expressed in bone marrow. *Mol Pharmacol* **2001,** *59* (3), 420-426, doi: 10.1124/mol.59.3.420.

31. Nguyen, T., Shapiro, D. A., George, S. R., Setola, V., Lee, D. K., Cheng, R., Rauser, L., Lee, S. P., Lynch, K. R., Roth, B. L., et al., Discovery of a novel member of the histamine receptor family. *Mol Pharmacol* **2001,** *59* (3), 427-433, doi: 10.1124/mol.59.3.427.

32. Oda, T., Morikawa, N., Saito, Y., Masuho, Y. & Matsumoto, S., Molecular cloning and characterization of a novel type of histamine receptor preferentially expressed in leukocytes. *J Biol Chem* **2000,** *275* (47), 36781-36786, doi: 10.1074/jbc.M006480200.

33. Morse, K. L., Behan, J., Laz, T. M., West, R. E., Greenfeder, S. A., Anthes, J. C., Umland, S., Wan, Y., Hipkin, R. W., Gonsiorek, W., et al., Cloning and characterization of a novel human histamine receptor. *J Pharmacol Exp Ther* **2001,** *296* (3), 1058-1066.

34. Zhu, Y., Michalovich, D., Wu, H., Tan, K. B., Dytko, G. M., Mannan, I. J., Boyce, R., Alston, J., Tierney, L. A., Li, X., et al., Cloning, expression, and pharmacological characterization of a novel human histamine receptor. *Mol Pharmacol* **2001,** *59* (3), 434-441, doi: 10.1124/mol.59.3.434.

35. O'Reilly, M., Alpert, R., Jenkinson, S., Gladue, R. P., Foo, S., Trim, S., Peter, B., Trevethick, M. & Fidock, M., Identification of a histamine H4 receptor on human eosinophils- role in eosinophil chemotaxis. *J Recept Signal Transduct Res* **2002,** *22* (1-4), 431-448, doi: 10.1081/rrs-120014612.

36. Buckland, K. F., Williams, T. J. & Conroy, D. M., Histamine induces cytoskeletal changes in human eosinophils via the H4 receptor. *Br J Pharmacol* **2003,** *140* (6), 1117-1127, doi: 10.1038/sj.bjp.0705530.

37. Dijkstra, D., Leurs, R., Chazot, P., Shenton, F. C., Stark, H., Werfel, T. & Gutzmer, R., Histamine downregulates monocyte CCL2 production through the histamine H4 receptor. *J Allergy Clin Immunol* **2007,** *120* (2), 300-307, doi: 10.1016/j.jaci.2007.03.024.

38. Jemima, E. A., Prema, A. & Thangam, E. B., Functional characterization of histamine H4 receptor on human mast cells. *Molecular immunology* **2014,** *62* (1), 19-28, doi: 10.1016/j.molimm.2014.05.007.

39. Schneider, E. H., Schnell, D., Papa, D. & Seifert, R., High constitutive aactivity and a G-protein-independent high-affinity state of the human histamine H4-receptor. *Biochemistry* **2009,** *48* (6), 1424-1438, doi: 10.1021/bi802050d.

40. Olsen, R. H. J., DiBerto, J. F., English, J. G., Glaudin, A. M., Krumm, B. E., Slocum, S. T., Che, T., Gavin, A. C., McCorvy, J. D., Roth, B. L., et al., TRUPATH, an open-source biosensor platform for interrogating the GPCR transducerome. *Nat Chem Biol* **2020,** *16* (8), 841-849, doi: 10.1038/s41589-020-0535-8.

41. Okashah, N., Wan, Q., Ghosh, S., Sandhu, M., Inoue, A., Vaidehi, N. & Lambert, N. A., Variable G protein determinants of GPCR coupling selectivity. *Proc Natl Acad Sci U S A* **2019,** *116* (24), 12054-12059, doi: 10.1073/pnas.1905993116.

42. Avet, C., Mancini, A., Breton, B., Le Gouill, C., Hauser, A. S., Normand, C., Kobayashi, H., Gross, F., Hogue, M., Lukasheva, V., et al., Selectivity landscape of 100 therapeutically relevant GPCR profiled by an effector translocation-based BRET platform. *bioRxiv* **2020**, 2020.2004.2020.052027, doi: 10.1101/2020.04.20.052027.

43. Conklin, B. R., Farfel, Z., Lustig, K. D., Julius, D. & Bourne, H. R., Substitution of three amino acids switches receptor specificity of Gqα to that of Giα. *Nature* **1993,** *363* (6426), 274-276, doi: 10.1038/363274a0.

44. Flock, T., Hauser, A. S., Lund, N., Gloriam, D. E., Balaji, S. & Babu, M. M., Selectivity determinants of GPCR-G-protein binding. *Nature* **2017,** *545* (7654), 317-322, doi: 10.1038/nature22070.

45. Rasmussen, S. G., DeVree, B. T., Zou, Y., Kruse, A. C., Chung, K. Y., Kobilka, T. S., Thian, F. S., Chae, P. S., Pardon, E., Calinski, D., et al., Crystal structure of the β2 adrenergic receptor–Gs protein complex. *Nature* **2011,** *477* (7366), 549-555, doi: 10.1038/nature10361.

46. Inoue, A., Raimondi, F., Kadji, F. M. N., Singh, G., Kishi, T., Uwamizu, A., Ono, Y., Shinjo, Y., Ishida, S., Arang, N., et al., Illuminating G-protein-coupling selectivity of GPCRs. *Cell* **2019,** *177* (7), 1933-1947 e1925, doi: 10.1016/j.cell.2019.04.044.

47. Carpenter, B. & Tate, C. G., Engineering a minimal G protein to facilitate crystallisation of G protein-coupled receptors in their active conformation. *Protein Eng Des Sel* **2016,** *29* (12), 583-594, doi: 10.1093/protein/gzw049.

48. Nehmé, R., Carpenter, B., Singhal, A., Strege, A., Edwards, P. C., White, C. F., Du, H., Grisshammer, R. & Tate, C. G., Mini-G proteins: Novel tools for studying GPCRs in their active conformation. *PLoS One* **2017,** *12* (4), e0175642, doi: 10.1371/journal.pone.0175642.

49. Wan, Q., Okashah, N., Inoue, A., Nehmé, R., Carpenter, B., Tate, C. G. & Lambert, N. A., Mini G protein probes for active G protein-coupled receptors (GPCRs) in live cells. *J Biol Chem* **2018,** *293* (19), 7466-7473, doi: 10.1074/jbc.RA118.001975.

50. Wouters, E., Marin, A. R., Dalton, J. A. R., Giraldo, J. & Stove, C., Distinct dopamine D2 receptor antagonists differentially impact D2 receptor oligomerization. *Int J Mol Sci* **2019,** *20* (7), doi: 10.3390/ijms20071686.

51. Wouters, E., Walraed, J., Robertson, M. J., Meyrath, M., Szpakowska, M., Chevigne, A., Skiniotis, G. & Stove, C., Assessment of biased agonism among distinct synthetic cannabinoid receptor agonist scaffolds. *ACS Pharmacol Transl Sci* **2020,** *3* (2), 285-295, doi: 10.1021/acsptsci.9b00069.

52. Pottie, E., Tosh, D. K., Gao, Z. G., Jacobson, K. A. & Stove, C. P., Assessment of biased agonism at the A3 adenosine receptor using β-arrestin and miniGαi recruitment assays. *Biochem Pharmacol* **2020,** *177*, 113934, doi: 10.1016/j.bcp.2020.113934.

53. Pottie, E., Dedecker, P. & Stove, C. P., Identification of psychedelic new psychoactive substances (NPS) showing biased agonism at the 5-HT2AR through simultaneous use of β-arrestin 2 and miniG αq bioassays. *Biochem Pharmacol* **2020**, 114251, doi: 10.1016/j.bcp.2020.114251.

54. Höring, C., Seibel, U., Tropmann, K., Grätz, L., Mönnich, D., Pitzl, S., Bernhardt, G., Pockes, S. & Strasser, A., A dynamic, split-luciferase-based mini-G protein sensor to functionally characterize ligands at all four histamine receptor subtypes. *Int J Mol Sci* **2020,** *21* (22), 8440.

55. Garcia-Nafria, J., Lee, Y., Bai, X., Carpenter, B. & Tate, C. G., Cryo-EM structure of the adenosine A2A receptor coupled to an engineered heterotrimeric G protein. *Elife* **2018,** *7*, doi: 10.7554/eLife.35946.

56. Zhuang, Y., Xu, P., Mao, C., Wang, L., Krumm, B., Zhou, X. E., Huang, S., Liu, H., Cheng, X., Huang, X. P., et al., Structural insights into the human D1 and D2 dopamine receptor signaling complexes. *Cell* **2021,** *184* (4), 931-942.e918, doi: 10.1016/j.cell.2021.01.027.

57. Lin, X., Li, M., Wang, N., Wu, Y., Luo, Z., Guo, S., Han, G.-W., Li, S., Yue, Y., Wei, X., et al., Structural basis of ligand recognition and self-activation of orphan GPR52. *Nature* **2020,** *579* (7797), 152-157, doi: 10.1038/s41586-020-2019-0.

58. Garcia-Nafria, J., Nehmé, R., Edwards, P. C. & Tate, C. G., Cryo-EM structure of the serotonin 5-HT1B receptor coupled to heterotrimeric Go. *Nature* **2018,** *558* (7711), 620-623, doi: 10.1038/s41586-018-0241-9.

59. Kim, K., Che, T., Panova, O., DiBerto, J. F., Lyu, J., Krumm, B. E., Wacker, D., Robertson, M. J., Seven, A. B., Nichols, D. E., et al., Structure of a hallucinogen-activated Gq-coupled 5-HT2A serotonin receptor. *Cell* **2020,** *182* (6), 1574-1588 e1519, doi: 10.1016/j.cell.2020.08.024.

60. Kooistra, A. J., Mordalski, S., Pándy-Szekeres, G., Esguerra, M., Mamyrbekov, A., Munk, C., Keserű, G. M. & Gloriam, David E., GPCRdb in 2021: Integrating GPCR sequence, structure and function. *Nucleic Acids Res* **2020,** *49* (D1), D335-D343, doi: 10.1093/nar/gkaa1080.

61. Zhang, X., Johnson, R. M., Drulyte, I., Yu, L., Kotecha, A., Danev, R., Wootten, D., Sexton, P. M. & Belousoff, M. J., Evolving cryo-EM structural approaches for GPCR drug discovery. *Structure* **2021**, doi: 10.1016/j.str.2021.04.008.

62. Xia, R., Wang, N., Xu, Z., Lu, Y., Song, J., Zhang, A., Guo, C. & He, Y., Cryo-EM structure of the human histamine H1 receptor/Gq complex. *Nat Commun* **2021,** *12* (1), 2086, doi: 10.1038/s41467-021-22427-2.

63. Kaczor, A. A., Rutkowska, E., Bartuzi, D., Targowska-Duda, K. M., Matosiuk, D. & Selent, J., Computational methods for studying G protein-coupled receptors (GPCRs). *Methods Cell Biol* **2016,** *132*, 359-399, doi: 10.1016/bs.mcb.2015.11.002.

64. Wang, J. & Miao, Y., Recent advances in computational studies of GPCR-G protein interactions. *Adv Protein Chem Struct Biol* **2019,** *116*, 397-419, doi: 10.1016/bs.apcsb.2018.11.011.

65. Torrens-Fontanals, M., Stepniewski, T. M., Aranda-Garcia, D., Morales-Pastor, A., Medel-Lacruz, B. & Selent, J., How do Molecular Dynamics data complement static structural data of GPCRs. *Int J Mol Sci* **2020,** *21* (16), doi: 10.3390/ijms21165933.

66. Nygaard, R., Zou, Y., Dror, R. O., Mildorf, T. J., Arlow, D. H., Manglik, A., Pan, A. C., Liu, C. W., Fung, J. J., Bokoch, M. P., et al., The dynamic process of β 2-adrenergic receptor activation. *Cell* **2013,** *152* (3), 532-542, doi: 10.1016/j.cell.2013.01.008.

67. Mafi, A., Kim, S. K. & Goddard, W. A., 3rd, The atomistic level structure for the activated human kappa-opioid receptor bound to the full Gi protein and the MP1104 agonist. *Proc Natl Acad Sci U S A* **2020,** *117* (11), 5836-5843, doi: 10.1073/pnas.1910006117.

68. Lazim, R., Suh, D. & Choi, S., Advances in Molecular Dynamics Simulations and Enhanced Sampling Methods for the Study of Protein Systems. *Int J Mol Sci* **2020,** *21* (17), doi: 10.3390/ijms21176339.

69. Miao, Y., Feher, V. A. & McCammon, J. A., Gaussian accelerated Molecular Dynamics: Unconstrained enhanced sampling and free energy calculation. *J Chem Theory Comput* **2015,** *11* (8), 3584-3595, doi: 10.1021/acs.jctc.5b00436.

70. Pang, Y. T., Miao, Y., Wang, Y. & McCammon, J. A., Gaussian accelerated Molecular Dynamics in NAMD. *J Chem Theory Comput* **2017,** *13* (1), 9-19, doi: 10.1021/acs.jctc.6b00931.

71. Miao, Y. & McCammon, J. A., Gaussian accelerated Molecular Dynamics: Theory, implementation, and applications. *Annu Rep Comput Chem* **2017,** *13*, 231-278, doi: 10.1016/bs.arcc.2017.06.005.

72. Wang, J., Arantes, P. R., Bhattarai, A., Hsu, R. V., Pawnikar, S., Huang, Y.-m. M., Palermo, G. & Miao, Y., Gaussian accelerated molecular dynamics: Principles and applications. *WIREs Computational Molecular Science* **2021,** *n/a* (n/a), e1521, doi: 10.1002/wcms.1521.

73. Miao, Y., Feixas, F., Eun, C. & McCammon, J. A., Accelerated molecular dynamics simulations of protein folding. *J Comput Chem* **2015,** *36* (20), 1536-1549, doi: 10.1002/jcc.23964.

74. Miao, Y. & McCammon, J. A., Graded activation and free energy landscapes of a muscarinic G-protein–coupled receptor. *Proc Natl Acad Sci U S A* **2016,** *113* (43), 12162-12167, doi: 10.1073/pnas.1614538113.

75. Miao, Y. & McCammon, J. A., Mechanism of the G-protein mimetic nanobody binding to a muscarinic G-protein-coupled receptor. *Proc Natl Acad Sci U S A* **2018,** *115* (12), 3036-3041, doi: 10.1073/pnas.1800756115.

76. Wang, J. & Miao, Y., Mechanistic insights into specific G protein interactions with adenosine receptors. *J Phys Chem B* **2019,** *123* (30), 6462-6473, doi: 10.1021/acs.jpcb.9b04867.

77. Conrad, M., Soldner, C. A., Miao, Y. & Sticht, H., Agonist Binding and G Protein Coupling in Histamine H2 Receptor: A Molecular Dynamics Study. *Int J Mol Sci* **2020,** *21* (18), doi: 10.3390/ijms21186693.

78. Sali, A. & Blundell, T. L., Comparative protein modelling by satisfaction of spatial restraints. *J Mol Biol* **1993,** *234* (3), 779-815, doi: 10.1006/jmbi.1993.1626.

79. Söldner, C. A., Horn, A. H. C. & Sticht, H., Binding of histamine to the H1 receptor-a molecular dynamics study. *J Mol Model* **2018,** *24* (12), 346, doi: 10.1007/s00894-018-3873-7.

80. Hornak, V., Abel, R., Okur, A., Strockbine, B., Roitberg, A. & Simmerling, C., Comparison of multiple Amber force fields and development of improved protein backbone parameters. *Proteins* **2006,** *65* (3), 712-725, doi: 10.1002/prot.21123.

81. D.A. Case, D.S. Cerutti, T.E. Cheatham III, T.A. Darden, R.E. Duke, T.J. Giese, H. Gohlke, A.W. Goetz, D. Greene, N. Homeyer, et al., AMBER 2017. *University of California, San Francisco* **2017.**

82. Berendsen, H. J. C., van der Spoel, D. & van Drunen, R., GROMACS: A message-passing parallel molecular dynamics implementation. *Comput Phys Commun* **1995,** *91* (1), 43-56, doi: 10.1016/0010-4655(95)00042-E.

83. Siu, S. W., Vacha, R., Jungwirth, P. & Bockmann, R. A., Biomolecular simulations of membranes: Physical properties from different force fields. *J Chem Phys* **2008,** *128* (12), 125103, doi: 10.1063/1.2897760.

84. Toukan, K. & Rahman, A., Molecular-dynamics study of atomic motions in water. *Phys Rev B Condens Matter* **1985,** *31* (5), 2643-2648, doi: 10.1103/physrevb.31.2643.

85. Pándy-Szekeres, G., Munk, C., Tsonkov, T. M., Mordalski, S., Harpsøe, K., Hauser, A. S., Bojarski, A. J. & Gloriam, D. E., GPCRdb in 2018: Adding GPCR structure models and ligands. *Nucleic Acids Res* **2017,** *46* (D1), D440-D446, doi: 10.1093/nar/gkx1109.

86. Fiser, A., Do, R. K. G. & Šali, A., Modeling of loops in protein structures. *Protein Sci* **2000,** *9* (9), 1753-1773, doi: 10.1110/ps.9.9.1753.

87. Fiser, A. & Sali, A., ModLoop: Automated modeling of loops in protein structures. *Bioinformatics (Oxford, England)* **2003,** *19* (18), 2500-2501, doi: 10.1093/bioinformatics/btg362.

88. Miao, Y., Sinko, W., Pierce, L., Bucher, D., Walker, R. C. & McCammon, J. A., Improved reweighting of accelerated Molecular Dynamics simulations for free energy calculation. *J Chem Theory Comput* **2014,** *10* (7), 2677-2689, doi: 10.1021/ct500090q.

89. D.A. Case, I.Y. Ben-Shalom, S.R. Brozell, D.S. Cerutti, T.E. Cheatham III, V.W.D. Cruzeiro, T.A. Darden, R.E. Duke, D. Ghoreishi, M.K. Gilson, et al., AMBER 2018. *University of California, San Francisco* **2018.**

90. Kollman, P. A., Massova, I., Reyes, C., Kuhn, B., Huo, S., Chong, L., Lee, M., Lee, T., Duan, Y., Wang, W., et al., Calculating structures and free energies of complex molecules: Combining molecular mechanics and continuum models. *Accounts of chemical research* **2000,** *33* (12), 889-897, doi: 10.1021/ar000033j.

91. Genheden, S. & Ryde, U., The MM/PBSA and MM/GBSA methods to estimate ligand-binding affinities. *Expert Opin Drug Discov* **2015,** *10* (5), 449-461, doi: 10.1517/17460441.2015.1032936.

92. Wang, E., Sun, H., Wang, J., Wang, Z., Liu, H., Zhang, J. Z. H. & Hou, T., End-point binding free energy calculation with MM/PBSA and MM/GBSA: Strategies and applications in drug design. *Chem Rev* **2019,** *119* (16), 9478-9508, doi: 10.1021/acs.chemrev.9b00055.

93. Shannon, P., Markiel, A., Ozier, O., Baliga, N. S., Wang, J. T., Ramage, D., Amin, N., Schwikowski, B. & Ideker, T., Cytoscape: A software environment for integrated models of biomolecular interaction networks. *Genome Res* **2003,** *13* (11), 2498-2504, doi: 10.1101/gr.1239303.

94. Thomsen, W., Frazer, J. & Unett, D., Functional assays for screening GPCR targets. *Curr Opin Biotechnol* **2005,** *16* (6), 655-665, doi: 10.1016/j.copbio.2005.10.008.

95. Mehta, P., Miszta, P. & Filipek, S., Molecular modeling of histamine receptors - recent advances in drug discovery. *Molecules* **2021,** *26* (6), doi: 10.3390/molecules26061778.

96. Fleetwood, O., Matricon, P., Carlsson, J. & Delemotte, L., Energy landscapes reveal agonist's control of GPCR activation via microswitches. *bioRxiv* **2019**, 627026, doi: 10.1101/627026.

97. Dai, H., Fu, Q., Shen, Y., Hu, W., Zhang, Z., Timmerman, H., Leurs, R. & Chen, Z., The histamine H3 receptor antagonist clobenpropit enhances GABA release to protect against NMDA-induced excitotoxicity through the cAMP/protein kinase A pathway in cultured cortical neurons. *Eur J Pharmacol* **2007,** *563* (1-3), 117-123, doi: 10.1016/j.ejphar.2007.01.069.

98. Glukhova, A., Draper-Joyce, C. J., Sunahara, R. K., Christopoulos, A., Wootten, D. & Sexton, P. M., Rules of Engagement: GPCRs and G Proteins. *ACS Pharmacol Transl Sci* **2018,** *1* (2), 73-83, doi: 10.1021/acsptsci.8b00026.

99. Kenakin, T. & Onaran, O., The ligand paradox between affinity and efficacy: Can you be there and not make a difference? *Trends Pharmacol Sci* **2002,** *23* (6), 275-280, doi: 10.1016/s0165-6147(02)02036-9.

100. Lee, D., Lee, J. & Seok, C., What stabilizes close arginine pairing in proteins? *Phys Chem Chem Phys* **2013,** *15* (16), 5844-5853, doi: 10.1039/C3CP00160A.

101. Vondrášek, J., Mason, P. E., Heyda, J., Collins, K. D. & Jungwirth, P., The molecular origin of like-charge arginine−arginine pairing in water. *J Phys Chem B* **2009,** *113* (27), 9041-9045, doi: 10.1021/jp902377q.

102. Baumeister, P., Erdmann, D., Biselli, S., Kagermeier, N., Elz, S., Bernhardt, G. & Buschauer, A., [3H]UR-DE257: Development of a tritium-labeled squaramide-type selective histamine H2 receptor antagonist. *ChemMedChem* **2015,** *10* (1), 83-93, doi: 10.1002/cmdc.201402344.

103. Lim, H. D., van Rijn, R. M., Ling, P., Bakker, R. A., Thurmond, R. L. & Leurs, R., Evaluation of histamine H1-, H2-, and H3-receptor ligands at the human histamine H4 receptor: Identification of 4-methylhistamine as the first potent and selective H4 receptor agonist. *J Pharmacol Exp Ther* **2005,** *314* (3), 1310-1321, doi: 10.1124/jpet.105.087965.

104. Zhou, Q., Yang, D., Wu, M., Guo, Y., Guo, W., Zhong, L., Cai, X., Dai, A., Jang, W., Shakhnovich, E. I., et al., Common activation mechanism of class A GPCRs. *Elife* **2019,** *8*, doi: 10.7554/eLife.50279.

7. Summary

7.1. Summary and Outlook

In GPCR research, there is great interest in developing high-affinity and selective ligands as pharmacological tools and ultimately as drugs.[1-3] Traditionally, G protein-dependent functional responses have been assessed in [^{35}S]GTPγS binding assays reporting on the degree of G protein activation in response to agonists by the accumulation of nonhydrolyzable [^{35}S]GTPγS bound to Gα.[4-5] However, [^{35}S]GTPγS binding assays are confounded by the use of radionucleotides, the non-homogenous performance and low assay signal amplitudes that represent a major drawback for weakly expressed GPCRs. Therefore, the primary aim of this thesis was the development of an alternative G protein assay, which should overcome the latest disadvantages of [^{35}S]GTPγS binding assays and, in particular, be amenable to weakly expressed GPCRs, such as the histamine H_4 receptor.

In 2018, the utility of engineered mini-G proteins in live cell assays in addition to stabilizing active GPCR conformations for crystallization purposes was demonstrated by Wan and co-workers.[6] Motivated by the idea that the cytosolic nature of mini-G proteins in combination with the split-luciferase complementation (SLC) principle should improve assay sensitivity (i.e., signal-to-noise ratio) and signal-to-background (S/B) ratios compared to G protein sensors that make use of membrane-bound G proteins resulting in high background signals due to pre-association with GPCRs, SLC-based mini-G protein sensors were developed. For this purpose, the sequences encoding split-NanoLuc fragments, NlucC and NlucN, were fused to the C-termini of receptors and the N-termini of the mini-G proteins, mGs, mGsi and mGsq, respectively. In response to agonists, receptor conformational change promoted the recruitment of the corresponding mini-G protein, allowing the reconstitution of a functional luciferase. Advantageously, released bioluminescence, which was proportional to the amount of activated receptor, could be measured in real time. In particular, the use of the bright split-NanoLuc[7] luciferase allowed for the investigation of weakly expressed receptors.

One subproject of this thesis was dedicated to the development of mini-G protein sensors for the histamine receptor (HR) family comprising H_1R, H_2R, and $H_{3,4}$R (cf. Chapter 2), since these receptors have constituted well-studied drug targets at the institute. To demonstrate the suitability of mini-G protein recruitment assays for the pharmacological characterization of ligands as alternative to [^{35}S]GTPγS binding assays, H_1R/mGsq, H_2R/mGs and $H_{3,4}$R/mGsi sensors were characterized in detail. In general, excellent assay quality was obtained, including significantly higher signal amplitudes (H_1R: 12.56, H_2R: 4.39, H_3R: 6.61, H_4R: 1.75 fold over [^{35}S]GTPγS) and Z' factors between 0.5 and 1.0 (H_1R: 0.78 ± 0.07, H_2R: 0.85 ± 0.02, H_3R: 0.79 ± 0.04, H_4R: 0.68 ± 0.05; cf. Chapter 2).[8] Moreover, developed sensors served for the pharmacological characterization of standard agonists and

antagonists as well as example ligands, which were synthesized at the institute (UR-KUM530, UR-PI294).

Subsequently, the assay concept was applied to other GPCRs of interest at the institute, including dopamine $D_{1,2,5}$ receptors, muscarinic acetylcholine $M_{1,2,4,5}$ receptors, neuropeptide Y $Y_{2,4}$ receptors, the neurotensin NTS_1 receptor and the chemokine receptor CXCR4 (cf. Chapter 3). It is worth mentioning that the mGsi assay was the first assay available for CXCR4 at the institute, thus now offering the opportunity to characterize potential CXCR4 ligands, the development of which has recently become a research project in our laboratory. The determination of binding sites per cell in radioligand binding assays revealed that the receptor number did not correlate with obtained signal amplitudes, suggesting that each receptor provided an individual mini-G protein turnover. Furthermore, the mini-G protein sensor reversibility was confirmed by demonstrating that SLC responses could be completely blocked in all systems after the agonist has been displaced by an antagonist.

Since mini-G protein recruitment assays could be performed at low level receptor density recombinantly expressed in cells (~40,000 binding sites per cell, e.g., for H_3R and M_2R), it was of interest to determine whether mini-G protein sensors would detect the activation of endogenously expressed receptors (cf. Chapter 4). For this purpose, CRISPR/Cas9 experiments[9-10] were designed for attaching the small split-Nanoluc fragment, NlucC, to endogenous $\beta_{1,2}$AR in HEK293T cells. Albeit, most likely not all gene loci of the utilized aneuploid HEK293T cells were modified by CRISPR/Cas9 reactions, mGs sensors were able to report on the activation of $\beta_{1,2}$AR-NlucC at the endogenous receptor level. Despite significantly lower signal amplitudes (S/B) compared with overexpressed sensors, mGs sensors specifically recognized receptor activation in response to full and partial agonists at the endogenous receptor level. In the future, the generation of $\beta_{1,2}$AR-NlucC fusion proteins under endogenous promotion should enable the evaluation of other signal transducer interactions, including β-arrestins, G protein-coupled receptor kinases (GRKs), or mini-G proteins of other G-protein families, when fused to NlucN.

Another subproject of this thesis was dedicated to the elucidation of GPCR – G protein coupling profiles using mini-G protein sensors (cf. Chapter 5). Due to the chimeric nature of mini-G proteins, it was of particular interest to examine whether obtained coupling profiles were consistent with reported interactions. Since a correlation between assay signal amplitudes and mini-G protein expression was observed for histamine receptors in Chapter 2, the amounts of plasmid DNA used were optimized to obtain comparable protein expression in HEK293T cells after transient transfection. Overall, 22 GPCRs were characterized and, in addition to appropriate primary G protein coupling,[11] strong secondary interaction was obtained for D_1R, adenosine A_{2B} receptor, H_1R, M_1R, M_5R and NTS_1R with mGsi. In future projects, it may be of interest to determine whether

the observed GPCR - G protein coupling profiles can be altered by ligands, thus providing a drug target.

In a computer-based approach, the dynamics of mini-G protein binding were assessed more in detail for H_2R and H_4R using Gaussian accelerated molecular dynamics (GaMD) simulations. In GaMD, a harmonic boost potential is applied to the system to cross high energy barriers and thus allow the system to achieve another conformation.[12-13] Overall, the canonical systems, H_2R-mGs and H_4R-mGsi, were the most stable systems and the weaker coupled systems, H_2R-mGsi and H_2R-mGsq were more dynamic. With the knowledge from the mini-G protein recruitment assays that H_2R interacted with both mGs, mGsi, and mGsq, the observation that all mini-G proteins occupied a Gs-like position in complex with H_2R gained significance. In agreement with the hypothesis that GPCRs accommodate G proteins in a designated position, GaMD revealed that mGs and mGsq, in contrast to mGsi, could not occupy the Gi-like position at H_4R, which exclusively coupled to mGsi in mini-G recruitment assays.

In summary, a modern G protein-dependent assay platform has been established for the functional characterization of ligands at a total of 22 different GPCRs. Not least, its usefulness for pharmacological testing is highlighted by the fact that the mini-G protein recruitment concept has become widely accepted in drug discovery during the preparation of this thesis.[14-21] In addition to the development of protocols for the routine testing of full, partial and inverse agonists as well as antagonists, assay and data analysis protocols have been established for the investigation of GPCR – G protein coupling profiles under uniform mini-G protein expression levels. In addition, the computational analysis of $H_{2,4}R$ coupling profiles to mGs, mGsi, and mGsq using GaMD simulations provided dynamic insight into the respective complex formation and suggested that GPCRs need to allow a specific orientation of the G protein in the receptor binding cavity (e.g., in a Gs- or Gi-like position) as a prerequisite for successful coupling. Ultimately, as a proximal G protein-dependent cell assay of high quality, the mini-G protein recruitment assay should be well suited to assess structure-activity relationships of ligands in terms of pathway bias for different types of G proteins or β-arrestins, optionally at the endogenous receptor level.

7.2. References

1. Hauser, A. S., Attwood, M. M., Rask-Andersen, M., Schioth, H. B. & Gloriam, D. E., Trends in GPCR drug discovery: New agents, targets and indications. *Nat Rev Drug Discov* **2017,** *16* (12), 829-842, doi: 10.1038/nrd.2017.178.
2. Wacker, D., Stevens, R. C. & Roth, B. L., How ligands illuminate GPCR molecular pharmacology. *Cell* **2017,** *170* (3), 414-427, doi: 10.1016/j.cell.2017.07.009.
3. Conner, J. W., Poole, D. P., Jorg, M. & Veldhuis, N. A., New small molecule fluorescent probes for G protein-coupled receptors: Valuable tools for drug discovery. *Future Med Chem* **2021,** *13* (1), 63-90, doi: 10.4155/fmc-2019-0327.
4. Strange, P. G., Use of the GTP γ S ([35S]GTP γ S and Eu-GTP γ S) binding assay for analysis of ligand potency and efficacy at G protein-coupled receptors. *Br J Pharmacol* **2010,** *161* (6), 1238-1249, doi: 10.1111/j.1476-5381.2010.00963.x.
5. Milligan, G., Principles: Extending the utility of [35S]GTP γ S binding assays. *Trends Pharmacol Sci* **2003,** *24* (2), 87-90, doi: 10.1016/s0165-6147(02)00027-5.
6. Wan, Q., Okashah, N., Inoue, A., Nehmé, R., Carpenter, B., Tate, C. G. & Lambert, N. A., Mini G protein probes for active G protein-coupled receptors (GPCRs) in live cells. *J Biol Chem* **2018,** *293* (19), 7466-7473, doi: 10.1074/jbc.RA118.001975.
7. Dixon, A. S., Schwinn, M. K., Hall, M. P., Zimmerman, K., Otto, P., Lubben, T. H., Butler, B. L., Binkowski, B. F., Machleidt, T., Kirkland, T. A., et al., NanoLuc complementation reporter optimized for accurate measurement of protein interactions in cells. *ACS Chem Biol* **2016,** *11* (2), 400-408, doi: 10.1021/acschembio.5b00753.
8. Zhang, J. H., Chung, T. D. & Oldenburg, K. R., A simple statistical parameter for use in evaluation and validation of high throughput screening assays. *J Biomol Screen* **1999,** *4* (2), 67-73, doi: 10.1177/108705719900400206.
9. Cong, L., Ran, F. A., Cox, D., Lin, S., Barretto, R., Habib, N., Hsu, P. D., Wu, X., Jiang, W., Marraffini, L. A., et al., Multiplex genome engineering using CRISPR/Cas systems. *Science* **2013,** *339* (6121), 819-823, doi: 10.1126/science.1231143.
10. Doudna, J. A. & Charpentier, E., The new frontier of genome engineering with CRISPR-Cas9. *Science* **2014,** *346* (6213), 1258096, doi: doi:10.1126/science.1258096.
11. Alexander, S. P. H., Christopoulos, A., Davenport, A. P., Kelly, E., Mathie, A., Peters, J. A., Veale, E. L., Armstrong, J. F., Faccenda, E., Harding, S. D., et al., The concise guide to pharmacology 2019/20: G protein-coupled receptors. *Br J Pharmacol* **2019,** *176* (S1), S21-S141, doi: 10.1111/bph.14748.
12. Miao, Y. & McCammon, J. A., Gaussian accelerated Molecular Dynamics: Theory, implementation, and applications. *Annu Rep Comput Chem* **2017,** *13*, 231-278, doi: 10.1016/bs.arcc.2017.06.005.
13. Wang, J., Arantes, P. R., Bhattarai, A., Hsu, R. V., Pawnikar, S., Huang, Y.-m. M., Palermo, G. & Miao, Y., Gaussian accelerated molecular dynamics: Principles and applications. *WIREs Computational Molecular Science* **2021,** *n/a* (n/a), e1521, doi: 10.1002/wcms.1521.
14. Wouters, E., Marin, A. R., Dalton, J. A. R., Giraldo, J. & Stove, C., Distinct dopamine D2 receptor antagonists differentially impact D2 receptor oligomerization. *Int J Mol Sci* **2019,** *20* (7), doi: 10.3390/ijms20071686.
15. Wouters, E., Walraed, J., Robertson, M. J., Meyrath, M., Szpakowska, M., Chevigne, A., Skiniotis, G. & Stove, C., Assessment of biased agonism among distinct synthetic cannabinoid receptor agonist scaffolds. *ACS Pharmacol Transl Sci* **2020,** *3* (2), 285-295, doi: 10.1021/acsptsci.9b00069.

16. Vasudevan, L., Vandeputte, M., Deventer, M., Wouters, E., Cannaert, A. & Stove, C. P., Assessment of structure-activity relationships and biased agonism at the μ opioid receptor of novel synthetic opioids using a novel, stable bio-assay platform. *Biochem Pharmacol* **2020,** *177*, 113910, doi: 10.1016/j.bcp.2020.113910.

17. Pottie, E., Dedecker, P. & Stove, C. P., Identification of psychedelic new psychoactive substances (NPS) showing biased agonism at the 5-HT2AR through simultaneous use of β-arrestin 2 and miniG αq bioassays. *Biochem Pharmacol* **2020**, 114251, doi: 10.1016/j.bcp.2020.114251.

18. Pottie, E., Tosh, D. K., Gao, Z. G., Jacobson, K. A. & Stove, C. P., Assessment of biased agonism at the A3 adenosine receptor using β-arrestin and miniG αi recruitment assays. *Biochem Pharmacol* **2020,** *177*, 113934, doi: 10.1016/j.bcp.2020.113934.

19. Martemyanov, K. A. & Garcia-Marcos, M., Making useful gadgets with miniaturized G proteins. *J Biol Chem* **2018,** *293* (19), 7474-7475, doi: 10.1074/jbc.H118.002879.

20. Bondar, A. & Lazar, J., Optical sensors of heterotrimeric G protein signaling. *The FEBS journal* **2021,** *288* (8), 2570-2584, doi: 10.1111/febs.15655.

21. Jullié, D., Valbret, Z. & Stoeber, M., Optical tools to study the subcellular organization of GPCR neuromodulation. *J Neurosci Methods* **2022,** *366*, 109408, doi: 10.1016/j.jneumeth.2021.109408.

8. Appendix

8.1. Appendix to Chapter 2

```
>mGs (mini-Gs393)
MIEKQLQKDKQVYRATHRLLLLGADNSGKSTIVKQMRILHGGSGGSGGTSGIFETKFQVDKVNFHMFDVGGQRDER
RKWIQCFNDVTAIIFVVDSSDYNRLQEALNDFKSIWNNRWLRTISVILFLNKQDLLAEKVLAGKSKIEDYFPEFAR
YTTPEDATPEPGEDPRVTRAKYFIRDEFLRISTASGDGRHYCYPHFTCAVDTENARRIFNDCRDIIQRMHLRQYELL

>mGsi (miniGs/i43)
MIEKQLQKDKQVYRATHRLLLLGADNSGKSTIVKQMRILHGGSGGSGGTSGIFETKFQVDKVNFHMFDVGGQRDER
RKWIQCFNDVTAIIFVVDSSDYNRLQEALNDFKSIWNNRWLRTISVILFLNKQDLLAEKVLAGKSKIEDYFPEFAR
YTTPEDATPEPGEDPRVTRAKYFIRDEFLRISTASGDGRHYCYPHFTCAVDTENARRIFNDVTDIIIKMNLRDCGLF

>mGsq (miniGs/q71)
MIEKQLQKDKQVYRRTLRLLLLGADNSGKSTIVKQMRILHGGSGGSGGTSGIFETKFQVDKVNFHMFDVGGQRDER
RKWIQCFNDVTAIIFVVDSSDYNRLQEALNDFKSIWNNRWLRTISVILFLNKQDLLAEKVLAGKSKIEDYFPEFAR
YTTPEDATPEPGEDPRVTRAKYFIRKEFVDISTASGDGRHICYPHFTCAVDTENARRIFNDCKDIILQMNLREYNLV
```

Figure A1. Protein sequences of utilized mini-G proteins mGs, mGsi and mGsq according to Nehmé et al.[1]

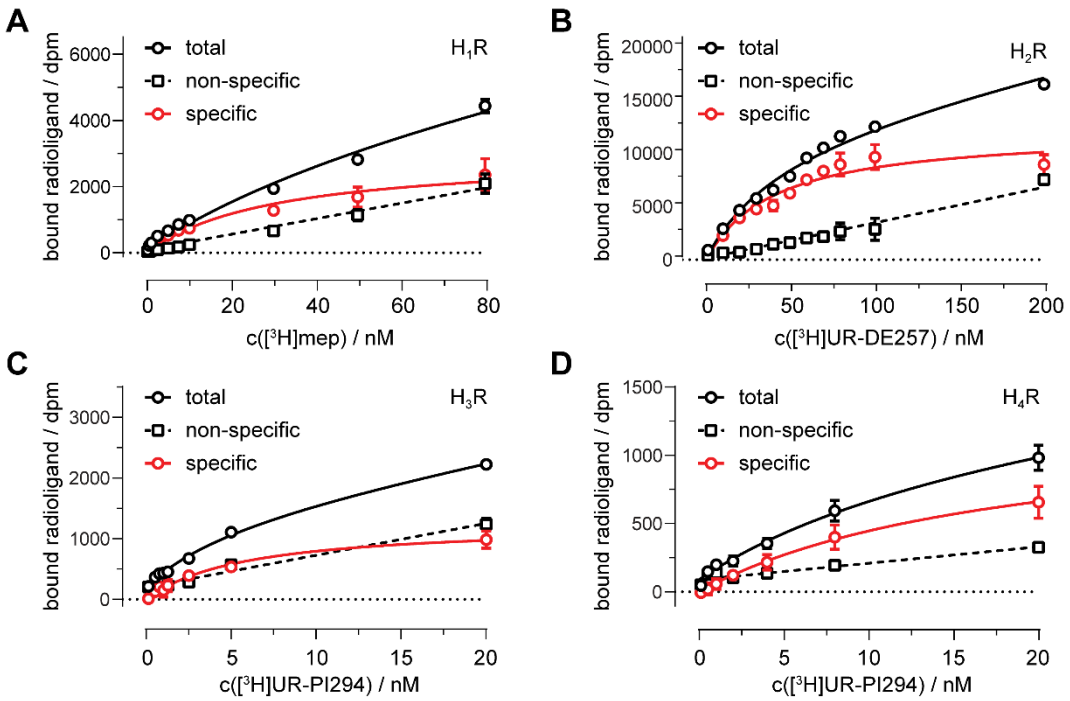

Figure A2. Representative binding isotherms from radioligand saturation binding assays using HEK293T cells stably co-expressing the histamine H_{1-4} receptors in combination with either mGsq, mGs or mGsi. Representative data from saturation binding experiments of A) [^{3}H]mepyramine ([^{3}H]mep) at the H_1R, B) [^{3}H]UR-DE257 at the H_2R and C) [^{3}H]UR-PI294 at the H_3R and D) H_4R are plotted. The nonspecific binding of each radioligand concentration was determined in the presence of either 10 µM diphenhydramine (H_1R), famotidine (H_2R), histamine (H_3R) or thioperamide (H_4R), respectively.

Table A1. Dissociation constants (pK_d) of radioligands determined in saturation binding experiments using HEK293T cells stably co-expressing either the H_1R-NlucC/ NlucN-mGsq, H_2R-NlucC/NlucN-mGs, H_3R-NlucC/NlucN-mGsi or H_4R-NlucC/NlucN-mGsi. Presented data are means ± SEM of at least three experiments (*N* = 3) each performed in triplicate.

		Radioligand Saturation Binding			Literature
Subtype	Radioligand	pK_d ± SEM	B_{max} ± SEM	Binding Sites / Cell ± SEM	pK_d
H_1R	[^{3}H]mep	7.59 ± 0.08	2224 ± 364	377,111 ± 61,750	8.35[2]
H_2R	[^{3}H]DE257	7.35 ± 0.08	10070 ± 1664	1,038,127 ± 171,508	7.26[3]
H_3R	[^{3}H]PI294	8.37 ± 0.12	1130 ± 118	41,103 ± 4,300	8.96[4]
H_4R	[^{3}H]PI294	7.85 ± 0.07	1568 ± 503	50,848 ± 12,349	8.29[4]

Reference pK_d values were obtained for the indicated radioligands in radioligand saturation binding experiments using membrane preparations of *Sf*9 cells (co-) expressing either the hH_1R and RGS4[2a], hH_2R-Gα_s fusion protein[3] or hH_3R, Gα_{i2} and G$\beta_1\gamma_2$.[4]

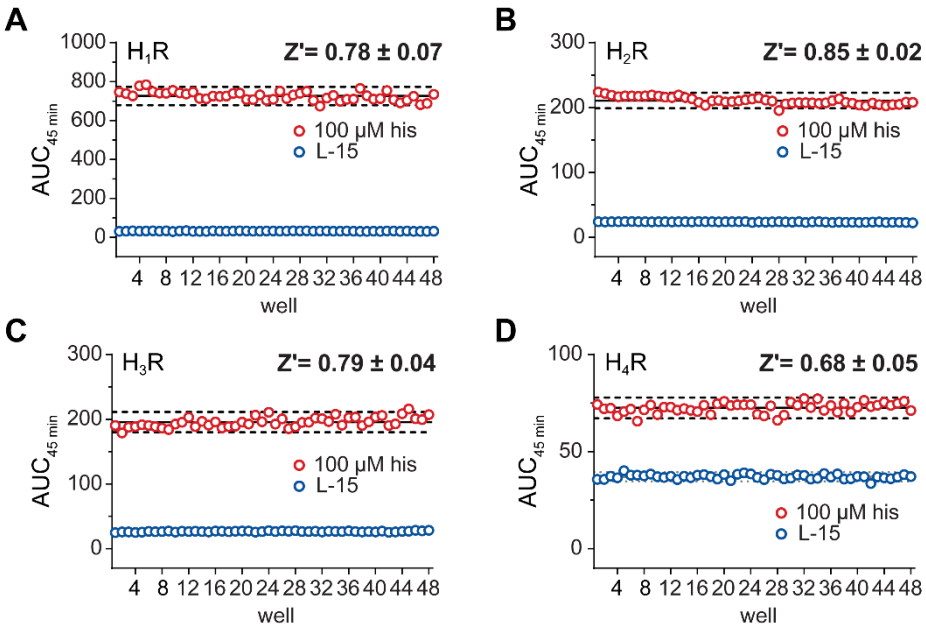

Figure A3. Representative signals used for the determination of the Z' factor. Area under curves (AUC) of 100 µM histamine and Leibovitz' L-15 as buffer control for each well using HEK293T cells stably co-expressing A) NlucN-mGsq/H_1R-NlucC, B) NlucN-mGs/H_2R-NlucC, C) NlucN-mGsi/H_3R-NlucC or D) NlucN-mGsi/H_4R-NlucC fusion proteins are plotted. Presented data are from representative plates. Indicated Z' are means ± SEM of at least three experiments (*N* = 3).

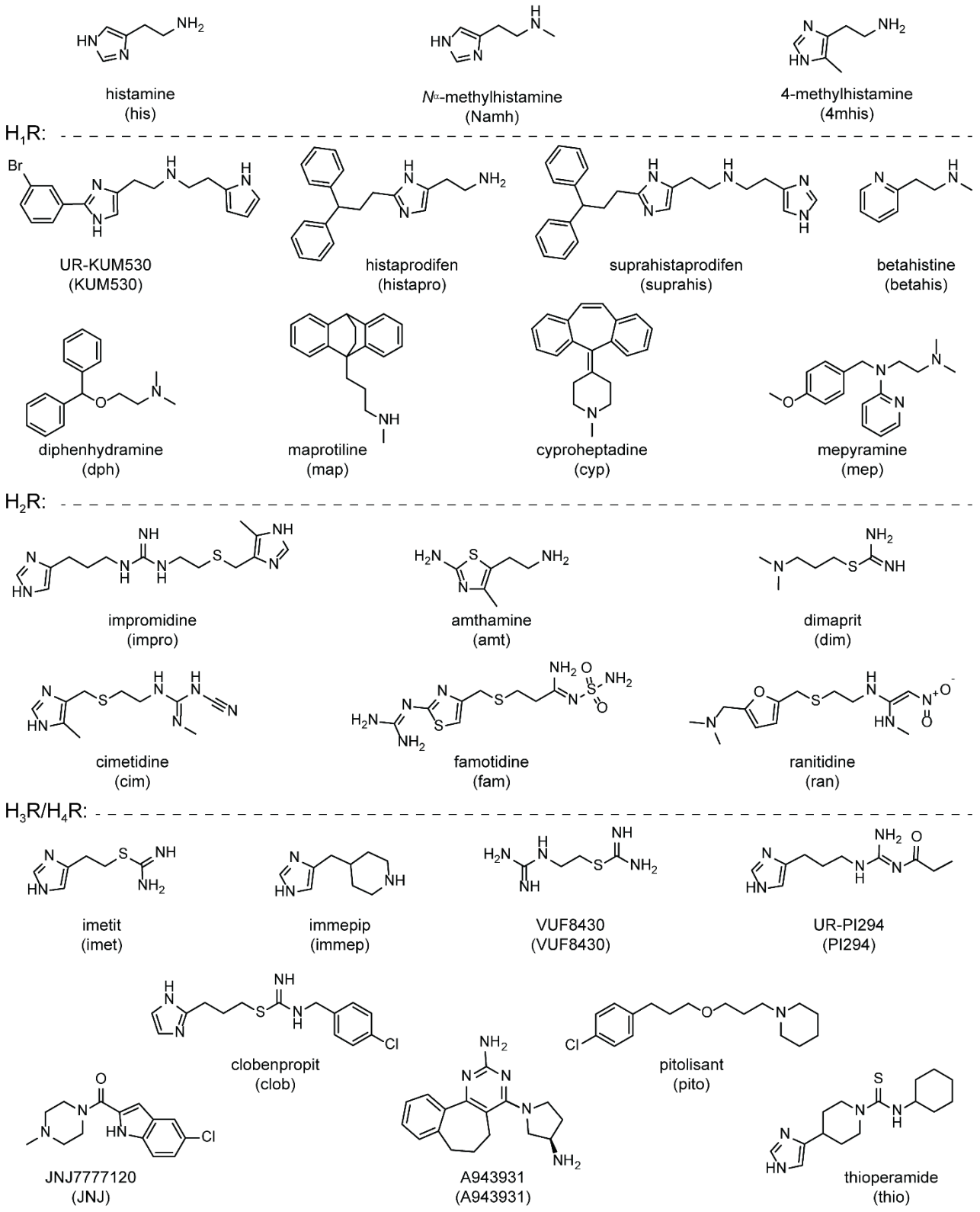

Figure A4. Structures of investigated histamine receptor ligands.

Method A1. [^{35}S]GTPγS binding assay at the H_1R (protocol) performed by Ulla Seibel-Ehlert.

Cloning and protein expression.

The pcDNA3.1 vector encoding the human H_1 receptor, the $G\alpha_q$, the $G\beta_1$ or the $G\gamma_2$ sequences were from the cDNA Resource Center (Rolla, MO, USA). For cloning of H_1R into the pFastBac1 vector,[7] the receptor was amplified using the PCR protocol for Phusion® DNA polymerase (New England Biolabs, Frankfurt a. M., Germany). A *Bam*HI restriction site was added at the 5'-end, followed by HA and FLAG tag and a *Hin*dIII restriction site at the 3'-end. This construct was inserted into the linearized vector according to the NEBuilder HiFi DNA Assembly Reaction Protocol (New England Biolabs, Frankfurt a. M.). The cDNA of the G proteins was amplified as described above, introducing a *Bam*HI restriction site at the 5'- and a *Hin*dIII at the 3'-end, and cloned into the pFastBac1 backbone via restriction endonuclease reaction protocol. The sequences were verified by sequencing. These pFastBac1 constructs were subsequently used for the generation of recombinant bacmids according to the manufacturer's instructions (Invitrogen). The H_1R and the G proteins $G\alpha_q$, $G\beta_1$ and $G\gamma_2$ were co-expressed using the Bac-to-Bac Baculovirus Expression System (Invitrogen). *Spodoptera frugiperda* (*Sf*9) cells were seeded into a 6-well plate (Sarstedt, Nümbrecht, Germany) at a density of 0.8 x 10^6 cells/well in InsectXpress medium (Lonza, USA) without FCS. The transfection with bacmids was performed as described in manufacturer's instructions (Invitrogen) but using XtremeGENE™ HP (Roche Diagnostics, Mannheim, Germany) as transfection reagent. After an incubation period of 5 h at 27 °C the transfection mixture was replaced by 2 mL of full growth medium (InsectXpress supplemented with 5% FCS). The P1 baculoviruses were isolated after the *Sf*9 cells were incubated for 72 h at 27 °C, when signs of infection were visible. Amplification of the virus stock was achieved by infecting 30 mL of Sf9 cells (2 x 10^6 cells/mL) with 2 mL of P1 and P2 baculoviruses were harvested after 48 h. A further amplification step was performed using 50 mL Sf9 cells (1 x 10^6 cells/mL) and 2.5 mL of P2 to obtain high-titer P3 baculoviruses after 48 h of incubation at 27 °C. To prepare membranes from *Sf*9 cells co-expressing the H_1R + $G\alpha_q$ + $G\beta_1$ + $G\gamma_2$, the cells (50 mL, 1 x 10^6 cells/mL) were co-infected with 2.5 mL of the corresponding P3 virus stocks and incubated for 48 h at 27 °C. Isolation and storage of the membranes as well as the determination of protein concentration was performed as described previously.[8-9] The receptor expression was determined with saturation binding experiments using [^{3}H]mepyramine as radiolabeled tracer as described previously[10] and 0.5 – 1 µg protein/well. The determined pK_d = 7.93 ± 0.06 nM differs slightly from the literature value (pK_d = 8.35).[11-12]

[^{35}S]GTPγS binding assay procedure.

The [^{35}S]GTPγS assay was essentially performed as described previously by Lazewska et al. (2019) with following modifications:[13] The amount of protein was reduced to 1 µg/well and the saponin concentration was decreased to 50 µg/mL. The antagonist mode was performed in the presence of 30 µM histamine.

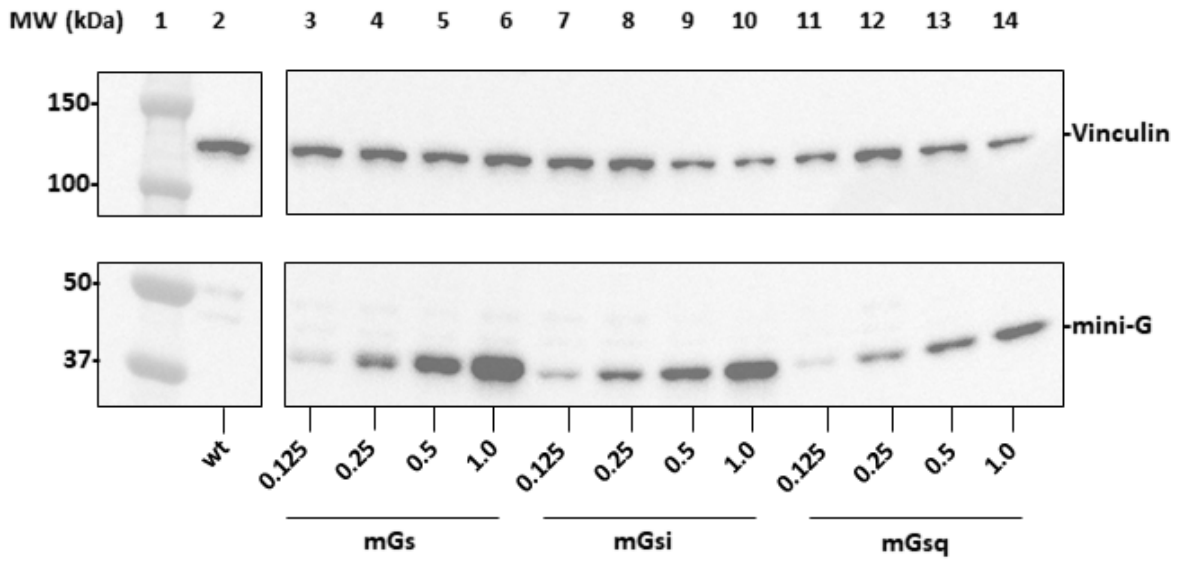

Figure A5. Western blot analysis of HEK293T cell lysates expressing the NlucN-mini-G fusion proteins. Lanes contain a protein marker (lane 1) and cell lysates of either HEK293T wildtype (wt; lane 2) as negative control or HEK293T cells expressing NlucN-mGs (lanes 3-6), NlucN-mGsi (lanes 7-10) or NlucN-mGsq (lanes 11-14) that were transiently transfected with indicated plasmid DNA amounts (µg) encoding NlucN-mG fusion proteins. For primary staining, α-Nluc (rat; 1:5,000 in PBS-T) and α-vinculin (mouse; 1:500 in PBS-T) antibodies were used and for secondary staining α-rabbit (HRP-conjugated; 1:10,000 in PBS-T) and α-mouse (HRP-conjugated; 1:100,000 in PBS-T) were used, both raised against IgG. Shown is a superposition of the colorimetric and Chemi Hi resolution images captured with a ChemiDoc MP imager (Bio-Rad).

Table A2. Binding affinities (pK_i, $pK_{i,low}$, $pK_{i,high}$) of ligands at the H_2R. 50 nM [^{3}H]UR-DE257 were displaced by the indicated H_2R ligand. Utilized HEK293T cells either stably co-expressed the H_2R-NlucC and NlucN-mGs constructs or were transiently transfected with indicated plasmid DNA amounts (µg; H_2R + mGs) of the latter. Data represent means ± SEM of at least three independent experiments each performed in triplicate for stable transfectants and in duplicate for transient transfectants.

Cell Strain		Radioligand Competition Binding			Literature
(µg DNA)	Compound	$pK_{b,low}$ ± SEM	$pK_{b,high}$ ± SEM	pK_b ± SEM	pK_b
stable	his	3.87 ± 0.13	6.94 ± 0.14	--	6.27[a,3], 4.37[b,5]
stable	fam	--	--	7.68 ± 0.01	7.8[c,6]
transient (1.0 + 0.0)	his	--	--	3.55 ± 0.09	
transient (1.0 + 0.25)	his	3.14 ± 0.17	5.98 ± 0.12	--	
transient (1.0 + 0.5)	his	3.63 ± 0.80	6.49 ± 0.08	--	
transient (1.0 + 1.0)	his	3.90 ± 0.18	7.37 ± 0.12	--	

Reference data is reported from experiments using [a,b][^{3}H]UR-DE257 with membrane preparations of *Sf*9 cells expressing a hH_2R-$G\alpha_s$ fusion protein[3,5] or [c][^{125}I]iodoaminopotentidine with membrane preparations of CHO cells expressing the hH_2R[6]. While assay buffers for [a] were without NaCl, the assay buffers for [b] contained 145 mM NaCl.

8.2. Appendix to Chapter 3

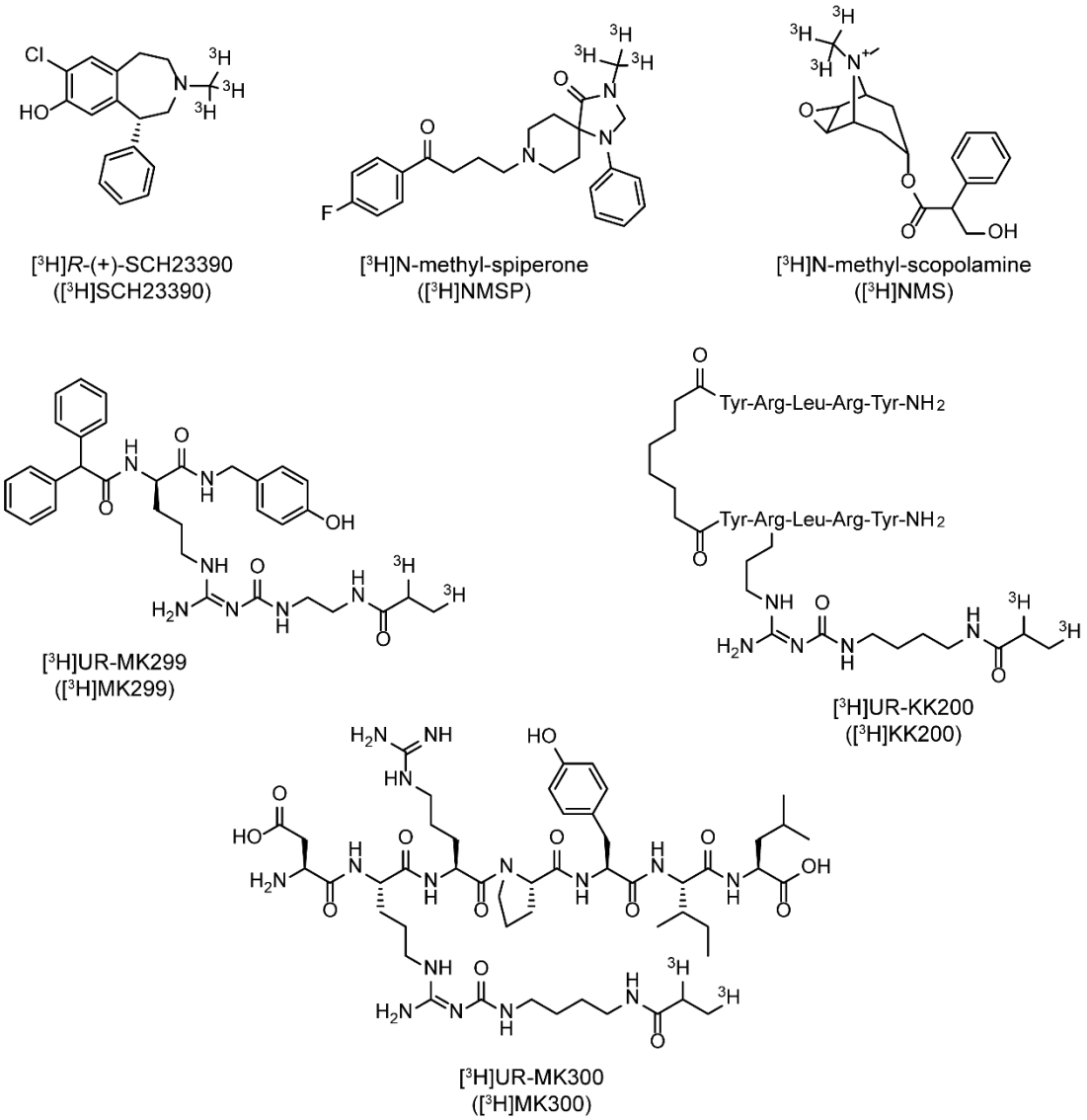

Figure A6. Structures of utilized radioligands.

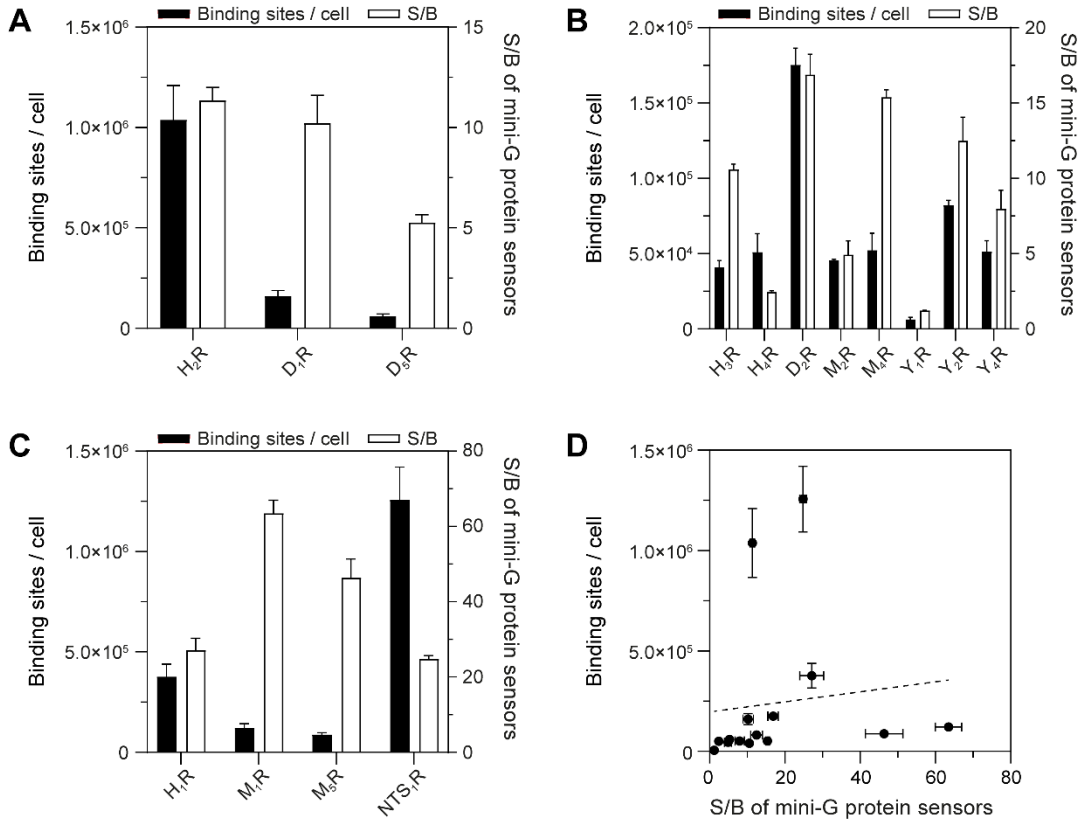

Figure A7. Number of binding sites per cell and signal-to-background (S/B) ratios of mini-G sensors consisting of given GPCR-NlucC and A) NlucN-mGs, B) NlucN-mGsi and C) NlucN-mGsq fusion proteins. For each cell strain, the number of binding sites per cell was determined by radioligand saturation binding as described in section 3.2.5. S/B ratios were calculated using peak or plateau values of the relative increase in luminescence upon receptor stimulation using the endogenous or reference agonist at maximal concentration, respectively. D) A scatter plot of the number of binding sites and S/B ratios demonstrating the missing correlation between the data sets. The dashed regression line (Y = 2,491*x + 197,124) was calculated using a simple linear regression. Data represent mean ± SEM of at least three independent experiments (*N* = 3), each performed in triplicate.

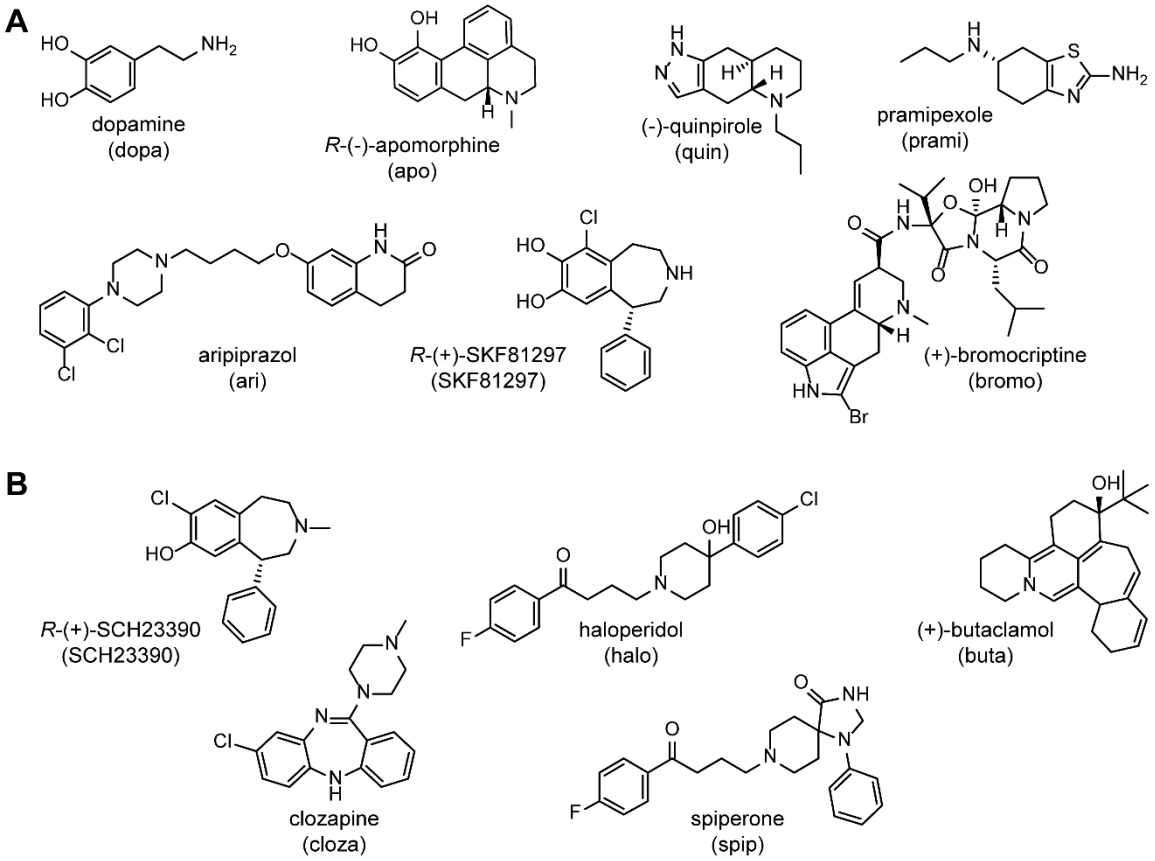

Figure A8. Structures of investigated dopamine receptor ligands classified as A) agonists and B) antagonists.

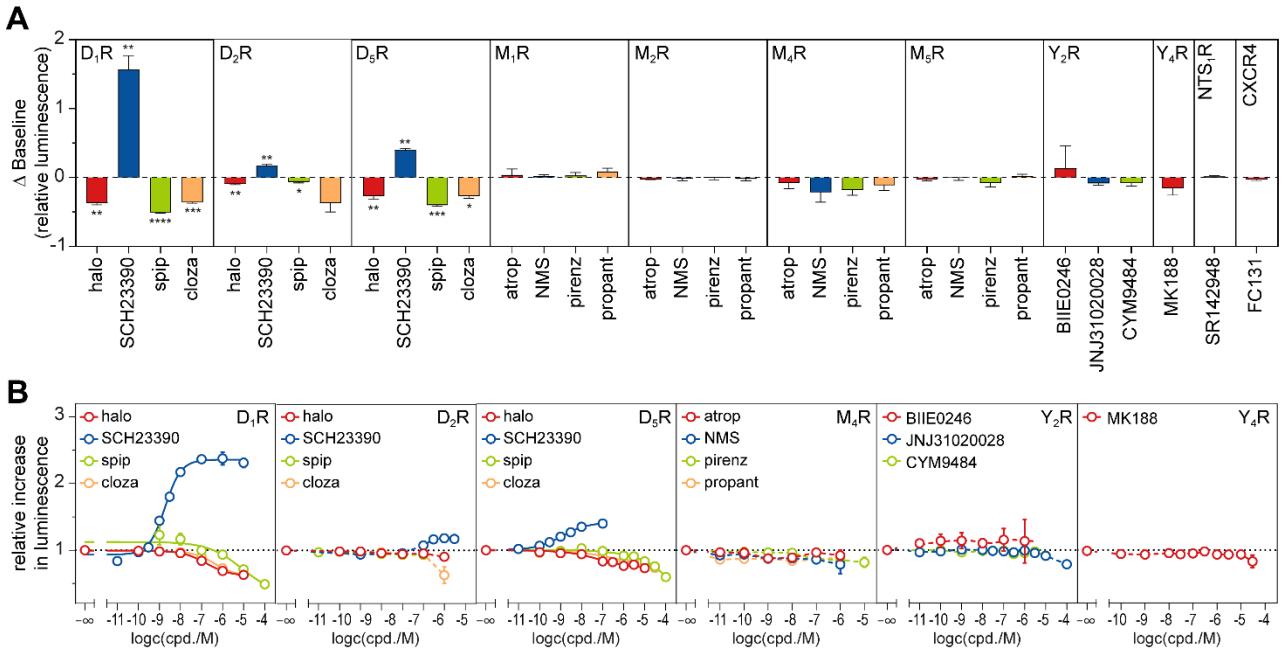

Figure A9. A) Changes in the relative increase in luminescence (Δ Baseline = (Ligand (max. conc.) - L-15)*100%) for ligands reported as antagonists at HEK293T cells stably co-expressing D_1R-NlucC/NlucN-mGs, D_2R-NlucC/NlucN-mGsi, D_5R-NlucC/NlucN-mGs, M_1R-NlucC/NlucN-mGsq, M_2R-NlucC/NlucN-mGsi, M_4R-NlucC/NlucN-mGsi, M_5R-NlucC/NlucN-mGsq, NTS_1R-NlucC/NlucN-mGsq, Y_2R-NlucC/NlucN-mGsi, Y_4R-NlucC/NlucN-mGsi or CXCR4-NlucC/NlucN-mGsi fusion proteins. Signals obtained for the maximal antagonist concentration and L-15 after 15 min incubation were considered. B) Full concentration response curves of antagonist signals at GPCRs with noticeable changes in basal luminescence shown in (A) calculated using the relative increase in luminescence after 15 min obtained in the mini-G protein recruitment assay. Data represent means ± SEM of at least three independent experiments (*N* = 3) performed in triplicate. Significant changes in relative luminescence were observed for dopamine receptor antagonists using a one sample t test (*: $p < 0.05$; **: $p < 0.01$; ***: $p < 0.005$; ****: $p < 0.001$).

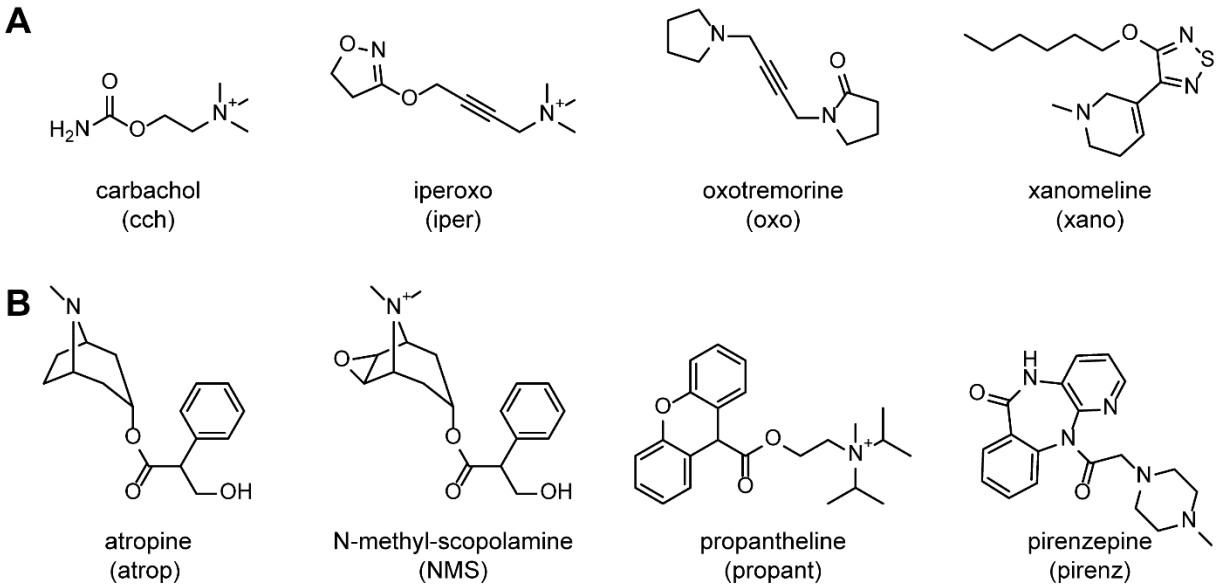

Figure A10. Structures of investigated muscarinic acetylcholine receptor ligands classified as A) agonists and B) antagonists.

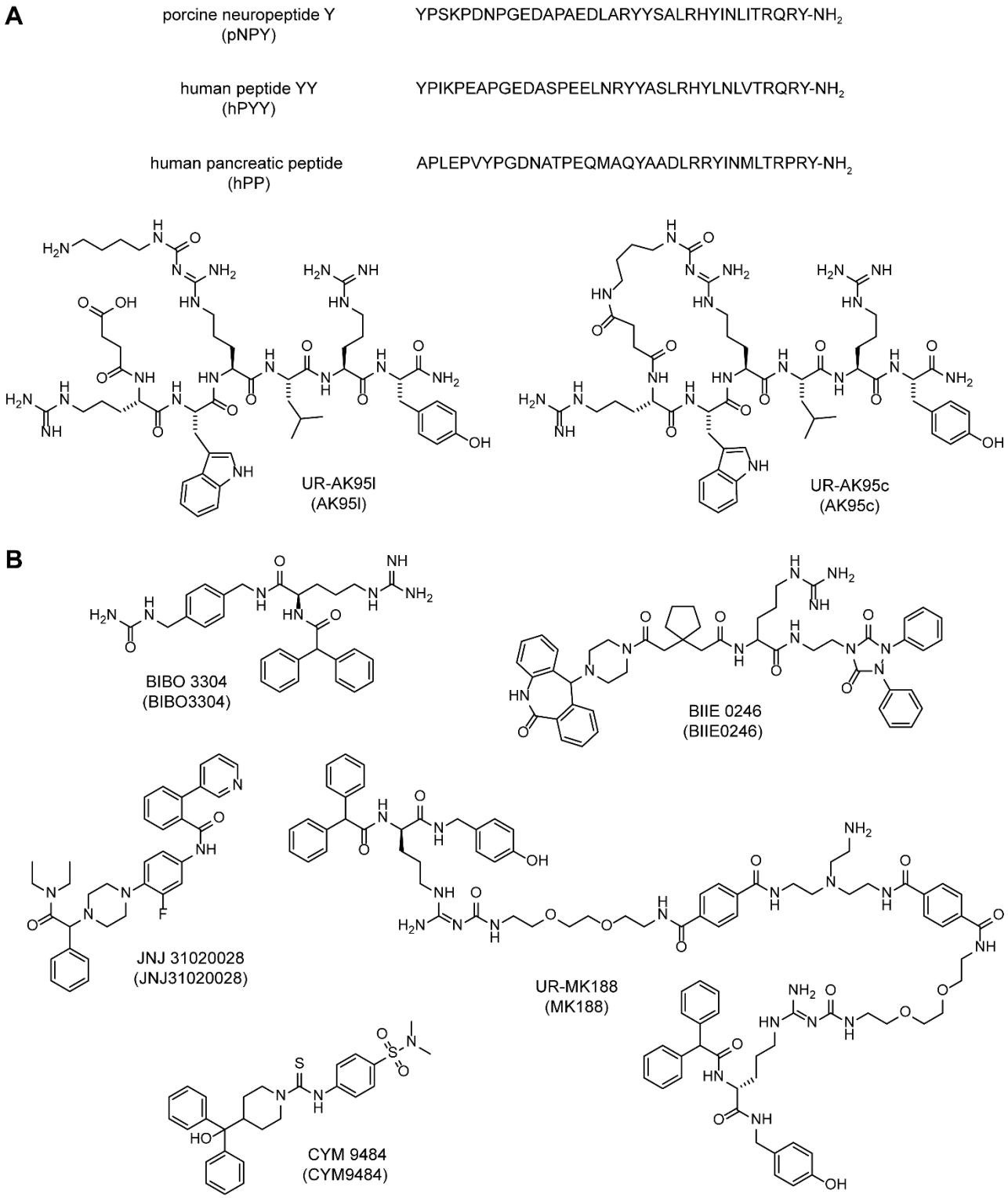

Figure A11. Protein sequences or structures of investigated neuropeptide Y receptor ligands classified as A) agonists and B) antagonists.

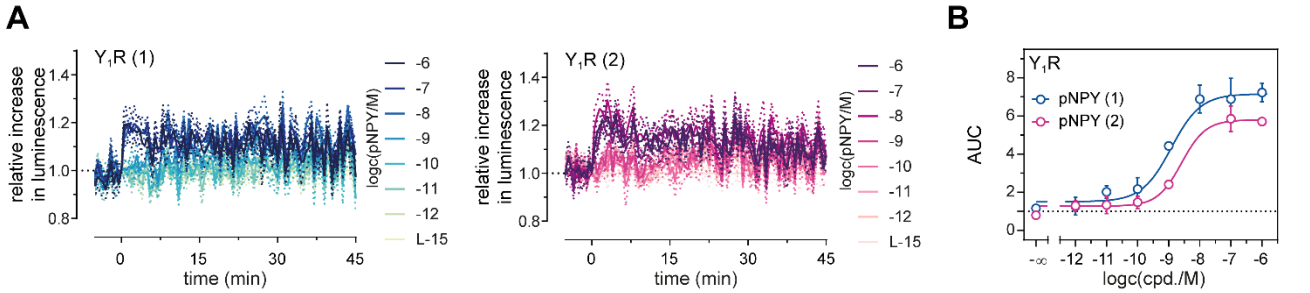

Figure A12. A) Relative increases in luminescence over time upon Y_1R stimulation obtained in the mini-G protein recruitment assay. HEK293T cells stably co-expressing NlucN-mGsi and Y_1R-NlucC fusion proteins were stimulated using various pNPY concentrations. B) Concentration response curves of pNPY were obtained using the area under curve (AUC) of the luminescent traces.

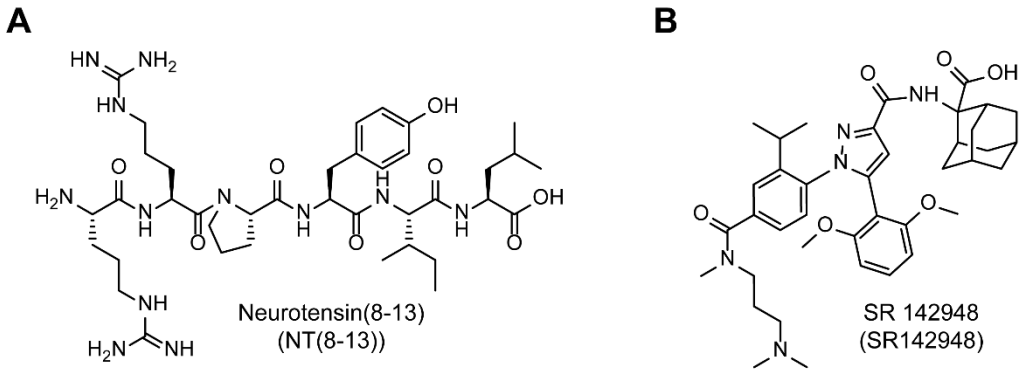

Figure A13. Structures of investigated NTS_1R ligands classified as A) agonist and B) antagonist.

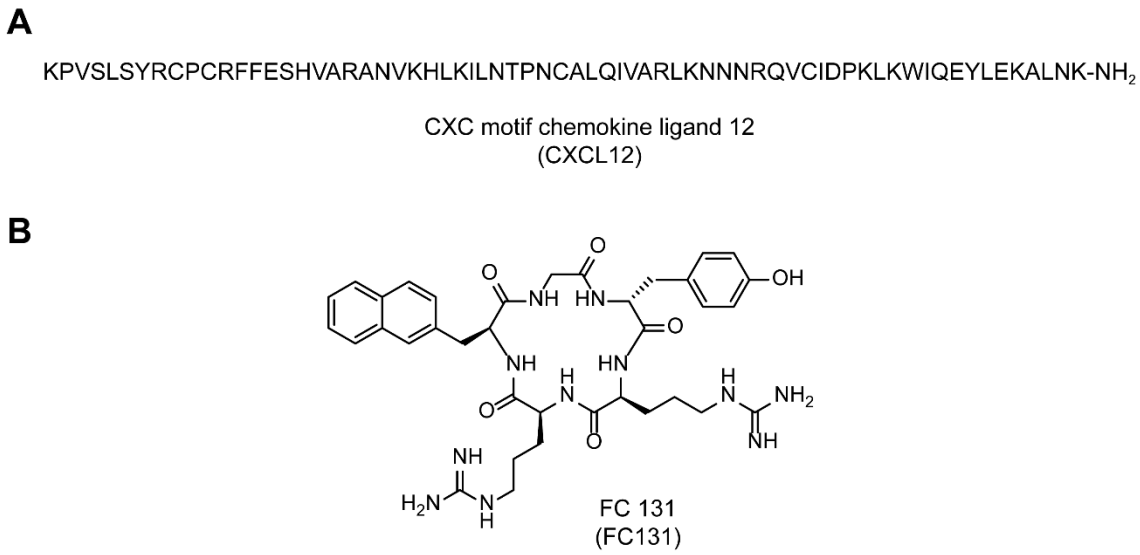

Figure A14. Protein sequences or structures of investigated CXCR4 ligands classified as A) agonist and B) antagonist.

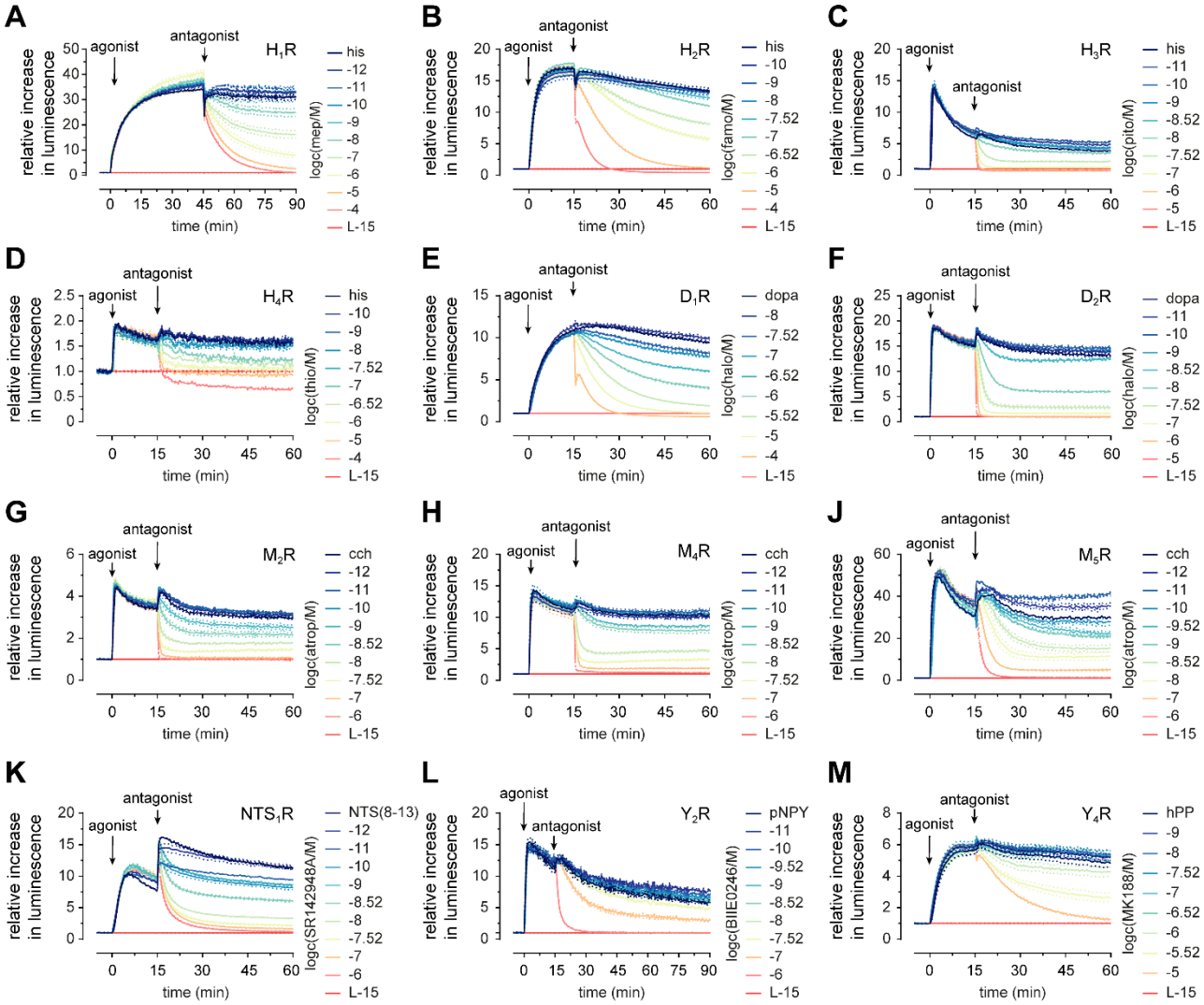

Figure A15. Reversibility of mini-G sensors. HEK293T cells stably co-expressing GPCR-NlucC/NlucN-mG fusion proteins were stimulated with a reference agonist (H_1R/mGsq: 10 µM histamine (his), H_2R/mGs: 1 µM his, H_3R/mGsi: 1 µM his, H_4R/mGsi: 1 µM his, D_1R/mGs: 100 nM dopamine (dopa), D_2R/mGsi: 1 µM dopa, M_2R/mGsi: 100 µM carbachol (cch), M_4R/mGsi: 100 µM cch, M_5R/mGsq: 100 µM cch, NTS_1R/mGsq: 5 nM NTS(8-13), Y_2R/mGsi: 50 nM pNPY, Y_4R/mGsi: 10 nM MK188). After 15 min, mini-G protein recruitment was terminated by the addition of indicated antagonists at various concentrations. Presented data show representative luminescent traces from at least three independent experiments (*N* = 3), each performed in triplicate.

8.3. Appendix to Chapter 4

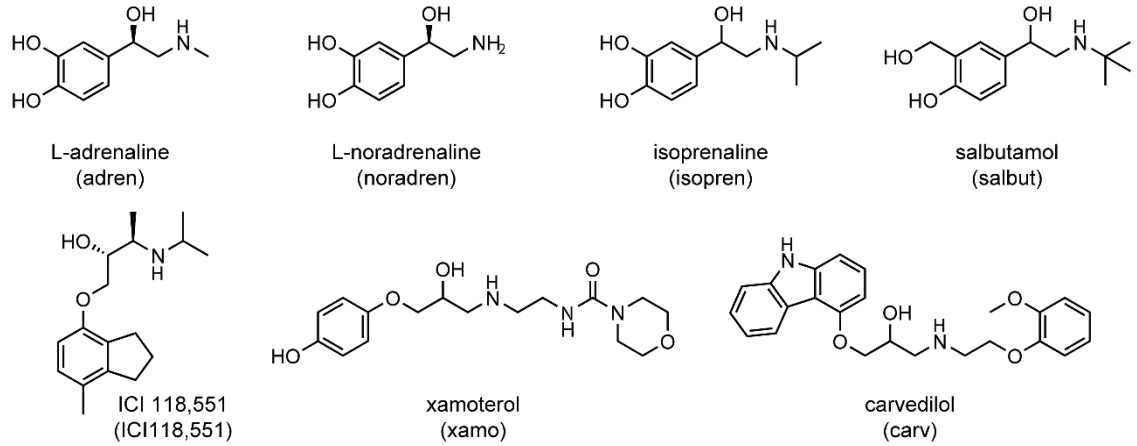

Figure A16. Structures of investigated $\beta_{1,2}$AR ligands.

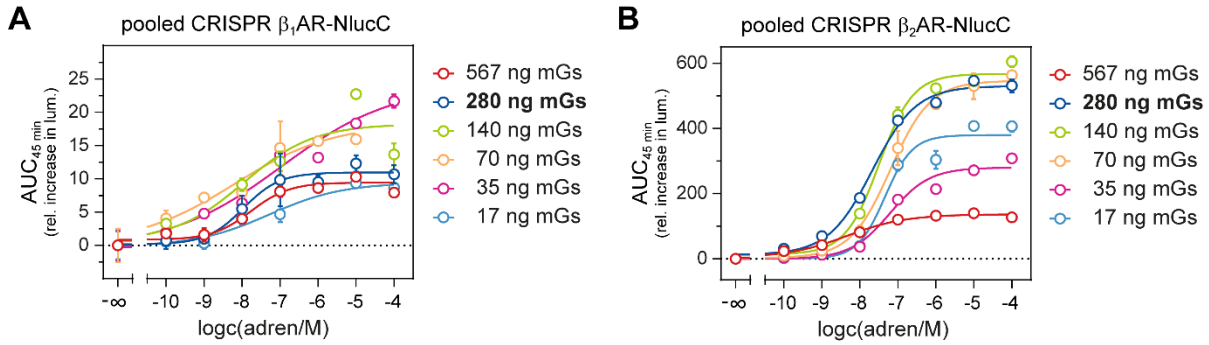

Figure A17. Concentration response curves of adrenaline obtained by mGs recruitment to endogenously expressed A) β_1AR-NlucC and B) β_2AR-NlucC. CRISPR/Cas9 modified HEK293T cells were transiently transfected with indicated amounts of pIRESpuro3 NlucN-mGs plasmid DNA on one hand to verify the CRISPR/Cas9 edit, and on the other hand to evaluate the plasmid DNA amount for optimal assay signals. Thus, in the following experiments, 280 ng of pIRESpuro3 NlucN-mGs plasmid DNA was used for transfection.

Table A3. Oligonucleotide sequences (O1-O22) used for the generation and verification of HEK293T CRISPR $\beta_{1,2}$AR-NlucC cells. Nucleotides complementary to template DNA are indicated by underlining.

	Oligo name	Sequence
O1	β_1AR gRNA fw	CACCGCCTCGGAATCCAAGGTGTA
O2	β_1AR gRNA rv	AAACTACACCTTGGATTCCGAGGC
O3	β_2AR gRNA fw	CACCGATAACATTGATTCACAAGGG
O4	β_2AR gRNA rv	AAACCCCTTGTGAATCAATGTTATC
O5	β_1AR diag fw	CTGCTACAACGACCCCAAGT
O6	β_1AR diag rv	TCCCCTAACCCACCCATCTT
O7	β_2AR diag fw	TCCCCTTATCTACTGCCGGA
O8	β_2AR diag rv	AACAGGTGCAATGAAGGCAT
O9	pFETCh(-)FLAG fw	CGCTCAGAGACCCGCGTAAG
O10	pFETCh(-)FLAG rv	GTTTCAGGAAGCGGAGCTAC
O11	NlucC fw	AGTTAGTAGCTCCGCTTCCTGAAACGAGAATCTCCTCGAACAGCCG
O12	NlucC rv	GAGACCTTACGCGGGTCTCTGAGCGGAGGAGGTGGCGGATCCGGT
O13	β_1AR HOM1 fw	TCCCCGACCTGCAGCCCAGCTTGCTACAACGACCCCAAG
O14	β_1AR HOM1 rv	ATCCGCCACCTCCTCCGCTCCCCACCTTGGATTCCGAGGC
O15	β_1AR HOM2 fw	AGTTCTTCTGATTCGAACATCTAGCTGCCCGGCGCGGGGC
O16	β_1AR HOM2 rv	TGGAGAGGACTTTCCAAGCCCAGGCGCGCGGGGGAC
O17	β_2AR HOM1 fw	TCCCCGACCTGCAGCCCAGCTAGAATAAGGCCCGGGTGATCATTCT
O18	β_2AR HOM1 rv	ATCCGCCACCTCCTCCGCTCCCCAGCAGTGAGTCATTTGTACTACAATTT
O19	β_2AR HOM2 fw	AGTTCTTCTGATTCGAACATCTAAAGCAGTTTTTCTACT
O20	β_2AR HOM2 rv	TGGAGAGGACTTTCCAAGAGACTCAAAGGCAAATGA
O21	β_2AR CRISPR control fw	AAGCTGCTCCTCAAATCCCT
O22	β_2AR CRISPR control rv	CCTTACCTCCTTCTTGCCCA

8.4. Appendix to Chapter 5

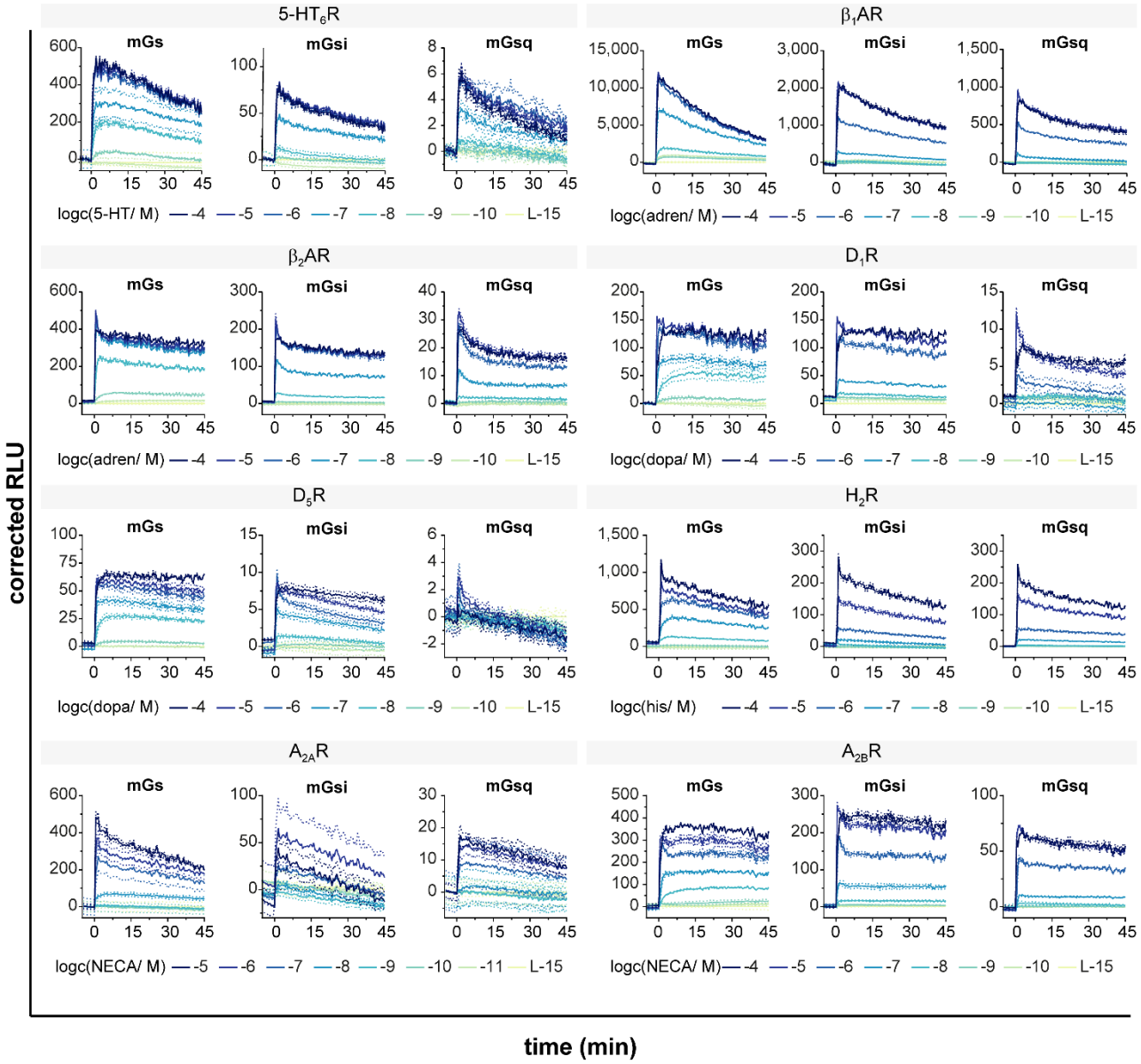

Figure A18. Representative luminescent traces obtained for Gs-coupled GPCRs under distinct mini-G protein conditions. Signals (corrected relative luminescent units (RLU)) in response to indicated reference agonists were obtained in mini-G protein recruitment assays using HEK293T cells transiently expressing GPCR-NlucC/NlucN-mini-G protein fusion proteins. Representative data are shown from at least three independent experiments (*N* = 3), each performed in triplicate.

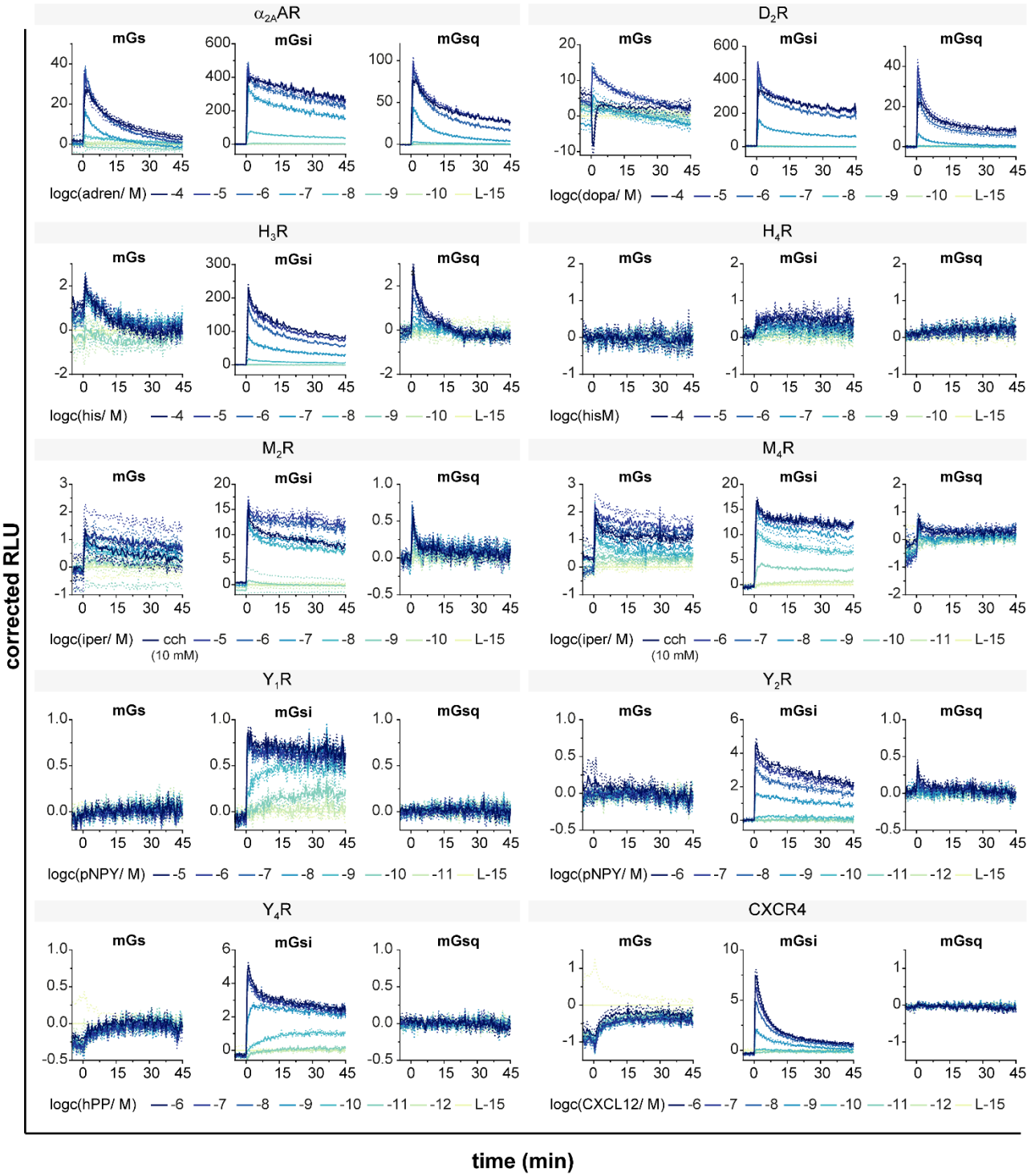

Figure A19. Representative luminescent traces obtained for Gi/o-coupled GPCRs under distinct mini-G protein conditions. Signals (corrected relative luminescent units (RLU)) in response to indicated reference agonists were obtained in mini-G protein recruitment assays using HEK293T cells transiently expressing GPCR-NlucC/NlucN-mini-G protein fusion proteins. Representative data are shown from at least three independent experiments (*N* = 3), each performed in triplicate.

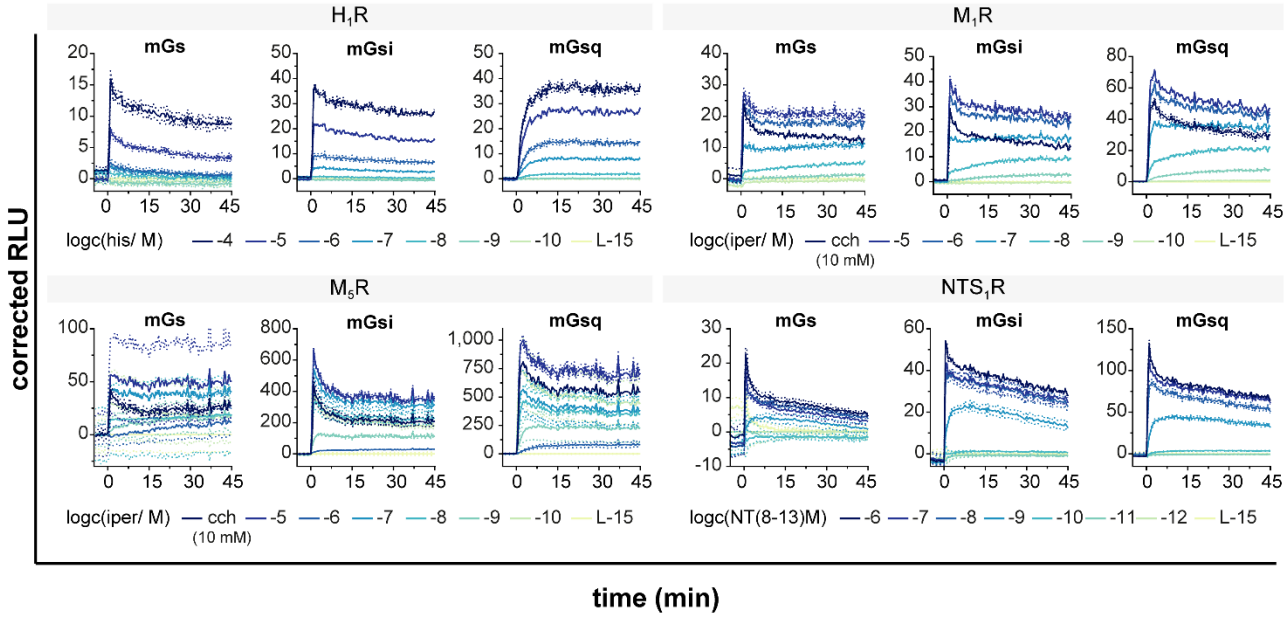

Figure A20. Representative luminescent traces obtained for Gq/11-coupled GPCRs under distinct mini-G protein conditions. Signals (corrected relative luminescent units (RLU)) in response to indicated reference agonists were obtained in mini-G protein recruitment assays using HEK293T cells transiently expressing GPCR-NlucC/NlucN-mini-G protein fusion proteins. Representative data are shown from at least three independent experiments (*N* = 3), each performed in triplicate.

Table A4. Comparison of utilized full agonists in presented mini-G protein recruitment assays and [a]TGF-a shedding assays by Inoue et al. (2019)[14] and [b]G protein-dependent effector translocalization assays (GEMTA) by Avet et al. (2020)[15]; n.a. = not available.

Subtype	mini-G Protein Recruitment	TGF-α Shedding[a]	GEMTA[b]
5-HT_6R	5-hydroxytryptamine	5-hydroxytryptamine	n.a.
β_1AR	adrenaline	(-)-isoprenaline	noradrenaline
β_2AR	adrenaline	(-)-isoprenaline	noradrenaline
D_1R	dopamine	dopamine	dopamine
D_5R	dopamine	dopamine	dopamine
H_2R	histamine	histamine	histamine
A_{2A}R	NECA	adenosine	adenosine
A_{2B}R	NECA	adenosine	adenosine
α_{2A}AR	adrenaline	noradrenaline	noradrenaline
D_2R	dopamine	dopamine	dopamine
H_3R	histamine	histamine	n.a.
H_4R	histamine	histamine	n.a.
M_2R	iperoxo	acetylcholine	acetylcholine
M_4R	iperoxo	acetylcholine	acetylcholine
Y_1R	porcine NPY	n.a.	human NPY
Y_2R	porcine NPY	n.a.	n.a.
Y_4R	human PP	n.a.	n.a.
CXCR4	CXCL12	n.a.	CXCL12
H_1R	histamine	histamine	histamine
M_1R	iperoxo	acetylcholine	acetylcholine
M_5R	iperoxo	acetylcholine	n.a.
NTS_1R	NT(8-13)	neurotensin	n.a.

8.5. Appendix to Chapter 6

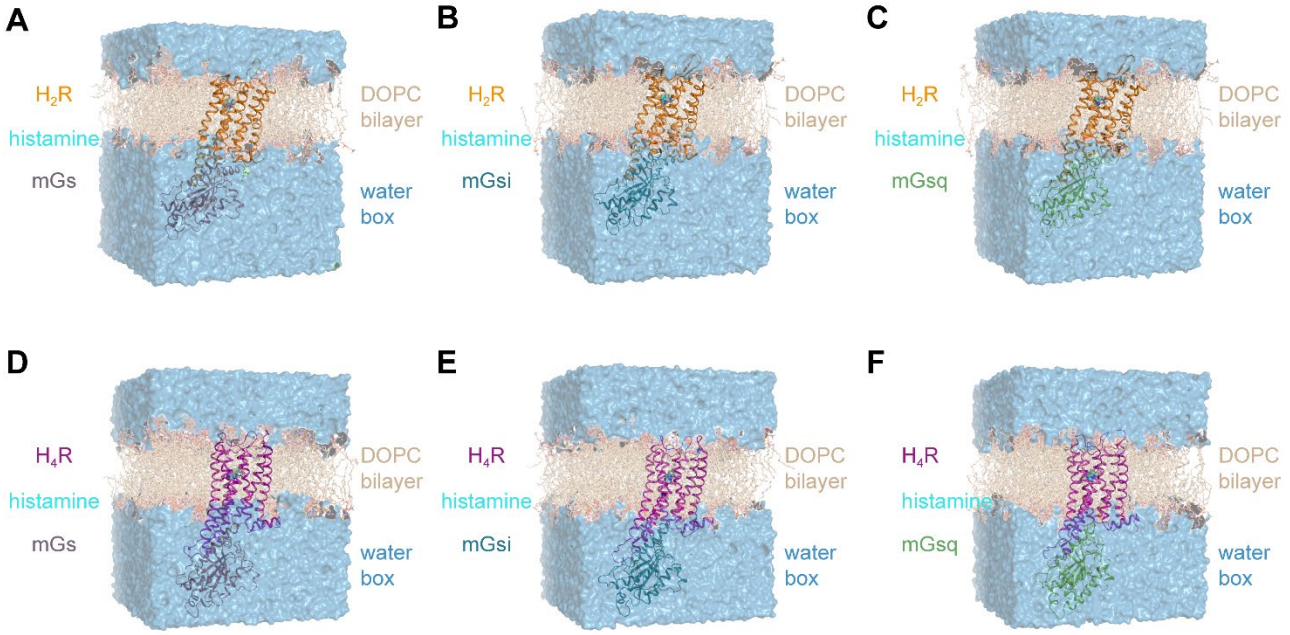

Figure A21. Computational model of GaMD simulation systems containing the H_2R in complex with A) mGs, B) mGsi and C) mGsq as well as the H_4R in complex with D) mGs, E) mGsi and F) mGsq. The histamine-bound receptors complexed by mini-G proteins were embedded into a dioleoylphosphatidylcholine (DOPC) bilayer and solvated in a TIP3 water box with Cl^- as counter ions.

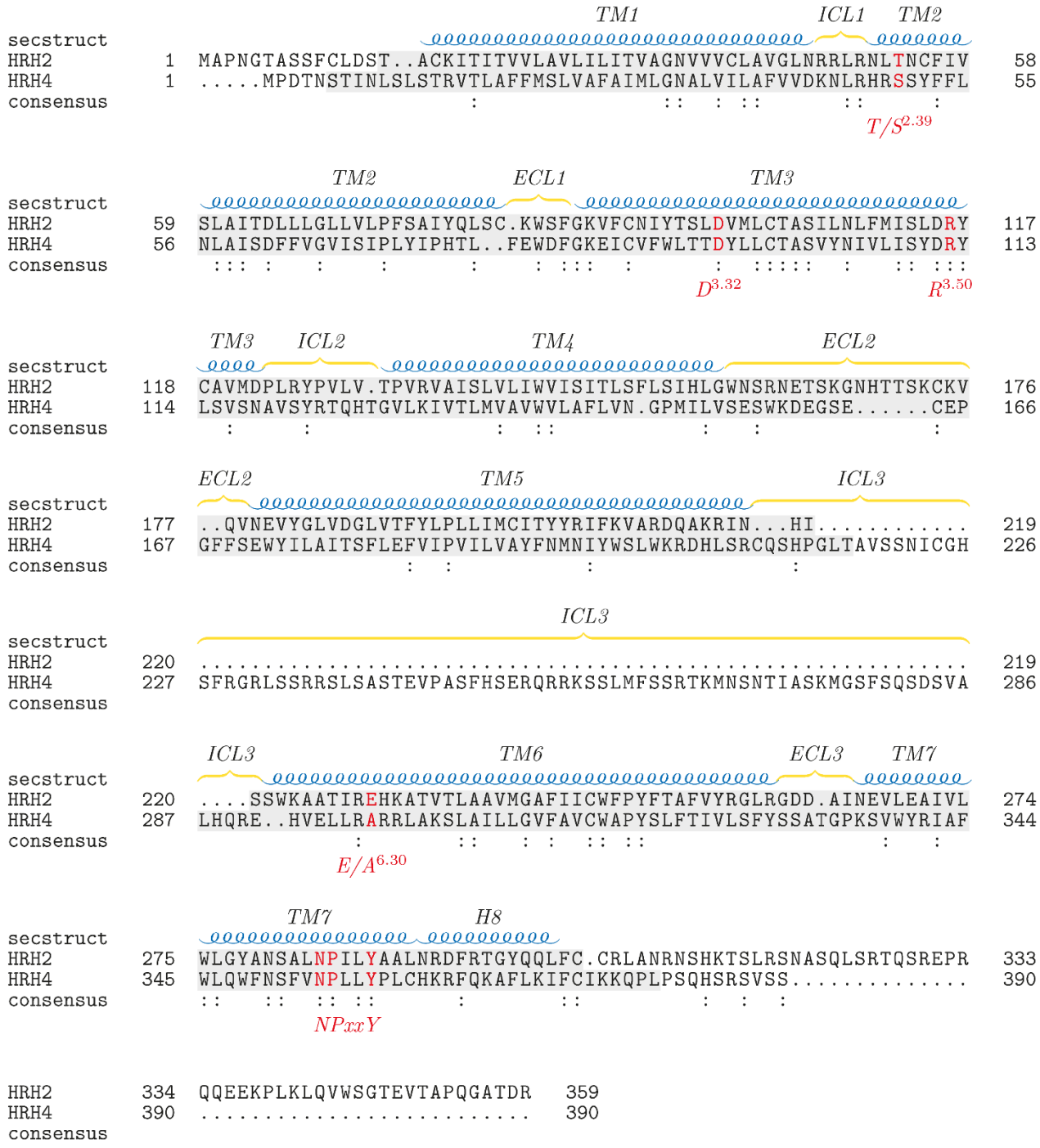

Figure A22. Sequence alignment of the human histamine receptor subtypes H_2 and H_4 (HRH2, HRH4). Residues present in computational receptor models used are highlighted in gray; missing residues are not shaded. Secondary structure elements of α-helical transmembrane (TM) domains are highlighted as blue coils and extracellular or intracellular loops (ECL, ICL) as yellow brackets. Residues considered for extraction of reaction coordinates and subsequent calculation of free energy profiles are indicated in red. The sequence consensus indicates identical receptor residues (:).

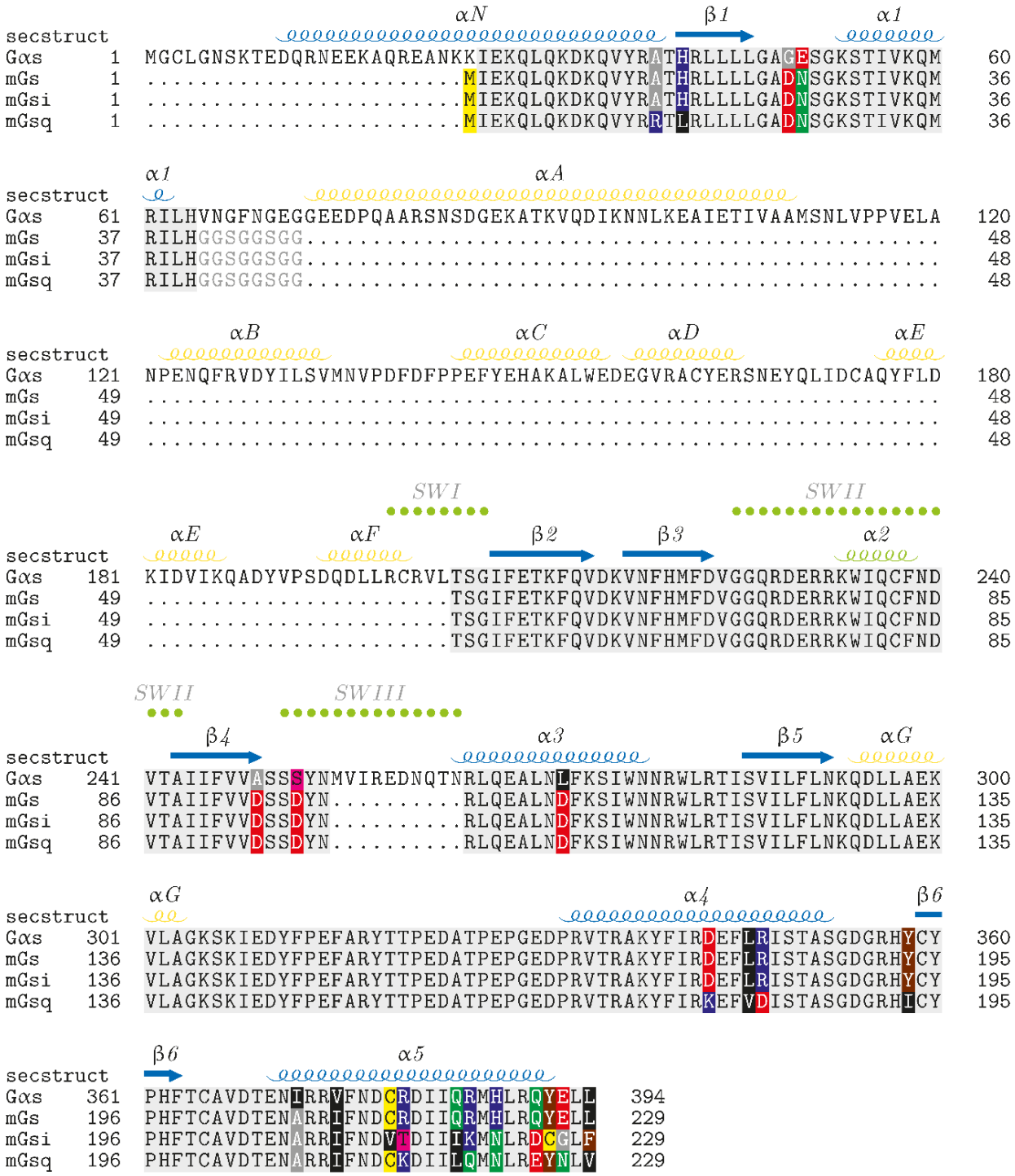

Figure A23. Sequence alignment of the Gαs subunit and the utilized mini-G proteins mGs, mGsi and mGsq. Secondary structure elements of Gαs, such as α helices and β sheets, are highlighted as loops and arrows, respectively, in blue (GTPase domain) and yellow (helical domain). The switch regions (SWI, SWII and SWIII) are labeled in green. Identical residues of the sequences are colored in light grey. Sequence differences are highlighted due to the chemical properties of the residue functional groups (acidic: red, aliphatic: black, aliphatic (small): grey, amide: green, aromatic: brown, basic: blue, hydroxyl: pink, imino: orange, sulfur: yellow). Residues only present in Gαs are not shaded.

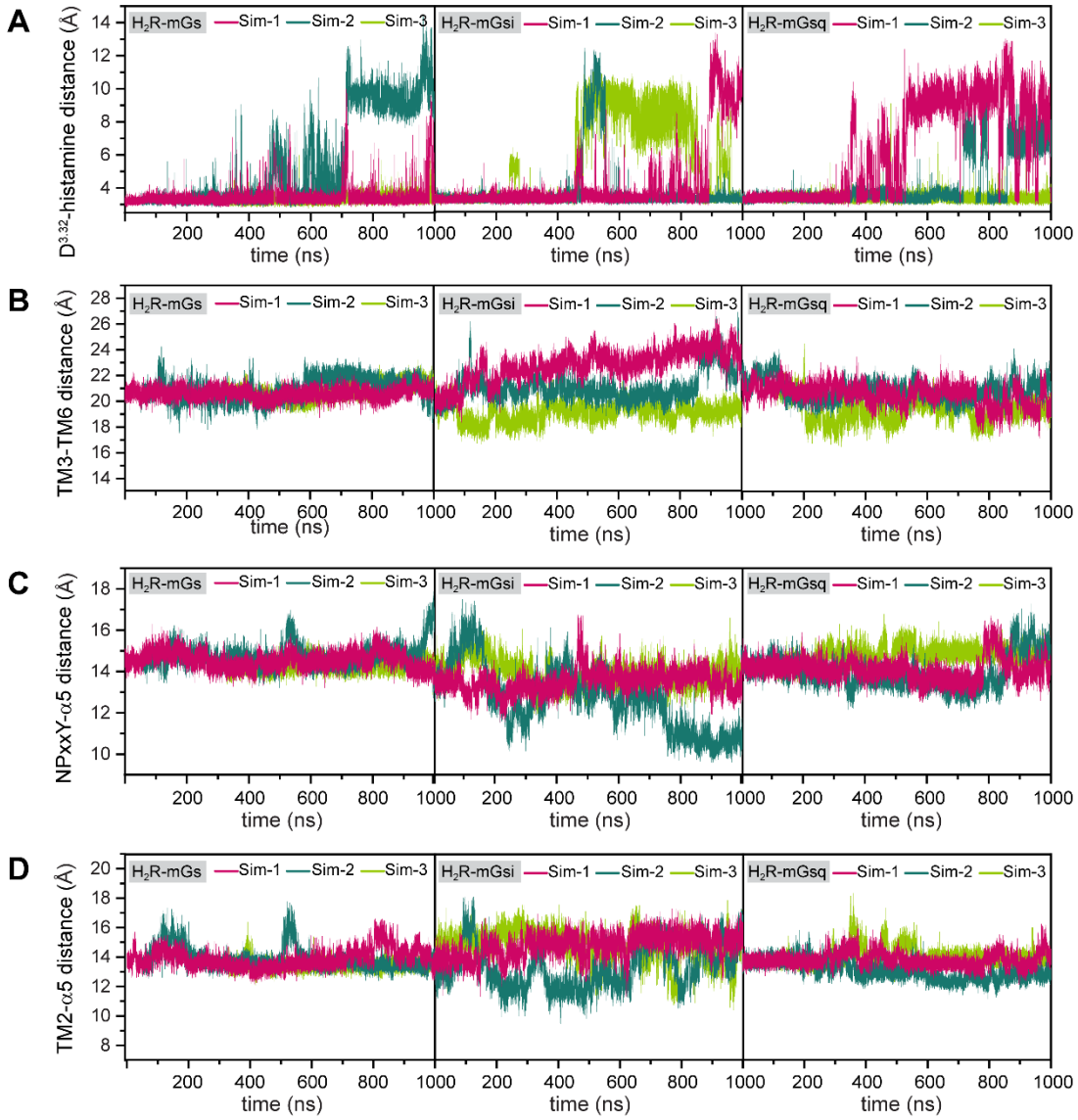

Figure A24. Time courses of the reaction coordinates in H_2R systems (H_2R-mGs, H_2R-mGsi and H_2R-mGsq) used for energetic reweighting. A) Distance between $D^{3.32}$ and histamine using the Cγ atom of $D^{3.32}$ and Nα of histamine. B) Distance between TM3 and TM6 of the H_2R. The Cα, C and N atoms of residues $R^{3.50}$ and $E^{6.30}$ were used to calculate the distance. C) Distance between the NPxxY motif and α5 helix of the respective mini-G protein. The distance was calculated using the center of mass of the NPxxY motif and the last five residues of α5 helix. D) Distance between TM2 of the H_2R and the α5 helix of the respective mini-G protein. To calculate the distance, the Cα, C and N atoms of $T^{2.39}$ and the geometric center of the last five residues of α5 were used.

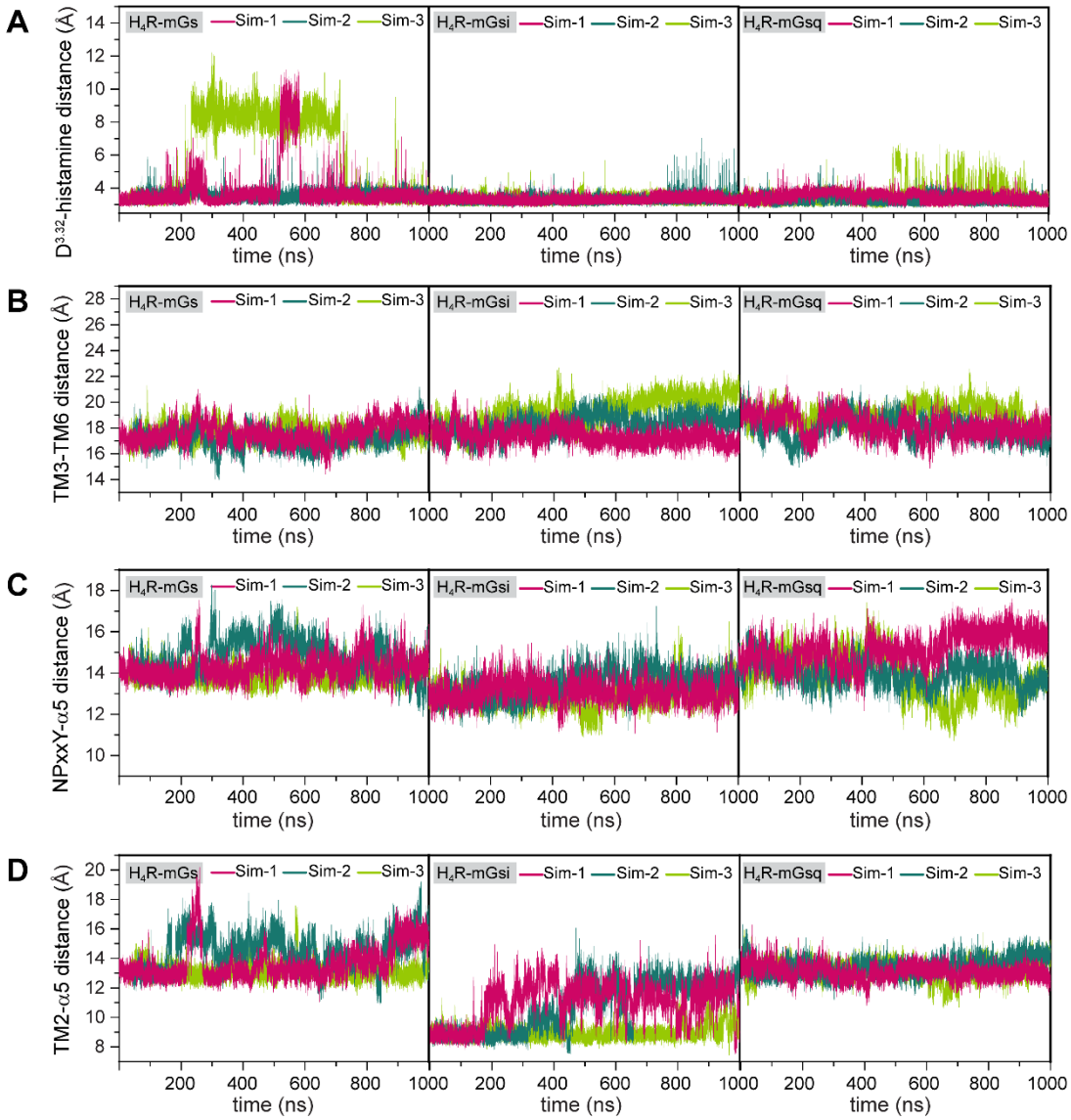

Figure A25. Time courses of the reaction coordinates in H_4R systems (H_4R-mGs, H_4R-mGsi and H_4R-mGsq) used for energetic reweighting. A) Distance between $D^{3.32}$ and histamine using the Cγ atom of $D^{3.32}$ and Nα of histamine. B) Distance between TM3 and TM6 of the H_4R. The Cα, C and N atoms of residues $R^{3.50}$ and $A^{6.30}$ were used to calculate the distance. C) Distance between the NPxxY motif and α5 helix of the respective mini-G protein. The distance was calculated using the center of mass of the NPxxY motif and the last five residues of α5 helix. D) Distance between TM2 of the H_4R and the α5 helix of the respective mini-G protein. To calculate the distance, the Cα, C and N atoms of $S^{2.39}$ and the geometric center of the last five residues of α5 were used.

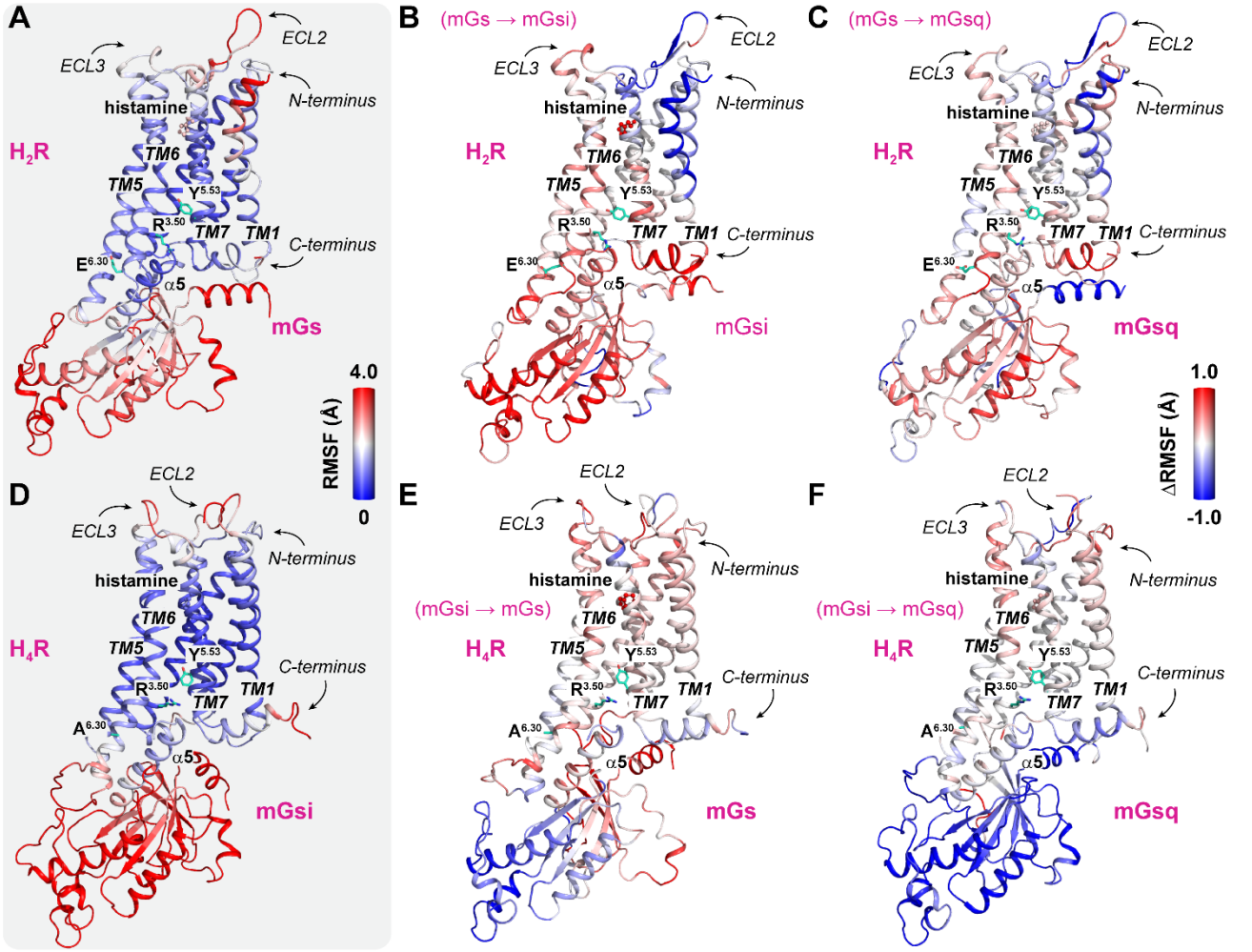

Figure A26. Comparison of the structural flexibility in H_2R and H_4R complexes with mini-G proteins. A) Overall structural flexibility (RMSF) of the H_2R-mGs complex and changes in structural flexibility (ΔRMSF) in the H_2R complexes, when mGs was exchanged by mGsi (B) or mGsq (C). D) Overall structural flexibility (RMSF) of the H_4R-mGsi complex and changes in structural flexibility (ΔRMSF) in the H_4R complexes, when mGsi was exchanged by mGs (E) or mGsq (F). For RMSFs, a color scale of 0.0 Å (blue) to 4.0 Å (red) was used. In case of ΔRMSF, the color scale ranged from -1.0 Å (blue) to 1.0 Å (red). (Δ)RMSF values were assigned to the starting structure of each system.

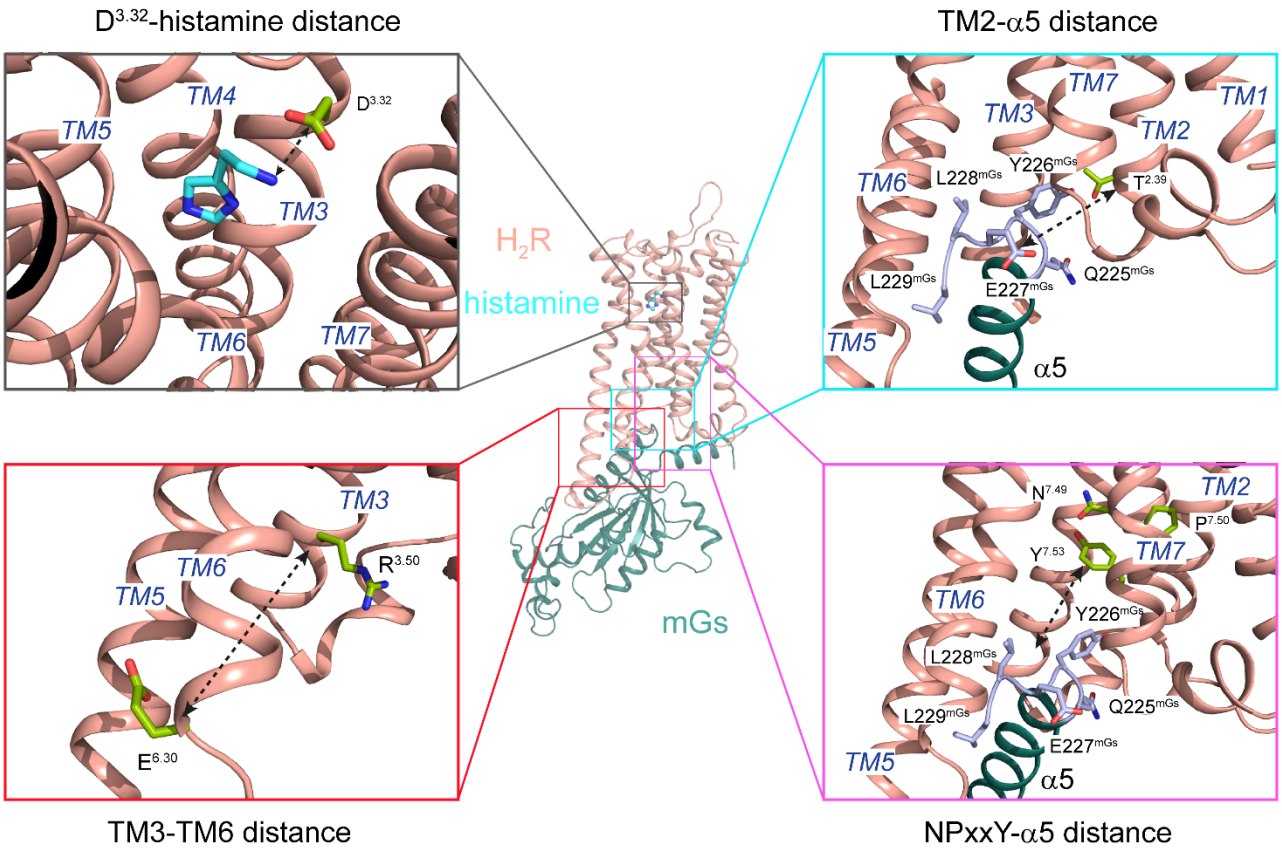

Figure A27. Schematic illustration of the reaction coordinates used for energetic reweighting exemplarily shown for the H_2R in complex with mGs. The distance between $D^{3.32}$ and histamine was calculated using the Cγ atom of $D^{3.32}$ and Nα of histamine. The distance between TM3 and TM6 was assessed using the Cα, C and N atoms of residues $R^{3.50}$ and $E^{6.30}$. The distance between the NPxxY motif and α5 helix of mGs was calculated using the center of mass of the NPxxY motif ($N^{7.49}$, $P^{7.50}$ and $Y^{7.53}$) and the last five residues of mGs α5 helix (Q225, Y226, E227, L228 and L229). The distance between TM2 of the H_2R and the α5 helix of mGs was determined using the Cα, C and N atoms of $T^{2.39}$ and the geometric center of the last five residues of mGs α5 helix (Q225, Y226, E227, L228 and L229).

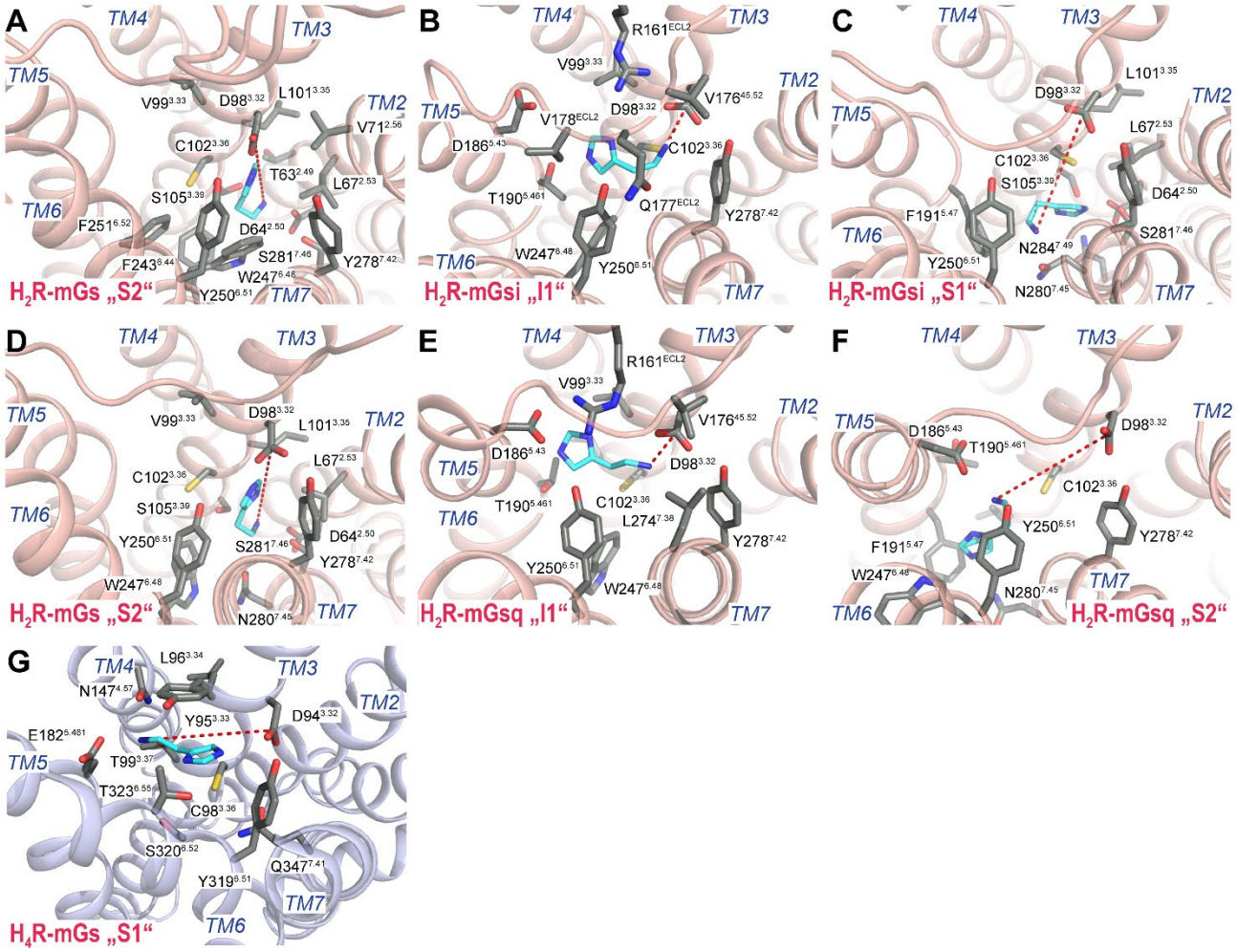

Figure A28. Binding modes of histamine (light blue) within the orthosteric binding pocket of the H_2R (salmon) and the H_4R (purple). Structures representing the separated histamine state "S2" in H_2R-mGs (A), the intermediately bound state "I1" (B) and the separated histamine states "S1" (C) and "S2" (D) in H_2R-mGsi, the intermediately bound state "I1" (E) and the separated histamine states "S2" (F) in H_2R-mGsq complexes, as well as the separated histamine state "S1" in the H_4R-mGs complex (G) are shown. Contact residues within 4 Å of the ligand are highlighted as sticks (dark grey). The histamine-$D^{3.32}$ distance is highlighted with a red, dashed line.

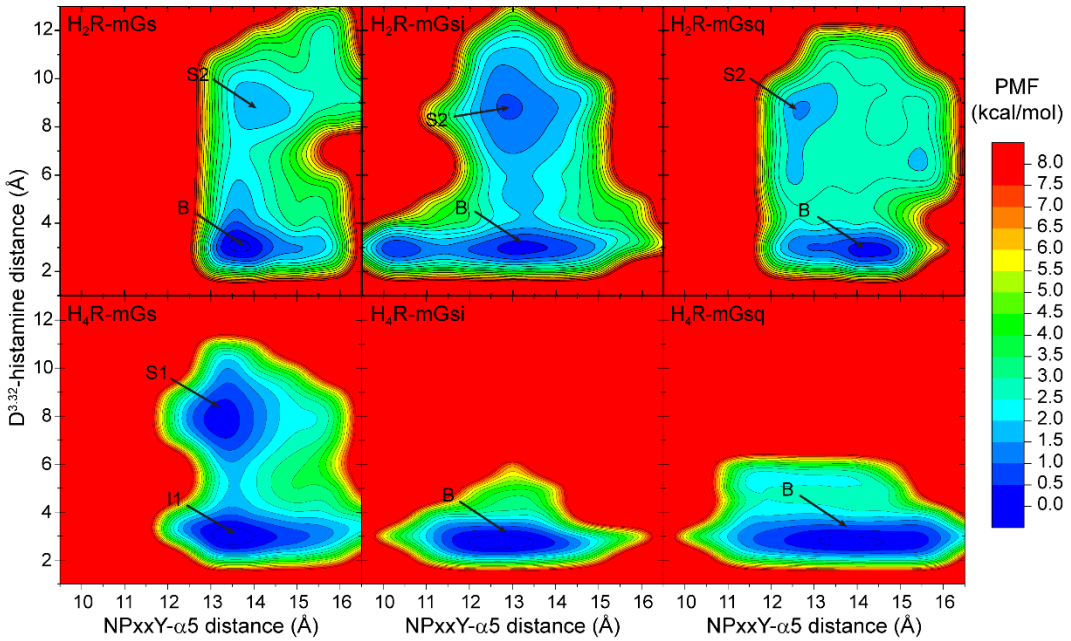

Figure A29. Free energy profiles of GaMD simulations with complexes of either the H_2R or the H_4R in combination with mGs, mGsi or mGsq. Distances (Å) between $D^{3.32}$ (Cγ atom) and the amino group of histamine (Nα atom) as well as of the NPxxY - α5 helix distance were used as reaction coordinates. The NPxxY distance was determined using the center-of-mass (COM) distance between the receptors' NPxxY motif and the last 5 residues of the mG α5 helix. For each system, three independent GaMD simulations were used for analysis. (Labels: "B" indicates representative low energy wells of fully active receptors bound to histamine, "I1" indicates low energy wells of intermediate receptor conformation bound to histamine. "S1" and "S2" indicate low energy wells containing conformations with histamine separated from $D^{3.32}$, cf. Chapter 6, Figure 6.1).

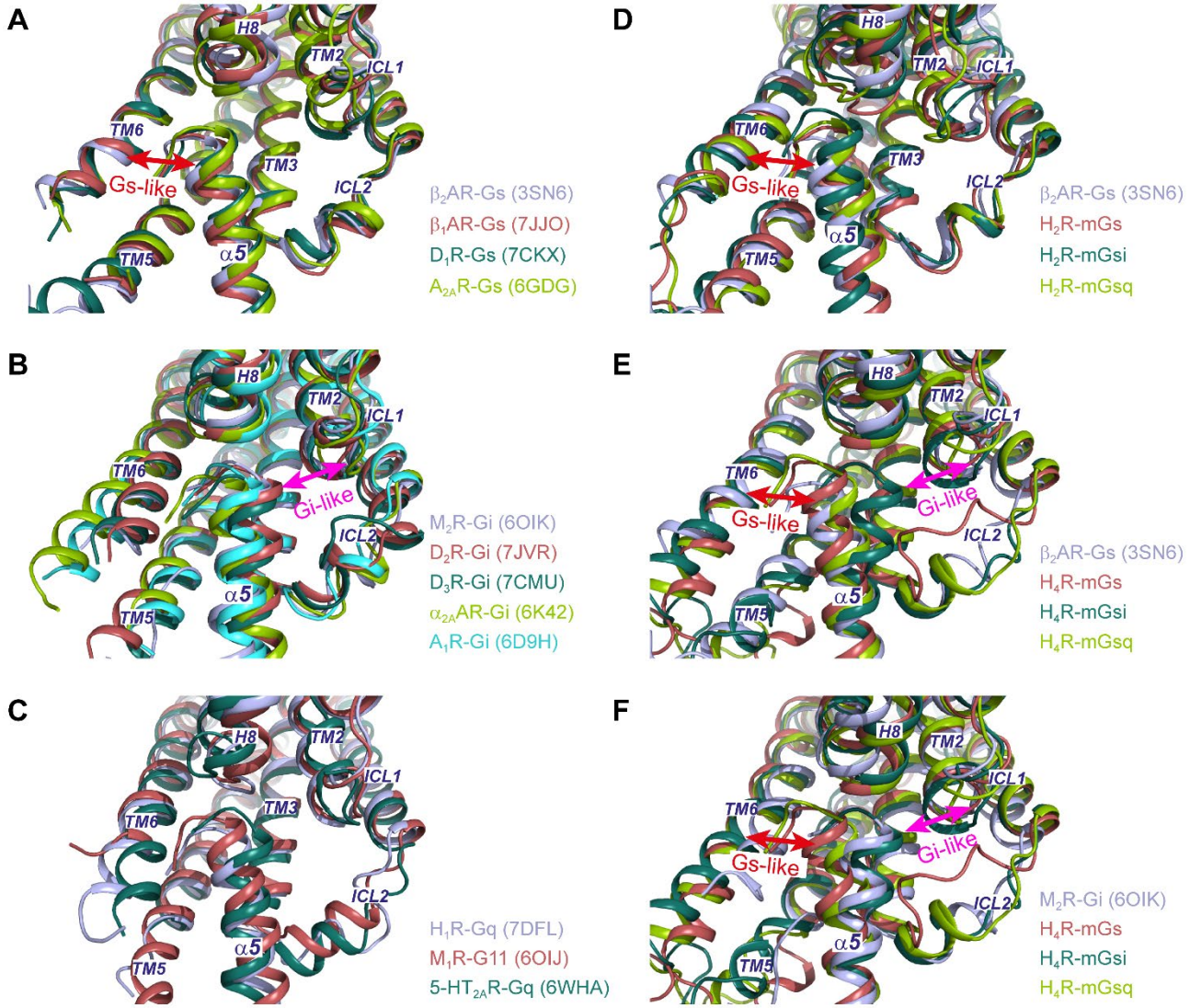

Figure A30. Comparison of the α5 helix orientation at the GPCR - G protein interface. Cytoplasmatic view of the α5 helix orientation of exemplary A) GPCR-Gs complexes (β_2AR, pdb-id.: 3SN6, purple; β_1AR, pdb-id: 7JJO, light red; D_1R, pdb-id.: 7CKX, dark green; A_{2A}R, pdb-id.: 6GDG, light green), B) GPCR-Gi complexes (M_2R, pdb-id.: 6OIK, purple; D_2R, pdb-id.: 7JVR, light red; D_3R, pdb-id.: 7CMU, dark green; α_{2A}AR, pdb-id.: 6K42, light green; A_1R, pdb-id.: 6DH9, blue) and GPCR-Gq complexes (H_1R, pdb-id.: 7DFL, purple; M_1R, pdb-id.: 6OIJ, light red; 5-HT_{2A}R, pdb-id.: 6WHA, dark green). D) Comparison of the α5 helix orientation in the β_2AR-Gs complex (purple) and the representative structures of low energy wells containing the fully active receptors bound to histamine ("B" states, cf. Fig. 1) of the H_2R-mGs (light red), H_2R-mGsi (dark green) and H_2R-mGsq (light green) complexes obtained in GaMD simulations. The α5 helix orientation in representative histamine bound structures of H_4R-mGs ("I1" state, light red), H_4R-mGsi ("B" state, dark green) and H_4R-mGsq ("B" state, light green) complexes are compared to the E) β_2AR-Gs (purple) and F) M_2R-Gi (purple) complexes. The Gs-like α5 orientation towards TM6 is highlighted in red and the Gi-like α5 orientation towards TM2 in pink.

8.6. Abbreviations

5-HT_6R	Human serotonin 5-HT_6 receptor
α_{2A}AR	Human α_{2A} adrenoceptor
A_{2A}R	Human adenosine A_{2A} receptor
A_{2B}R	Human adenosine A_{2B} receptor
AC	Adenylyl cyclase
α_s	Specific activity
ATP	adenosine-5'-triposphate
AUC	Area under curve
β_1AR	Human β_1 adrenoceptor
β_2AR	Human β_2 adrenoceptor
B_{max}	maximum number of binding sites
BRET	Bioluminescence resonance energy transfer
c	Concentration
cAMP	3'-5'-cyclic adenosine monophosphate
Cas	CRISPR associated protein
cDNA	Complementary DNA
CHO	Chinese hamster ovary cells
Ci	Curie
CNS	Central nervous system
cpm	Counts per minute
CRISPR	Clustered regularly interspaced short palindromic repeats
CRC	Concentration response curve
CXCR4	Human CXC-motif chemokine receptor 4
D_1R	Human dopamine D_1 receptor
D_2R	Human dopamine D_2 receptor (long splice variant)
D_5R	Human dopamine D_5 receptor
Da	Dalton
DAG	Diacyl glycerol
DMEM	Dulbecco's Modified Eagle's Medium
DMSO	Dimethyl sulfoxide
DNA	Desoxyribonucleic acid
DPBS	Dulbecco's phosphate-buffered saline
dpm	Disintegrations per minute
EC_{50}	Half maximal effective concentration of an agonist, refers to the agonist concentration that induces 50% of the maximal effect
EDTA	Ethylenediaminetetraacetic acid

E_{max}	Maximal response of a ligand in a functional assay
ER	Endoplasmatic reticulum
ERK1/2	Extracellularly regulated kinase 1 and 2
FCS	Fetal calf serum
FRET	Förster resonance energy transfer
G418	Geneticin
GaMD	Gaussian accelerated molecular dynamics
GDP	Guanosine 5-diphosphate
GFP	Green fluorescent protein
G protein	Guanine nucleotide-binding protein
GPCR	G protein-coupled receptor
GTP	Guanosine 5'-triphosphate
GTPγS	Guanosine 5'-O-[γ-thio]triphosphate
h	Hour(s)
HEK293T	Human embryonic kidney cells
H_1R	Human histamine H_1 receptor
H_2R	Human histamine H_2 receptor
H_3R	Human histamine H_3 receptor
H_4R	Human histamine H_4 receptor
HEPES	4-(2-Hydroxyethyl)piperazine-1-ethanesulfonic acid
IC_{50}	a) Ligand concentration that displaces 50% of a labeled compound from the binding site
	b) Antagonist concentration that suppresses 50% of an agonist induced response
IP_3	inositol trisphosphate
K_b	Equilibrium dissociation constant of a ligand determined in a functional assay
K_d	Equilibrium dissociation constant of a ligand determined in saturation binding experiments
K_i	Equilibrium dissociation constant of a ligand determined in competition binding experiments
L	Liter
L-15	Leibovitz' L-15 medium
M_1R	Human muscarinic acetylcholine M_1 receptor
M_2R	Human muscarinic acetylcholine M_2 receptor
M_4R	Human muscarinic acetylcholine M_4 receptor
M_5R	Human muscarinic acetylcholine M_5 receptor
M	Molar (mol/L)
MAP	Mitogen-activated protein

min	Minute(s)
mol	Mole(s)
NlucC	C-terminal, smaller NanoLuc fragment (amino acids 1-11)
NlucN	N-terminal, larger NanoLuc fragment (amino acids 12-170)
NTS_1R	Human neurotensin NTS_1 receptor
PBS	Phosphate-buffered saline
PCR	Polymerase chain reaction
PLC-β	Phospholipase C-β
RET	Resonance energy transfer
rpm	Revolutions per minute
RT	Room temperature
s	Second(s)
S/B ratio	Signal-to-background ratio
SEM	Standard error of the mean
*Sf*9	Insect cell line derived from *Spopoptera frugiperda*
SLC	Split-luciferase complementation
TALEN	Transcription activator-like effector nuclease
Tris	2-amino-2-(hydroxymethyl)propane-1,3-diol
Y_1R	Human neuropeptide Y Y_1 receptor
Y_2R	Human neuropeptide Y Y_2 receptor
Y_4R	Human neuropeptide Y Y_4 receptor
ZFN	Zinc-finger nuclease

8.7. References

1. Nehmé, R., Carpenter, B., Singhal, A., Strege, A., Edwards, P. C., White, C. F., Du, H., Grisshammer, R. & Tate, C. G., Mini-G proteins: Novel tools for studying GPCRs in their active conformation. *PLoS One* **2017,** *12* (4), e0175642, doi: 10.1371/journal.pone.0175642.
2. Seifert, R., Wenzel-Seifert, K., Burckstummer, T., Pertz, H. H., Schunack, W., Dove, S., Buschauer, A. & Elz, S., Multiple differences in agonist and antagonist pharmacology between human and guinea pig histamine H1-receptor. *J Pharmacol Exp Ther* **2003,** *305* (3), 1104-1115, doi: 10.1124/jpet.103.049619.
3. Baumeister, P., Erdmann, D., Biselli, S., Kagermeier, N., Elz, S., Bernhardt, G. & Buschauer, A., [3H]UR-DE257: Development of a tritium-labeled squaramide-type selective histamine H2 receptor antagonist. *ChemMedChem* **2015,** *10* (1), 83-93, doi: 10.1002/cmdc.201402344.
4. Igel, P., Schnell, D., Bernhardt, G., Seifert, R. & Buschauer, A., Tritium-labeled N1-[3-(1H-imidazol-4-yl)propyl]-N2-propionylguanidine ([3H]UR-PI294), a high-affinity histamine H3 and H4 receptor radioligand. *ChemMedChem* **2009,** *4* (2), 225-231, doi: 10.1002/cmdc.200800349.
5. Gratz, L., Tropmann, K., Bresinsky, M., Muller, C., Bernhardt, G. & Pockes, S., NanoBRET binding assay for histamine H2 receptor ligands using live recombinant HEK293T cells. *Sci Rep* **2020,** *10* (1), 13288, doi: 10.1038/s41598-020-70332-3.
6. Leurs, R., Smit, M. J., Menge, W. M. & Timmerman, H., Pharmacological characterization of the human histamine H2 receptor stably expressed in Chinese hamster ovary cells. *Br J Pharmacol* **1994,** *112* (3), 847-854, doi: 10.1111/j.1476-5381.1994.tb13157.x.
7. Yang, Z., Han, S., Keller, M., Kaiser, A., Bender, B. J., Bosse, M., Burkert, K., Kogler, L. M., Wifling, D., Bernhardt, G., et al., Structural basis of ligand binding modes at the neuropeptide Y Y1 receptor. *Nature* **2018,** *556* (7702), 520-524, doi: 10.1038/s41586-018-0046-x.
8. Kelley, M. T., Burckstummer, T., Wenzel-Seifert, K., Dove, S., Buschauer, A. & Seifert, R., Distinct interaction of human and guinea pig histamine H2-receptor with guanidine-type agonists. *Mol Pharmacol* **2001,** *60* (6), 1210-1225, doi: 10.1124/mol.60.6.1210.
9. Houston, C., Wenzel-Seifert, K., Burckstummer, T. & Seifert, R., The human histamine H2-receptor couples more efficiently to Sf9 insect cell Gs-proteins than to insect cell Gq-proteins: Limitations of Sf9 cells for the analysis of receptor/Gq-protein coupling. *J Neurochem* **2002,** *80* (4), 678-696, doi: 10.1046/j.0022-3042.2001.00746.x.
10. Bartole, E., Littmann, T., Tanaka, M., Ozawa, T., Buschauer, A. & Bernhardt, G., [3H]UR-DEBa176: A 2,4-diaminopyrimidine-type radioligand enabling binding studies at the human, mouse, and rat histamine H4 receptors. *J Med Chem* **2019,** *62* (17), 8338-8356, doi: 10.1021/acs.jmedchem.9b01342.
11. Bosma, R., Witt, G., Vaas, L. A. I., Josimovic, I., Gribbon, P., Vischer, H. F., Gul, S. & Leurs, R., The target residence time of antihistamines determines their antagonism of the G protein-coupled histamine H1 receptor. *Front Pharmacol* **2017,** *8*, 667, doi: 10.3389/fphar.2017.00667.
12. Strasser, A., Striegl, B., Wittmann, H. J. & Seifert, R., Pharmacological profile of histaprodifens at four recombinant histamine H1 receptor species isoforms. *J Pharmacol Exp Ther* **2008,** *324* (1), 60-71, doi: 10.1124/jpet.107.129601.
13. Lazewska, D., Mogilski, S., Hagenow, S., Kuder, K., Gluch-Lutwin, M., Siwek, A., Wiecek, M., Kaleta, M., Seibel, U., Buschauer, A., et al., Alkyl derivatives of 1,3,5-triazine as histamine H4 receptor ligands. *Bioorg Med Chem* **2019,** *27* (7), 1254-1262, doi: 10.1016/j.bmc.2019.02.020.
14. Inoue, A., Raimondi, F., Kadji, F. M. N., Singh, G., Kishi, T., Uwamizu, A., Ono, Y., Shinjo, Y., Ishida, S., Arang, N., et al., Illuminating G-protein-coupling selectivity of GPCRs. *Cell* **2019,** *177* (7), 1933-1947 e1925, doi: 10.1016/j.cell.2019.04.044.

15. Avet, C., Mancini, A., Breton, B., Le Gouill, C., Hauser, A. S., Normand, C., Kobayashi, H., Gross, F., Hogue, M., Lukasheva, V., et al., Selectivity landscape of 100 therapeutically relevant GPCR profiled by an effector translocation-based BRET platform. *bioRxiv* **2020**, 2020.2004.2020.052027, doi: 10.1101/2020.04.20.052027.

Ich erkläre hiermit an Eides statt, dass ich die vorliegende Arbeit ohne unzulässige Hilfe Dritter und ohne Benutzung anderer als der angegebenen Hilfsmittel angefertigt habe; die aus anderen Quellen direkt oder indirekt übernommenen Daten und Konzepte sind unter Angabe des Literaturzitats gekennzeichnet.

Einige der experimentellen Arbeiten wurden in Zusammenarbeit mit anderen Institutionen und Personen durchgeführt. Vermerke zu den Beiträgen der betreffenden Personen finden sich in den jeweiligen Kapiteln und unter „Acknowledgments".

Weitere Personen waren an der inhaltlich-materiellen Herstellung der vorliegenden Arbeit nicht beteiligt. Insbesondere habe ich hierfür nicht die entgeltliche Hilfe eines Promotionsberaters oder anderer Personen in Anspruch genommen. Niemand hat von mir weder unmittelbar noch mittelbar geldwerte Leistungen für Arbeiten erhalten, die im Zusammenhang mit dem Inhalt der vorgelegten Dissertation stehen.

Die Arbeit wurde bisher weder im In- noch im Ausland in gleicher oder ähnlicher Form einer anderen Prüfungsbehörde vorgelegt

Regensburg, den 28.06.2022

_____

Carina Höring